

ABSTRACT

Title of Document: Ultra-High Molecular Weight Nonlinear Bisphenol A
Polycarbonates by Solid State Polymerization in Micro-
Layers

In Hak Baick, Doctor of Philosophy

Directed By: Professor Kyu Yong Choi
Department of Chemical and Biomolecular Engineering

The solid-state polymerization of bisphenol A polycarbonate (BPAPC) has been studied in amorphous and partially crystallized micro-layers (SSP_m) of low molecular weight prepolymers in presence of $LiOH \cdot H_2O$ catalyst at a temperature between the glass transition temperature and the melting point. When the prepolymers (14,000 g/mol) in micro-layers of a thickness range from 5 μm to 35 μm were solid-state polymerized at 230 °C, the polymer molecular weight increased rapidly to above 100,000 g/mol, exceeding the highest molecular weight obtainable by the conventional solid-state polymerization in micro-particles. It has also been observed that the final molecular weight reached as high as 600,000 g/mol even in presence of significant stoichiometric imbalances of end group mole ratios when the prepolymer having 21,000 g/mol is used at 230°C under low pressure (10 mmHg). Most notably, amorphous

prepolymer micro-layers showed significantly higher increase in molecular weight than partially crystallized prepolymer micro-layers.

The chain branching and partially cross-linked structures in high molecular weight polycarbonates have been confirmed by ^1H -NMR spectroscopic analysis as well as pyrolysis-gas chromatography mass spectrometry (Py-GC/MS). ^{13}C -NMR analysis and SSP theoretical model simulation have shown that conventional linear step-growth polymerization is not responsible for the additional increase in molecular weight beyond 50,000 g/mol of polycarbonate MW. The ultra-high molecular weight is contributed to the formation of branched and partially cross-linked structures via Fries or Kolbe-Schmitt rearrangement reactions and radical recombination reaction, respectively. Micro-radical polycarbonate species can be produced via chain scission reaction and hydrogen abstraction at the solid-state polymerization temperature. The formation of cross-linked polymers by radical recombination reactions was attributed to the near complete removal of phenol (i.e. radical scavenger) from the micro-layers during the solid state polymerization. Branched structure polycarbonate was also confirmed by atomic force microscopy (AFM).

The presence of branched and cross-linked polymers contributed to the insolubility of the polymer in solvents such as chloroform, tetrahydrofuran (THF), and methylene chloride. As SSPm process extends for a long reaction time at 230°C, about 95% of the polymer was insoluble with excellent transparency (90-93% light transmission). Properties of ultra-high molecular weight nonlinear polycarbonates (SSP_m PCs) have been investigated by differential scanning calorimetry (DSC), dynamic mechanical analysis (DMA), and rheometer.

The development of Multi-Layer Deposit and Reaction (MLDR) technique has shown that the SSP_m process is not limited to 5-35μm scale. The layer thickness can be expanded while keeping the merits (e.g. high transparency, good solvent resistance, and obtaining high molecular weight in short reaction time) of the SSP_m technique developed in this study.

Ultra-High Molecular Weight Nonlinear Bisphenol A
Polycarbonates by Solid State Polymerization in Micro-Layers

By

In Hak Baick

Dissertation Submitted to the Faculty of the Graduate School of the

University of Maryland, College Park, in partial fulfillment

Of the requirements for the degree of

Doctor of Philosophy

2013

Advisory Committee:

Professor Kyu Yong Choi, Chair

Professor Panagiotis Dimitrakopoulos

Professor Srinivasa Raghavan

Professor Nam Sun Wang

Professor Bongtae Han

© Copyright by

In Hak Baick

2013

Acknowledgements

I would like to express my sincere gratitude for my advisor, Prof. Kyu Yong Choi, for giving me this invaluable opportunity. During my time at the University of Maryland, his support and guidance allowed me to successfully complete my studies. I would especially like to acknowledge his patience in dealing with the many problems that were encountered. I would also like to thank my committee members, Profs. Panos Dimitrakopoulos, Srinivasa Raghavan, Nam Sun Wang, and Bongtae Han for their valuable suggestions and advice on this project.

I would like to acknowledge the support for this project received from The National Science Foundation (NSF, CBET-1033071). My study at UMD was made possible by their financial support.

I would like to thank my lab mates, Sangyool Lee, Yunju Jung, and Woo Jic Yang. I also express my thanks to former lab mates, Dr. Joong Jin Han, Dr. Yuesheng Ye, Dr. Carla Luciani, and Laleh Emdadi. My time in this lab was made much more enjoyable thanks to them.

There were many individuals who gave me valuable technical assistance for this project. I would like to thank Dr. Yiu-Fai Lam from the Analytical NMR Service & Research Center, Dr. Kwang Ho Song (Korea University) and Dr. Yun Gyong Ahn (Korea Basic Science Institute, Seoul, Korea) for pyrolysis-GC/MS, Wonseok Hwang (AFM, DMA), Hyuntaek Oh (rheological analysis, Prof. Raghavan's laboratory) and Dr. Xin Zhang (spin coating, Prof. Briber's laboratory).

All of this would not have been possible without the loving support from my wife, Yungkyung Han, and my son, Brandon Baick. Finally, I would like to thank my family, my

parents Seungyong Baick and Hunyoung Lee, my sister and her husband Junhee Baick and Seho Yang.

Table of Contents

Chapter1: Introduction.....	1
1.1 Background	1
1.1.1 Bisphenol A Polycarbonate	1
1.2 Synthesis of Bisphenol A Polycarbonate	5
1.2.1 Interfacial Phosgenation Process	5
1.2.2 Melt Polymerization Process	7
1.2.3 Solid-State Polymerization Process.....	9
1.2.4 Ring-Opening Polymerization Process.....	11
1.3 Branched and Cross-linked Polycarbonate	12
1.3.1 Branched Polycarbonate	12
1.3.1 Cross-linked Polycarbonate	15
1.4 Research Objectives	16
Chapter2: Solid-State Polymerization of Bisphenol A Polycarbonate in Micro-Layers: Experimental Study.....	18
2.1 Introduction	18
2.2 Experimental	23
2.2.1 Materials	23
2.2.2 Preparation of Low Molecular Weight Precursor Polymers	23
2.2.3 Preparation of Amorphous, Crystalline Micro-Layers and Crystalline Micro-Particles	26
2.3 Results and Discussion.....	31
2.3.1 Solid State Polymerization in Micro-Layers and Micro-Particles.....	31
2.3.2 SSP Theoretical Model Prediction	42
2.3.3 Effect of End-Group Ratio	47
2.3.4 Effect of Amorphous Micro-Layer Thickness.....	50
2.3.5 Effect of Reaction Temperature	52
2.4 Conclusions	56

Chapter3: Reaction Mechanisms for SSP _m in an Amorphous Polymer Micro-Layers	58
3.1 Introduction	58
3.2 Experimental	60
3.2.1 Characterizations	60
3.3 Results and Discussion.....	61
3.3.1 ¹³ C-NMR Analysis	61
3.3.2 ¹ H-NMR Analysis.....	63
3.3.3 Pyrolysis-Gas Chromatography Mass Spectrometry (Py-GC/MS)	73
3.3.5 Atomic Force Microscopy (AFM) Analysis.....	91
3.4 Conclusions	95
Chapter4: Formation of Insoluble Amorphous Polycarbonate Synthesized in Micro-Layers	98
4.1 Introduction	98
4.2 Experimental	102
4.2.1 Materials	102
4.2.2 Characterization.....	103
4.3 Results and Discussion.....	104
4.3.1 Formation of Insoluble Polycarbonate in Amorphous Micro-Layers	104
4.3.2 Effect of Layer Thickness.....	118
4.3.3 Effect of Reaction Temperature and formation of Insoluble SSP _m PCs.	123
4.3.4 Effect of radical inhibitor on the molecular weight and insoluble fraction of PC.....	126
4.3.5 Multi-Layer Deposit & Reaction (MLDR).....	128
4.4 Conclusions	133
Chapter5: Thermal, Mechanical and Rheological Properties and Crystalline morphology of SSP _m PCs.....	134
5.1 Introduction	134
5.2 Experimental	136
5.2.1 Sample Preparation.....	136
5.2.2 Characterizations	137
5.3 Results and Discussion.....	139
5.3.1 Differential Scanning Calorimetry (DSC)	139

5.3.2 Dynamic Mechanical Analysis (DMA).....	141
5.3.4 Rheological Properties.....	149
5.3.5 Crystalline Morphology of SSP _m PCs.....	156
5.4 Conclusions.....	161
Chapter6: Summary and significance.....	163
Bibliography.....	167

List of Tables

Table 1.1 Physical and mechanical properties of bisphenol A polycarbonate in comparison with general purpose polystyrene (PS) and poly(methyl methacrylate) [5, 6].	3
Table 1.2 Catalyst activity of alkaline and alkaline-earth metals (2.16×10^{-7} mol/mL) in melt polycondensation process at 165°C [15].....	8
Table 2.1 Reaction conditions and molecular weights in solid state polymerization of BPAPC.	22
Table 2.2 Properties of PC prepolymers.	26
Table 2.3 Preparation of micro-layer in different thickness.....	29
Table 3.1 Mole fraction of cross-linkage and generation of insoluble fraction in amorphous micro-layers (10µm) at 230°C ($P=10$ mmHg, prepolymer B-14k).	71
Table 3.2 Ratio of methyl protons to aromatic protons in polycarbonates in partially crystallized micro-layers (10µm-crystalline) and amorphous micro-layers (10µm-amorphous) at 230°C ($P=10$ mmHg, prepolymer B-14k).....	73
Table 3.3 Model simulated phenol concentration profiles ($T=230^\circ\text{C}$, prepolymer B-14k) depending on micro-layer thickness and state (crystalline or amorphous) and generation of insoluble fraction.	83
Table 4.1 Formation of insoluble fraction at high temperature [40].....	99
Table 4.2 Experiment results of different micro-layer thickness (54 nm-20µm) at 180 min. ...	121
Table 5.1 Sample weight average molecular weight of soluble PCs, insoluble fraction (mass fraction), polydispersity, and mole fraction of cross-linkage with the reaction time for 10 µm-thick amorphous micro-layers (Precursor weight average molecular weight=14k g/mol, $P= 10$ mmHg, $T=230^\circ\text{C}$).	136

List of Figures

Figure 1.1 The major properties and applications of bisphenol A polycarbonate (BPAPC) (images were taken from google image).....	2
Figure 1.2 Bisphenol A (BPA) and diphenyl carbonate (DPC): structures and properties.	4
Figure 1.3 The two stage polymerization of phosgenation process.	6
Figure 1.4 Schematic description of Ring-Opening Polymerization of cyclic aromatic oligomeric carbonates.	12
Figure 1.5 Chemical structures of trifunctional branching agents [8].	13
Figure 1.6 Structure of resulting products by “Fries Rearrangement Reaction”.	14
Figure 2.1 Schematic diagrams illustrating a conventional SSP in partially crystallized prepolymer particles and the novel SSP _m in amorphous prepolymer micro-layers.....	21
Figure 2.2 Reaction mechanism of conventional linear step-growth polymerization of bisphenol A polycarbonate.	24
Figure 2.3 Prepolymer reactor system schematic.	25
Figure 2.4 Schematic description of amorphous precursor micro-layer sample preparation and SSP _m process of polycarbonate.....	28
Figure 2.5 Spherulitic morphology of solvent (acetone) induced crystalline PC micro-layers...	30
Figure 2.6 Weight-average molecular weight vs. reaction time profiles ($T=230^{\circ}\text{C}$, $P=10\text{ mmHg}$, prepolymer B-14k): (a) (◆) SSP _m (10μm layer, amorphous); (▲) SSP _m (10μm layer, crystalline). Solid and dashed lines represent the numerical simulations for the crystallized micro-layer (10μm-thick) and amorphous micro-layer (10μm-thick), respectively; (b) (●) SSP _p (10μm radius particles, crystalline); (■) SSP _p (350μm radius particles, crystalline). Solid lines represent the numerical simulations.	32
Figure 2.7 SEM images of partially crystallized particles having average radius of 10μm.	35
Figure 2.8 Size distribution of partially crystallized particles of 10μm-radius.	36
Figure 2.9 Partially crystallized particles of 350μm-radius (typical particle size in SSP): a) size distribution of crystalline particles, b) surface morphology of 350μm-radius particles.....	37

Figure 2.10 Polycarbonate crystalline micro-layers undergoing solid-state polymerization (SSP_m) ($T=230\text{ }^\circ\text{C}$, $P=10\text{ mmHg}$, prepolymer B-14k, $10\mu\text{m}$ -thick partially crystallized micro-layer). ... 37

Figure 2.11 Molecular weight distributions (MWD) of micro-layer and particle samples ($T=230\text{ }^\circ\text{C}$, $P=10\text{ mmHg}$, prepolymer B-14k) at 180 min: a, $10\mu\text{m}$ amorphous micro-layer; b, $10\mu\text{m}$ crystalline micro-layer (acetone induced crystallization); c, $10\mu\text{m}$ -radius crystalline particles. 38

Figure 2.12 Polydispersity of polymers vs. reaction time profile ($T=230\text{ }^\circ\text{C}$, $P=10\text{ mmHg}$, prepolymer B-14k): (\blacklozenge) SSP_m ($10\mu\text{m}$ layer-amorphous); (\blacktriangle) SSP_m ($10\mu\text{m}$ layer-crystalline); (\bullet) SSP ($10\mu\text{m}$ radius particles-crystalline). 39

Figure 2.13 (a) Evolution of the PC weight-average molecular weight with the reaction time using Sample A and D at $200\text{ }^\circ\text{C}$: (\bullet) Conventional SSP with pre-crystallized particles of about $100\text{ }\mu\text{m}$ in size (Sample A). (\blacksquare and \blacktriangle) SSP_m in amorphous polymer micro-layers of $10\text{ }\mu\text{m}$ -thickness (Sample A and D respectively). Lines represent the numerical simulations for different end-group ratios of the prepolymer sample (r_a'); (b) GPC chromatograms for high molecular weight samples collected at different reaction times in SSP_m 41

Figure 2.14 Effect of prepolymer end-group ratio on the evolution of weight-average MW in amorphous polymer micro-layers of $10\text{ }\mu\text{m}$ thickness ($T=230\text{ }^\circ\text{C}$, $P=10\text{ mmHg}$): amorphous micro-layer (solid line) and crystallized micro-layer (dashed line). Lines were added to guide the eyes only. 49

Figure 2.15 Effect of the amorphous micro-layer thickness on the evolution of the polymer molecular weight with the reaction time ($T=230\text{ }^\circ\text{C}$, $P=10\text{ mmHg}$, Prepolymer B-14k). Lines were added to guide the eyes only. 51

Figure 2.16 Maximum polymer molecular weight vs. micro-layer thickness after 180 min reaction time in amorphous polymer micro-layer (SSP_m) (prepolymer B-14k, δ =micro-layer thickness). 52

Figure 2.17 Effect of temperature on the evolution of the PC weight-average molecular weight with the reaction time ($P=10\text{ mmHg}$, micro-layer thickness= $10\text{ }\mu\text{m}$): (a) prepolymer A-8k; (\bullet) $168\text{ }^\circ\text{C}$; (\blacktriangle) $183\text{ }^\circ\text{C}$; (\blacksquare) $200\text{ }^\circ\text{C}$; (\blacklozenge) $223\text{ }^\circ\text{C}$; (\blacktriangledown) $237\text{ }^\circ\text{C}$; (b) prepolymer B-14k; (\blacktriangle) $235\text{ }^\circ\text{C}$; (\bullet) $230\text{ }^\circ\text{C}$; (\blacklozenge) $220\text{ }^\circ\text{C}$; (\blacksquare) $200\text{ }^\circ\text{C}$ 54

Figure 2.18 Morphology of crystallized polycarbonate prepolymers: (a1) surface of micro-layer (10 μ m-thickness), (b1) surface of bulk crystallized particles (10 μ m-radius), (a2) surface of micro-layer (10 μ m-thickness) after 2 hr reaction at 235 $^{\circ}$ C, (b2) surface of bulk particles (10 μ m-radius) after 2 hr reaction at 235 $^{\circ}$ C (Prepolymer: sample B-14k).	55
Figure 3.1 13 C NMR spectroscopic analysis of the SSP _m samples at different reaction times ($T=230$ $^{\circ}$ C, layer thickness=10 μ m, prepolymer B-14k).	62
Figure 3.2 Weight-average molecular weight vs. reaction time profiles ($T=230^{\circ}$ C, $P=10$ mmHg, prepolymer B-14k): (\blacklozenge) SSP _m (10 μ m layer, amorphous); (\blacktriangle) SSP _m (10 μ m layer, crystalline). Solid line is added to guide the eyes.	63
Figure 3.3 1 H NMR spectroscopic analysis of the amorphous micro-layer ($T=230$ $^{\circ}$ C, layer thickness=10 μ m, prepolymer B-14k). Arom. indicates aromatic protons.....	65
Figure 3.4 Kolbe-Schmitt and Fries rearrangement reactions leading to branched structures in polycarbonates [37, 40].....	66
Figure 3.5 Reaction mechanisms for the formation of cross-linked polycarbonates: R \bullet represents a macro-radical species generated in the system [40].....	67
Figure 3.6 Expanded methyl group on repeating unit and phenolic groups and ethyl group on cross-linkage region of two-dimensional (2D) heteronuclear single quantum coherence (HSQC) (2D 1 H- 13 C one bond) spectrum of SSP _m PC (30min at 230 $^{\circ}$ C).....	69
Figure 3.7 Expanded aromatic region of two-dimensional (2D) heteronuclear single quantum coherence (HSQC) (2D 1 H- 13 C one bond) spectrum of SSP _m PC (30min at 230 $^{\circ}$ C).	70
Figure 3.8 Pyrograms of prepolymer (B-14k) and amorphous micro-layer sample taken at 30 min in presence of TMAH.	74
Figure 3.9 Mass spectrum of peak 1. Peak 1 generated via reactive pyrolysis from structure A and B at 600 $^{\circ}$ C.	78
Figure 3.10 Mass spectrum of peak 2. Peak 2 generated via reactive pyrolysis from structure E at 600 $^{\circ}$ C.	79
Figure 3.11 Mass spectrum of peak 3. Peak 3 generated via reactive pyrolysis from structure C at 600 $^{\circ}$ C.	80

Figure 3.12 Mass spectrum of peak 4. Peak 4 generated via reactive pyrolysis from structure D at 600°C.	81
Figure 3.13 Model simulated phenol concentration profiles ($T=230^{\circ}\text{C}$, prepolymer B-14k): Solid lines represent average phenol concentration in amorphous micro-layers (5-35 μm thick); dashed lines represent average phenol concentration in crystallized micro-layers (10 μm and 100 μm thick).	84
Figure 3.14 The GPC chromatograms for the residual solvent (chloroform) in prepolymer (14k) after 2hr drying and in SSP _m PCs at different reaction times. a) prepolymer, b) 15 min, c) 60 min, d) 120 min.	85
Figure 3.15 Evolution of weight average molecular weight with reaction time using three different types of casing solvents (chloroform, NMP, and benzene) ($T=230^{\circ}\text{C}$, prepolymer B-14k).	87
Figure 3.16 Polydispersity of amorphous micro-layers with three different type of casting solvents (chloroform, NMP, and benzene) and crystalline micro-layers with chloroform as a casting solvent ($T=230^{\circ}\text{C}$, prepolymer B-14k).	88
Figure 3.17 Evolution of weight average molecular weight with reaction time using two different types of casing solvents (chloroform and THF) ($T=230^{\circ}\text{C}$, prepolymer B-14k).	89
Figure 3.18 Effect of acetone on SSP _m for the crystalline micro-layers ($T=230^{\circ}\text{C}$, prepolymer B-14k).	90
Figure 3.19 AFM images of single polycarbonate molecules. The AFM samples were prepared using Langmuir-Blodgett technique.	91
Figure 3.20 Accelrys Materials Studio Visualizer® Software provide diameter of linear PC (0.97 nm) and length of polymer chain in 10 repeating unit (7.89 nm).	92
Figure 3.21 The SSP _m PC molecules on the mica surface. The height and phase images for the 60min (A1 and A2) and 180 min (B1 and B2) samples. The AFM samples were prepared using spin coating technique at 2000rpm.	94
Figure 3.22 Summary of kinetic mechanism for a SSP _m in an amorphous polymer micro-layers.	97
Figure 4.1 Reaction scheme of BPAPC in amorphous micro-layers.	101

Figure 4.2 Evolution of soluble PC weight average molecular weight (\blacktriangle) and emergence of insoluble fractions (\blacklozenge) with the reaction time for 10 μm -thick amorphous micro-layers (Precursor weight average molecular weight=14k g/mol, $P=10\text{ mmHg}$, $T=230^\circ\text{C}$). Lines are added to guide the eyes.	105
Figure 4.3 Increase of insoluble fraction of BPAPC in solvent (chloroform) as reaction time extend ($T=230\text{ }^\circ\text{C}$, $P=10\text{ mmHg}$, Prepolymer: 14K g/mol).....	107
Figure 4.4 SEM image of insoluble BPAPC with reaction time of 720 min ($T=230\text{ }^\circ\text{C}$, $P=10\text{ mmHg}$, Prepolymer: 14K g/mol).	108
Figure 4.5 AFM height images of insoluble gel fractions onto the soluble PCs. Increment of insoluble gel fractions with reaction extend.	110
Figure 4.6 Height difference measurement between insoluble gel and soluble PC surface for the 60min and 420min samples.	111
Figure 4.7 ^1H NMR spectroscopic analysis of the amorphous micro-layer: a) prepolymer (14k g/mol), b) soluble fraction of amorphous micro-layer at the reaction time of 960min ($T=230\text{ }^\circ\text{C}$, layer thickness=10 μm , prepolymer: 14k g/mol).....	112
Figure 4.8 Pyrogram of insoluble gel obtained at the reaction time of 960 min ($T=230\text{ }^\circ\text{C}$, layer thickness=10 μm , prepolymer: 14k g/mol).....	114
Figure 4.9 Images of stand-alone insoluble PC gel recovered from glass substrate ($T=230\text{ }^\circ\text{C}$, layer thickness=10 μm , prepolymer: 14k g/mol, amorphous micro-layer at 960 min).	115
Figure 4.10 UV-vis spectra of (a) prepolymer (B-14k) and (b-e) amorphous micro-layers with reaction time ($T=230\text{ }^\circ\text{C}$, $P=10\text{ mmHg}$, Prepolymer B-14k).....	117
Figure 4.11 UV-vis spectra of (a) prepolymer (B-14k) and (b-e) bulk PCs using melt process with reaction time ($T=290\text{ }^\circ\text{C}$, $P=10\text{ mmHg}$, Prepolymer B-14k).....	117
Figure 4.12 Effect of the amorphous micro-layer thickness on the evolution of the polymer molecular weight with the reaction time ($T=230\text{ }^\circ\text{C}$, $P=10\text{ mmHg}$, Prepolymer B-14k). Lines were added to guide the eyes only.	119
Figure 4.13 Formation of insoluble fraction in amorphous micro-layers depending on thickness ($T=230\text{ }^\circ\text{C}$, $P=10\text{ mmHg}$, Prepolymer B-14K). Lines were added to guide the eyes only.	120

Figure 4.14 Model simulation of phenol concentration depending on micro-layer thickness ($T=230\text{ }^{\circ}\text{C}$, $P=10\text{ mmHg}$, Prepolymer B-14K).....	122
Figure 4.15 Effect of reaction temperature on the evolution of weight average molecular weight of soluble fraction in amorphous polymer micro-layers of $10\text{ }\mu\text{m}$ thickness ($T=170\text{-}245\text{ }^{\circ}\text{C}$, $P=10\text{ mmHg}$, Prepolymer B-14K). Lines were added to guide the eyes only.	124
Figure 4.16 Generation of insoluble fraction of BPAPC in amorphous micro-layers of $10\mu\text{m}$ thickness at the reaction temperature above $230\text{ }^{\circ}\text{C}$. Lines were added to guide the eyes only..	125
Figure 4.17 Evolution of effect of free radical inhibitor on weight average molecular weight (A) and insoluble fraction (B) with reaction time at $230\text{ }^{\circ}\text{C}$ ($T=230\text{ }^{\circ}\text{C}$, $P=10\text{ mmHg}$, Prepolymer B-14K).	127
Figure 4.18 Schematic description of Micro-Layer Deposit Reaction (MLDR).	128
Figure 4.19 Evolution of molecular weight and formation of insoluble gel using MLDR method ($T=230\text{ }^{\circ}\text{C}$, $P=10\text{ mmHg}$, Prepolymer B-14K). Multi layers were deposited every 180 min interval. Solution concentration was set to $10\mu\text{m}$ thickness. Lines are added to guide the eyes.	129
Figure 4.20 Evolution of molecular weight using MLDR method ($T=230\text{ }^{\circ}\text{C}$, $P=10\text{ mmHg}$, Prepolymer B-14K). Multi layers were deposited at an interval of every 30 min . Solution concentration was set to $5\mu\text{m}$ (■), $10\text{ }\mu\text{m}$ (●), and $20\text{ }\mu\text{m}$ (▲) in thickness.	131
Figure 4.21 Polydispersity of polymers vs. reaction time profile. Multi layers were deposited every 30 min interval ($T=230\text{ }^{\circ}\text{C}$, $P=10\text{ mmHg}$, Prepolymer B-14K). Solution concentration was set to $5\mu\text{m}$ (■), $10\text{ }\mu\text{m}$ (●), and $20\text{ }\mu\text{m}$ (▲) in thickness.	132
Figure 5.1 Structure of benzocyclobutene-terminated bisphenol A polycarbonate (BCB PC) and cross-linked BCB PC.	135
Figure 5.2 DSC thermograms of prepolymer (B-14k), amorphous micro-layers with reaction time ($T=230\text{ }^{\circ}\text{C}$, $P=10\text{ mmHg}$).	140
Figure 5.3 Strain-stress curves of SSPm PCs with reaction time: (a) SSPM-30, (b) SSPM-60, (c) SSPM-180, (d) SSPM-420, and (e) SSPM-960.	142
Figure 5.4 SSP _m PCs storage modulus as a function of temperature at 1 Hz with initial strain at 0.5% and preload force at 0.01N . SSP _m PCs were obtained at reaction temperature of $230\text{ }^{\circ}\text{C}$ with	

10 μ m thickness micro-layers: PRE-0 (■), SSPM-30 (⊖), SSPM-60 (⊕), SSPM-180 (✕), SSPM-420 (-Δ-), and SSPM-960 (-◆-)	144
Figure 5.5 Behavior of storage modulus above the glass transition temperature (T_g) with different reaction time samples: PRE-0 (■), SSPM-30 (⊖), SSPM-60 (⊕), SSPM-180 (✕), SSPM-420 (-Δ-), and SSPM-960 (-◆-)	145
Figure 5.6 Loss tangent ($\tan \delta$) as a function of temperature at 1 Hz with initial strain at 0.5% and preload force at 0.01N. Peak positions are marked as: PRE-0 (■), SSPM-30 (⊖), SSPM-60 (⊕), SSPM-180 (✕), SSPM-420 (-Δ-), and SSPM-960 (-◆-)	147
Figure 5.7 Behavior of loss tangent ($\tan \delta$) above the glass transition temperature (T_g) with different reaction time samples: PRE-0 (■), SSPM-30 (○), SSPM-60 (◇), SSPM-180 (✕), SSPM-420 (Δ), and SSPM-960 (◆)	148
Figure 5.8 Dynamic viscosity of prepolymer and SSP _m PCs over a frequency range of 0.01-100 rad/s. SSP _m PC samples were prepared at 230°C with 10 μ m thickness: PRE-0 (■), SSPM-30 (◇), SSPM-60 (Δ), SSPM-180 (○), SSPM-420 (◆)	151
Figure 5.9 Shear storage modulus (G') of prepolymer and SSP _m PCs over a frequency range of 0.01-100 rad/s. SSP _m PC samples were prepared at 230°C with 10 μ m thickness: PRE-0 (■), SSPM-30 (◇), SSPM-60 (Δ), SSPM-180 (○), SSPM-420 (◆)	153
Figure 5.10 Shear storage modulus (G') of prepolymer and SSP _m PCs over a frequency range of 0.01-100 rad/s. SSP _m PC samples were prepared at 230°C with 10 μ m thickness: PRE-0 (■), SSPM-30 (◇), SSPM-60 (Δ), SSPM-180 (○), SSPM-420 (◆)	154
Figure 5.11 Loss tangent ($\tan \delta$) of prepolymer and SSP _m PCs over a frequency range of 0.01-100 rad/s. SSP _m PC samples were prepared at 230°C with 10 μ m thickness: PRE-0 (■), SSPM-30 (◇), SSPM-60 (Δ), SSPM-180 (○), SSPM-420 (◆)	155
Figure 5.12 Acetone induced crystallization of prepolymer and SSP _m PCs: (a) PRE-0, (b) SSPM-180, (c) SSPM-420, and (d) SSPM-960	157
Figure 5.13 Cross-sectional area of prepolymer and SSP _m PCs with reaction time extend	158
Figure 5.14 Surface morphology of SSPM-960 (about 95% insoluble) samples	159
Figure 5.15 The secondary crystallization at the top of the primary structure (sample SSPM-960)	160

Chapter1: Introduction

1.1 Background

1.1.1 Bisphenol A Polycarbonate

Linear step-growth polymerization (or polycondensation) is a polymerization technique in which bi-functional single monomers (A-B type) or two monomers (A-A, B-B types) react first to produce long chain polymers with low molecular weight polycondensation byproducts. Bisphenol A polycarbonate (BPAPC), poly(L-lactic acid) (PLLA), polyethylene terephthalate (PET), polyamide, and polyurethane are the most well-known industrial condensation polymers. Molecular weight (MW), molecular weight distribution (MWD), and chain structures (*i.e.*, branching and cross-linking) are the important parameters that impact the polymer's physical, mechanical, and rheological properties. Among these polymers, bisphenol A polycarbonate (BPAPC) is an important material in many applications such as automotives, electronic displays, data storage, medical, environmental, energy, and aerospace industries [1]. Figure 1.1 shows major properties and applications of bisphenol A polycarbonate [2]. The high glass transition temperature ($\sim 150^{\circ}\text{C}$), optical clarity (88-96 % light transmission of visible light), and exceptional impact resistance are the major merits of polycarbonates [2, 3]. PCs having MWs larger than 54,000 g/mol maintain its transparency even after 400 h of continuous exposure to high temperature environment (120°C) [4]. Table 1.1 illustrates physical and mechanical

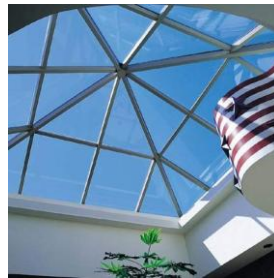
properties of two commercial BPAPC (Dow and General Electric) in comparison with general purpose polystyrene (PS) and poly(methyl methacrylate).

Characteristics of Amorphous Bisphenol A Polycarbonate

- High Glass Transition Temperature
- High Heat Resistance
- Excellent Optical Clarity
- Excellent Impact Resistance
- Dimensional Stability



Data Storage



Windows



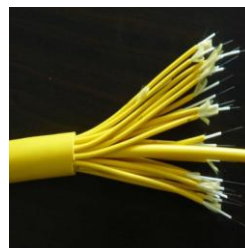
Automotives



Bullet Resistance Windows



Medical



Optical Fiber Core Material

Figure 1.1 The major properties and applications of bisphenol A polycarbonate (BPAPC) (images were taken from google image).

Table 1.1 Physical and mechanical properties of bisphenol A polycarbonate in comparison with general purpose polystyrene (PS) and poly(methyl methacrylate) [5, 6].

Property	unit	PC (Dow) ^a	PC (GE) ^b	PS	PMMA
Density	g/cm ³	1.20	1.20	1.05	1.2
Glass Transition Temperature	°C	147-150	147-150	100	105
Tensile strength	kpsi	9.8	9.0	6.4-8.2	10
Elongation	%	150	110	2-4	5
Flexible strength	kpsi	14.0	13.5	10	11
Notched Izod impact	ft-lb/in	14.0	12-16	0.4	0.3
Transmission (visible)	%	89	88-91	87	90

^aDow plastics grade, CALIBRE™ MEGARD™ 2081-15

^bGE plastics grade, Lexan 9034

For commercial applications, standard injection-molding grade PCs have molecular weights (M_w) of 35,000-70,000 g/mol. For instance, molecular weight PC of about 30,000 g/mol can be used as optical fiber core material for solid-state emitters and detectors with lower infrared absorption and higher heat resistance compared to those made of poly(methyl methacrylate) or polystyrene [5, 6]. Molecular weight PCs of 30,000-40,000 g/mol are widely used for CDs and DVDs. High transparency is also an important attribute required for the lamination of high molecular weight PC (~50,000-100,000 g/mol) with polyvinyl butyral in film applications such as automotive vehicles, building windows, skylights, retail (jewelry) casings and bullet-resistant windows [4]. Flow, physical, and mechanical properties of polymers depend not only on molecular weight and molecular weight distribution but also on its molecular structures [7]. For instance, while high molecular weight, linear PCs are not easy to melt process, long-chain branched PCs are relatively easier to process [8]. In recent years, branched and cross-linked PCs came into the spotlight in academia and in the industry due to their unique end use

properties. Crosslinkable PCs have found new uses as a binder in photoconductor applications and as an optical component in multilayer structures [9, 10].

The polycarbonate was discovered at Bayer (Germany) by Dr. Hermann Schnell and General Electric Company (USA) by Daniel Fox in 1953. About 75% of the polycarbonate market is held by “Lexan” and “Makrolon” polycarbonates which are produced by General Electric and Bayer, respectively [11]. While polycarbonates can be produced by a variety of polyfunctional hydroxy compounds, the most practical and commercially significant polycarbonate is derived from diphenyl compound and 4,4-dihydroxy-diphenyl-2,2-propane (Bisphenol A). Figure 1.2 shows the structures and properties of two monomers, bisphenol A (BPA) and diphenyl carbonate (DPC), used in the melt step-growth polymerization process to produce bisphenol A polycarbonate [12].

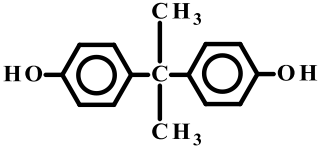
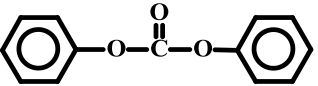
	T_m	Vapor Pressure (25°C)
 <p>Bisphenol A</p>	158°C	4×10^{-8} mmHg
 <p>Diphenyl Carbonate</p>	83°C	4×10^{-4} mmHg

Figure 1.2 Bisphenol A (BPA) and diphenyl carbonate (DPC): structures and properties.

1.2 Synthesis of Bisphenol A Polycarbonate

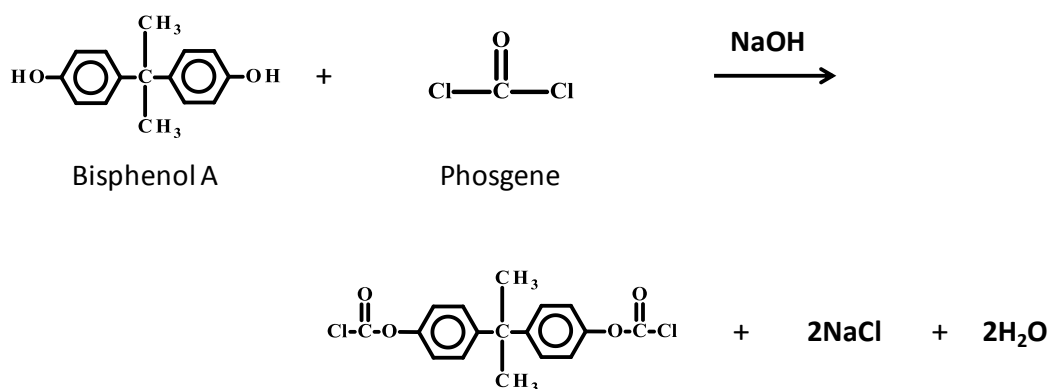
Several step-growth polymerization methods are used in industrial PC processes: interfacial phosgenation, direct melt polycondensation, and solid-state polymerization. In what follows, these processes are briefly discussed.

1.2.1 Interfacial Phosgenation Process

In the interfacial phosgenation process, gaseous phosgene is supplied to a two-phase liquid mixture of a methylene chloride-rich phase and an aqueous phase containing bisphenol A (BPA), sodium hydroxide, and a catalyst (triethylamine) [2, 13]. The interfacial phosgenation process is illustrated in Figure 1.3. In the aqueous phase, BPA reacts with NaOH to produce disodium Bisphenate, which in turn is available to react with phosgene, initiating the interfacial polymerization process. The intermediate species (BPA bis(chloroformate)) produced from this reaction is transported from the aqueous phase to the organic phase, due to its poor solubility in the aqueous phase, where polycondensation occurs, creating high molecular weight BPAPC. The molecular weight of the polymer is controlled in this process by the addition of a mono-functional chain stopper such as para-tertiary butyl phenol. Although the interfacial phosgenation process is an effective method to synthesize injection molding grade molecular weight BPAPCs (M_w up to 15,000-150,000 g/mol), it requires handling of a hazardous reactant (phosgene), and the treatment of a large amount of chlorinated solvent (e.g., methylene chloride) [14]. The complete removal of methylene chloride is impossible due to its strong affinity to polycarbonate

and it needs a massive amount of energy. As increase in demand of environmental friendly materials, the use of phosgene and chlorinated solvent become difficult.

(a) Phosgenation



(b) Polycondensation

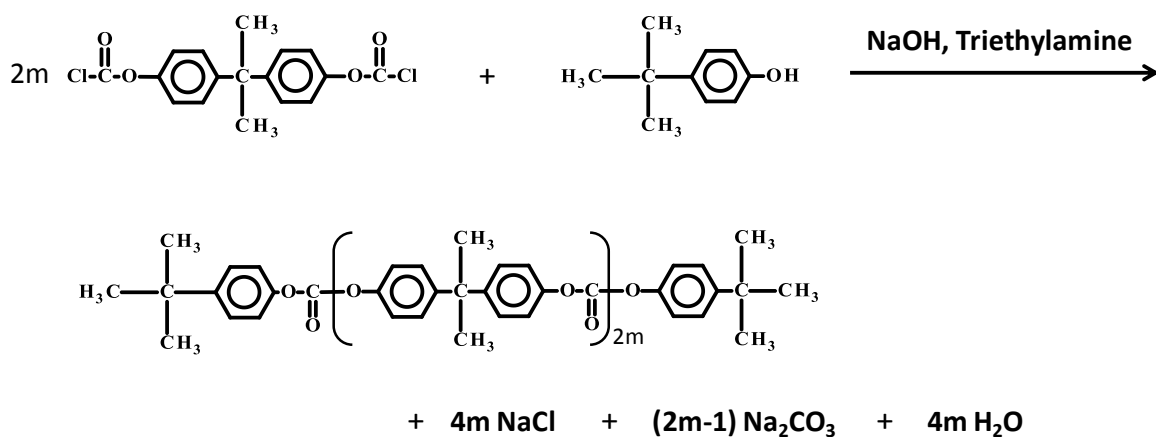


Figure 1.3 The two stage polymerization of phosgenation process.

1.2.2 Melt Polymerization Process

In the melt polycondensation process, bisphenol A (BPA) and diphenyl carbonate (DPC) monomers are reacted reversibly in either semibatch or continuous reactors under vacuum above the polymer melting temperature ($T_m \sim 260^\circ\text{C}$) in the presence of a catalyst such as lithium hydroxide monohydrate ($\text{LiOH}\cdot\text{H}_2\text{O}$). The list of possible catalysts used in the melt polycondensation process and catalyst activities are shown in Table 1.2 [15]. In the melt transesterification of BPA and DPC, alkaline and alkaline-earth metal compounds have confirmed higher catalyst activities compared to metal compounds. The byproduct of the reversible reaction is phenol. To drive the reaction to obtain high molecular weight polymer, phenol must be removed effectively from the high viscosity polymer mixture by applying low pressure (~ 0.1 mmHg) or using an inert purge gas. High reaction temperatures, long reaction times (4-5 h), and ineffective removal of phenol often lead to unwanted side reactions, causing discoloration of the final product [12, 16, 17]. If the reaction time is extended at high reaction temperatures to increase molecular weight, discoloration and gel formation may result [18-21]. Although the amount of such reaction products might be very small, their impact on the polymer quality is quite detrimental. One of the drawbacks of the melt BPAPC process is that obtaining molecular weights higher than 30,000 g/mol is difficult because very high viscosity of polycarbonate melt (e.g., 8,000-20,000 poise at 280°C) makes the removal of phenol very difficult [22]. For example, molecular weight of 30,000 g/mol of polycarbonate shows a melt viscosity of 5,000-500,000 poise at temperatures of 315°C and 245°C while poly(ethylene terephthalate) has 2,000 poise at 285°C with similar molecular weight [23].

Table 1.2 Catalyst activity of alkaline and alkaline-earth metals (2.16×10^{-7} mol/mL) in melt polycondensation process at 165°C [15].

Compound	$\frac{k}{10^{-6} \text{ mL}^2/\text{mol}^2 \text{ min}}$
(1) alkaline and alkaline-earth metals:	
LiOH	55.5
LiOH·H ₂ O	20.0
Potassium Hydrogenisophthalate	19.0
Ca(acac) ₂	56.0
Sr(acac) ₂	160.0
Ba(acac) ₂	390.0
(2) metal compounds:	
Ti(OBu) ₄	1.6
Zr(acac) ₄	1.3
Hf(acac) ₄	0.6
Mn(ac) ₂	0.3
Mn(acac) ₂	6.9
Fe(acac) ₂	2.4
Co(acac) ₂	0.3
Pd(acac) ₂	0.2

1.2.3 Solid-State Polymerization Process

Solid-state polymerization (SSP) is an alternative phosgene-free, post-direct melt polycondensation process that can be combined with a melt transesterification process to produce injection molding grade, high molecular weight PC. SSP is successfully used to industrially manufacture high molecular weight poly(ethylene terephthalate) (PET). SSP for polycarbonate has also been commercialized [22, 24]. In conventional SSP, semicrystalline low molecular weight prepolymer particles are first prepared by melt polycondensation and then polymerized in solid state using particle form to further increase the polymer molecular weight at a reaction temperature (*e.g.*, 210-220 °C) that is above the polymer's glass transition temperature ($T_g \sim 150$ °C) but quite below its melting point ($T_m \sim 260$ °C). In particular, it has been known that partial crystallization of low molecular weight BPAPC prepolymer is critical to carry out high conversion SSP processes. Amorphous BPAPC prepolymer can be partially crystallized by heat treatment at its crystallization temperature or by dissolving it in a solvent and precipitating/crystallizing it with a non-solvent such as acetone in a spray tower. There are also some reports on the solid state polymerization of BPAPC with supercritical CO₂ as a sweep fluid. The employment of low reaction temperature in SSP is advantageous over a higher temperature melt polycondensation process in minimizing the side reactions and discoloration. In order to obtain relatively high molecular weights ($M_w = 25,000-60,000$ g/mol) in a reasonable reaction time, the following conditions are required [25-30]:

- (i) Small prepolymer particles (several hundred microns) to minimize the diffusional resistance of byproduct (phenol).

- (ii) End group ratios close to the stoichiometric value (1.0).
- (iii) High reaction temperatures to reduce the system viscosity.
- (iv) High vacuum levels to induce an effective removal of phenol.
- (v) For the SSP of PC, crystallizing prepolymer is critical because the crystalline portions serve as a supporting frame to prevent the polymer particles from fusing.

The reaction temperature should also be properly controlled. If the reaction temperature is too close to the polymer melting point, the particles fuse together, thus reducing the reaction rate and making the operation of a continuous SSP reactor (*e.g.*, moving packed bed reactor) very difficult or even impossible [28, 30]. It is also to be noted that the molecular weights of PC produced by SSP are generally lower compared to those produced by interfacial polymerization. In either a high vacuum or an inert gas purging process of SSP to remove phenol from the polymer particles, the intra-particle phenol diffusion is frequently a rate controlling process. To obtain high molecular weight, the phenyl carbonate ($[-\text{OCO}-\text{C}_6\text{H}_5]$) to hydroxyl end group ($[-\text{OH}]$) ratio in the prepolymers for SSP should be close to the stoichiometric ratio but quite often, the end group ratio deviates from that target because of the loss of volatile reactants (DPC) during the prepolymerization stage (see figure 1.2) [31-33]. When large BPAPC prepolymer particles (*e.g.*, several hundred micrometer to a few millimeter) are used in SSP, there can be three possible rate determining processes:

- (i) Chemical reaction (chain growth reaction).
- (ii) Intra-particle diffusion of condensation byproduct (phenol).
- (iii) Mass transfer of phenol from the particle surface to the purge gas phase.

When a sufficiently high inert gas flow rate or low pressure is employed for the removal of phenol, the boundary layer mass transfer resistance at the particle surface becomes generally very small.

1.2.4 Ring-Opening Polymerization Process

Another method to prepare high molecular weight PC is a ring-opening polymerization (ROP). First, BPA bis(chloroformate) can be obtained from BPA in the presence of phosgene gas at low temperatures. Next, PC is obtained using ROP of cyclic aromatic oligomeric carbonates via an amine-catalyzed hydrolysis/condensation reaction of BPA bis(chloroformate) [34-36]. Figure 1.4 illustrates the schematic description of Ring-Opening Polymerization of cyclic aromatic oligomeric carbonates. Although the high molecular weight of polycarbonate can be obtainable without the generation of volatile byproducts, the ring-opening polymerization has been limited due to nonselective procedures for preparation of cyclic carbonates, low-yielding and high melting point ($\sim 350^{\circ}\text{C}$) of cyclic oligomers.

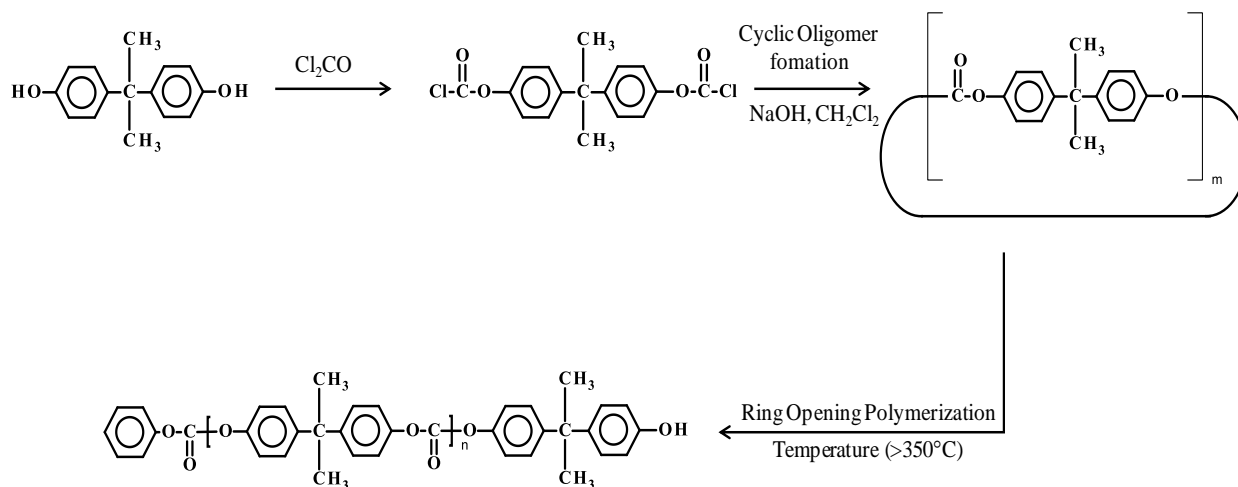


Figure 1.4 Schematic description of Ring-Opening Polymerization of cyclic aromatic oligomeric carbonates.

1.3 Branched and Cross-linked Polycarbonate

1.3.1 Branched Polycarbonate

A branched polycarbonates can be produced either by using several type of trifunctional branching agents resulting in degree of branching of about 0.5 (mol %) or by thermal rearrangement reactions at high melt polymerization temperature in the absence of branching agents [8, 37]. Figure 1.5 shows three different branching agents commonly used in melt processes [8].

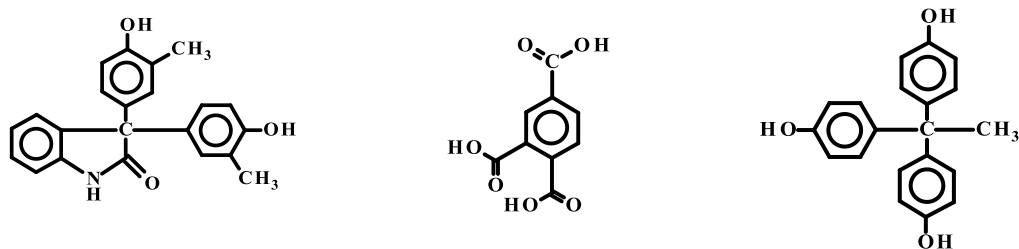
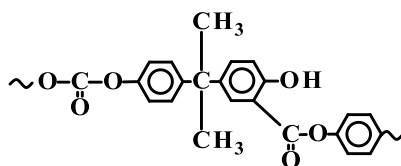


Figure 1.5 Chemical structures of trifunctional branching agents [8].

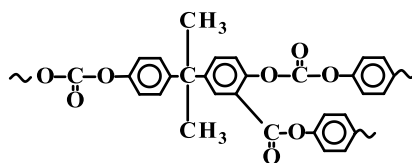
In the melt process, it is reported that the addition of alkali metal and alkaline compounds without trifunctional branching agents in the reaction mixture induces not only linear polycarbonate but also branched polymer by thermal rearrangement reaction known as “Fries Rearrangement Reaction” [38]. Structure of linear Fries product and branched Fries product are illustrated in Figure 1.6. Average number of branching units per chain of 0.017-0.434 is reported in the case of melt-polymerized BPAPC by thermal rearrangement reactions [37]. Depending on the chain length and structure, branched polymers are sorted into short-chain or long-chain branched polymer categories. Long-chain branch polymer is defined as having higher values of weight average molecular weight per arm (M_w/arm) than the critical molecular weight for entanglements, M_c (e.g., 4000-4800 g/mol). The molecular weight per arm (M_w/arm) can be defined as follows [39]:

$$M_w / arm = \frac{\sum_{i=1}^{N_{max}} (M_{w,i} / (2i + 1)) \times w_i}{\sum_{i=1}^{N_{max}} w_i} \quad (1.1)$$

Where, i is the number of branching per molecule, $M_{w,i}$ is M_w of molecules with i branches per chain, and w_i is weight fraction of i branching per molecule. Number of repeating units of commercially available long-chain branched BPAPC was estimated at about 39. Rheological properties and crystallization behavior of polycarbonate depend on its molecular structure as well as molecular weight. For instance, high molecular linear PCs are not easy to melt process. However, long-chain branched PCs are relatively easier. The higher mobility of polymer chains in long-chain branched polycarbonate compared to linear polycarbonate was reported using dielectric relaxation analysis [7]. Greater melt elasticity and shear rate sensitivity were observed while mechanical properties were not changed much at wide range of compositions (0-100 wt% of branched BPAPC) of linear and branched BPAPC blend in commercially available long-chain branched polycarbonate [7].



Linear Fries Product



Branched Fries Product

Figure 1.6 Structure of resulting products by “Fries Rearrangement Reaction”.

1.3.1 Cross-linked Polycarbonate

In the melt polycondensation process, it is also reported that cross-linking reaction occurs under high vacuum systems at high reaction temperature ranges (300-500°C) which is above the polycarbonate melting temperature and higher than temperatures typically applied in melt processes [18, 20]. At these higher temperature ranges, competitive reaction of chain scission and cross-linking is observed and when the volatile product, phenol, is effectively removed from the system, the cross-linked polymer fraction is pronounced to form an insoluble gel. Because of severe discoloration of the gel and its insoluble nature, most research work on the mechanism studies of insoluble formation is speculated. Structure of insoluble PCs were investigated using NMR, IR and GC-MS in the past [40-42] but recently pyrolysis-gas chromatography (Py-GC) in the presence of organic alkali has been reported as the most effective method for the characterization of cross-linked polycarbonates [40]. Several hypotheses of the mechanisms for the formation of insoluble fractions have been reported as follows:

- (i) The first involves the thermal rearrangement of the carboxyl group into a pendant carboxyl group, which undergoes further esterification leading to cross linking reactions.
- (ii) The second is the hydrogen abstraction from methyl and aromatic protons which generates radicals. Through radical recombination, the cross linking reaction occurs.

Recently, these two mechanisms have been confirmed via Py-GC/MS using reactive pyrolysis in the presence of tetramethyleammonium hydroxide (TMAH) which resulted in low molecular weight, decomposed products that are consistent with the proposed mechanisms [40].

1.4 Research Objectives

The research is concerned with the investigation of the solid-state polymerization in micro-layers (SSP_m) where ultra-high molecular weight PCs is produced in short reaction time. It is also the objective of study to characterize the nonlinear molecular structure of PCs that are formed at long reaction times.

The current research is aimed at developing a fundamental understanding of underlying chemical and physical principles of SSP_m process through experimentation and theoretical studies. In this research, the following reaction conditions are used:

- (i) Reaction is carried out in two-dimensionally confined reaction space in which high surface/ volume ratio promote faster removal of byproduct. The thickness of micro-layers can be range of 1-100 μm , although it has been found that 5-35 μm thickness was the most effective.
- (ii) Precursor PCs are amorphous. Pre-crystallization of precursors is not required in SSP_m process.

- (iii) Reaction temperature is very close to the polymer's melting point (T_m) but higher than its glass transition temperature (T_g) under the reduced pressure (~ 10 torr).

The major research objectives in the thesis are summarized as follows:

- 1) To investigate the phenomenological aspects of solid-state polymerization in micro-layers under various reaction conditions;
- 2) To develop an understanding of the reaction mechanism for the formation of high molecular weight polycarbonates with nonlinear chain structures;
- 3) To investigate the physical and mechanical properties of the ultrahigh MW polycarbonates;
- 4) To develop a theoretical model to estimate the molecular weight, the molecular structures, and the concentration of byproduct in a micro-layer during the polymerization.

Chapter2: Solid-State Polymerization of Bisphenol A Polycarbonate in Micro-Layers: Experimental Study

2.1 Introduction

According to the literature, the molecular weight of BPAPC obtained in SSP processes is generally below 42,000 g/mol and the reaction time is longer than 15 hr when large polymer particles (~ 300 μm) are used [24, 30, 43]. Table 2.1 summarizes typical reaction conditions and molecular weight data for the solid state polymerization of polycarbonate reported in the literature. In the solid state polymerization within a single spherical particle, diffusion resistance for the transport of phenol (condensation byproduct) results in a non-uniform concentration gradient. The diffusion and reaction in a polycarbonate prepolymer particle under solid-state polymerization conditions have been studied by many researchers in the past. In our laboratory, a fundamental modeling of solid-state polymerization in a single particle has been studied by Dr. Yuesheng Ye [32, 44]. From the previous study of diffusion and reaction phenomena in our laboratory, the idea of isolating a thin layer of the outer region of a polymerizing particle was conceived. The preliminary experimental data showed surprisingly high molecular weight of polycarbonate when the solid-state polymerization was carried out in thin micro-layers at typical solid-state polymerization temperatures (180-200°C). It was very interesting that extremely high molecular weight polymer was obtained in very short reaction time (less than 1-2 h). Figure 2.1 illustrates schematically the intraparticle concentration gradient for phenol and the concept of

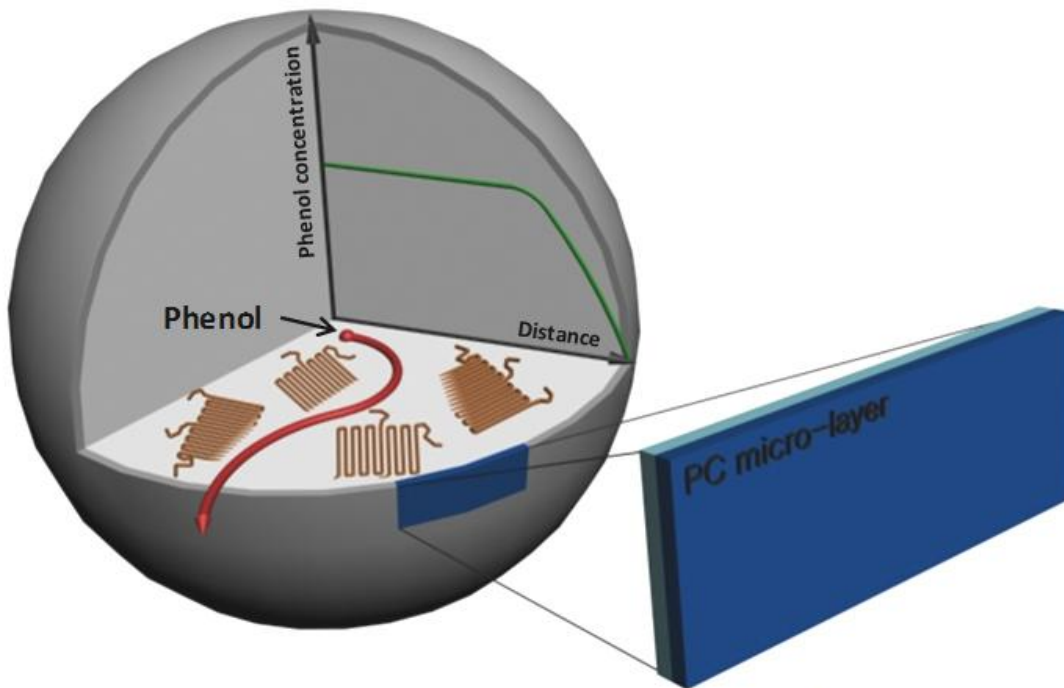
isolated particle ‘skin’ layer where maximum molecular weight is expected. A typical polycarbonate solid particle used in the traditional solid-state polymerization is semi-crystalline because otherwise, the amorphous polymer fraction easily fuses and the integrity of a polymerizing particle is lost. If that happens, the solid-state polymerization in a continuous flow reactor will be very difficult or impossible because the particles will agglomerate. Therefore, polycarbonate prepolymers are crystallized prior to solid-state polymerization to make the polymer particles fusion-resistance during the solid-state polymerization. The presence of a crystalline fraction in the particle has an effect of concentrating the end group concentrations as well as the catalyst in an amorphous phase. But it is also to be noted that the crystalline region poses a diffusion barrier for the removal of phenol.

Since the removal of phenol from the region close to the particle surface is much faster than from the center region of the particle, it is likely that a molecular weight non-uniformity may develop across the radial direction. The MW of the outer region is expected to have higher molecular weight because of a rapid removal of phenol but it will also hinder the removal of phenol diffusing out from the particle interior. Goodner et al. experimentally investigated the molecular weights of spherical particles at three different regions (*i.e.*, core, middle, and shell) and reported that the molecular weight in the shell region was about four times as high as that in the core region [43]. However, under their experimental conditions, the highest molecular weight at the particle surface region was only about 16,000 g/mol. In mathematical model simulation of SSP, Ye et al. [25] in our laboratory have also shown that the molecular weight of BPAPC at the external surface of the polymer particle can be much larger than the molecular weight in the particle core. Thus, the idea was to “isolate” the surface layer (PC micro-layer in Figure 2.1) that

would mimic the external surface region of the particles used in the conventional SSP in which diffusional resistance of byproduct is minimal.

In this thesis, we have exploited the idea of solid-state polymerization in micro-layers based on the preliminary study in the Polymer Reaction Engineering Laboratory at Maryland through experimentation. To distinguish our solid-state polymerization technique from the conventional solid-state polymerization in spherical particles, we shall call the SSP used in this work as SSP_m (solid state polymerization in micro-layers). As will be discussed later, the SSP_m of BPAPC shows quite interesting and unusual kinetic phenomena which deviate from linear step-growth polymerization kinetics. The dimension of the micro-layers employed in this study is far smaller than the dimension of polymer particles commonly used in typical solid-state polymerization studies reported in the literature.

Semi-Crystalline Particle



SSP_m in Amorphous Polymer Micro-Layer on the Glass Substrate

Figure 2.1 Schematic diagrams illustrating a conventional SSP in partially crystallized prepolymer particles and the novel SSP_m in amorphous prepolymer micro-layers.

Table 2.1 Reaction conditions and molecular weights in solid state polymerization of BPAPC.

Temperature (°C)	Pressure	Particle size (μm)	Reaction time (h)	Prepolymer MW (g/mol)	Final MW (g/mol)	Reference
190-220	2-5 mmHg	n.a.	14	6,200 (M _w)	28,000 (M _w)	[22]
220	N ₂ purge	180-230	50	3,300 (M _w)	18,000 (M _w)	[24]
			40	3,100 (M _w)	10,300 (M _w)	
230	0.07 mmHg	n.a.	16	9,700 (M _w)	41,500 (M _w)	[26]
180-230	N ₂ purge	3600	12	2,500 (M _w)	14,000 (M _w)	[43]
180	N ₂ purge	20	24	2,500 (M _w)	12,000 (M _w)	[27]
180-240			2,500 (M _w)	36,000 (M _w)		
120	in scCO ₂ (204 bar)	20	24	4,500 (M _w)	23,000 (M _w)	
165	N ₂ purge	75-125	10	4,300 (M _n)	15,000 (M _n)	[29]
120	in scCO ₂ (345 bar)	45-180	4	4,300 (M _n)	7,500 (M _n)	[28]
200	N ₂ purge or high vacuum	100	15	2.4 (scaled)	11.8 (scaled)	[25]
230	N ₂ purge	20-45	6	2,300 (M _n)	23,200 (M _n)	[45]
200	N ₂ purge or high vacuum	304	15	8,400 (M _w)	41,294 (M _w)	[30]
190	in scCO ₂ (207 bar)	20-45	10	3,800 (M _n)	16,000 (M _n)	[46]

2.2 Experimental

2.2.1 Materials

The chemical reagents including bisphenol A (BPA, 99.9%, Aldrich) and diphenyl carbonate (DPC, 99%, Aldrich) were recrystallized using methanol and water solution (1:1 v/v) and methanol, respectively. Lithium hydroxide monohydrate ($\text{LiOH}\cdot\text{H}_2\text{O}$, Aldrich) was used as received. The low molecular weight PC prepolymers were prepared by semi-batch melt polycondensation using BPA and DPC as monomers and $\text{LiOH}\cdot\text{H}_2\text{O}$ as a catalyst (1.75×10^{-4} M $[\text{LiOH}\cdot\text{H}_2\text{O}]/[\text{BPA}]$).

2.2.2 Preparation of Low Molecular Weight Precursor Polymers

For the polymerization of polycarbonate in micro-layers (SSP_m), low molecular weight precursor polymer (prepolymer) is needed. The precursor can be synthesized by conventional melt transesterification of diphenyl carbonate (DPC) and bisphenol A (BPA) with catalyst ($\text{LiOH}\cdot\text{H}_2\text{O}$). In our experiments, we used both industrially prepared prepolymers (LG Chemical Company) and our own prepolymer, which was prepared by same experimental procedure as described below. DPC and BPA have two phenyl carbonate ($[-\text{OCO}-\text{C}_6\text{H}_5]$) and hydroxyl ($[-\text{OH}]$) end groups at each end respectively so the reaction process is a typical -AA- , -BB- type polycondensation. Phenol, the byproduct of polycondensation reaction, should be removed from

the reactor using either vacuum or inert gas purging. The polymerization mechanism is shown below (Figure 2.2).

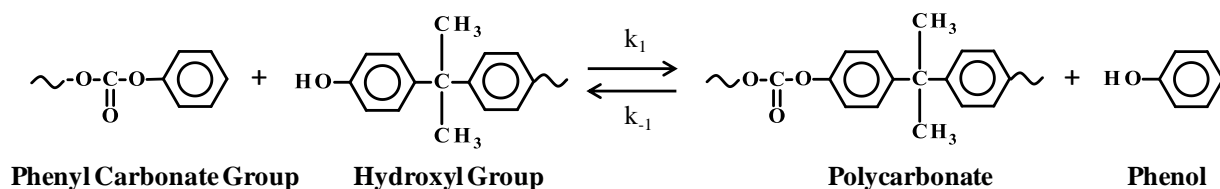


Figure 2.2 Reaction mechanism of conventional linear step-growth polymerization of bisphenol A polycarbonate.

Melt polycondensations were carried out by adding almost equimolar quantities of purified BPA and DPC and lithium hydroxide monohydrate ($\text{LiOH}\cdot\text{H}_2\text{O}$) was added at concentration of 1.75×10^{-4} M (catalyst/BPA mol) into a 500 ml glass reactor equipped with flux condenser temperature at 87°C on the top. A slight excess of DPC (1.06 DPC/BPA mol) was added to the reaction mixture to compensate the possible loss of DPC during the semi-batch reaction system [47]. The reaction mixture was agitated at 600 rpm and reaction temperature was gradually increased up to 250°C with nitrogen gas sweeping process (1090 ml/min). Figure 2.3 shows schematic description of melt polycondensation reactor system. The molecular weight and molecular weight distribution (MWD) of a prepolymer were measured by a gel permeation chromatography (GPC) system equipped with PLgel 10 μm MIXED-B columns (Polymer Laboratories) and a UV detector (Waters 484). HPLC grade chloroform was used as a mobile phase. The end group mole ratio in prepolymer (*i.e.*, phenyl carbonate ($[-\text{OCO-C}_6\text{H}_5]$) to hydroxyl groups) was determined by carbon nuclear magnetic resonance ($^{13}\text{C-NMR}$)

spectroscopy (Bruker DRX-500 spectrometer operating at 500 MHz using deuterated chloroform (CDCl_3) as a solvent). The ratios were obtained by comparing peak intensities of aromatic carbons on phenyl carbonate to aromatic carbons on phenolic groups (conducted by Dr. Yuesheng Ye). Table 2.2 shows the properties of four prepolymers achieved from direct melt polycondensation process used in this work. Samples A, B, and C were supplied by LG Chemical Company. These samples were produced by same procedure as described above. Sample D was prepared from our own reactor system with catalyst concentration of 1.0×10^{-4} M (catalyst/BPA mol) so slightly smaller concentration than that of sample A, B, and C (1.75×10^{-4} M (catalyst/BPA mol)).

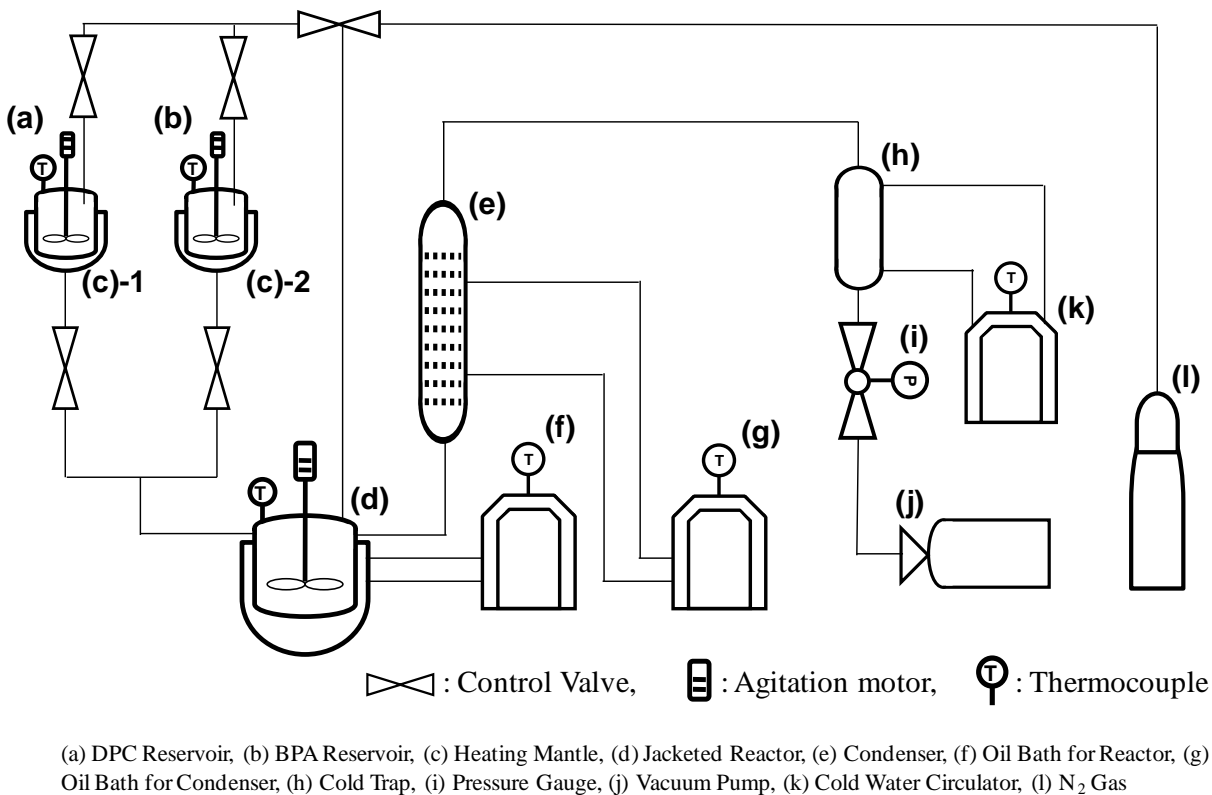


Figure 2.3 Prepolymer reactor system schematic.

Table 2.2 Properties of PC prepolymers.

Prepolymer	M_w (g/mol)	M_w/M_n	$r_a' = [-\text{OCO-C}_6\text{H}_5]/[-\text{OH}]$ (mol/mol)
A (8k)	8,300	1.95	0.66
B (14k)	14,000	1.97	0.80
C (21k)	21,000	2.00	0.90
D (8k)	8,400	1.90	N/A

2.2.3 Preparation of Amorphous, Crystalline Micro-Layers and Crystalline Micro-Particles

The following polymerization experiments were carried out: (i) polymerization in amorphous polymer micro-layers; (ii) polymerization in partially crystallized polymer micro-layers; (iii) conventional solid-state polymerization (SSP) of partially crystallized prepolymer particles for the purpose of comparison. Since the catalyst was not removed from the prepolymers, the catalyst content in each sample for the micro-layer polymerization was the same as the prepolymer produced from the melt polycondensation. Details of the sample preparation and polymerization procedures are described as follows.

2.2.3.1 Solid state polymerization in amorphous micro-layers (SSP_m)

Amorphous micro-layer polymer samples were prepared using a solvent casting technique. First, a predetermined amount of low molecular weight prepolymer sample (Table 2.2) was dissolved in a solvent (chloroform) at room temperature. Silica substrate ($2.5\text{cm} \times 7.5\text{cm}$) was cleaned with acetone for 10 min and then cleaned again with methanol for 5 min before rinsed with deionized water, and dried by nitrogen gas blow. The cleaned silica substrate was preheated and immersed in a bath of prepolymer solution and removed. The silica substrate coated with prepolymer was dried in a fume hood for 2h at ambient temperature and pressure. The coated prepolymer micro-layers prepared by this method were transparent and amorphous. The prepolymer micro-layers of different thickness ($5\text{-}35\mu\text{m}$) were obtained by varying the polymer concentration (e.g., 7.0 to 25.0 wt%) and the thickness measurement error was within $\pm 1.3 \mu\text{m}$ (see Table 2.3). The micro-layer thickness was measured by a Mitutoyo micrometer (Japan). When the micro-layer thickness was larger than $35\mu\text{m}$, partial crystallization occurred during the micro-layer preparation as the casting solvent evaporated from the sample and the micro-layer became opaque. Thus, we limited the maximum thickness of amorphous micro-layer samples studied in this work to $35\mu\text{m}$. For the solid state polymerization, a vacuum oven was used as a reaction chamber (Fisher Scientific™ Isotemp™ Model 281A Vacuum Oven, 0.65 cu. Ft.). The polymerization experiments were carried out in the reaction chamber at temperature range of $168\text{-}245 \text{ }^\circ\text{C}$ and 10 mmHg. For the analysis, the polymer samples were taken out of the reaction chamber at designated sampling times and polymer films were removed from glass substrate by ultrasonification (see Figure 2.4).

Table 2.3 Preparation of micro-layer in different thickness.

Prepolymer	Concentration [g/ml]	Casting Time [sec]	Micro-Layer Thickness [μm]
A (8k)	0.25		10 μm (± 1.3)
B (14k)	0.1		5 μm (± 1.3)
B (14k)	0.2	0.5-1.0 sec	10 μm (± 1.3)
B (14k)	0.35		35 μm (± 1.3)
C (21k)	0.19		10 μm (± 1.3)
D (8k)	0.25		10 μm (± 1.3)

2.2.3.2 Solid state polymerization in partially crystallized micro-layers (SSP_m)

Partially crystallized prepolymer micro-layers were prepared by treating the amorphous micro-layers with acetone. The resulting partially crystallized polycarbonate micro-layers exhibited three-dimensional spherulitic morphology as reported in the literature [48, 49] and Figure 2.5 shows morphology of solvent (acetone) induced crystalline morphology of PC micro-layers. The residual acetone was removed by air and vacuum drying at room temperature for 48h. The degree of crystallization of the partially crystallized BPAPC micro-layers was measured by differential scanning calorimetry (DSC) and it was about 32 % for most of the crystallized samples. The polymerization experiments were carried out in a reaction chamber at 230 °C and 10 mmHg.

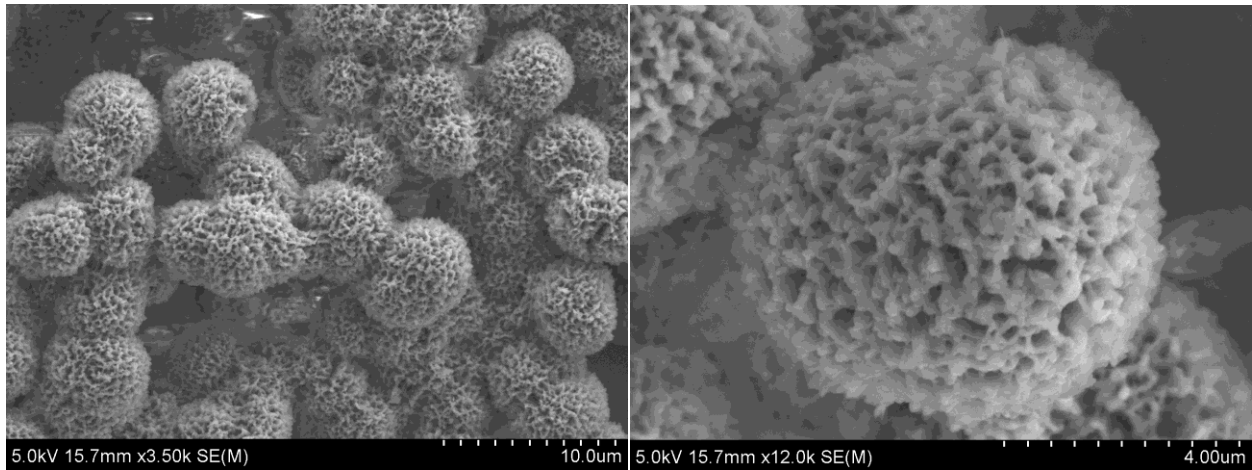


Figure 2.5 Spherulitic morphology of solvent (acetone) induced crystalline PC micro-layers.

2.2.3.3 Solid state polymerization of partially-crystallized polymer micro-particles (SSP_p)

To compare the performance of the solid-state polymerization in micro-layers (SSP_m), we have conducted conventional SSP experiments using the same prepolymers used in the SSP_m but in particle form. The prepolymer was first dissolved in chloroform and then precipitated in methanol. The precipitated prepolymer particles of about 10-350 μm -radius were dried in vacuum for 48h and crystallized in acetone, followed by drying under vacuum at room temperature for 48h. The degree of crystallinity measured by DSC was about 33 %, which was quite similar to that of the partially crystallized micro-layers (32 %). The scanning electron microscopy (SEM) analysis of these crystallized BPAPC particles showed that they were the aggregates of smaller precipitated particles. The particles were classified using sieve trays. The

conventional SSP was performed using the same reaction conditions as in SSP_m and the reaction chamber used for the micro-layer polymerization. Details of the experimental procedure for the conventional SSP can be found elsewhere [27-30, 43].

2.3 Results and Discussion

2.3.1 Solid State Polymerization in Micro-Layers and Micro-Particles

The first series of experiments were carried out using the prepolymer sample B-14K (Table 2.2) at 230°C and 10 mmHg for 180 min in four different settings:

- (i) SSP_m in 10µm-thick amorphous micro-layers;
- (ii) SSP_m in 10µm-thick partially crystallized micro-layers;
- (iii) SSP_p (solid-state polymerization in particles) in partially crystallized particles of 10µm-radius;
- (iv) SSP_p in partially crystallized particles of 350µm-radius (typical particle size in SSP).

Here, the micro-layer thickness (10µm) is a nominal value and the actual layer thickness varies within $\pm 1.3 \mu\text{m}$.

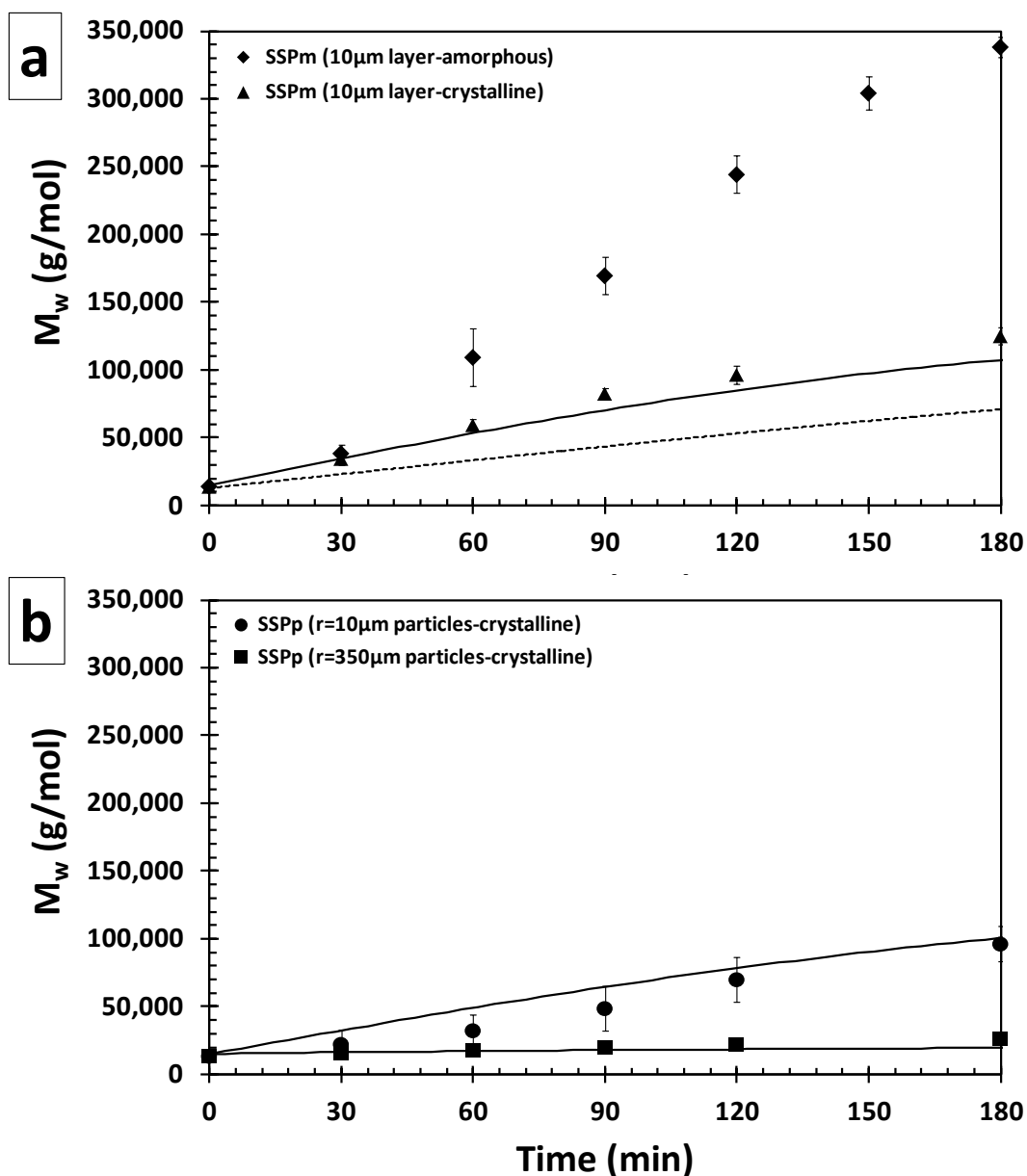


Figure 2.6 Weight-average molecular weight vs. reaction time profiles ($T=230^{\circ}\text{C}$, $P=10$ mmHg, prepolymer B-14k): (a) (\blacklozenge) SSP_m (10µm layer, amorphous); (\blacktriangle) SSP_m (10µm layer, crystalline). Solid and dashed lines represent the numerical simulations for the crystallized micro-layer (10µm-thick) and amorphous micro-layer (10µm-thick), respectively; (b) (\bullet) SSP_p (10µm radius particles, crystalline); (\blacksquare) SSP_p (350µm radius particles, crystalline). Solid lines represent the numerical simulations.

The most prominent result shown in Figure 2.6 (a) is that the molecular weight of 10 μm -thick amorphous prepolymer micro-layers (\blacklozenge) increased from 14,000 g/mol (prepolymer MW) to 340,000 g/mol in 180 min. Although a post-melt polymerization process such as solid-state polymerization can be used to raise the molecular weight of BPAPC to 36,000-42,000 g/mol in 16-24 hr at the temperature of 230°C [26, 27], the rapid increase to such a high molecular weight as illustrated in Figure 2.6 for BPAPC has never been reported in the literature. It is also seen that when the polymer micro-layer was partially crystallized (\blacktriangle), the polymer molecular weight increased to much lower value (about 100,000 g/mol) in 180 min, although the molecular weight of 100,000 g/mol is a very high value. Figure 2.6 (b) shows the molecular weight profiles when the solid state polymerization was carried out using polymer micro-particles. Note that when the prepolymer micro-particles of radius 10 μm (\bullet) were used with the same reaction conditions, the molecular weight increased to about 100,000 g/mol, which is slightly lower than the case of the solid state polymerization in partially crystallized micro-layers of 10 μm thickness (\blacktriangle in Figure 2.6 (a)). However, when larger crystallized polymer particles ($r = 350\mu\text{m}$) (\blacksquare) were used, molecular weight increased only to 26,500 g/mol in 180 min. The size of this polymer particle represents a typical particle size employed in conventional solid state polymerization processes.

Model simulation results for the end-group ratios of 0.80 (*i.e.*, prepolymer sample B-14k) are shown in Figure 2.6. The details of model equations are given in the section 2.3.2. The model-data match is quite good for the crystallized particles (Figure 2.6 (b), solid lines) and crystallized micro-layers (Figure 2.6 (a), solid line), indicating that the model and the model parameters used in the simulation are quite satisfactory for the partially crystallized polymer layers or particles. However, the model predictions of molecular weight for the amorphous

micro-layers (dashed lines in Figure 2.6 (a)) show significant deviations from the experimental data after 30 min of polymerization. It suggests that the solid state polymerization in amorphous micro-layers may not be adequately described by the classical diffusion and reaction model with a linear step-growth polymerization mechanism. One of the most likely reason for the rapid increase in molecular weight in thin amorphous micro-layers, as observed in the foregoing discussion, might be the short diffusion path for phenol. Here, it is to be noted again that the end group ratio of the prepolymer Sample B-14K used in our experiments was 0.8 (Table 2.2), which is a significant deviation from the stoichiometric ratio of 1.0. According to the theory of linear step-growth polymerization, such a stoichiometric imbalance of end groups prohibits the increase in polymer molecular weight even after the complete conversion of an end group present in smaller amount [50]. Therefore, the results obtained in our experimental study need further analysis.

We have also observed that the final polymer micro-layers were highly transparent without any discoloration. Discoloration of polycarbonate is known to be one of the problems in high temperature melt transesterification processes [12, 17]. For example, in conventional melt polycondensation processes at 260-280 °C and low pressure, the employment of long reaction time to obtain high molecular weight (30,000~60,000 g/mol) often leads to unwanted discoloration due to some unwanted side reactions (e.g., Kolbe-Schmitt type) that leading to a branched structure [51-54].

Figure 2.6 shows the experimentally measured weight-average molecular weight (M_w) vs. reaction time profiles for these four representative samples (symbols). The partially crystallized particles of 10 μ m radius have relatively larger particle size distributions than 350 μ m radius particles as shown in Figure 2.7 and Figure 2.9. Using SEM images, the number of particles in different size was counted and size distributions were obtained. Largest size particles observed in Figure 2.7 is around 25 μ m in radius and these are less than 2%. Figure 2.8 shows number of particles at each particle size and average radius of 10 μ m-radius particle samples (Figure 2.6(\bullet)) is 9.87 μ m. The particle size having range of 1-4 μ m radius is marked as 2.5 μ m.

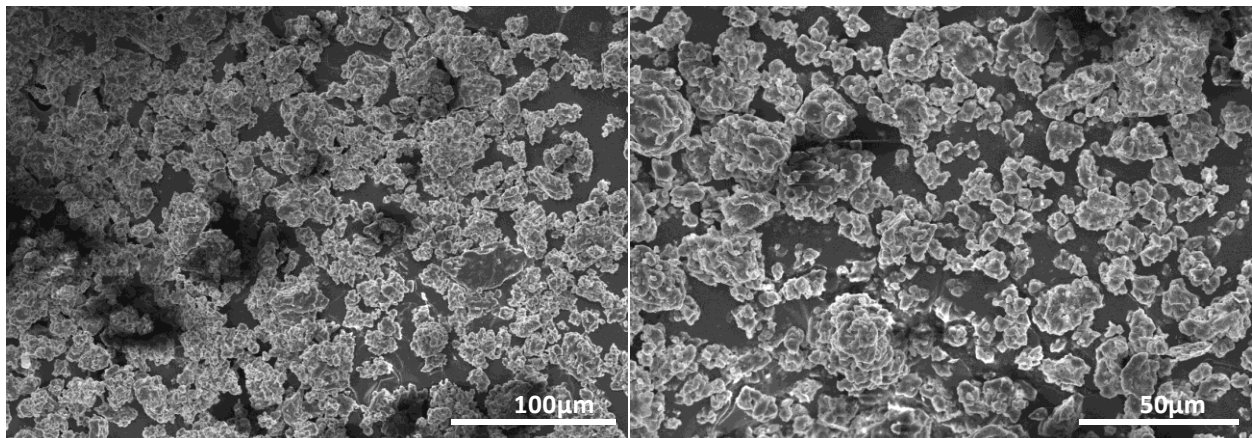


Figure 2.7 SEM images of partially crystallized particles having average radius of 10 μ m.

Figure 2.9 shows the SEM images of partially crystallized particles of 350 μ m-radius (typical particle size in SSP): a) size distribution of crystalline particles, b) surface morphology of 350 μ m-radius particles. The SEM analysis of these crystallized BPAPC particles shows that they are the aggregates of smaller spherulitic particles. Although not shown, the interior part of

large particles of 350 μm -radius does not have spherulitic subparticles and spherulitic morphology was observed only in about 20 μm -thick region from the surface.

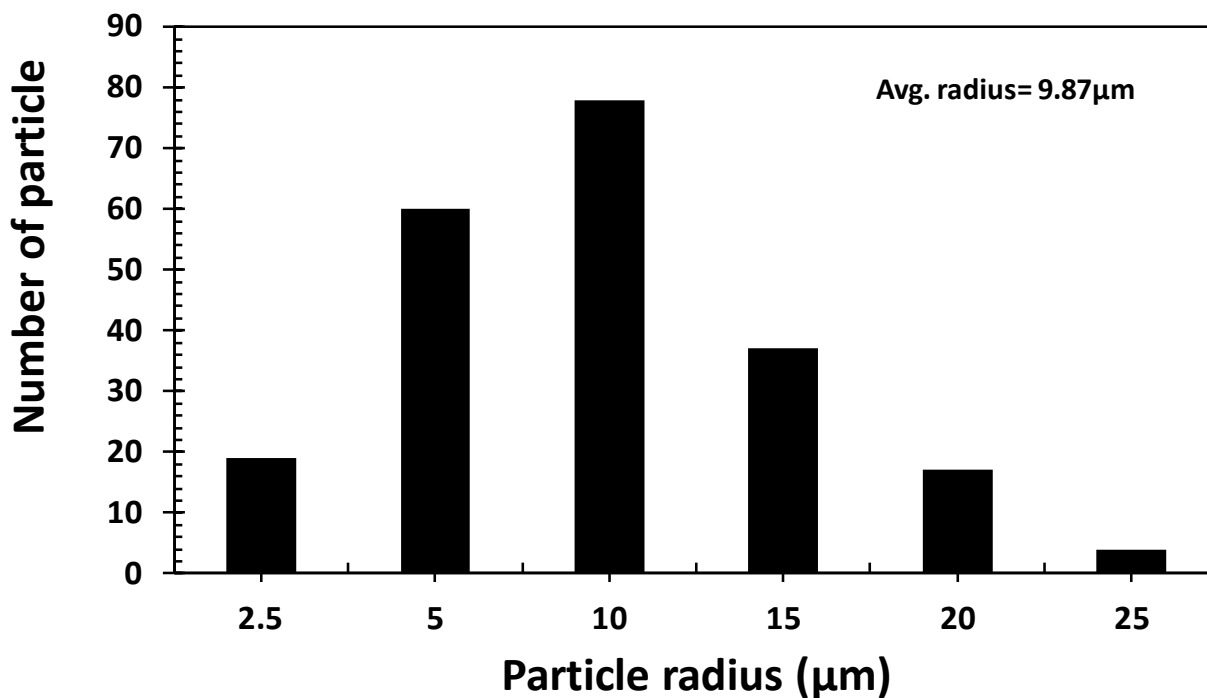


Figure 2.8 Size distribution of partially crystallized particles of 10 μm -radius.

Figure 2.10 shows the side and top views of the partially crystallized polymer micro-layers during the polymerization at 230 °C. Although the spherulitic particles do not completely melt, it is clearly seen that partial melting has occurred. The partial melting was due to the presence of a large fraction of amorphous polymers (c.a. 65%).

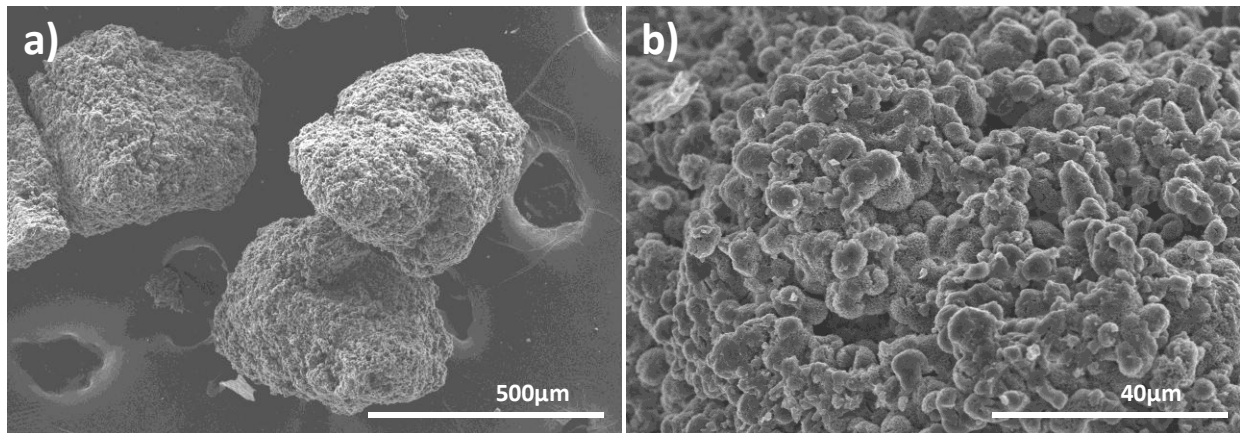


Figure 2.9 Partially crystallized particles of 350 μm -radius (typical particle size in SSP): a) size distribution of crystalline particles, b) surface morphology of 350 μm -radius particles.

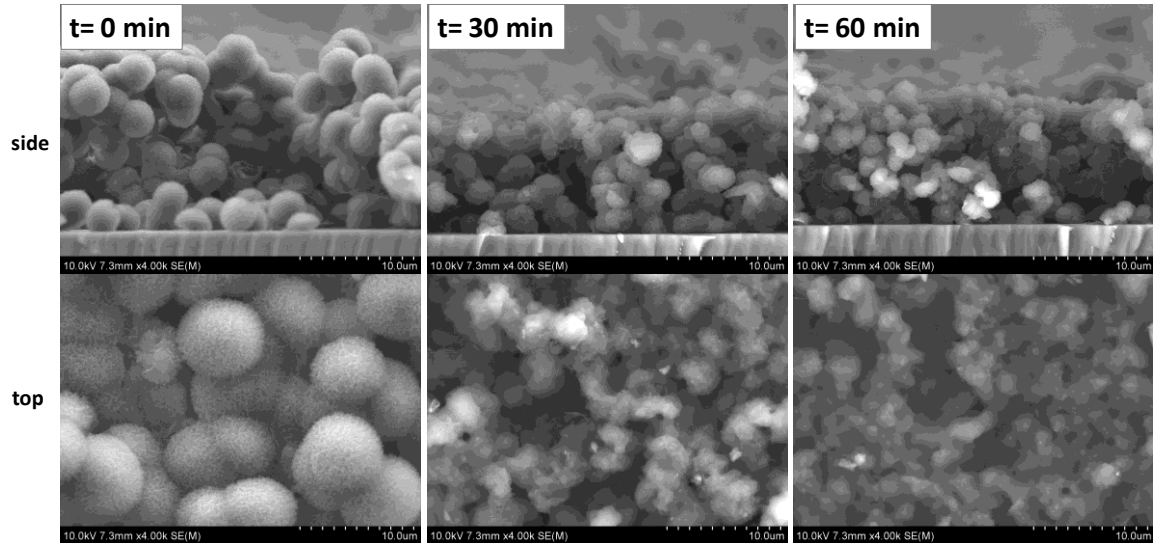


Figure 2.10 Polycarbonate crystalline micro-layers undergoing solid-state polymerization (SSP_m) ($T=230\text{ }^{\circ}\text{C}$, $P=10\text{ mmHg}$, prepolymer B-14k, 10 μm -thick partially crystallized micro-layer).

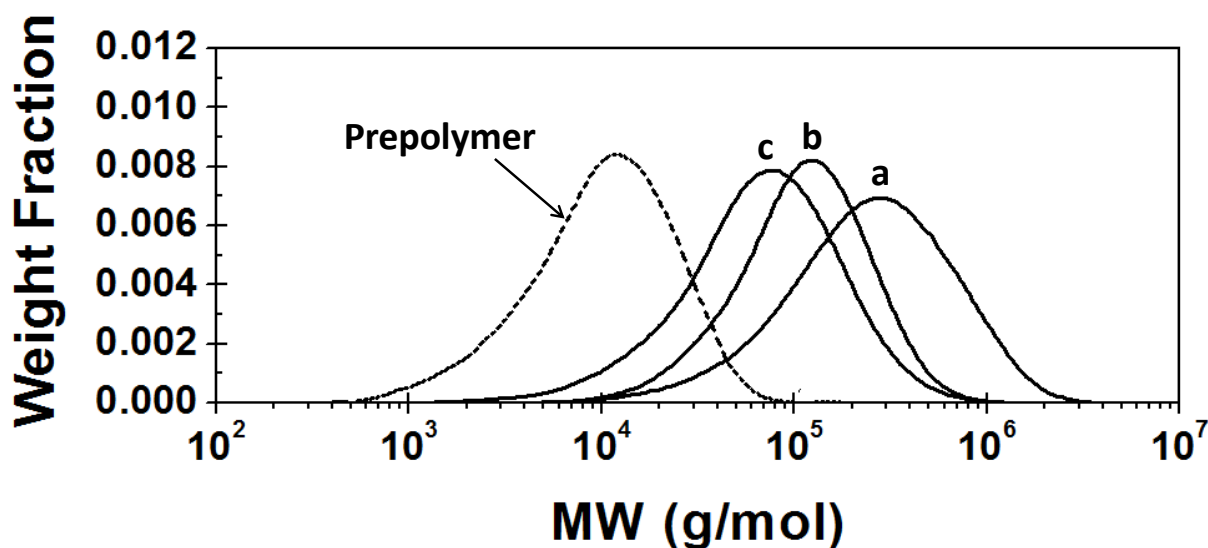


Figure 2.11 Molecular weight distributions (MWD) of micro-layer and particle samples ($T=230\text{ }^{\circ}\text{C}$, $P=10\text{ mmHg}$, prepolymer B-14k) at 180 min: a, $10\mu\text{m}$ amorphous micro-layer; b, $10\mu\text{m}$ crystalline micro-layer (acetone induced crystallization); c, $10\mu\text{m}$ -radius crystalline particles.

The molecular weight distributions (MWDs) of prepolymer and three polymerized samples are shown in Figure 2.11. We observe that the amorphous micro-layers (\blacklozenge in Figure 6) that have the highest molecular weight of all (peak **a**) show the presence of polymer chains ($\sim 10\text{ wt.}\%$) having molecular weight larger than 1 million g/mol. Also, we observed small increase in the polydispersity ($PD = \bar{M}_w / \bar{M}_n$) from 1.97 (prepolymer B-14k) to 2.17 ($10\mu\text{m}$ -radius crystalline particles), 2.15 ($10\mu\text{m}$ crystalline layer), and 2.57 ($10\mu\text{m}$ amorphous layer) (see figure 2.12). According to the linear step-growth polymerization theory, the polydispersity is close to 2.0 even for very high molecular weight polymers. Thus, the MWD broadening (i.e., deviations from $PD = 2.0$) observed in our experiments suggests that some deviation from the homogeneous linear step-growth polymerization might have occurred. For example, a spatial distribution of

phenol due to diffusion resistance might have been present or the polymer chain structures might have deviated from the linear configuration.

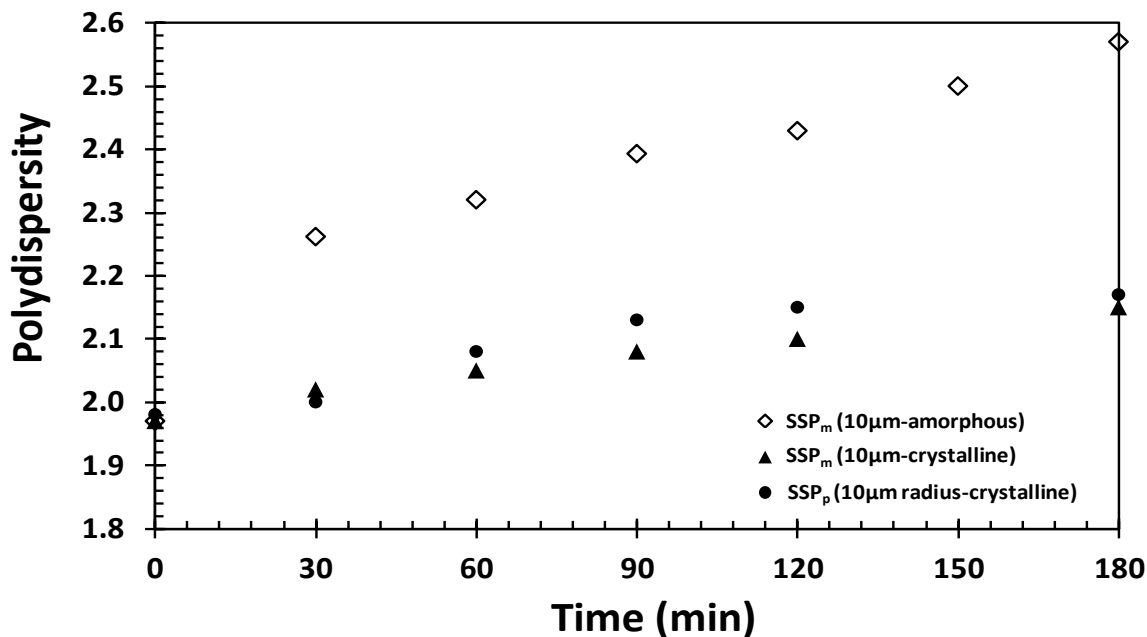


Figure 2.12 Polydispersity of polymers vs. reaction time profile ($T=230^{\circ}\text{C}$, $P=10$ mmHg, prepolymer B-14k): (◇) SSP_m (10µm layer-amorphous); (▲) SSP_m (10µm layer-crystalline); (●) SSP (10µm radius particles-crystalline).

Figure 2.13 (a) (symbols) shows the comparison of weight-average molecular weight buildup between a conventional SSP process using partially crystallized particles (100µm) (●) and the SSP_m process in amorphous micro-layers (10µm thick) (■ and ▲) for the prepolymer A and D ($M_w = 8,300$ g/mol and 8,400 g/mol respectively) which have lower precursor molecular weight than prepolymer B used in first series of experiment. By comparing molecular profile between prepolymer A (commercial BPAPC supplied from LG chemical company) and D (lab

produced), it is shown that SSP_m process has good reproducibility. As shown in Figure 2.13 (b), all the GPC chromatograms of high molecular weight PCs obtained from the SSP_m have unimodal distributions. Simulation model for the SSP was modified to describe the system of SSP_m process and simulation results of the SSP_m in the polymer micro-layers with the best case scenario (*i.e.*, stoichiometric value (1.0) and complete removal of phenol from the polymer micro-layers all the time) are indicated as dash line shown in Figure 2.13 (a). Table 2.2 show that sample A, B, and C exhibit two end group ratio deviates from the stoichiometric value (1.0). It is well known that in linear step-growth polymerization processes, the more the end group mole ratio deviates from the stoichiometric value, the smaller the maximum obtainable polymer molecular weight becomes. Obviously, this model cannot adequately explain the polymerization behavior of the SSP_m, indicating that the effective removal of phenol from the two-dimensional geometrically confined reaction space cannot be the only reason for the significant deviation of molecular weight buildup between SSP and SSP_m.

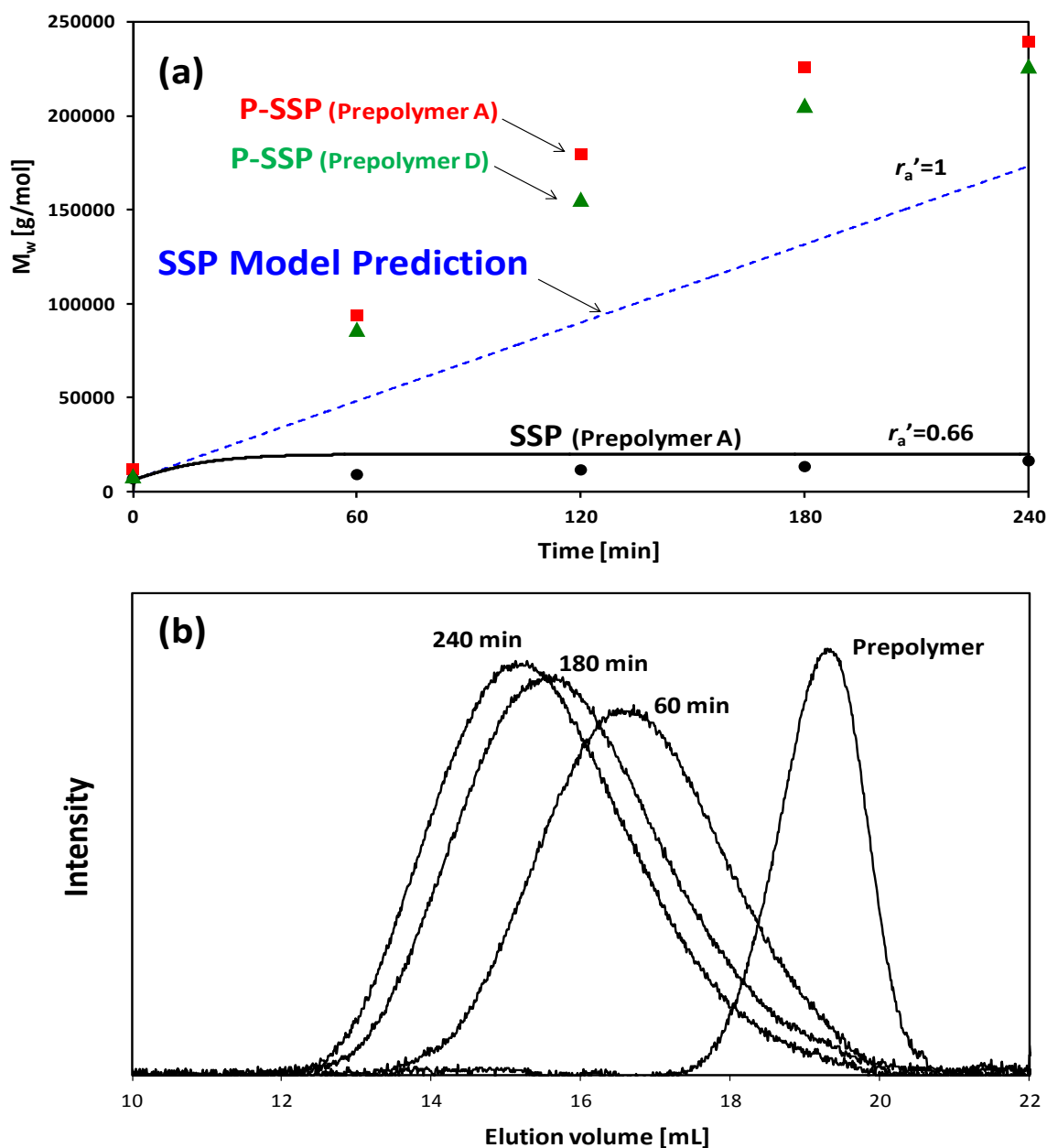
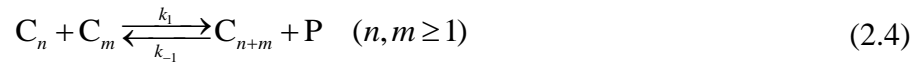
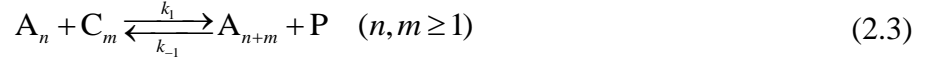
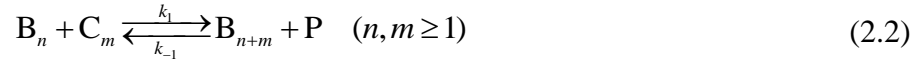
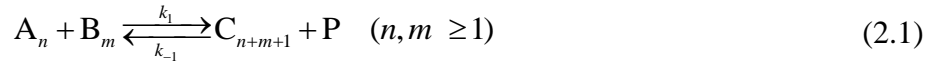


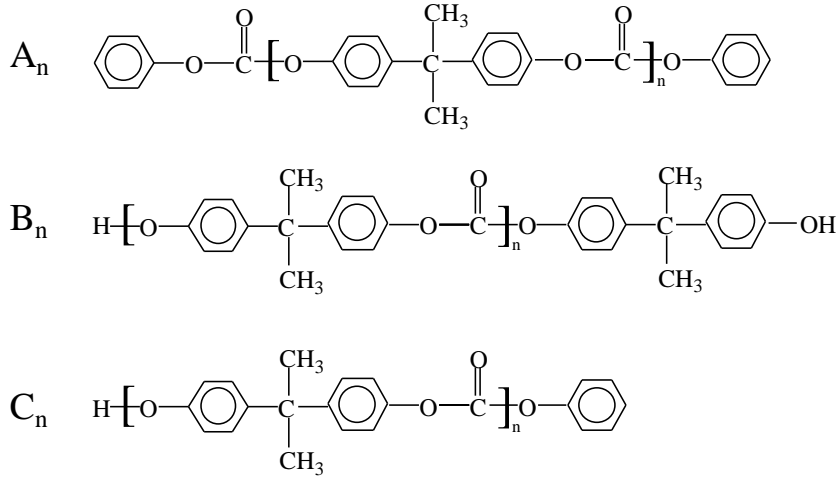
Figure 2.13 (a) Evolution of the PC weight-average molecular weight with the reaction time using Sample A and D at 200 °C: (●) Conventional SSP with pre-crystallized particles of about 100 μm in size (Sample A). (■ and ▲) SSP_m in amorphous polymer micro-layers of 10 μm -thickness (Sample A and D respectively). Lines represent the numerical simulations for different end-group ratios of the prepolymer sample (r_a'); (b) GPC chromatograms for high molecular weight samples collected at different reaction times in SSP_m.

2.3.2 SSP Theoretical Model Prediction

In order to develop some insight into the unusual characteristics of the SSP_m in amorphous polymer micro-layers, we have carried out the numerical simulations of the solid state polymerization using the solid state polymerization model reported in literatures [25, 32, 44]. To that purpose, we consider the reaction model represented by the following reaction scheme for a polycarbonate process [31]:



where A_n and B_n are chains with n repeating units (n -mer) with phenyl and phenolic groups at both ends, respectively. C_n is an n -mer end-capped by both phenyl and phenolic groups, and P is phenol. The molecular structures of A_n , B_n , and C_n type molecules are shown below. According to this notation, A_0 and B_0 represent DPC and BPA monomers, respectively. Kinetic constants k_1 and k_{-1} are for the polycondensation and the reverse reactions, respectively. No side reactions are assumed to be present in the reaction model.



To simulate the SSP process in micro-layer (SSP_m), the following set of partial differential equations is derived [25, 31]. Here, we assume that phenol ([P]) is the only diffusing species in the polymer phase:

$$\frac{\partial[A_0]}{\partial t} = -4k_1[A_0][B_0] - 2k_1[A_0] \sum_{n=1}^{\infty} (2[B_n] + [C_n]) + k_{-1}[P] \sum_{n=1}^{\infty} (2[A_n] + [C_n]) \quad (2.5)$$

$$\frac{\partial[B_0]}{\partial t} = -4k_1[A_0][B_0] - 2k_1[B_0] \sum_{n=1}^{\infty} (2[A_n] + [C_n]) + k_{-1}[P] \sum_{n=1}^{\infty} (2[B_n] + [C_n]) \quad (2.6)$$

$$\begin{aligned} \frac{\partial[P]}{\partial t} = & 4k_1 \sum_{n=0}^{\infty} \sum_{m=0}^{\infty} [A_n][B_m] + 2k_1 \sum_{n=1}^{\infty} \sum_{m=0}^{\infty} [C_n]([A_m] + [B_m]) + k_1 \sum_{n=1}^{\infty} \sum_{m=1}^{\infty} [C_n][C_m] \\ & + k_1 \sum_{m=1}^{\infty} [C_m]^2 - [P]k_{-1} \left(\sum_{n=1}^{\infty} (2n[A_n] + 2n[B_n] + n[C_n]) + \sum_{n=2}^{\infty} (n-1)[C_n] \right) \\ & + D_p \nabla^2 [P] \end{aligned} \quad (2.7)$$

$$\begin{aligned} \frac{\partial[A_n]}{\partial t} = & -4k_1[A_n] \sum_{m=0}^{\infty} [B_m] - 2k_1[A_n] \sum_{m=1}^{\infty} [C_m] + 2k_1 \sum_{m=1}^n [A_{n-m}][C_m] \\ & + k_{-1}[P] \left(\sum_{m=n+1}^{\infty} (2[A_m] + [C_m]) - 2n[A_n] \right) \quad n = 1, 2, \dots, \infty \end{aligned} \quad (2.8)$$

$$\begin{aligned} \frac{\partial[B_n]}{\partial t} = & -4k_1[B_n] \sum_{m=0}^{\infty} [A_m] - 2k_1[B_n] \sum_{m=1}^{\infty} [C_m] + 2k_1 \sum_{m=1}^n [B_{n-m}] [C_m] \\ & + k_{-1}[P] \left(\sum_{m=n+1}^{\infty} (2[B_m] + [C_m]) - 2n[B_n] \right) \quad n = 1, 2, \dots, \infty \end{aligned} \quad (2.9)$$

$$\begin{aligned} \frac{\partial[C_n]}{\partial t} = & 4k_1 \sum_{m=0}^{n-1} [A_{n-m-1}] [B_m] - 2k_1 [C_n] \sum_{m=0}^{\infty} ([A_m] + [B_m]) - 2k_1 [C_n] \sum_{m=1}^{\infty} [C_m] \\ & + k_1 \sum_{m=1}^{n-1} [C_m] [C_{n-m}] + 2k_{-1}[P] \left(\sum_{m=n+1}^{\infty} ([A_m] + [B_m] + [C_m]) \right) \\ & - k_{-1}n[P][C_n] \quad n = 1, 2, \dots, \infty \end{aligned} \quad (2.10)$$

In the above equations, D_P is the diffusivity of phenol in the polymer phase. The following initial and boundary conditions are used to solve Equations (2.5)-(2.10):

$$[P(0, z)] = P_0 \quad (2.11)$$

$$[A_n(0, z)] = [A_n]_0 \quad n = 0, 1, 2, \dots, \infty \quad (2.12)$$

$$[B_n(0, z)] = [B_n]_0 \quad n = 0, 1, 2, \dots, \infty \quad (2.13)$$

$$[C_n(0, z)] = [C_n]_0 \quad n = 0, 1, 2, \dots, \infty \quad (2.14)$$

$$\frac{\partial[P(t, 0)]}{\partial z} = 0 \quad (2.15)$$

$$[P(t, \delta_{\text{layer}})] = P^* \quad (2.16)$$

where z is the distance from the substrate surface and δ_{layer} is the polymer micro-layer thickness, and P_0 and P^* are the concentration of residual phenol in the prepolymer and the concentration of phenol at the layer surface during the SSP, respectively. The above model can also be applied to a spherical polymer particle.

The above molecular species model consists of the population balance equations for these three polymeric species (A_n , B_n , and C_n). The polymer molecular weight moments are also derived and solved to calculate the molecular weight averages. The derivation of molecular weight moments can be found elsewhere [44]. Here, the k -th molecular weight moments of molecular species A_n , B_n and C_n are defined as

$$\mu_{A,k} = \sum_{n=1}^{\infty} n^k [A_n], \quad \mu_{B,k} = \sum_{n=1}^{\infty} n^k [B_n], \quad \mu_{C,k} = \sum_{n=1}^{\infty} n^k [C_n] \quad (n = 1, 2, \dots; k = 0, 1, 2) \quad (2.17)$$

where $[A_n]$, $[B_n]$ and $[C_n]$ represent the concentrations of corresponding species. The number-average and the weight-average molecular weights of the polymer are calculated as

$$\bar{M}_n = w_m \frac{\mu_1}{\mu_0}, \quad \bar{M}_w = w_m \frac{\mu_2}{\mu_1} \quad (2.18)$$

where w_m is the molecular weight of a repeating unit and μ_k ($k = 0, 1, 2$) is the k -th molecular weight moment ($\mu_k = \mu_{A,k} + \mu_{B,k} + \mu_{C,k}$). One of the difficulties in modeling the SSP with a given prepolymer is that molecular weight moments of three polymeric species in a given prepolymer are not known. To calculate the polymer molecular weight in SSP where only prepolymer molecular weight averages and end group ratio data are available, we need to estimate the molecular weight moments of three polymeric species defined in the above model.

In this work, we used a computational method reported in the literature to estimate the molecular weight moment values of a prepolymer using molecular weight averages and end group ratio [44]. Here, if the prepolymer molecular weight averages are $\bar{M}_{n,0}$ and $\bar{M}_{w,0}$, and the end group ratio in a prepolymer is r'_a , the initial end group ratio in the prepolymer synthesis stage (r_a) and the end group conversion (p) can be estimated by the following equations [44]:

$$r_a = \frac{1 - r_a' - (1 + r_a')(2\overline{M}_{n,0} / w_m)}{r_a' - 1 - (1 + r_a')(2\overline{M}_{n,0} / w_m)} \quad (2.19)$$

$$p = 1 - \frac{1 + r_a - (1 - r_a)(2\overline{M}_{n,0} / w_m)}{2r_a(2\overline{M}_{n,0} / w_m)} \quad (2.20)$$

where w_m is the molecular weight of a repeating unit and $\overline{M}_{n,0}$ is the number average molecular weight of a prepolymer. Then, the molecular weight moments can be calculated as follows [44]:

$$\mu_{A,k} = \frac{\rho_p}{\overline{M}_{n,0}} \sum_{n=1}^{\infty} n^k \left[p^{2n} r_a^n \frac{(1-p)^2}{1 + \frac{1}{r_a} - 2p} \right] \quad (2.21)$$

$$\mu_{B,k} = \frac{\rho_p}{\overline{M}_{n,0}} \sum_{n=1}^{\infty} n^k \left[p^{2n} r_a^{n-1} \frac{(1-r_a p)^2}{1 + \frac{1}{r_a} - 2p} \right] \quad (2.22)$$

$$\mu_{C,k} = \frac{\rho_p}{\overline{M}_{n,0}} \sum_{n=1}^{\infty} n^k \left[p^{2n-1} r_a^n \frac{2(1-p)(1-r_a p)}{1 + r_a - 2r_a p} \right] \quad (2.23)$$

where ρ_p is the polymer density, $\mu_{A,k}$, $\mu_{B,k}$ and $\mu_{C,k}$ are the k-th moments of polymer species A_n , B_n , and C_n .

Also, from the estimated values of r_a and p , the concentrations of three molecular weight species in the prepolymer ($[A_n]_0$, $[B_n]_0$, and $[C_n]_0$) can be estimated using the following equations [44, 55]:

$$[A_n]_0 = p^{2n} r_a^n \frac{(1-p)^2}{1 + 1/r_a - 2p} \sum_{n=1}^{\infty} ([A_n]_0 + [B_n]_0 + [C_n]_0) \quad (2.24)$$

$$[B_n]_0 = p^{2n} r_a^{n-1} \frac{(1-r_a p)^2}{1+1/r_a-2p} \sum_{n=1}^{\infty} ([A_n]_0 + [B_n]_0 + [C_n]_0) \quad (2.25)$$

$$[C_n]_0 = p^{2n-1} r_a^n \frac{2(1-p)(1-r_a p)}{1+r_a-2r_a p} \sum_{n=1}^{\infty} ([A_n]_0 + [B_n]_0 + [C_n]_0) \quad (2.26)$$

The reaction rate constant values used in our simulations at 230°C with the catalyst (LiOH·H₂O) concentration of 1.75×10⁻⁴ M [11] are: $k_1=1.551 \times 10^{-1}$ (L/mol/min) and $k_{-1}=1.619 \times 10^{-1}$ (L/mol/min).

2.3.3 Effect of End-Group Ratio

In a linear step-growth polymerization, the end-group ratio is an important parameter that affects the rate of polymerization and the polymer molecular weight. For an AA-BB type of polycondensation process (e.g., bisphenol A polycarbonate synthesis from bisphenol A and diphenyl carbonate), any deviation from the stoichiometric end group ratio (i.e., $r_a'=1.0$) is unfavorable for the growth of polymer chain length. For example, when BPAPC prepolymer is synthesized from BPA and DPC at high reaction temperature and reduced pressure, a partial loss of volatile DPC occurs, making the end group ratio difficult to maintain at its stoichiometric value in the reaction mixture during the course of polymerization [25, 29]. To compensate for the loss of DPC during the polymerization, a slight excess amount of DPC is generally used. Indeed, the three prepolymer samples we prepared show the end group ratios deviating from 1.0 (Table 2.2). We used these three prepolymer samples to investigate the effect of end group ratio on the rate of polymerization in micro-layer.

Figure 2.14 shows the increase of molecular weights as a function of reaction time. Here, three amorphous prepolymer micro-layers and three partially crystallized prepolymer micro-layer samples were used and the thickness of each micro-layer was kept constant at 10 μm within experimental error. For all samples, amorphous polymer micro-layers showed much higher molecular weights than the partially crystallized samples. As observed in the prepolymer B-14K (Figure 2.6), all samples show the similar results of rapid molecular weight increments even with the stoichiometric imbalance. The amorphous sample C-21k, which has the end group mole ratio ($[-\text{OCO}-\text{C}_6\text{H}_5]/[-\text{OH}]$) closest to 1.0 among three samples tested (Table 2.2), gives the highest molecular weight of all as expected. Notice that, after 150 min of reaction, the amorphous micro-layer of prepolymer sample C-21k has reached a molecular weight of 600,000 g/mol. Such a high molecular weight and soluble polycarbonate has not been reported in the literature. The MW value obtained using amorphous micro-layers is truly remarkable and it can be considered as an ultra-high molecular weight PC. Notice that all these samples exhibit a phenyl ($[-\text{OCO}-\text{C}_6\text{H}_5]$) to phenolic end group ($[-\text{OH}]$) ratios (r_a') significantly deviating from the stoichiometric value of 1.0 (Table 2.2). Figure 2.14 also shows that the molecular weight difference between Samples B and C in amorphous micro-layers is much higher than that of the crystalline micro-layers. Although the end group mol ratio (phenyl/phenolic) of Sample C (0.9) is larger than that of Sample B (0.8), and hence more favorable for faster chain growth, the observed molecular weight difference between these samples as shown in Figure 2.14 is so large thus the end group mol ratio does not seem to be the only one reason for the difference. Furthermore, the presence of long polymer chains from the very beginning of the polymerization seems to accelerate the reaction for the production of very high molecular weight. Thus, other reactions involving long

polymer chains, which are not dependent on either the end group concentration or the end group mol ratio, may occur during the SSP_m results in high molecular weight polycarbonates. Even the crystallized micro-layers of sample C-21K has the molecular weight about 300,000 g/mol after 240 min.

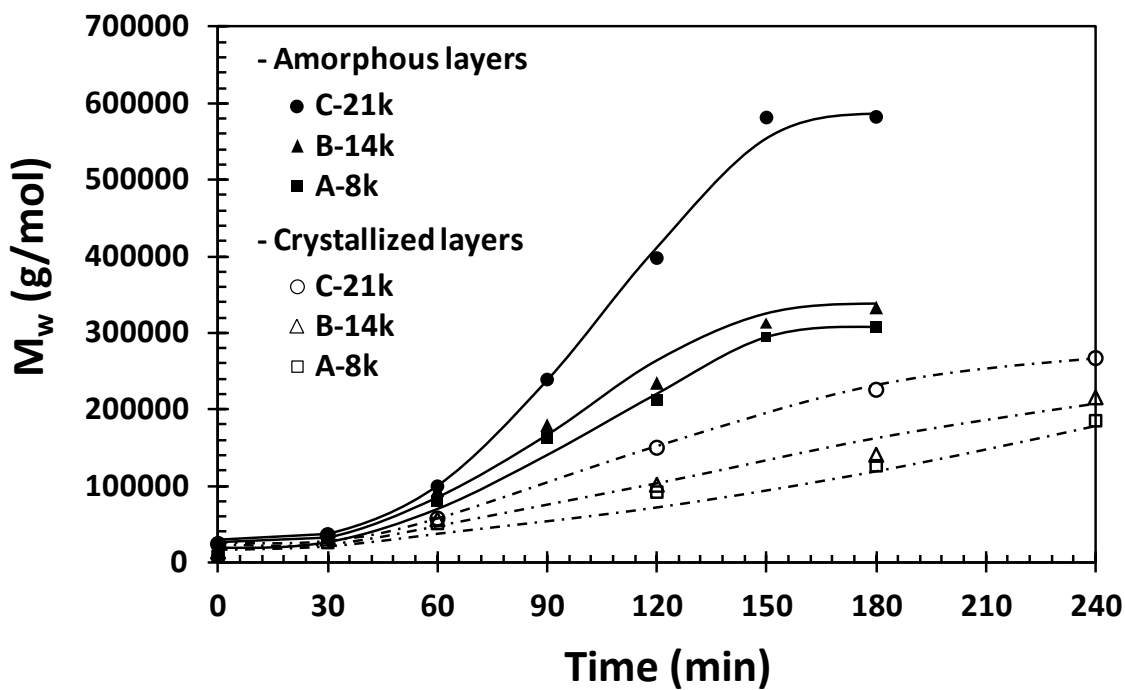


Figure 2.14 Effect of prepolymer end-group ratio on the evolution of weight-average MW in amorphous polymer micro-layers of 10 μm thickness ($T=230\text{ }^{\circ}\text{C}$, $P=10\text{ mmHg}$): amorphous micro-layer (solid line) and crystallized micro-layer (dashed line). Lines were added to guide the eyes only.

2.3.4 Effect of Amorphous Micro-Layer Thickness

In the foregoing, we have shown that amorphous micro-layers yielded the highest molecular weight in solid-state polymerization. Figure 2.15 shows the molecular weight vs. reaction time profiles for the amorphous micro-layers of thickness from 5 μm to 35 μm at 230°C with B-14K prepolymer samples. All these samples were solvent (chloroform)-cast and they were transparent during the entire period of solid-state polymerization. It was observed that partial crystallization occurred during the polymerization when the micro-layers of thickness larger than 35 μm were used. It is clearly seen in Figure 2.15 that molecular weight increases with the decrease in the micro-layer thickness. It is understandable because the diffusion path for the condensate (phenol) is shorter in thinner micro-layers. In 180 min of SSP_m with amorphous micro-layers, the molecular weight reached as large as 400,000 g/mol for the 5 μm -thick micro-layers. Figure 2.16 shows a plot of the maximum polymer molecular weight vs. micro-layer thickness after 3 hr reaction. Interestingly, the molecular weight is almost linearly dependent on the micro-layer thickness and its correlation is expressed as $M_w = 4.533 \times 10^5 - 1.083 \times 10^4 \delta$, where δ in μm .

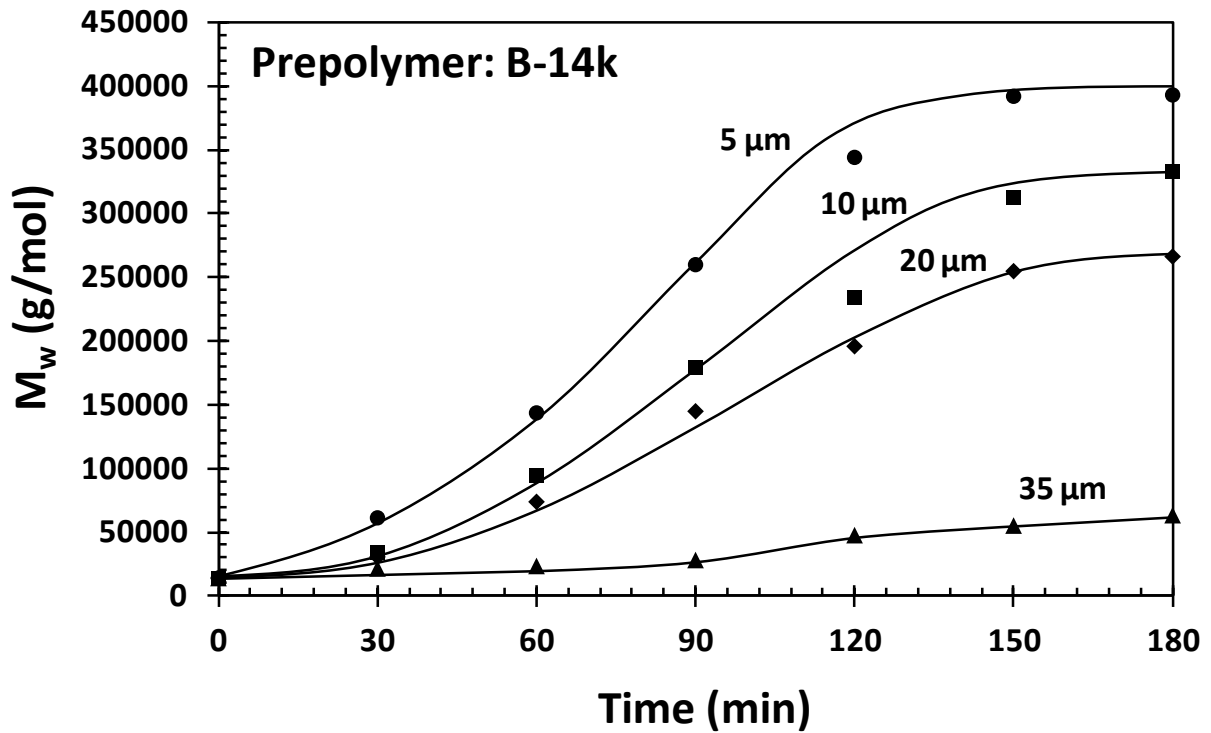


Figure 2.15 Effect of the amorphous micro-layer thickness on the evolution of the polymer molecular weight with the reaction time ($T=230\text{ }^\circ\text{C}$, $P=10\text{ mmHg}$, Prepolymer B-14k). Lines were added to guide the eyes only.

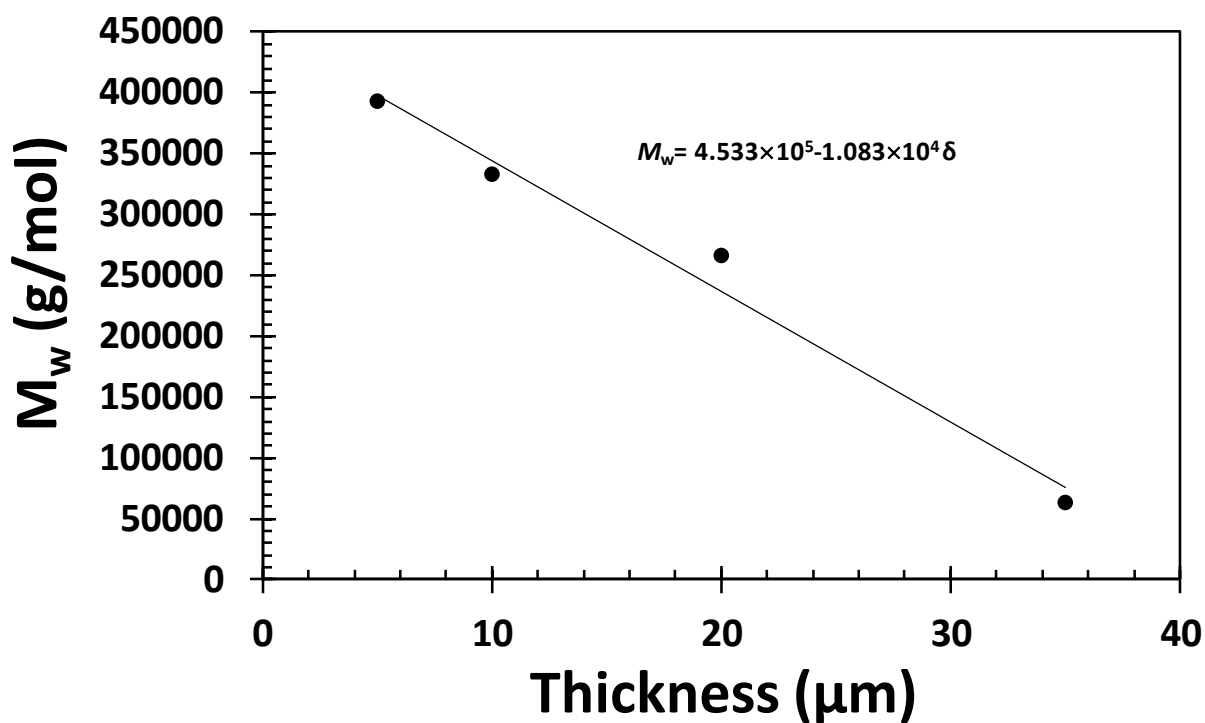


Figure 2.16 Maximum polymer molecular weight vs. micro-layer thickness after 180 min reaction time in amorphous polymer micro-layer (SSP_m) (prepolymer B-14k, δ =micro-layer thickness).

2.3.5 Effect of Reaction Temperature

In a conventional SSP of BPAPC, the maximum reaction temperature must be sufficiently below the polymer's melting point ($\sim 260^{\circ}\text{C}$) because otherwise, partial melting or fusion of the polymer particles occurs and the operation of a continuous flow reactor (e.g., fluidized bed reactor, moving packed bed reactor) becomes very difficult or impossible.

Therefore, in conventional SSP of BPAPC, much lower temperature ($< 220\text{ }^{\circ}\text{C}$) is employed and it makes the polymerization proceed very slowly. Figure 2.18 (a1) and (b1) show the SEM images of the crystallized prepolymer micro-layer surface of thickness $10\mu\text{m}$ and the crystallized prepolymer particle surface of $10\mu\text{m}$ -radius. When these partially crystallized prepolymers were polymerized at $235\text{ }^{\circ}\text{C}$ for 60 min, the resulting polymer morphologies are shown in Figures 2.18 (a2) and (b2). In the micro-layer polymerization, however, the reaction temperature much higher than in the SSP processes can be used because the reaction occurs in a stationary amorphous micro-layer. In our experiments, we carried out SSP_m experiments at different temperatures. Figure 2.17 shows the effect of reaction temperature on the molecular weight of $10\mu\text{m}$ -thickness amorphous polymer layers prepared using prepolymer Sample A-8k (Figure 2.17 (a)) and Sample B-14k (Figure 2.17 (b)). In the temperature range of $168\text{-}237\text{ }^{\circ}\text{C}$ (prepolymer A-8k) and $200\text{-}235\text{ }^{\circ}\text{C}$ (prepolymer B-14k), the reaction temperature has a strong effect on MW, indicating that the polymerization in micro-layers is kinetically controlled. In our experiments, it was observed that when the reaction temperature was below $200\text{ }^{\circ}\text{C}$ (Figure 2.17 (a)), the polymer micro-layers partially crystallized by a very small amount of residual casting solvent (chloroform). The reduced polymer chain mobility in crystalline regions and low reaction temperature might have contributed to the reduced molecular weight at low temperatures. But, it should be noted that the molecular weight values obtained at $183\text{-}200\text{ }^{\circ}\text{C}$ are still much higher than those obtainable by conventional SSP using spherical particles of larger sizes.

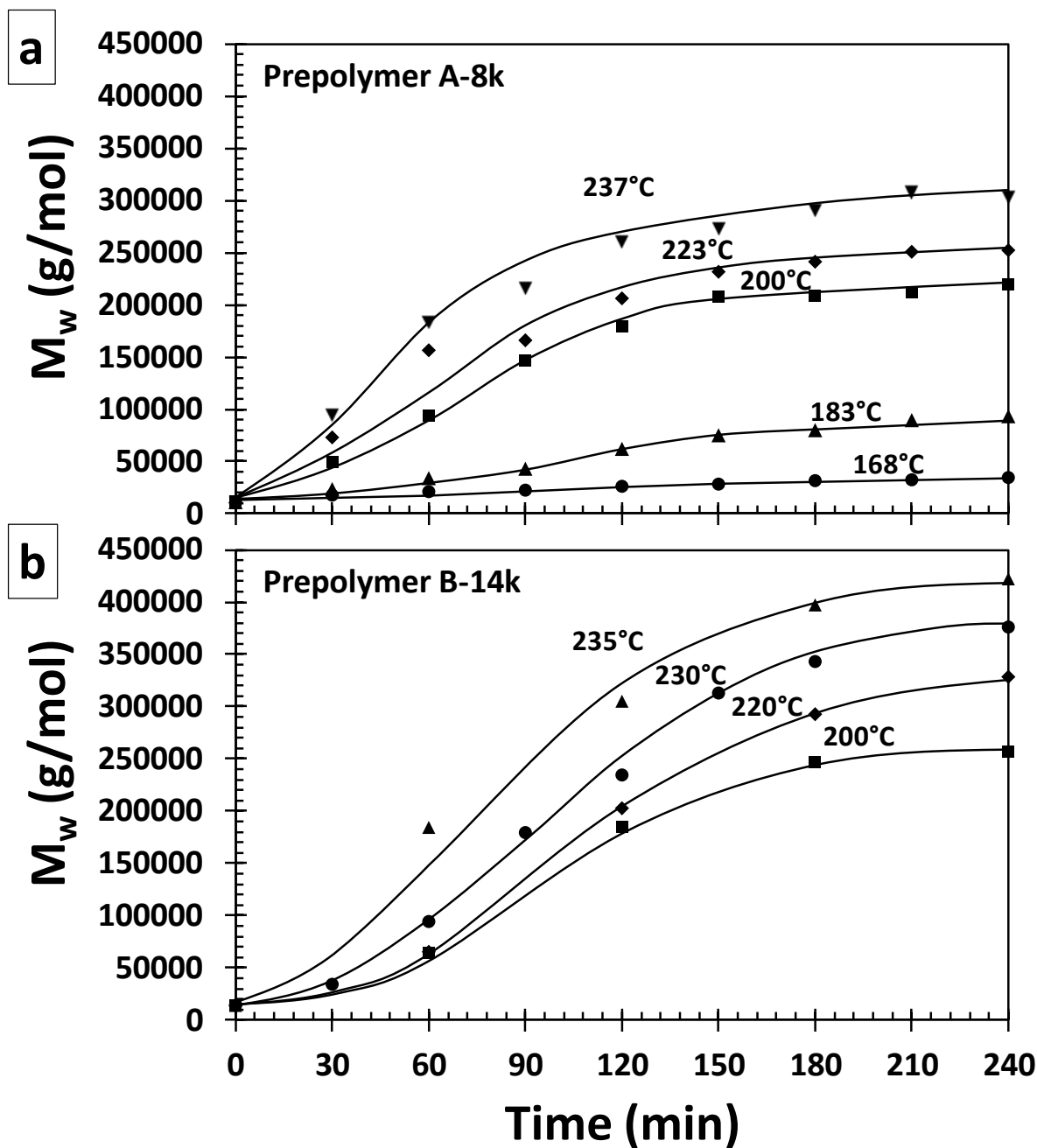


Figure 2.17 Effect of temperature on the evolution of the PC weight-average molecular weight with the reaction time ($P=10$ mmHg, micro-layer thickness= $10 \mu\text{m}$): (a) prepolymer A-8k; (●) 168°C ; (▲) 183°C ; (■) 200°C ; (◆) 223°C ; (▼) 237°C : (b) prepolymer B-14k; (▲) 235°C ; (●) 230°C ; (◆) 220°C ; (■) 200°C .

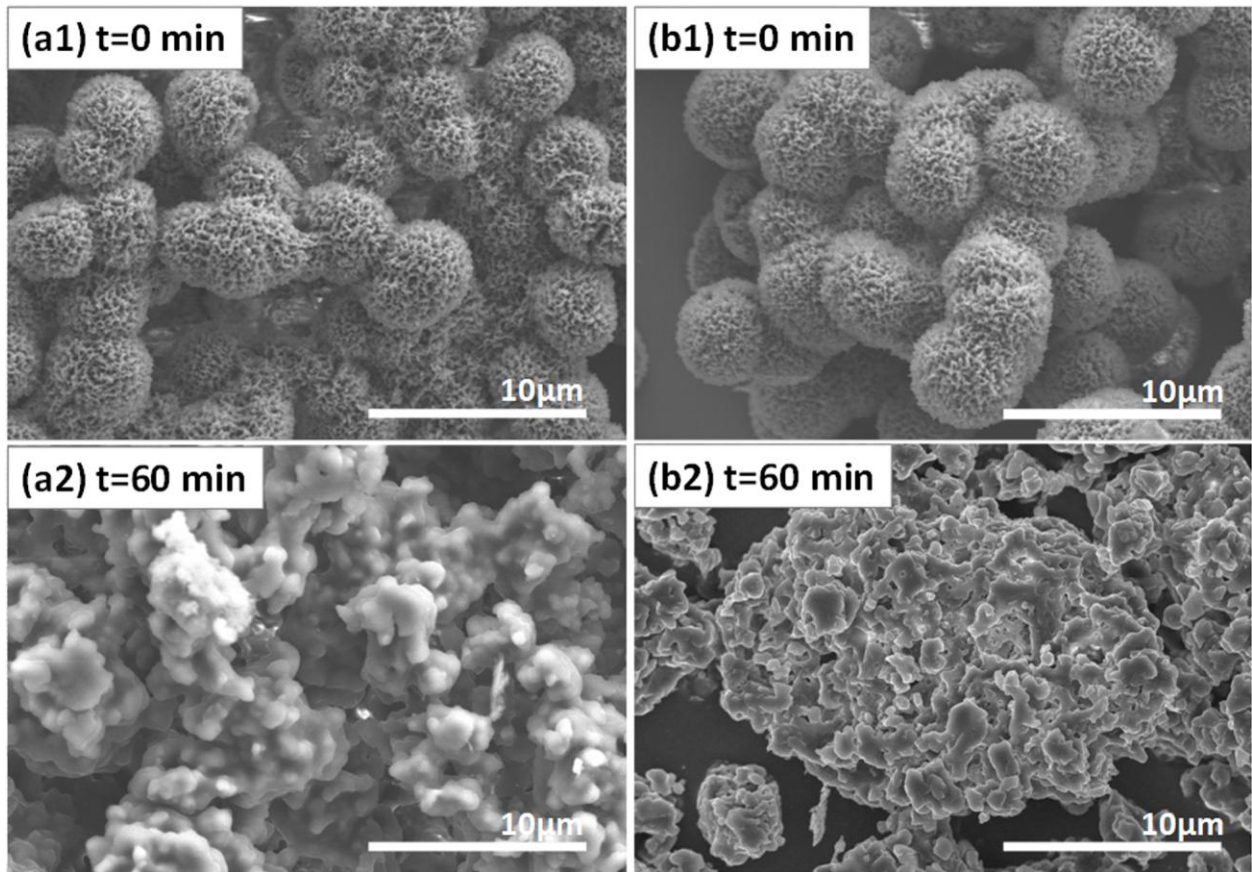


Figure 2.18 Morphology of crystallized polycarbonate prepolymers: (a1) surface of micro-layer (10μm-thickness), (b1) surface of bulk crystallized particles (10μm-radius), (a2) surface of micro-layer (10μm-thickness) after 2 hr reaction at 235 °C, (b2) surface of bulk particles (10μm-radius) after 2 hr reaction at 235 °C (Prepolymer: sample B-14k).

2.4 Conclusions

In this chapter, we have presented new experimental study on the solid-state polymerization of BPAPC in micro-layers (SSP_m) at the similar temperature range (200-235 °C) employed in conventional solid-state polymerization process but very close to the polymer's melting point. In SSP process, the reaction temperature should also be properly controlled. If the reaction temperature is too close to the polymer melting point, the particles fuse together, thus reducing the reaction rate and making the operation of a continuous SSP reactor (*e.g.*, moving packed bed reactor) very difficult or even impossible. The particle fusing of partially crystallized particles at relative high temperature were observed. In the micro-layer polymerization, the reaction temperature much higher than in the SSP processes can be used because the reaction occurs in a stationary amorphous micro-layer. Thus partial melting or fusing during the reaction are not of concern. Quite unexpectedly, ultra-high molecular weight polymers were obtained in very short reaction time when amorphous prepolymer micro-layers were used at 200-235 °C. It was observed that thin micro-layer thickness promotes very efficient removal of the polycondensation byproduct but other factors such as the amorphous state, temperature, end-group ratio and the prepolymer molecular weight seem to affect the progress of polymerization in the SSP_m. Through the SSP theoretical simulation model prediction, unlike in conventional solid-state polymerization using partially crystallized micro-particles, the SSP_m in amorphous micro-layers is not ruled by conventional linear step-growth polymerization theory. Also, broadening of MWD and polydispersity were observed. The polydispersity of amorphous micro-layers are far higher than 2.0 which is theoretical value of maximum polydispersity of linear

step-growth polymers in homogeneous conditions. Interestingly, the molecular weight is almost linearly dependent on the micro-layer thickness and its correlation is expressed as

$M_w = 4.533 \times 10^5 - 1.083 \times 10^4 \delta$, where δ in μm . Temperature dependent molecular weight in

SSP_m process indicate that this process is kinetically controlled.

Chapter3: Reaction Mechanisms for SSP_m in an Amorphous Polymer Micro-Layers

3.1 Introduction

In the foregoing, we have seen that the SSP kinetics in amorphous micro-layers (SSP_m) deviate from the kinetics of conventional SSP in that the polymer molecular weight increases rapidly in a short reaction time even with a significant stoichiometric imbalance of end groups ([$\text{OCO-C}_6\text{H}_5$]/ [-OH]) being present in a starting prepolymer and linear step-grow polymerization kinetic cannot explain such a fast buildup of molecular weight using SSP_m and final molecular weight of amorphous 5-20 μm thickness micro-layers. To understand the unusually high molecular weight in our polymer samples, particularly in amorphous micro-layers, we postulate that the polymer chain structure may not be perfectly linear but may have some nonlinear structures such as branching and partial cross-linking. In fact, in a melt polymerization of polycarbonate at high reaction temperatures (260-290 °C) a small amount of branched polycarbonate can be formed by Kolbe-Schmitt rearrangement or Fries rearrangement reactions [37, 40]. Although the concentration of branched polymers (often called Fries product) in linear polycarbonates is usually quite small (~450 ppm), they can adversely affect melt flow properties and ductility and hence much efforts have been made to minimize the formation of Fries products [37, 40, 56-58]. The polydispersity values obtained in our high molecular weight polycarbonates were as high as 2.3-2.57, broadening of polydispersity, suggesting that branching

might be a strong possibility. The polydispersity of precursors provided in table 2.2 were 1.90 – 2.00 which is typical values can be achieved via homogeneous melt polycondensation process [50].

Another possible nonlinear chain structure in the high molecular weight BPAPC obtained in our study is a partial cross-linking. The formation of a cross-linked structure in polycarbonate during melt polymerization has been known to be possible at high reaction temperature ranges (300-500°C) which is above the polycarbonate melting temperature and higher than temperatures typically applied in melt processes or solid-state polymerization process [18, 20] and this temperature range is much higher than temperature applied in our study using thin amorphous micro-layers. At 1965, Davis et al. [18] reported a formation of insoluble gel with severe discoloration at high temperature range (300-500°C) when the volatile product, phenol, is effectively removed from the system. Also, it was proposed that the cross-linking can occur via radical recombination of two macro-radical species or formation of pendant carboxyl group followed by esterification reaction [19, 59, 60].

3.2 Experimental

3.2.1 Characterizations

The polycarbonate molecular architectures have been analyzed using high resolution ^{13}C -NMR and ^1H -NMR spectroscopy (Bruker AV III spectrometer at 150.9 and 600 MHz, respectively), and pyrolysis-gas chromatography mass spectrometry (Py-GC/MS). For the ^{13}C -NMR and ^1H -NMR spectroscopy analysis, polymer samples taken from the SSP_m experiments were dissolved in deuterated chloroform (CDCl_3). Py-GC/MS analysis was conducted in Korea by Dr. Yun Gyong Ahn (Korea Basic Science Institute, Seoul, Korea) and Dr. Kwang Ho Song (Korea University)). For the Py-GC/MS analysis, a Frontier Lab PY-2020iD pyrolyzer (Koriyama, Fukushima, Japan) was used. It was connected to an Agilent GC/MS system composed of an Agilent 6890 gas chromatograph and an Agilent 5975i mass spectrometer (Palo Alto, CA, USA) to separate and obtain the mass spectra of the compounds in each sample. Measurement conditions for the GC were: A DB-5 MS capillary column (length, 30 m; internal diameter, 250 μm ; film thickness, 0.25 μm , 5% diphenyl-95% dimethylsiloxane phase, J&W Scientific, Folsom, CA, USA); carrier gas helium running at a constant flow rate of 1 mL/min (37 cm/s); split mode (50:1 ratio). The initial temperature of oven was 60 $^\circ\text{C}$, then a 10 $^\circ\text{C}/\text{min}$ gradient was applied to 320 $^\circ\text{C}$ (15 min). The column was interfaced directly to the electron impact (EI) ion source of the mass spectrometer. The ion source was operated at 70 eV. The injection port, transfer line and ion source temperature were set at 300, 300 and 230 $^\circ\text{C}$, respectively. The mass spectrometer was scanned in the 50-800 m/z range. An aqueous solution

(25 wt %) of tetramethylammonium hydroxide [(CH₃)₄NOH; TMAH] (Aldrich) was used as the reagent for methylation of the product samples. About 100 μg of sample and 10 μL of the aqueous solution of TMAH taken in a platinum sample cup were introduced into the furnace at 600 °C. Then, the temperature program of the gas chromatograph oven was started.

3.3 Results and Discussion

3.3.1 ¹³C-NMR Analysis

Figure 3.1 shows the ¹³C-NMR spectral data for an amorphous prepolymer and three SSP_m samples, all in 10 μm micro-layers, taken at different reaction times (15min, 30 min, and 60 min). Prepolymer B (14,000 g/mol) in Table 2.2 which has end functional group ratio ([-OCO-C₆H₅]/[-OH]) of 0.8 was used for the preparation of SSP_m amorphous BPAPC samples. Reaction temperature was set to 230°C and SSP_m was conducted at reduced pressure (10 Torr). Result of molecular weight obtained via SSP_m process with amorphous micro-layers (10μm) is provided in figure 3.2 (♦). Carbon peaks in PC were assigned on the basis of detailed studies available in the literature [37, 61]. Here, we note that phenolic group (peak 5,6,7, and 8 in Figure 3.1) and phenyl group (peak 1,2,3, and 4 in Figure 3.1) decreased to insignificant levels after 30 min, and therefore, linear step-growth polymerization via end group reactions practically ceases to occur afterwards. In other word, no functional group is available to react to produce higher molecular weight linear polycarbonate. However, according to the polymerization data in Figure

3.2 polymer molecular weight continued to increase after 30 min, suggesting that some other reactions might have led to the continued growth of polymer chains and molecular weight.

^{13}C -NMR

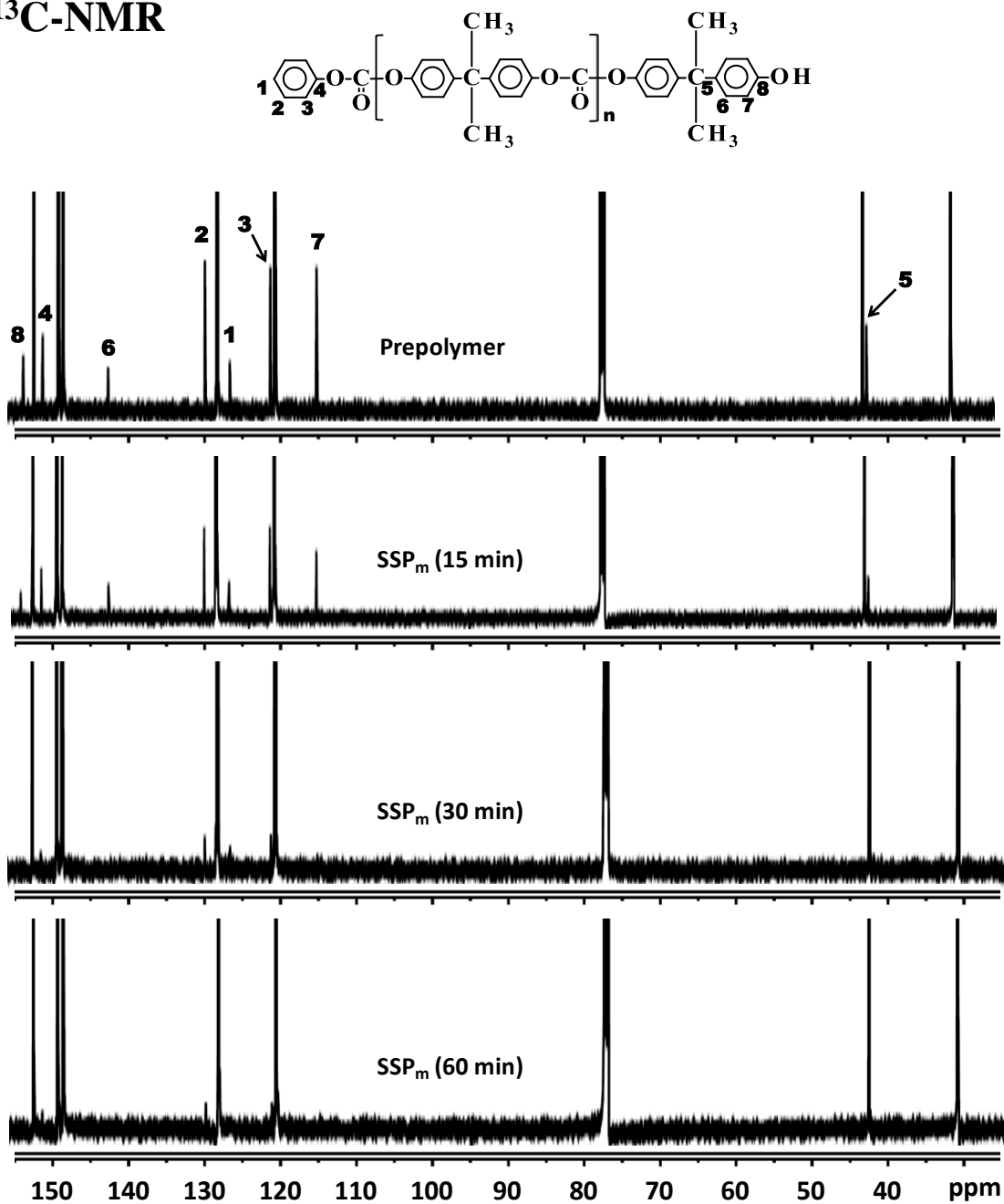


Figure 3.1 ^{13}C NMR spectroscopic analysis of the SSP_m samples at different reaction times ($T=230\text{ }^{\circ}\text{C}$, layer thickness= $10\text{ }\mu\text{m}$, prepolymer B-14k).

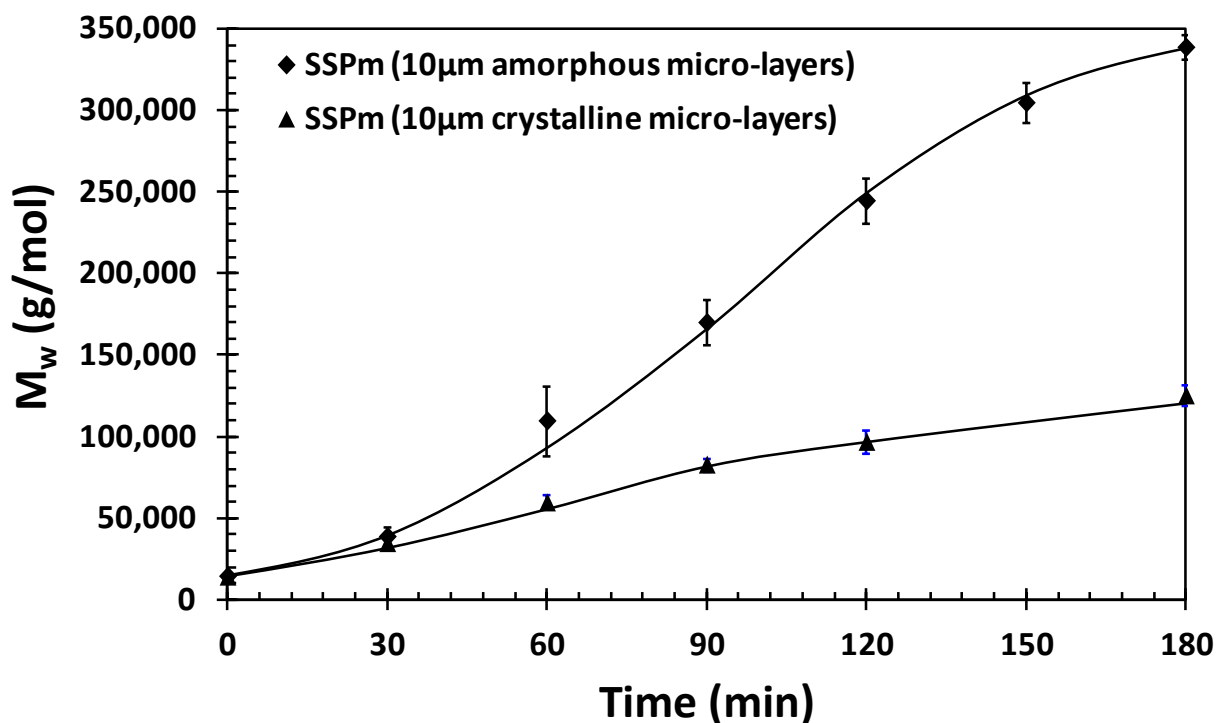


Figure 3.2 Weight-average molecular weight vs. reaction time profiles ($T=230^{\circ}\text{C}$, $P=10$ mmHg, prepolymer B-14k): (\blacklozenge) SSP_m (10 μm layer, amorphous); (\blacktriangle) SSP_m (10 μm layer, crystalline). Solid line is added to guide the eyes.

3.3.2 ^1H -NMR Analysis

The ^1H -NMR spectroscopy data of prepolymer, high molecular weight amorphous micro-layer samples at different reaction times (30min and 180min), and crystalline micro-layer sample (180min) are shown in Figure 3.3. The molecular weight of amorphous micro-layers and crystalline micro-layers of 10 μm thickness are shown in Figure 3.2. For the amorphous polymers, the aromatic regions (peak assignment 3''' at 8.0-8.1 ppm in Figure 3.3) for phenyl salicylate

phenyl carbonate (PhSALPhC, Structure B in Figure 3.4) and peak assignment 6" at 2.1-2.2 ppm (Structure C in Figure 3.5) indicate the presence of anomalous chain structures (branched and cross-linked structures) in the high molecular weight samples obtained after 30 min. Note that these peak assignments (peak assignment 3" and 6", branching and cross-linking, respectively) were absent in the low molecular weight prepolymers and crystalline micro-layers (Figure 3.2) used in our study (see Figure 3.3). In the literature, the presence of the branched units has been reported [37]. For example, the concentration of PhSALPhC structure units (i.e., branching density) in the fractionated polycarbonate samples of molecular weight (M_w) of 11,400-39,200 (g/mol) was reported to increase quasi linearly with molecular weight, suggesting that the branching units were not homogeneously distributed across the molecular weight distribution.

Although the sample molecular weights in this reference are much lower than those obtained in our experiments, we performed the following simple calculations: The data in ref. [37] can be correlated as followed:

$$Y = 0.1125M_w + 822.5 \quad (3.1)$$

Where, Y is the modified concentration of PhSALPhC (in ppm) and M_w is the weight average molecular weight (g/mol). According to this correlation, as polycarbonate molecular weight increases from 14,000 (prepolymer B-14K in our experiment) to 40,000 g/mol ($t = 30$ min), the branching unit concentration increases from 0.24% to 0.5%. If the correlation is also applied to higher MW sample (e.g., 340,000 g/mol) as observed in our study (Figure 3.2 (♦)), the calculated branching unit concentration is as large as 3.8 %, which is about 16 times the unit concentration in the prepolymer. It is to be noted that, none of the peaks in Figures 3.1 and 3.3

shows the presence of phenol, indicating that phenol was effectively removed from the polymer micro-layers.

¹H-NMR

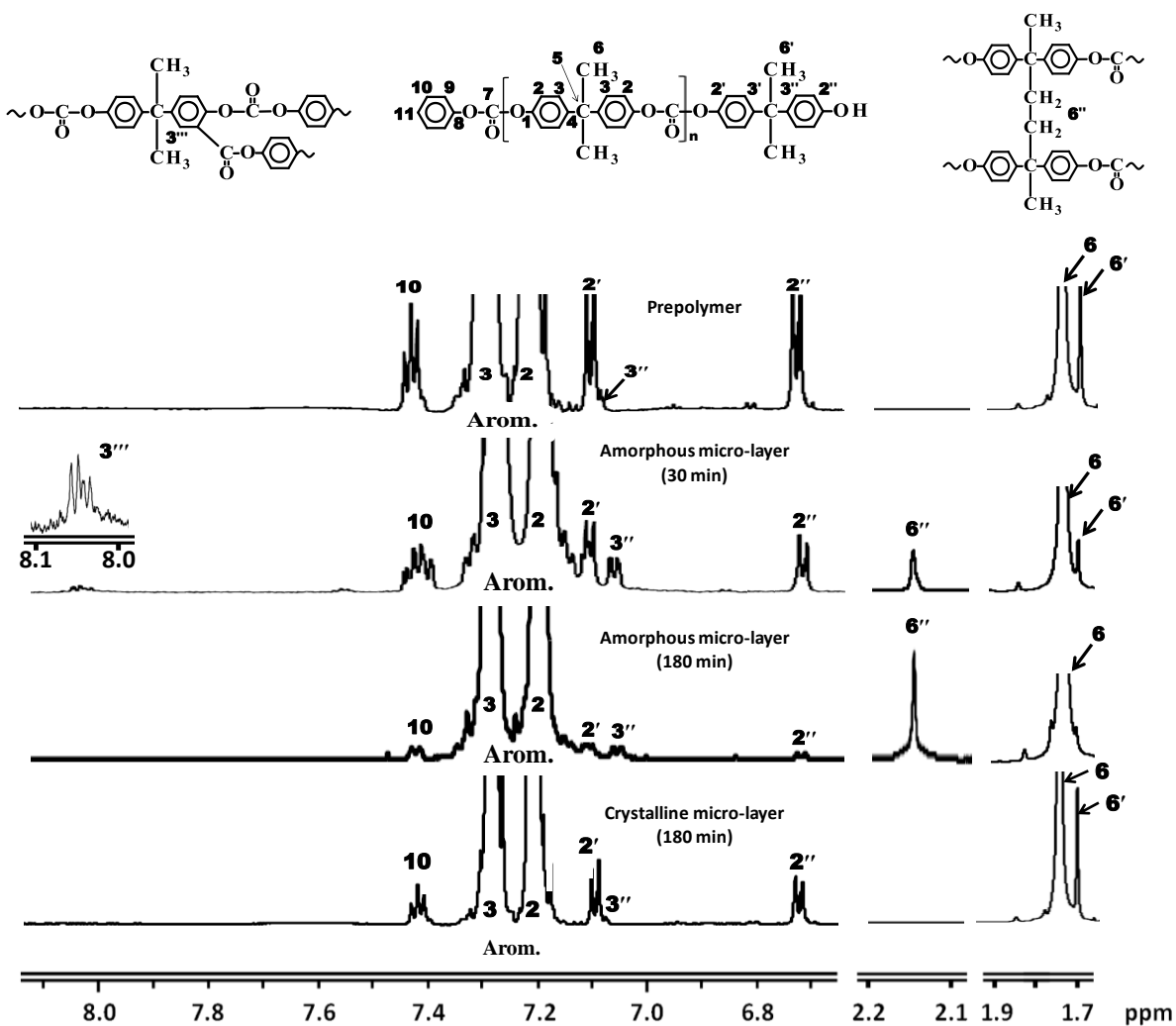


Figure 3.3 ¹H NMR spectroscopic analysis of the amorphous micro-layer ($T=230$ °C, layer thickness=10 μ m, prepolymer B-14k). Arom. indicates aromatic protons.

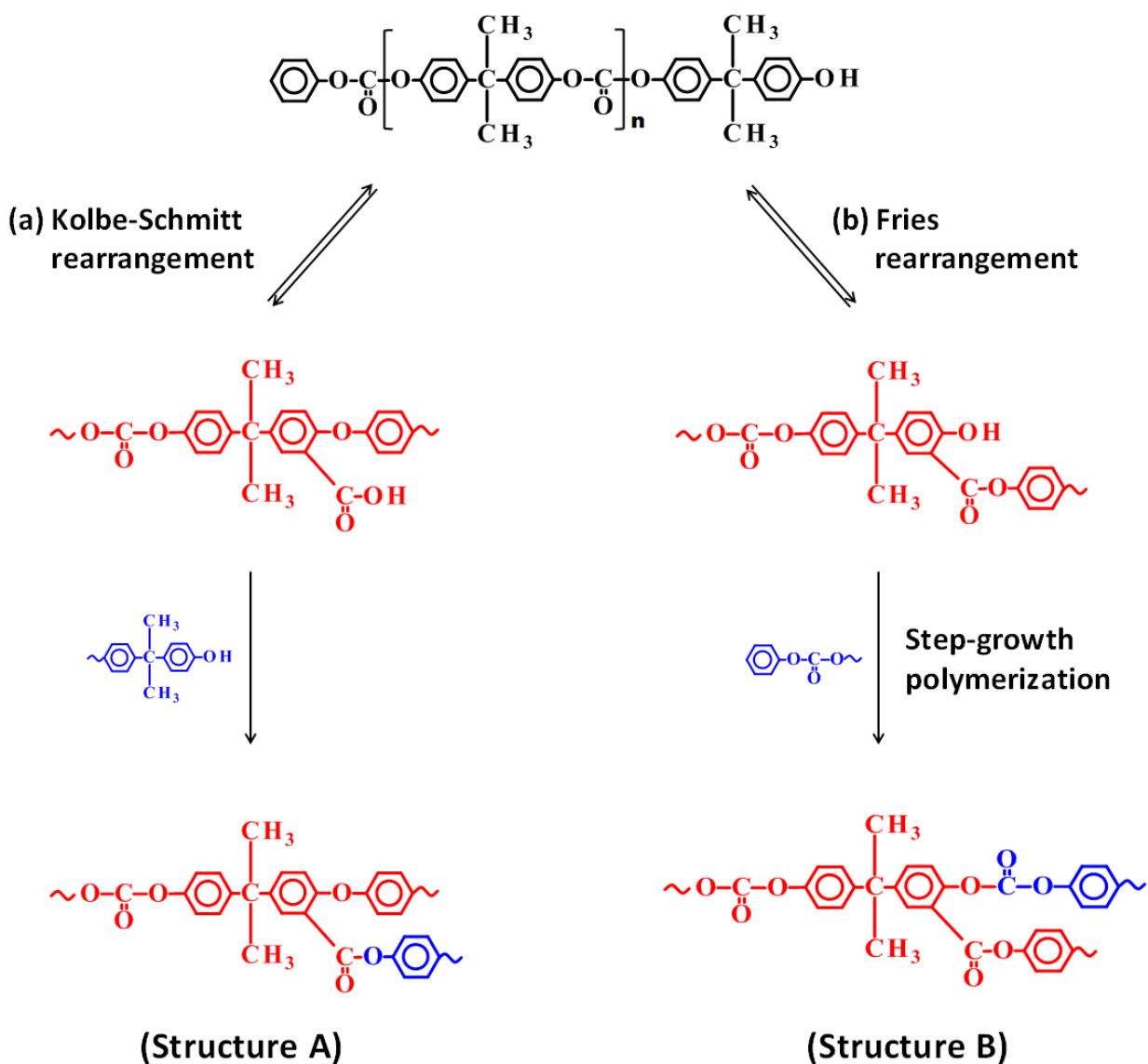


Figure 3.4 Kolbe-Schmitt and Fries rearrangement reactions leading to branched structures in polycarbonates [37, 40].

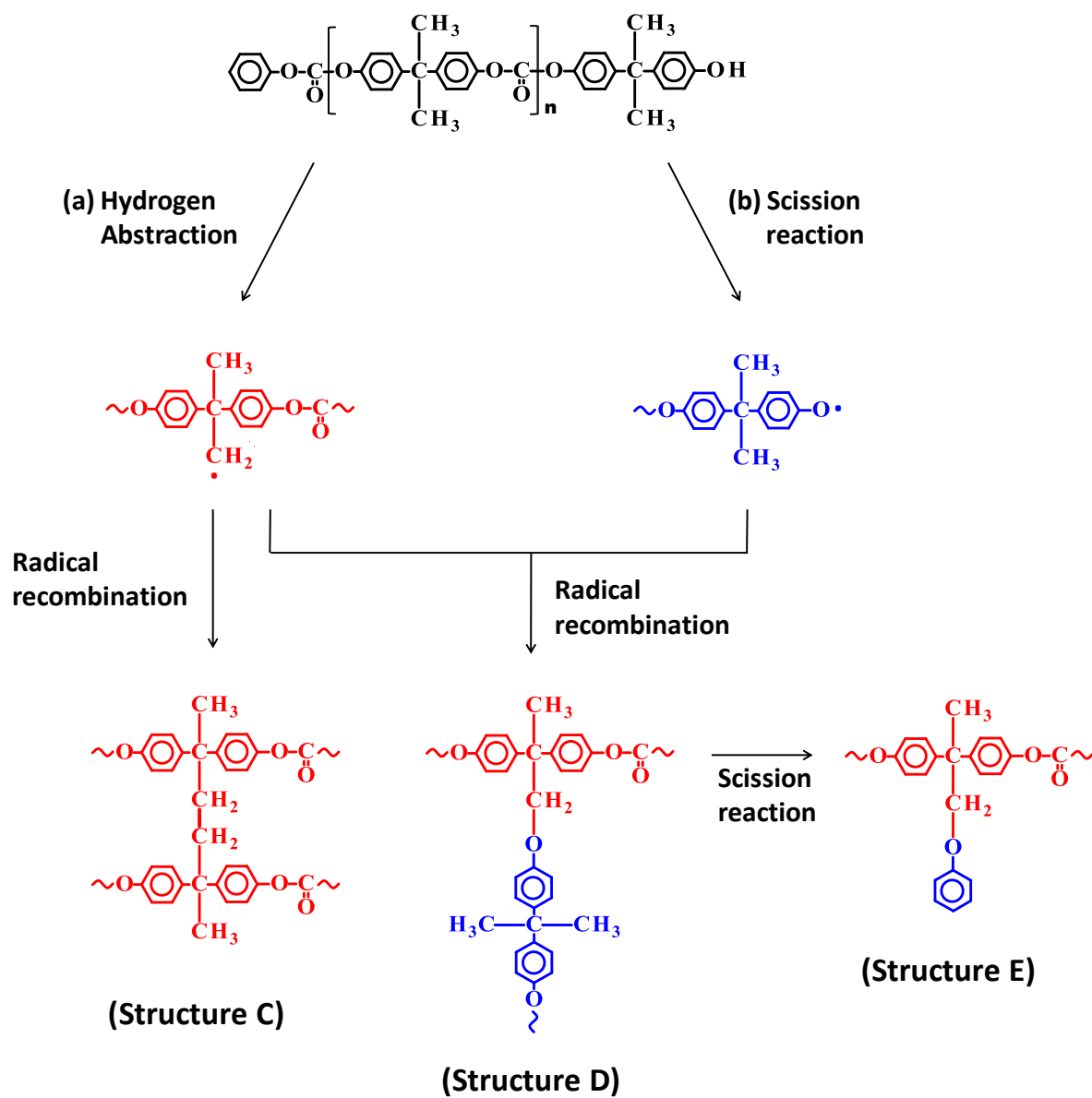


Figure 3.5 Reaction mechanisms for the formation of cross-linked polycarbonates: R^\bullet represents a macro-radical species generated in the system [40].

Another possible nonlinear chain structure in the high molecular weight BPAPC obtained in our study is a partial cross-linking. The formation of a cross-linked structure in polycarbonate during melt polymerization has been known to be possible at high reaction temperature (300-500°C) under evacuate system and it was proposed that the cross-linking can occur by radical recombination as illustrated in Figure 3.5 [40]. Note that temperature applied in our reaction system is much lower than the temperature that induces formation of cross-linking reported in the literature (i.e., 300-500 °C). The reaction scheme includes the hydrogen abstraction from a methyl group (Figure 3.5 (a)) and scission of oxygen and carbonyl linkage (Figure 3.5 (b)) to generate radicals that lead to the cross-linked structures through recombination [40, 62]. Two radical species via hydrogen abstraction and chain scission reaction can be combined either between same species or two different species to form a cross-linking Structure C and D. From the ^1H NMR analysis of amorphous micro-layers, only Structure C (peak assignment 6'' at 2.1-2.2 ppm) was confirmed.

The 6, 6', and 6'' peaks in NMR spectra were assigned using 2D heteronuclear single quantum coherence (HSQC) NMR (Bruker AV-400Mhz high resolution). As shown in Figure 3.6, the methyl protons for the repeating unit (peak 6), phenolic end group (peak 6'), and ethyl protons in cross-linkage (peak 6'') are clearly isolated. However, these peaks are overlapped in one carbon peak assignment around 31.0 ppm thus separation of carbon assignment for the cross-linkage was not obtained. Figure 3.7 shows expanded aromatic region of two-dimensional (2D) heteronuclear single quantum coherence (HSQC) (2D ^1H - ^{13}C one bond) spectrum of SSP_m PC (30min at 230°C). These peak assignments are corresponds to that of given in 3.1 and 3.3 for the ^{13}C -NMR and ^1H -NMR, respectively.

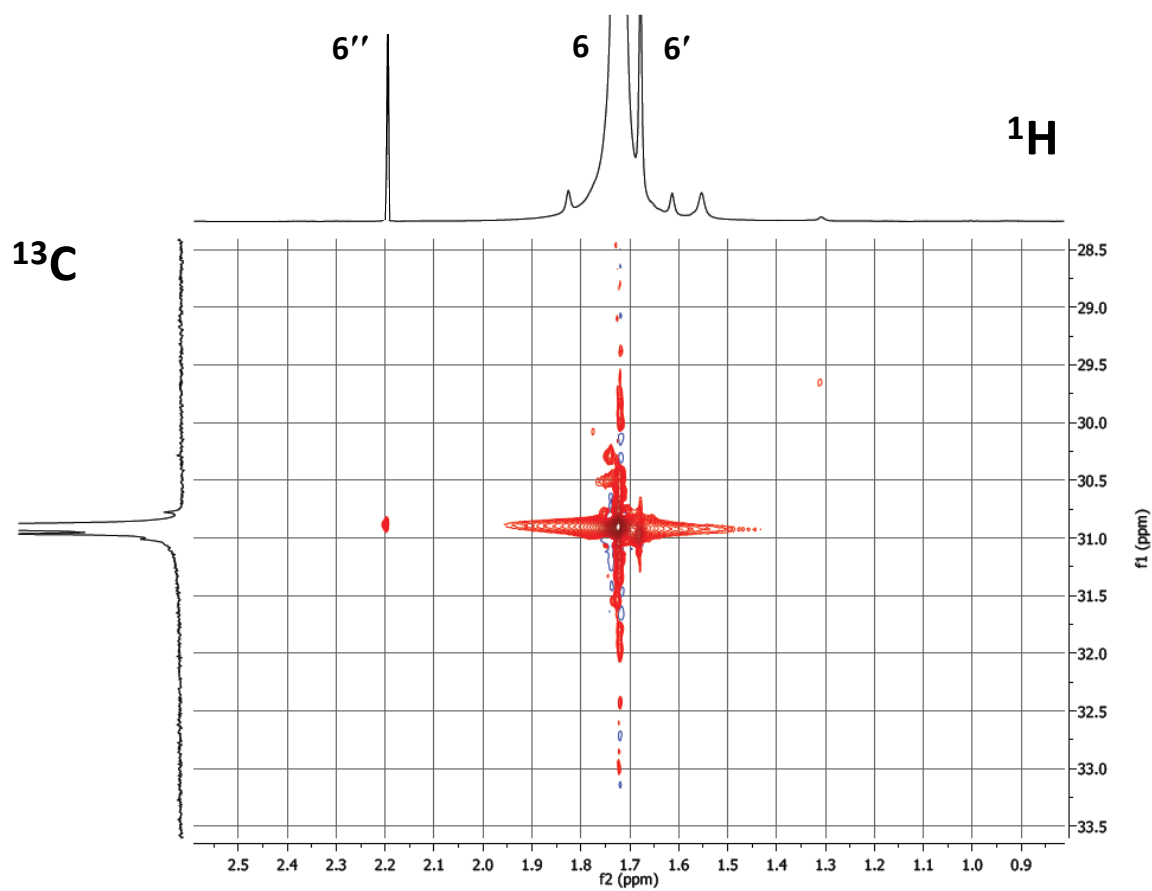


Figure 3.6 Expanded methyl group on repeating unit and phenolic groups and ethyl group on cross-linkage region of two-dimensional (2D) heteronuclear single quantum coherence (HSQC) ($2D\ ^1\text{H}-^{13}\text{C}$ one bond) spectrum of SSP_mPC (30min at 230°C).

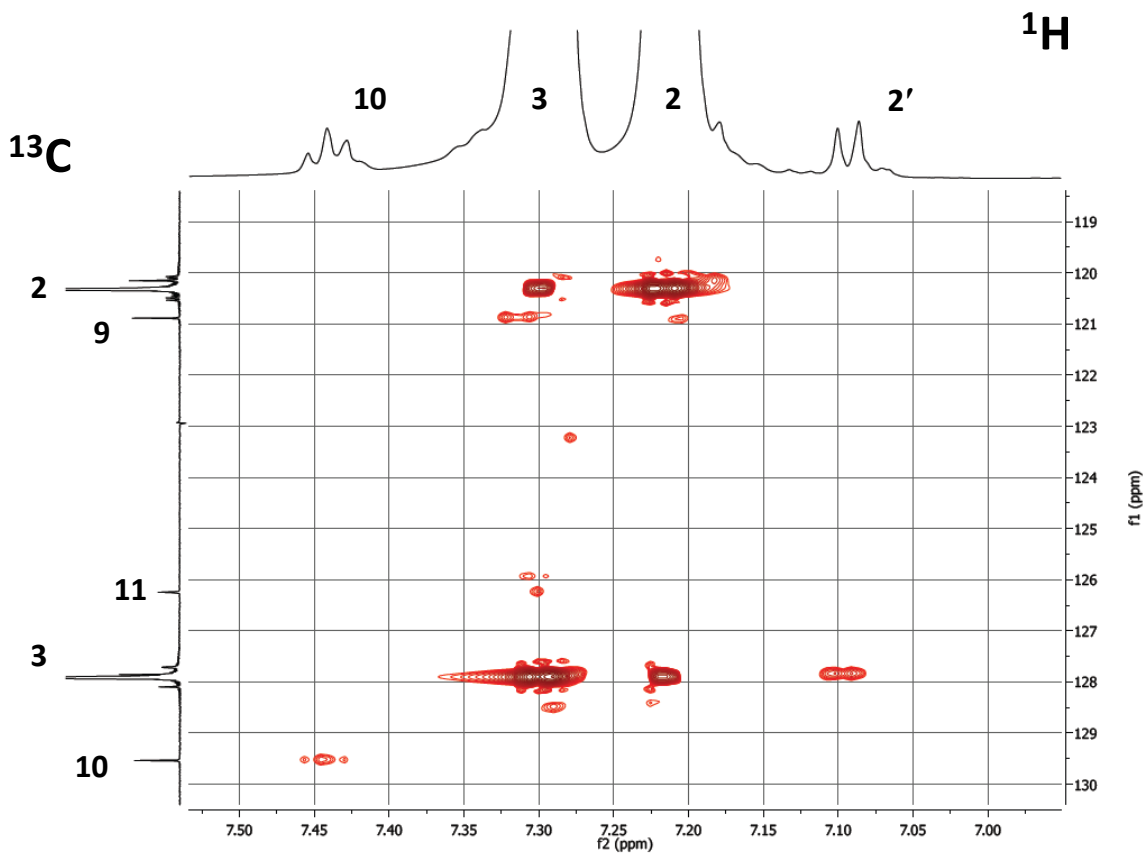


Figure 3.7 Expanded aromatic region of two-dimensional (2D) heteronuclear single quantum coherence (HSQC) (2D ^1H - ^{13}C one bond) spectrum of SSP_m PC (30min at 230°C).

The mole fractions of cross-linkages (peak assignment 6" at 2.1-2.2 ppm) in sample B-14k from amorphous micro-layers at 230 °C, estimated using the area intensity of methyl proton and ethyl proton in repeating unit and cross-linkage as followed:

$$(\text{Mole fraction of cross-linkages}) = \frac{\text{peak6}"/4}{\text{peak6}"/6 - \text{peak6}"/4 + \text{peak6}"/2} \quad (3.2)$$

The mole fractions of cross-linkages were 3.55×10^{-4} and 4.26×10^{-2} at 30 min and 180min, respectively (see figure 3.3), indicating that the cross-linkages have increased about two orders of magnitude in 180 min of solid state polymerization in micro-layers. In fact, small amount of insoluble fraction of polymer was obtained after 180 min (e.g., 4.8 wt% in 10 μ m-amorphous thickness sample). The generation of insoluble gel is probably because of the formation long-chain branched or cross-linked polycarbonate. Table 3.1 shows mole fraction of cross-linkage and generation of insoluble fraction in amorphous micro-layers (10 μ m) at 230°C.

Table 3.1 Mole fraction of cross-linkage and generation of insoluble fraction in amorphous micro-layers (10 μ m) at 230°C ($P=10$ mmHg, prepolymer B-14k).

Time (min)	10 μ m-amorphous micro-layers		
	M_w (g/mol)	Insoluble Fraction (wt %)	Mole Fraction of Cross-linkage
0	14,000	0	0
30	39,000	N/A	3.55×10^{-4}
60	109,000	2.3	8.89×10^{-4}
180	338,000	4.8	4.26×10^{-2}

Table 3.2 shows the mole ratio of methyl protons to aromatic protons in the amorphous and crystalline polycarbonate micro-layer samples at different reaction times (30 min, 60 min, and 180 min in Figure 3.2 (◆)). The ratio was obtained using the sum of area intensity of methyl protons and aromatic protons at repeating units and phenolic end groups as indicated below:

$$\left(\begin{array}{l} \text{Ratio of methyl protons} \\ \text{to aromatic protons} \end{array} \right) = \frac{\text{sum of methyl protons } 6, 6' \text{ peak area}}{\text{sum of aromatic protons } 2, 2', 2'' \text{ and } 3, 3', 3'' \text{ peak area}} \quad (3.3)$$

It is seen that the ratio remains constant in the 10 μm thick crystalline micro-layers (Figure 3.2 (▲)), while the ratio decreases with the progress of reaction when the amorphous micro-layers (Figure 3.2 (◆)) of 10 μm thickness due to the consumption of methyl protons via radical recombination reactions. If only linear step growth polymerization occurs, this ratio will remain constant but if radical recombination reactions occur (see structure C, D, and E in Figure 3.5), this ratio will decrease. The assignment of proton peaks used in equation (3.3) is provided in Figure 3.3.

Table 3.2 Ratio of methyl protons to aromatic protons in polycarbonates in partially crystallized micro-layers (10 μ m-crystalline) and amorphous micro-layers (10 μ m-amorphous) at 230 $^{\circ}$ C ($P=10$ mmHg, prepolymer B-14k).

Time (min)	Ratio of methyl protons to aromatic protons			
	10 μ m-crystalline Micro-layer	M_w (g/mol)	10 μ m-amorphous micro-layers	M_w (g/mol)
0	0.716	14,000	0.716	14,000
30	0.713	35,000	0.703	39,000
60	0.714	59,000	0.639	109,000
180	0.716	123,000	0.598	338,000

3.3.3 Pyrolysis-Gas Chromatography Mass Spectrometry (Py-GC/MS)

The formation of anomalous chain structures such as branched and cross-linked structures in the amorphous micro-layer samples has been investigated using pyrolysis gas chromatography mass spectrometry (Py-GC/MS). Py-GC/MS technique enables the characterization of macromolecular complexes and it has been found to be a very effective technique for the qualitative analysis of various condensation polymers. In this method, the polycarbonate chains in presence of tetramethylammonium hydroxide (TMAH) decompose selectively at high temperatures (e.g., 400 $^{\circ}$ C) at carbonate linkages to yield methyl derivatives

of the components for a given polymer sample. The mass spectrum of each peak provides the identity of a specific chain structure of the polycarbonate sample.

Figure 3.8 shows the pyrograms obtained by the reactive pyrolysis of the prepolymer and the amorphous micro-layer samples after 30 min of SSP_m in the presence of TMAH at 600 °C. Here, we note four peaks (1, 2, 3, 4) that correspond to anomalous polycarbonate chain structures [40]. Mass spectra of these four peaks are shown in Figure 3.9-12. These peaks 1-4 are more pronounced in the sample obtained by polymerization of amorphous micro-layers than in the prepolymer. In what follows, we shall present the analysis of these peaks and relevant reaction pathways and resulting chain structures.

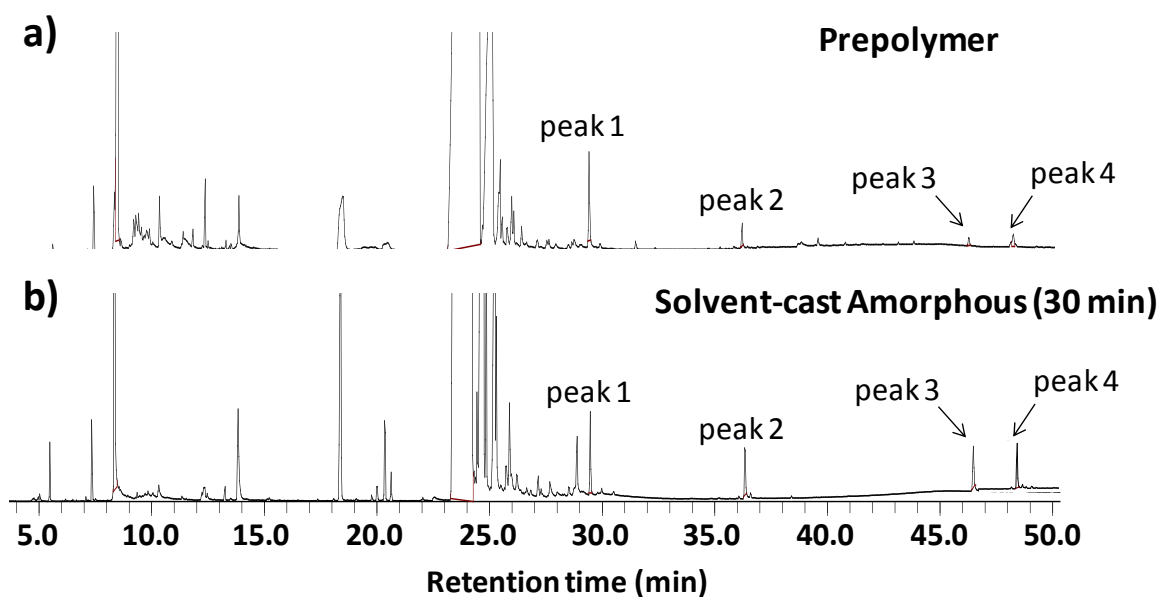


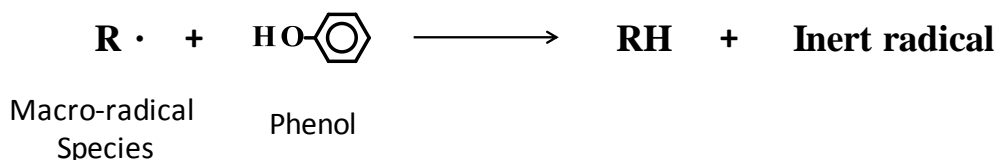
Figure 3.8 Pyrograms of prepolymer (B-14k) and amorphous micro-layer sample taken at 30 min in presence of TMAH.

Rearrangement of the carbonate group in BPAPC can form a pendant carboxyl group, ortho to an ether link, and through ester exchange reaction with another BPAPC chain, it can form branching structure (Kolbe-Schmitt rearrangement, Figure 3.4 (a)). The branching structure can also be formed by Fries rearrangement reaction (see Figure 3.4 (b)). The possibility of homolytic scission of carbonate group at high temperature between the oxygen and carbonyl group in BPAPC and hydrogen abstraction in the system can generate radicals that may lead to cross-linking reaction (see Figure 3.5) [40]. The branching and cross-linking studies on polycarbonate reported in the literature were mostly on the thermal degradation of polycarbonate in the temperature range of 300-500 °C, and this temperature is far higher than the temperature of polymerization in micro-layers employed in our study (< 235 °C).

The mass spectrum in the pyrogram (Peak 1 in Figure 3.8) corresponds to carboxylic branching structure by Kolbe-Schmitt rearrangement and Fries rearrangement reaction [37, 40]. Here, the molecular ion at m/z 314 and the base fragment ions at m/z 299 are formed through elimination of a methyl group from an isopropylidene group of the polycarbonate molecule. The fragment ions at m/z 283 and 267 are formed through elimination of a methoxy and methyl groups from the polymer (see Figure 3.9). The pendant carboxylic group in ortho-position can react with phenolic end group in BPAPC to a branching structure. Fries rearrangement (Figure 3.4) is an alternative pathway leading to another branching structure.

The reaction pathways leading to the formation of cross-linked structure shown in Figure 3.5 involve the recombination of macro-radical species generated in the system. In a bulk melt polycondensation of BPAPC, even if radicals are generated, they quickly react with phenol

which acts as a free-radical scavenger [63, 64]. R^\bullet represents a macro-radical species generated in the system.



Unlike in bulk (melt) polymerization and polymerization in partially crystallized polymer micro-layers and particles, the polymerization in amorphous polymer micro-layers provides a very efficient removal of phenol due to either very short diffusion path and absence of crystalline structure which gives extra diffusional resistance of phenol. The presence of a residual amount of casting solvent might have acted as a plasticizer also to ease the transport of phenol to the micro-layer surface by diffusion. The concentrations of residual casting solvent (chloroform) in solvent cast amorphous micro-layer samples at 230 °C were measured by gel permeation chromatography (GPC) and amount with reaction extend are: 7.51 wt.% (0 min), 1.93 wt.% (30 min), 0.98 wt.% (60 min), and 0.03 wt.% (120 min). The residual amount of solvent (chloroform) in solution casted BPAPC micro-layer was determined using GPC equipped with a refractive index detector (Waters 2414) with tetrahydrofuran (THF) as a mobile phase. Eventually, the recombination of macro-radicals may lead to the formation of cross-linked structures. In the thickness range of 5-10 μm of micro-layers, a small amount of insoluble BPAPC present in the sample (e.g., 4.8 wt% in 10 μm thickness sample at 180min) can also be regarded as an indirect evidence of cross-linked polymers. Peaks 3 and 4 (corresponding to structure C and D in Figure 3.5, respectively) in Figures 3.11 and 3.12 observed in our high molecular weight polycarbonate

samples indicate that such reactions might have occurred in the polymerization in micro-layers at 230 °C.

Peak 2 (structure E in Figure 3.5) is formed by the scission of C-C linkage between isopropylidene group and the aromatic ring of Structure D at high reaction temperature. Thus, peak 2 detected by Py-GC/MS (Figure 3.10) is a supporting evidence of structure D formed by the recombination of methylene radical and phenoxy radical. The formation of D is also confirmed by the mass spectrum of peak 4 shown in Figure 3.8.

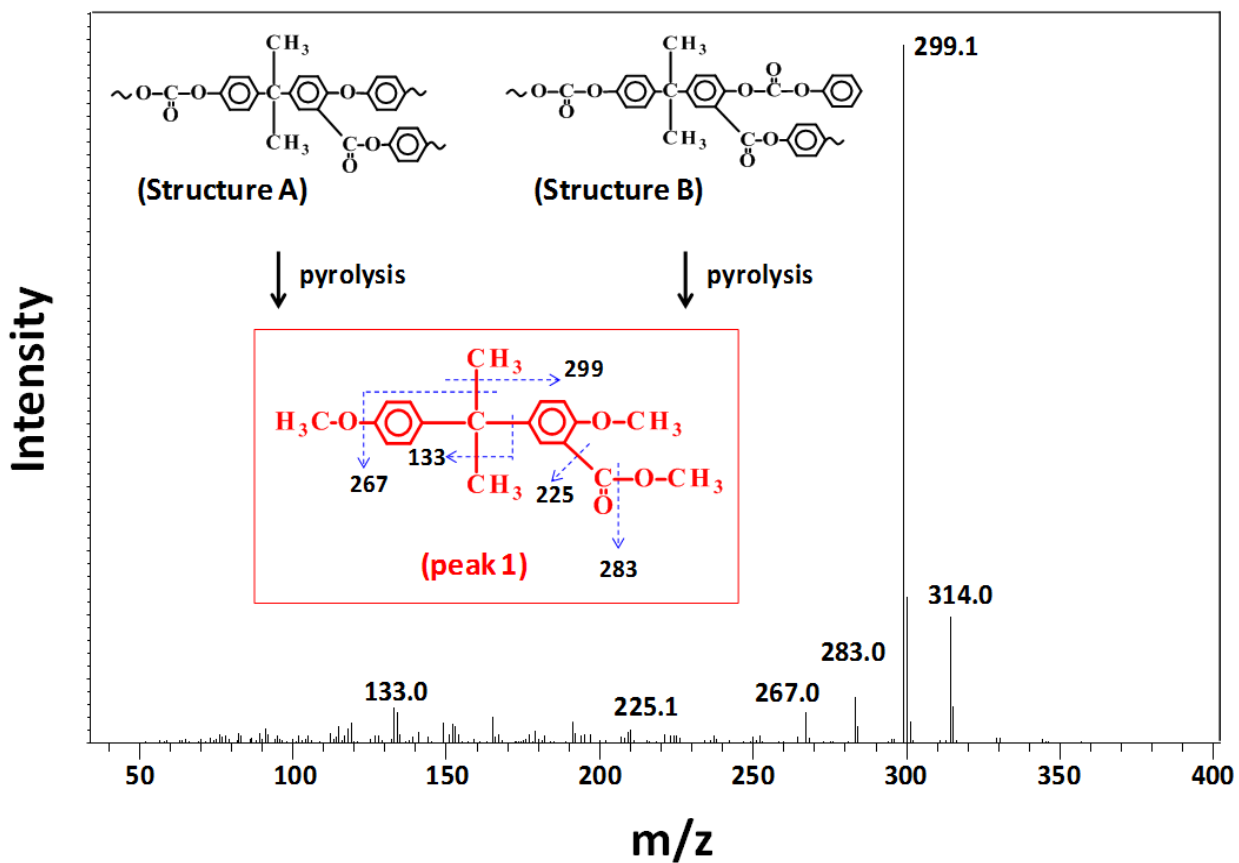


Figure 3.9 Mass spectrum of peak 1. Peak 1 generated via reactive pyrolysis from structure A and B at 600°C.

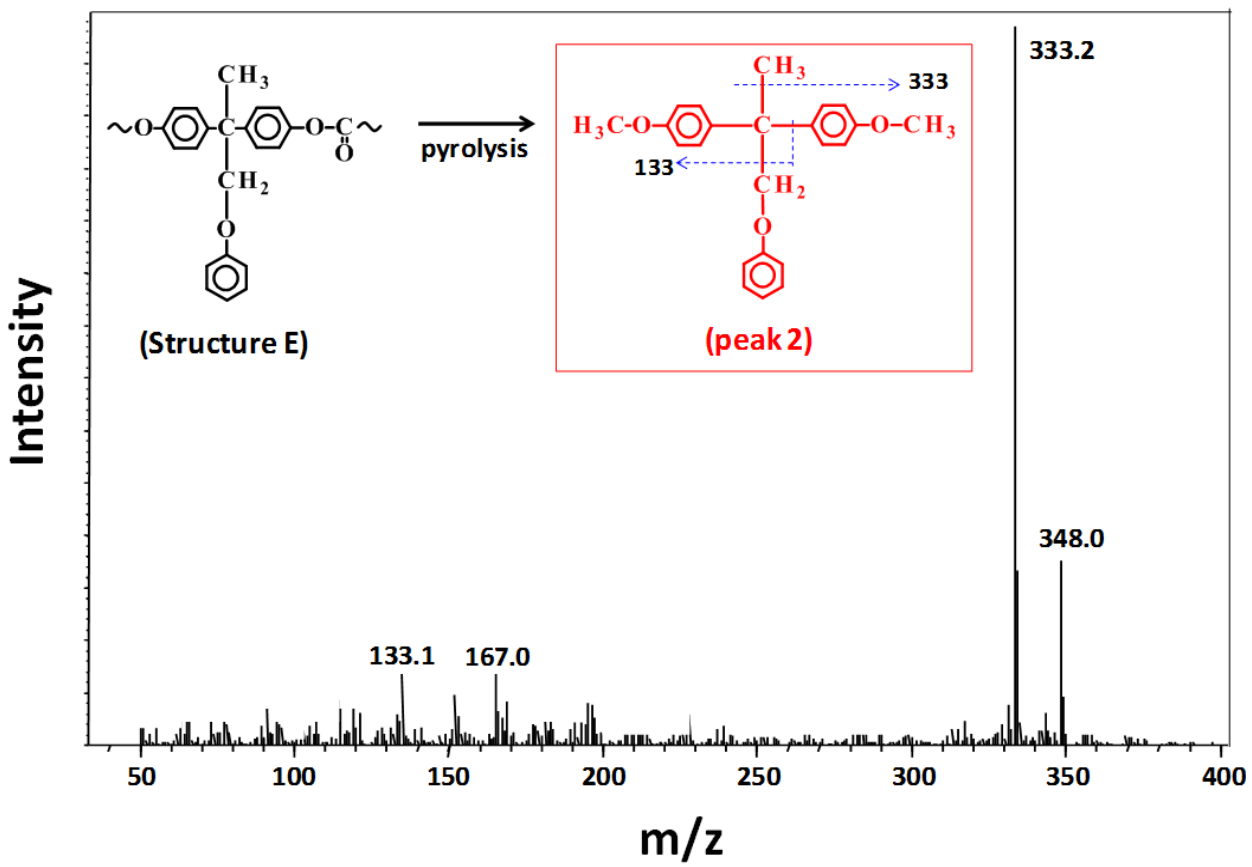


Figure 3.10 Mass spectrum of peak 2. Peak 2 generated via reactive pyrolysis from structure E at 600°C.

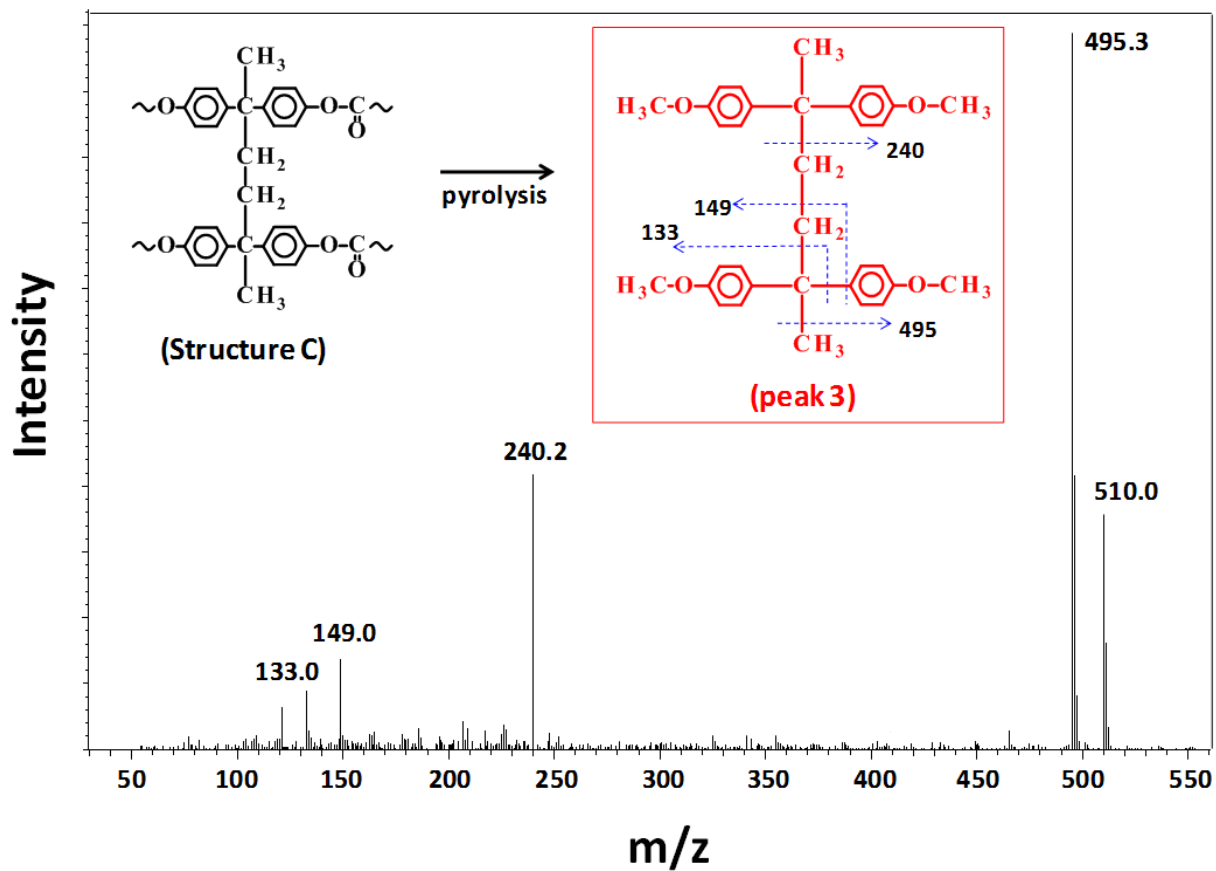


Figure 3.11 Mass spectrum of peak 3. Peak 3 generated via reactive pyrolysis from structure C at 600°C.

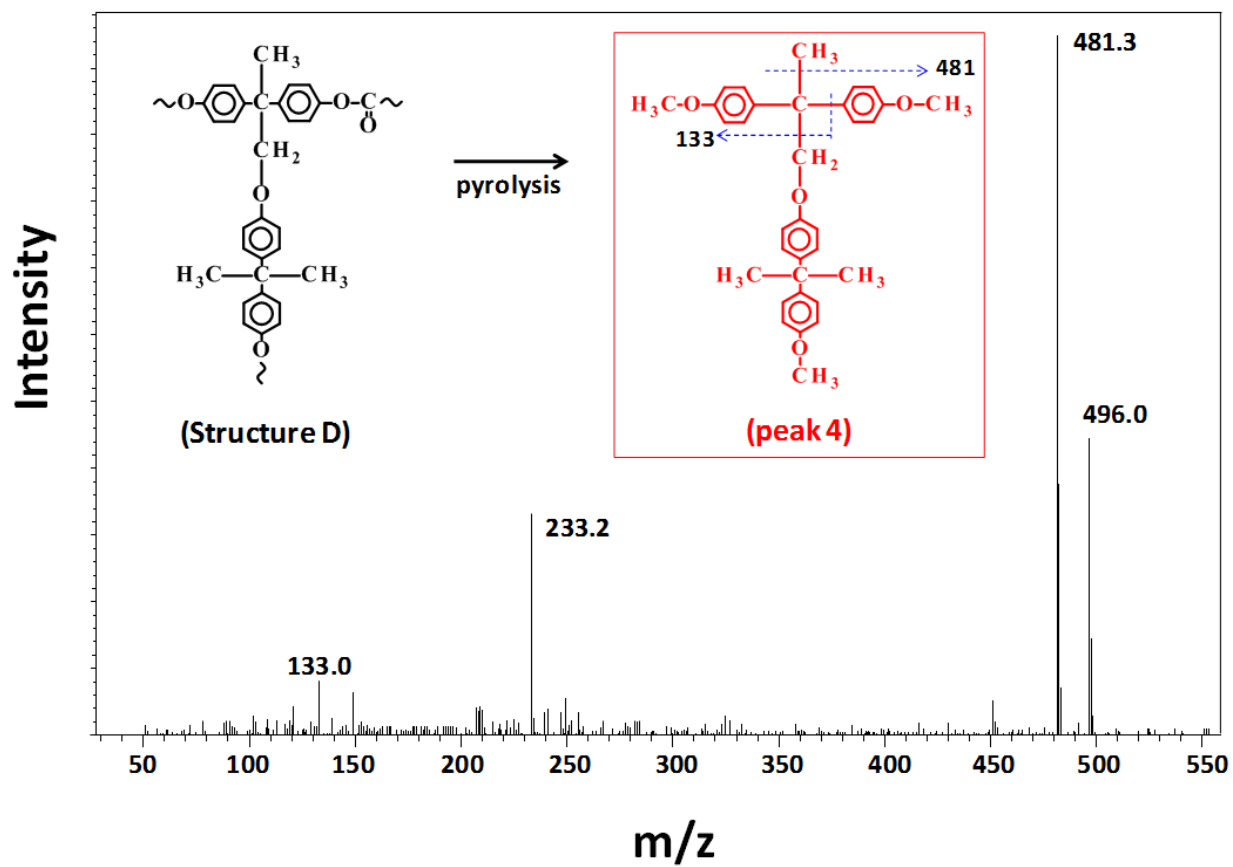


Figure 3.12 Mass spectrum of peak 4. Peak 4 generated via reactive pyrolysis from structure D at 600°C.

To identify the efficiency of phenol removal from the micro-layers, we have used a numerical simulation model provided in Chapter 2 for the amorphous and partially crystalline polymer micro-layers and the simulation results are illustrated in Figure 3.13. In the numerical simulation model, the average phenol concentrations in micro-layers are calculated by the following equations:

$$\bar{P} = \frac{1}{\delta} \int_0^{\delta} P(z) dz \quad (3.4)$$

First of all, it is seen that the phenol concentrations rapidly drops to a very small values in 5-10 μm micro-layers with a given initial phenol concentration (5.8×10^{-3} mol/L) in 14000 g/mol prepolymer,. In 1 min of SSP_m at 230°C, phenol concentrations of 5-10 μm micro-layers show $1.0\text{-}3.6 \times 10^{-4}$ (mole/L) which are about one order of magnitude lower than phenol concentrations in crystallized micro-layers and thicker micro-layers. As mentioned earlier, 35 μm thick amorphous sample shows partial crystallization during the course of polymerization and this sample does not generate insoluble fraction until 180min of reaction time (see Table 3.3). As expected, the partially crystalline micro-layers show higher residual phenol concentration. These results also suggest that the high phenol concentration due to slower diffusion in thick micro-layers and crystallized micro-layers reduce the radical induced recombination reactions and mobility of polymer chain that lead to the formation of cross-linked structures.

Table 3.3 Model simulated phenol concentration profiles ($T=230^{\circ}\text{C}$, prepolymer B-14k) depending on micro-layer thickness and state (crystalline or amorphous) and generation of insoluble fraction.

Partially Crystallized and Amorphous Micro-Layers			
Thickness (μm)	Initial Crystallinity (%)	Phenol Concentration at 1 min (mol/L)	Insoluble Fraction After 180 min
100 (crystalline)	33	3.8×10^{-3}	-
10 (crystalline)	32	1.4×10^{-3}	-
35 (amorphous)	0 *	1.5×10^{-3}	0
20 (amorphous)	-	1.0×10^{-3}	2.0
10 (amorphous)	-	3.6×10^{-4}	4.8
5 (amorphous)	-	1.1×10^{-4}	6.3

* The partial crystallization occurs during the SSP_m

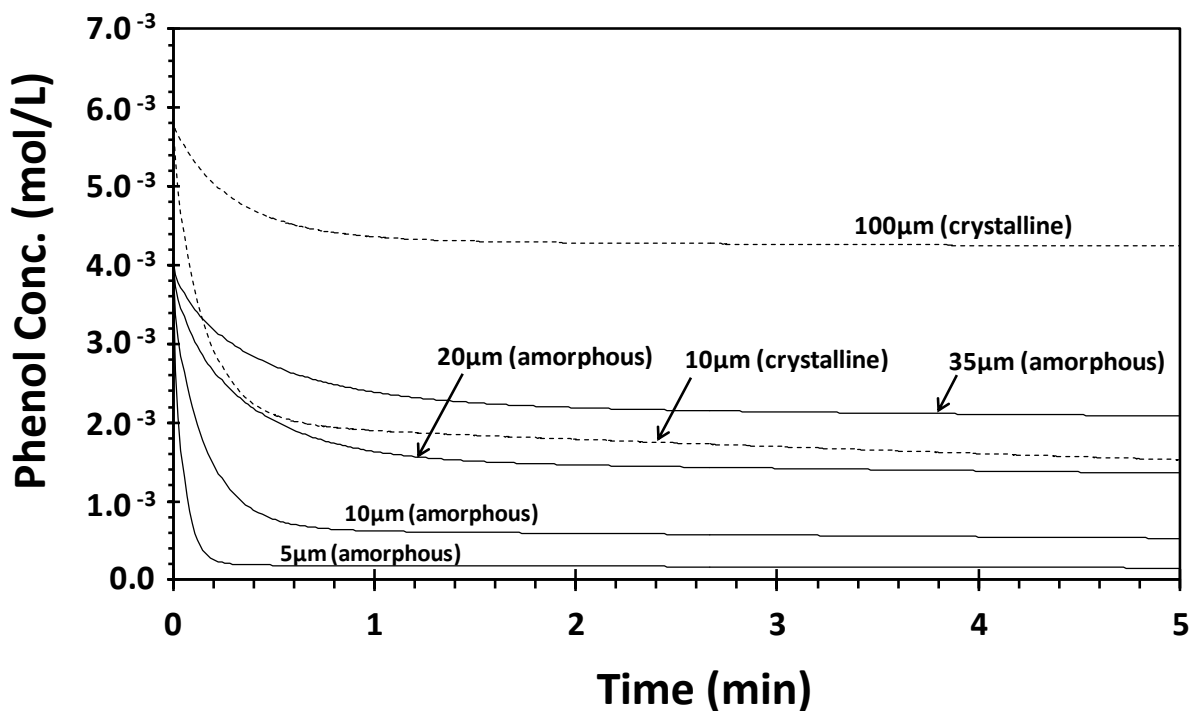
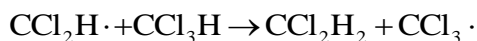
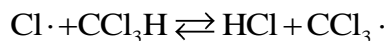


Figure 3.13 Model simulated phenol concentration profiles ($T=230^{\circ}\text{C}$, prepolymer B-14k): Solid lines represent average phenol concentration in amorphous micro-layers (5-35 μm thick); dashed lines represent average phenol concentration in crystallized micro-layers (10 μm and 100 μm thick).

The reaction pathways leading to the formation of cross-linked structure shown in Figure 3.5 involve free radicals. At high temperatures (451-526 $^{\circ}\text{C}$), chloroform decomposes to produce active chlorinated radicals as follows [65, 66]:



The concentrations of residual casting solvent (chloroform) in solvent cast amorphous micro-layer samples at 230 °C were measured by gel permeation chromatography (GPC): 7.51 wt.% (0 min), 1.93 wt.% (30 min), 0.98 wt.% (60 min), and 0.03 wt.% (120 min). Figure 3.14 shows GPC chromatograms for the residual solvent (chloroform) in prepolymer (14k) and SSP_m PCs at different reaction times. Our temperature employed in SSP_m process is far below than temperature reported for the decomposition of chloroform. Therefore, it is unlikely that the radicals are generated by the chloroform at the reaction temperature employed in this study.

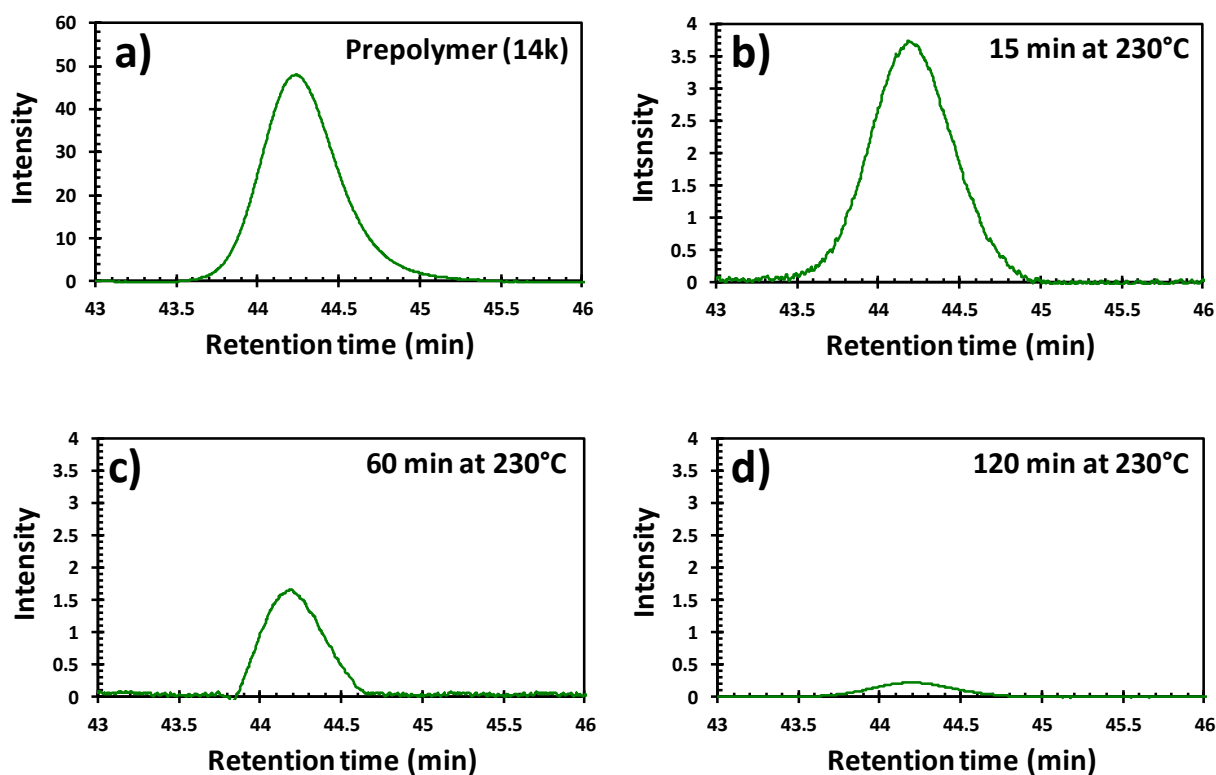


Figure 3.14 The GPC chromatograms for the residual solvent (chloroform) in prepolymer (14k) after 2hr drying and in SSP_m PCs at different reaction times. a) prepolymer, b) 15 min, c) 60 min, d) 120 min.

To evaluate the possible radical generation from solvent molecules, SSP_m experiments were carried out using different types of solvents which do not decompose or contain any radical species when they decompose at high temperature. Benzene does not decompose at temperatures below 900°C and it decomposes above 1000°C [67, 68].

N-Methyl-2-pyrrolidone (NMP) decomposes above 315°C [69]. The prepolymer having 14,000 g/mol can be dissolved in benzene and NMP as well. The decomposition temperature of benzene and NMP is far higher than the temperature used in SSP_m process. Thus, the free radicals generated from these solvents should not affect the polymerization in micro-layers. The 20g/100ml PC (14k)/benzene solution was prepared to make 10µm thick prepolymer amorphous micro-layers. To avoid solvent induced crystallization during the casting process, the PC/benzene solution and glass substrate were preheated at temperature of 90°C. For the NMP, 28g/100ml solution was prepared and glass substrate was preheated at temperature of 250°C due to a high boiling point (202-204°C). These 10µm-thick amorphous micro-layers prepared using three different solvents were polymerized at 230°C under the low pressure (10mmHg). The molecular weight vs. time profile for the amorphous using three different solvents (chloroform, benzene, and NMP) and crystalline micro-layers using two different solvents (chloroform and benzene) are shown in Figure 3.15. The molecular weights obtained from three amorphous micro-layers are very similar. Also, two crystalline micro-layers using two different solvents show very good molecular weight consistency. Figure 3.16 shows polydispersity of these samples and amorphous micro-layers have broader MWD compared to the crystalline micro-layers.

Tetrahydrofuran (THF) also used as casting solvent. Decomposition of THF occurs above the 546°C as reported in the literature [70]. The solvent induced crystallization was observed at micro-layer thickness around 10 μ m when THF used, thus SSP_m experiments were conducted using 5 μ m-thick amorphous micro-layers. 28g/100ml solution was used and glass substrate was preheated at 70°C prior to the solvent casting of prepolymer. As shown in Figure 3.17, the casting solvent (THF) does not affect on molecular weight buildup for the SSP_m process. During the course of polymerization, all amorphous micro-layers were amorphous and transparent.

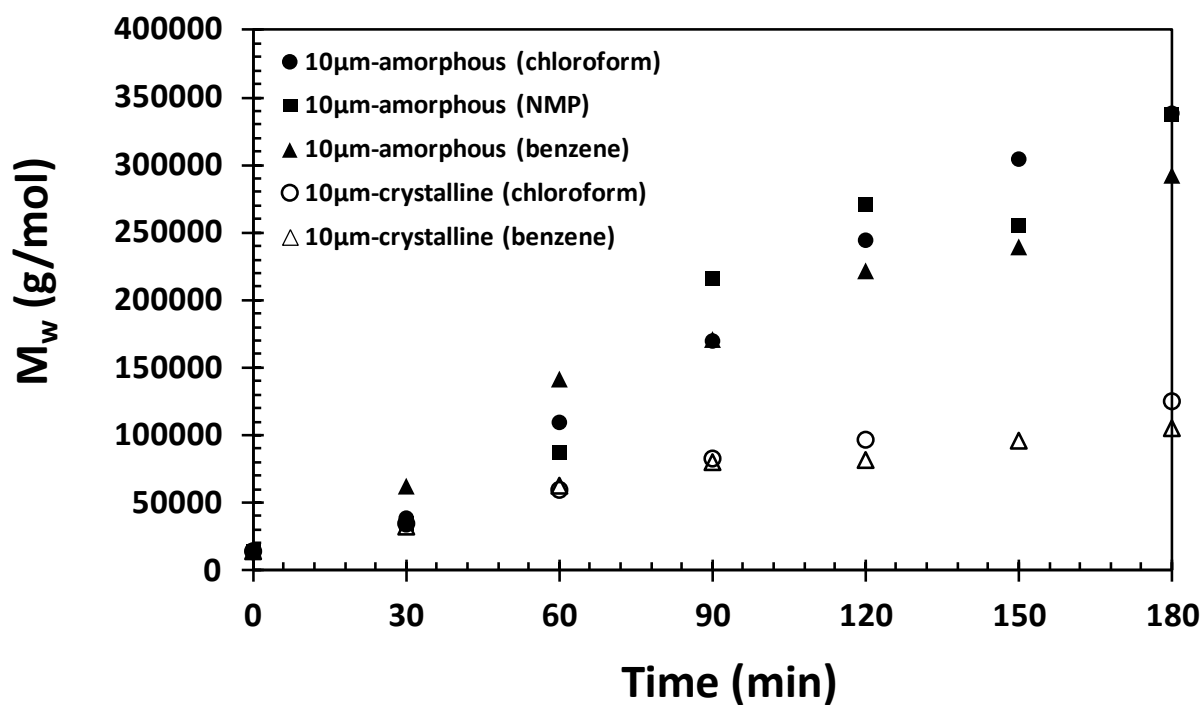


Figure 3.15 Evolution of weight average molecular weight with reaction time using three different types of casing solvents (chloroform, NMP, and benzene) ($T=230^{\circ}\text{C}$, prepolymer B-14k).

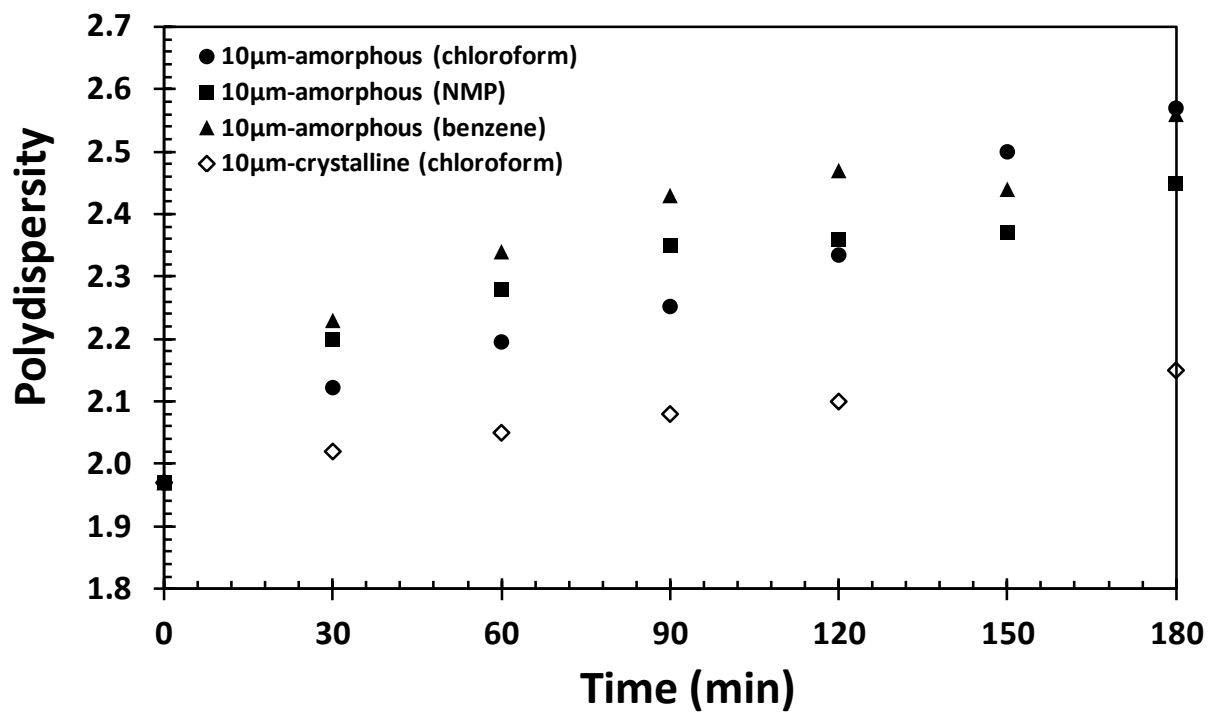


Figure 3.16 Polydispersity of amorphous micro-layers with three different type of casting solvents (chloroform, NMP, and benzene) and crystalline micro-layers with chloroform as a casting solvent ($T=230^{\circ}\text{C}$, prepolymer B-14k).

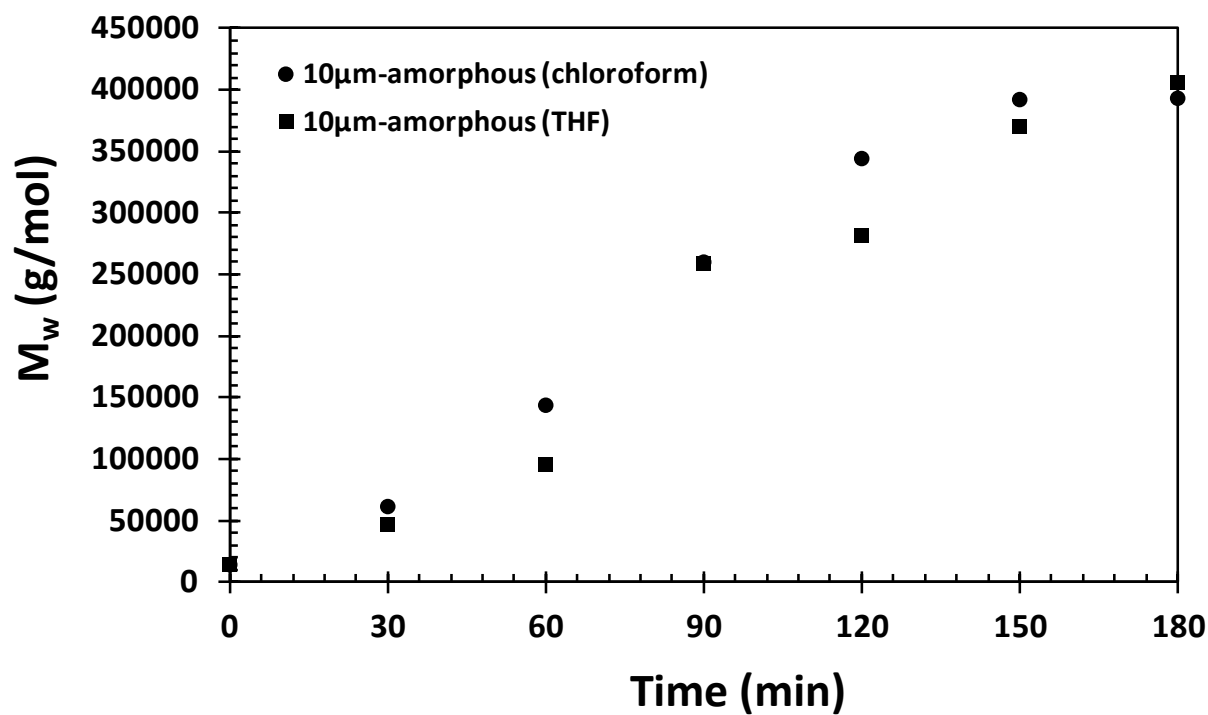
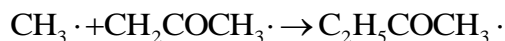
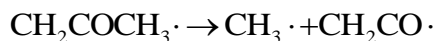
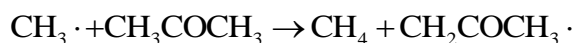
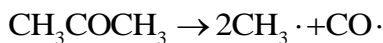


Figure 3.17 Evolution of weight average molecular weight with reaction time using two different types of casing solvents (chloroform and THF) ($T=230^{\circ}\text{C}$, prepolymer B-14k).

Effect of acetone (crystallization solvent) on SSP_m process for the crystallized micro-layers was investigated. Decomposition of acetone was studied at 570°C as follows [71]:



The experiment was carried out with micro-layers having two different solvent drying time and conditions. As shown in Figure 3.18, the swelling solvent agent for the crystallization do not affect on molecular weight buildup for the SSP_m process.

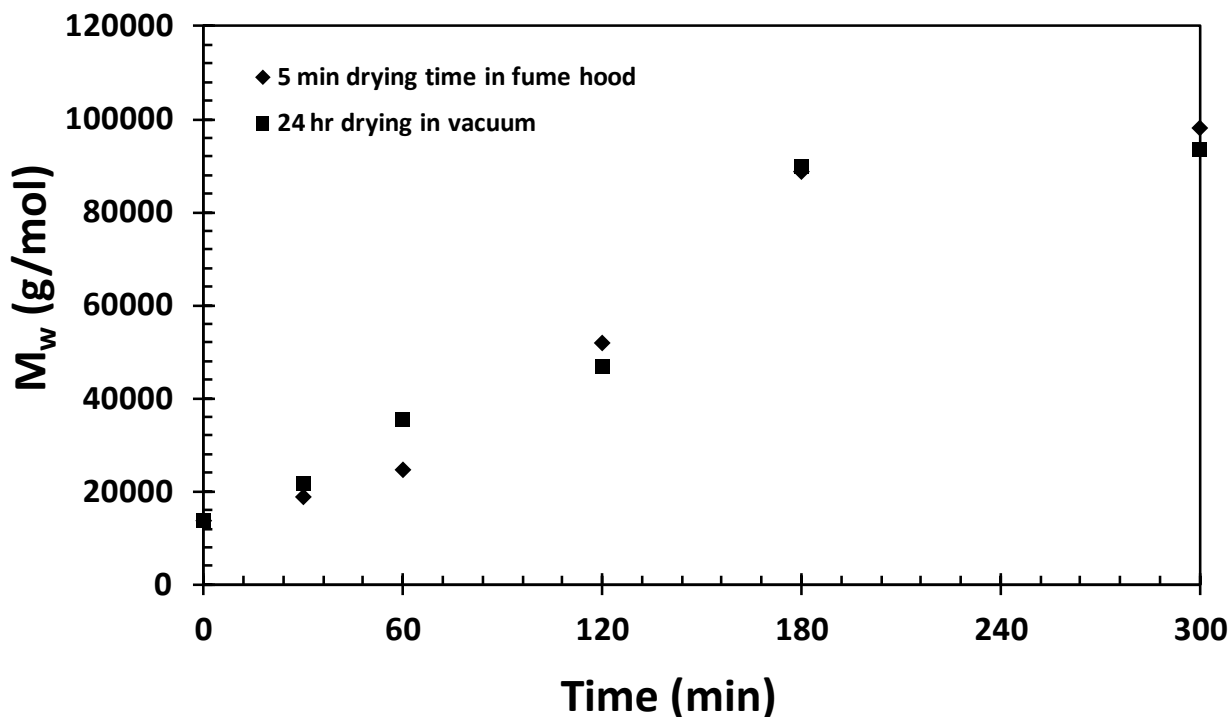


Figure 3.18 Effect of acetone on SSPm for the crystalline micro-layers ($T=230^\circ\text{C}$, prepolymer B-14k).

3.3.5 Atomic Force Microscopy (AFM) Analysis

The branched and/or network structures of the insoluble polymers confirmed by $^1\text{H-NMR}$ analysis and Py-GC mass spectroscopy were further analyzed using atomic force microscopy (AFM) (Veeco D-3000 AFM). The polymer sample was a $10\mu\text{m}$ -thick amorphous micro-layer polymerized at 230°C for 30 min. To prepare for an AFM analysis, a very dilute polymer solution (10 ppm solution in chloroform) was made and dropped onto the interface of water and air. After complete evaporation of the solvent from the surface, a polymer film formed was carefully removed from the interface and transferred onto a mica surface. Similar technique is reported to obtain an image of single molecules [72-76]. We used a tapping mode with the scan rate of 0.5 line/s. AFM images were obtained using Hi'RES-C14/Cr-Au probe of 1 nm radius (MicroMasch) at a resonance frequency of 160 kHz with the force constant 5.7N/m. Figure 3.19 shows the AFM images of the polycarbonate molecules.

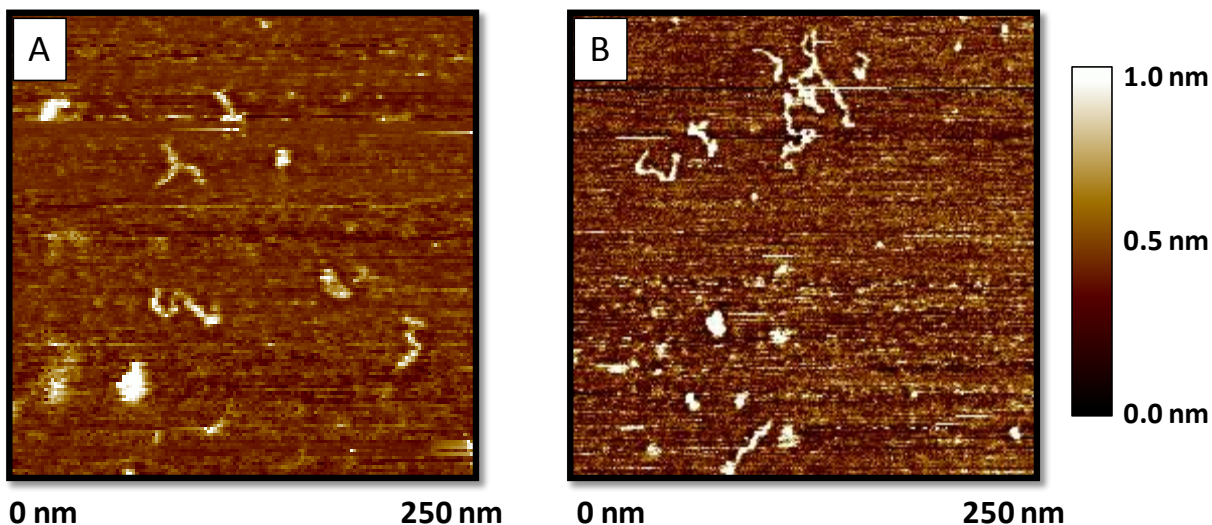


Figure 3.19 AFM images of single polycarbonate molecules. The AFM samples were prepared using Langmuir-Blodgett technique.

Some aggregated molecules and linear polymers are seen in Figure 3.19 A and B, but a nonlinear structured polymer is also clearly seen and it has a Y-branch shape with each branch length of 20 nm, 22 nm, and 25 nm. The length of a polycarbonate chain with 10 repeat units and molecule diameter calculated using Accelrys Materials Studio Visualizer® is 7.86 nm and 0.97 nm, respectively. Figure 3.20 shows linear polycarbonate with 10 repeating units obtained using visualizer software. If this value is applied to the polymer chain (branched polymer), then each branch segment has a chain length of 25, 28, and 32 repeat units per segment, respectively. These values are similar to those of obtained from commercial branched polycarbonate using tri-functional agents [77]. It is noted that the branched polymer molecule shown in Figure 3.19 may not be the most representative image of all the branched polymers formed in our experiments.

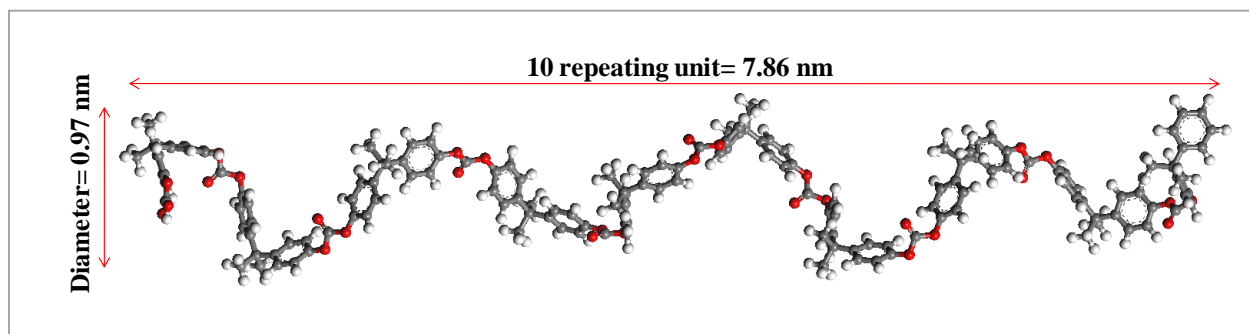


Figure 3.20 Accelrys Materials Studio Visualizer® Software provide diameter of linear PC (0.97 nm) and length of polymer chain in 10 repeating unit (7.89 nm).

In Figure 3.19, we used the Langmuir-Blodgett technique to visualize the SSP_m PC single molecules. We also use spin coating technique to prepare thin layers on the mica surface with very dilute solutions (0.05mg/L) using chloroform. A 0.1ml of dilute solution was dropped onto the mica surface and spincoater (Speedline Technologies, Model P6700 series) rotation rate was set to 200 rpm for 2 min to give enough time to evaporate solvent from thin polymer layers. The similar technique has been reported in the literature to obtain the images of single molecules [78, 79].

Figure 3.21 shows height and phase images of 60 min (A1 and A2 in Figure 3.21) and 180 min (B1 and B2 in Figure 3.21) samples. All images of the spin-coated samples show globular shapes. It has been reported that results of 2D coil or 3D compressed globules on a substrate depends on surface characteristic, contribution of nonelectrostatic interactions with substrate, and solvent quality [80]. The sample for longer reaction time (180 min) show larger globules than shorter reaction time sample (60 min) which has lower molecular weight and also lower degree of cross-linking.

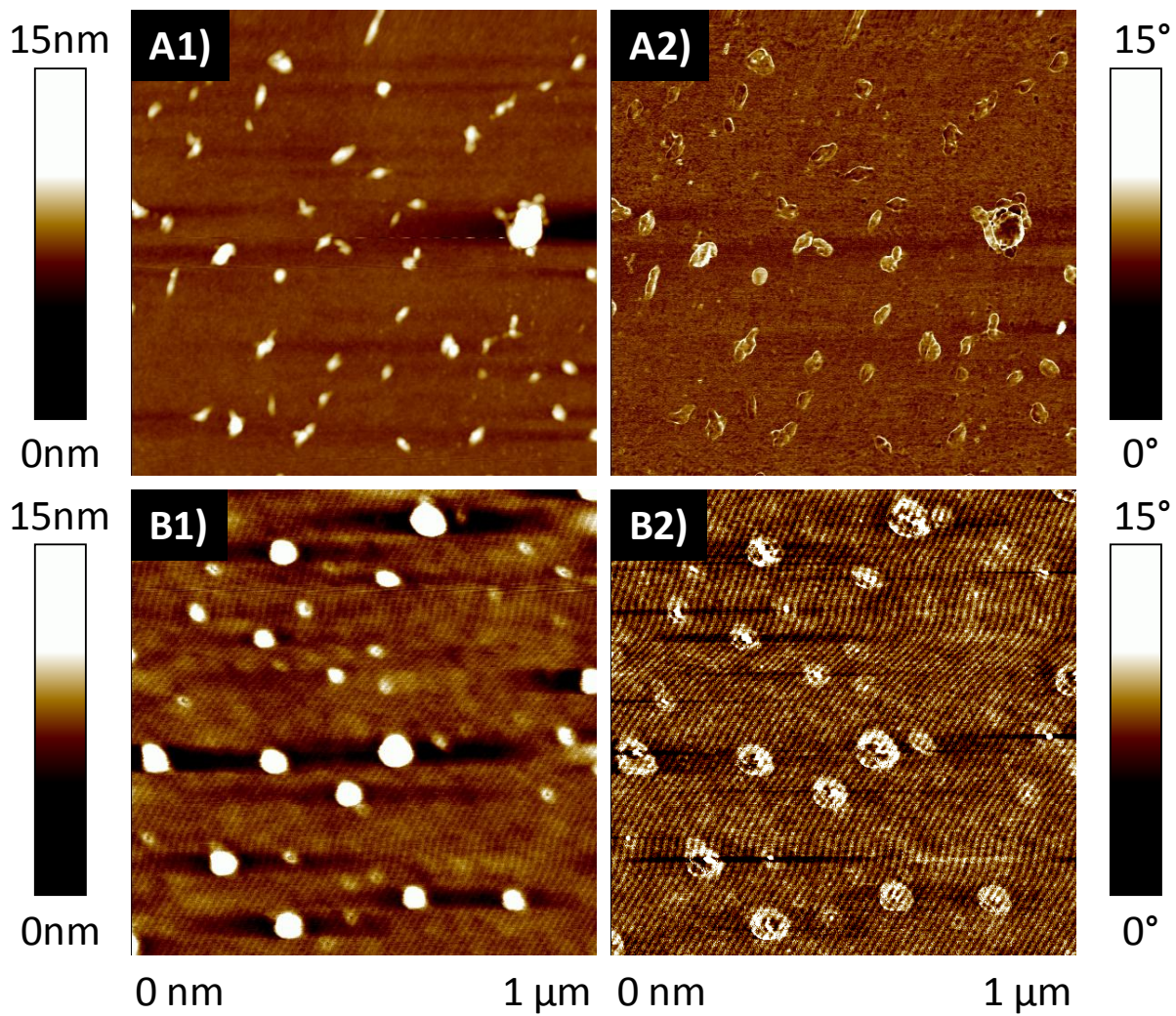


Figure 3.21 The SSP_m PC molecules on the mica surface. The height and phase images for the 60min (A1 and A2) and 180 min (B1 and B2) samples. The AFM samples were prepared using spin coating technique at 2000rpm.

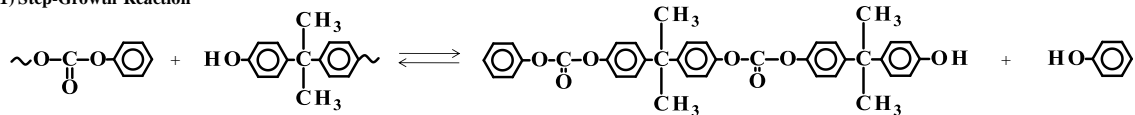
3.4 Conclusions

In Chapter 2, we have presented new experimental results on the polymerization of BPAPC in micro-layers to ultra-high molecular weight polymers in very short reaction time when amorphous prepolymer micro-layers of thickness smaller than 35 μm were polymerized at 230 $^{\circ}\text{C}$. The amorphous micro-layers exhibited faster increase to ultrahigh molecular weight (300,000-600,000 g/mol) than the partially crystallized micro-layers. The end group mole ratios of the prepolymer samples used in our study deviated from the stoichiometric ratio of 1.0 and hence, Chapter 3 is focused on finding the mechanisms that can lead to the formation of such high molecular weight polymers.

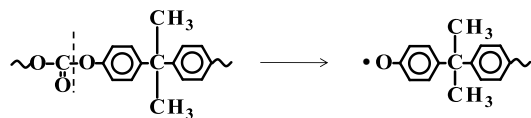
The ^{13}C NMR and ^1H NMR analysis as well as Py-GC/MS spectrometry have shown that a fair amount of anomalous polymer microstructures such as branching and partial cross-linking are present in the high molecular weight polymers. The presence of branched polymer molecules was also observed by atomic force microscopy. If the polycarbonate chain length of 10 repeating unit obtained using Accelrys Materials Studio Visualizer[®] is applied to the polymer chain (branched polymer), then each branch segment has a chain length of 25, 28, and 32 repeat units per segment, respectively. We proposed a hypothesis that intermolecular rearrangement reactions (Kolbe-Schmitt rearrangement and Fries rearrangement reactions) and radical recombination reactions might have led to the formation of non-linear chain structures. At the reaction temperature ($< 235^{\circ}\text{C}$) of our reaction system applied using amorphous micro-layers, the cross-linked structure is not reported in the literature. In the step-growth polymerization process, the byproduct, phenol, acts as radical scavenger is reported. The rapid removal of

phenol (radical scavenger) from thin micro-layers is believed to have promoted the formation of partial cross-linking. We have also observed that a small amount of insoluble polymer was present, which indirectly suggests that the cross-linking reaction might have progressed only partially so that the polymer was still mostly soluble in chloroform. A very small amount of branching and insoluble gels in low molecular weight linear polycarbonate is known to have adverse effects on the polymer quality and hence they need to be removed after reaction processes. The ultra-high molecular weight polycarbonates with branching and partial cross-linking structures are readily soluble in a solvent (chloroform). It suggests that the ultra-high molecular weight polycarbonate with nonlinear chain structures obtained in our study might be an interesting new type of polycarbonate. Figure 3.22 shows summary of reaction mechanisms for SSP_m in an Amorphous Polymer Micro-Layers.

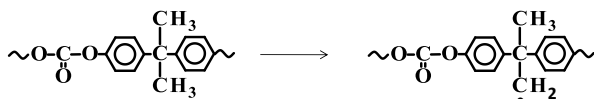
(1) Step-Growth Reaction



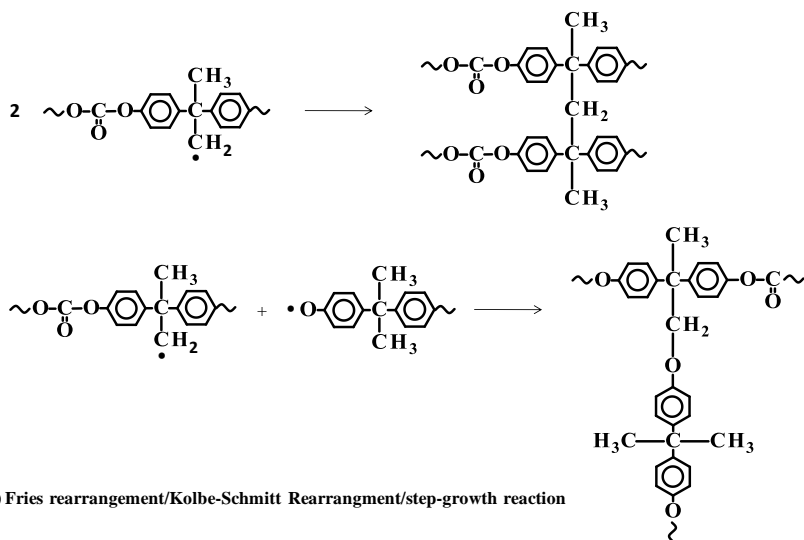
(2) Generation of Macro-Radicals by Scission Reaction



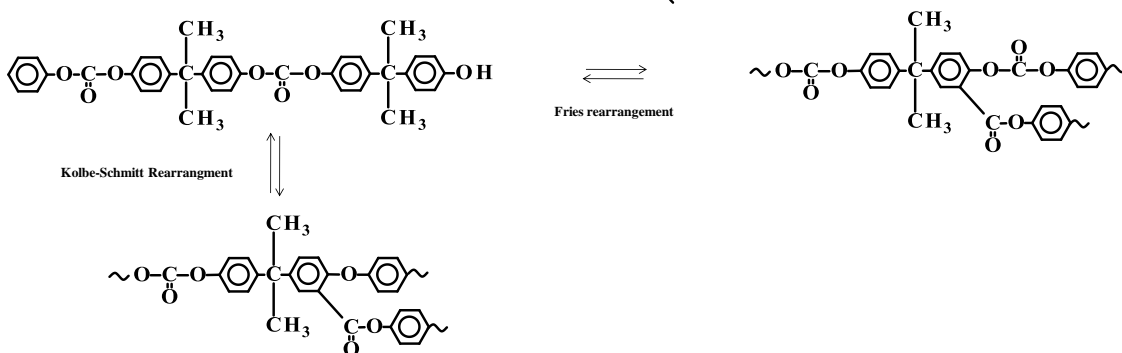
(3) Generation of Macro-Radicals by Hydrogen Abstraction



(4) Recombination of Radicals



(5) Fries rearrangement/Kolbe-Schmitt Rearrangement/step-growth reaction



(6) Free-radical inhibition reaction



Figure 3.22 Summary of kinetic mechanism for a SSP_m in an amorphous polymer micro-layers.

Chapter4: Formation of Insoluble Amorphous Polycarbonate Synthesized in Micro-Layers

4.1 Introduction

Bisphenol A polycarbonate (BPAPC) is an important material in many applications such as automotives, electronic displays, data storage, medical, environmental, energy, and aerospace industries [1]. The high glass transition temperature ($\sim 150^{\circ}\text{C}$), optical clarity (88-96 % light transmission of visible light), and exceptional impact resistance are the major merits of polycarbonates [2, 3]. Although linear BPAPCs have many outstanding properties, relatively poor solvent resistance, low surface hardness and low scratch resistance are disadvantages of current commercially available linear bisphenol A polycarbonate [81, 82].

A small amount of insoluble gel produced as a side product with severe discoloration is generated during the melt polycondensation process at high decomposition temperatures ($> 300^{\circ}\text{C}$) under low pressure [18-21, 59]. At lower temperature ranges ($< 300^{\circ}\text{C}$), very minor fraction of insoluble gel is formed [40, 83]. Table 4.1 shows formation of insoluble PC at high reaction temperature. It is known to pendant carboxyl group, ortho to an ether link, via thermal rearrangement reaction react with another PC to form an insoluble polymer gel. At high temperatures, decomposition of diphenyl carbonate results in 2-phenoxybenzoic acid [19].

Table 4.1 Formation of insoluble fraction at high temperature [40].

Sample	Preparation Method	M_n	M_w	M_w/M_n
PC-1	Melt Polymerization	1.3×10^4	3.2×10^4	2.5
PC-2	Insoluble fraction in CHCl_3 for thermally treated PC-1 at 300°C	-	-	-
PC-3	Soluble fraction in CHCl_3 for thermally treated PC-1 at 300°C	1.8×10^3	1.2×10^4	6.7
PC-4	Solvent Method	2.3×10^4	5.8×10^4	2.5

Also, Mcneill et al. [41, 84] and Montaudo et al. [60, 85-87] investigated the thermal decomposition of BPAPC at high temperature. In both studies, they observed the formation of fractionated insoluble gel when PCs undergo thermal decomposition at high temperature range of $300\text{-}700^\circ\text{C}$. However, they proposed different mechanisms for the branched and cross-linked structures. Mcneill et al. used IR spectroscopy and GC-MS to identify the decomposition products [41, 84]. They postulated that homolytic scission between the isopropylidene and the aromatic ring produce macro-radical species followed by end-biting reaction resulting in cyclic dimers. The formation of polymer radicals via hydrogen abstraction from a methyl group can form a cross-linking structure when two macro-radical species are recombined [41, 84]. However,

Montaudo et al. [60, 85] hypothesized that cross-linked structures can be obtained by intermolecular ester exchange processes to form a pendant carboxyl groups which undergo esterification rather than homolysis scission reactions [42, 60, 85-87]. Although their hypotheses on the formation of insoluble gels are different, insoluble gel is obtained at similar reaction conditions:

- (i) Higher temperatures (300-500°C) than normally applied in commercial polycondensation process.
- (ii) Reactions conducted at lower pressure (0.01-20 mmHg).

However, in both studies, direct evidence of pyrolytic products for the cross-linking structures was not identified.

Recently, Oba et al. investigated the pyrolysis products using pyrolysis gas chromatography technique and successfully identified pyrolysis products via ester exchange and hydrogen abstraction [40, 56, 88-90]. In this study, both thermal rearrangement and hydrogen abstraction were confirmed. Py-GC/MS technique enables the characterization of macromolecular complexes and it has been found to be a very effective technique for the qualitative analysis of various condensation polymers. In this method, the polycarbonate chains in the presence of tetramethylammonium hydroxide (TMAH) are decomposed selectively at high temperatures (e.g., 400 °C) at carbonate linkages to yield methyl derivatives of the components for a given polymer sample. Because of the insoluble nature and discoloration, these insoluble products are regarded as side products. Thus far, researches on these phenomena have been done in order to avoid the formation of insoluble fractions during the melt process.

In Chapter 2, we investigated the reaction mechanism for the formation of nonlinear structures (i.e., branched and cross-linked structure of polycarbonate) and fast build-up of molecular weight in soluble fractions even at a lower temperature range (<235°C) than temperatures generally applied to obtain an insoluble gel. The reaction scheme is shown in Figure 4.1.

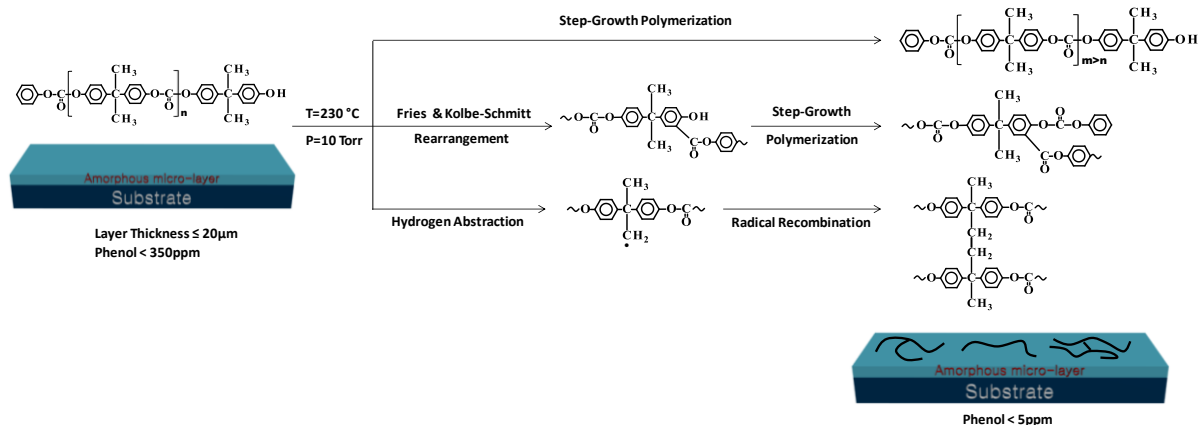


Figure 4.1 Reaction scheme of BPAPC in amorphous micro-layers.

4.2 Experimental

4.2.1 Materials

Amorphous micro-layer polymer samples were prepared using a solvent casting technique. First, a predetermined amount of low molecular weight prepolymer sample (B-14k in Table 2.2) was dissolved in a solvent (chloroform) at room temperature. Silica substrate (2.5cm × 7.5cm) was cleaned with acetone for 10 min and then cleaned again with methanol for 5 min before being rinsed with deionized water, and dried by nitrogen gas flow. The cleaned silica substrate was preheated, immersed in a bath of prepolymer solution, and removed. The silica substrate coated with prepolymer was dried in a fume hood for 2h at ambient temperature and pressure. The coated prepolymer micro-layers prepared by this method were transparent and amorphous. For the solid state polymerization, a vacuum oven was used as a reaction chamber (Fisher Scientific™ Isotemp™ Model 281A Vacuum Oven, 0.65 cu. Ft.). The polymerization experiments were carried out in a reaction chamber at 230 °C and 10 mmHg. For the analysis, the polymer samples were taken out of the reaction chamber at designated sampling times.

To investigate the effect of free radicals, a free radical inhibitor was used in the polymer micro-layers. To avoid the possibility of side reactions between the radical inhibitor and phenyl carbonate end groups in polymer, phenothiazine was selected as it does not contain hydroxyl groups [91, 92].

4.2.2 Characterization

The molecular weight and molecular weight distribution (MWD) of the prepolymer were measured by a gel permeation chromatography (GPC) system equipped with PLgel 10 μm MIXED-B columns (Polymer Laboratories) and a UV detector (Waters 484). Chloroform was used as the mobile phase and a narrow polystyrene standard was used for the calibration of MW. We analyzed the polycarbonate molecular architecture using high resolution $^1\text{H-NMR}$ spectroscopy (Bruker AV III spectrometer at 600 MHz). For the $^1\text{H-NMR}$ spectroscopy analysis, polymer samples taken from the SSP_m experiments were dissolved in deuterated chloroform (CDCl_3). For the analysis of insoluble gel fractions, Py-GC/MS (Frontier Lab PY-2020iD pyrolyzer) was used equipped with an Agilent GC/MS system composed of an Agilent 6890 gas chromatograph and an Agilent 5975i mass spectrometer for analysis. Py-GC/MS analysis was conducted in Korea by Dr. Yun Gyong Ahn (Korea Basic Science Institute, Seoul, Korea) and Dr. Kwang Ho Song (Korea University). An aqueous solution (25 wt %) of tetramethylammonium hydroxide [$(\text{CH}_3)_4\text{NOH}$; TMAH] (Aldrich) was used as the reagent for methylation of the product samples. Insoluble polycarbonate morphology was visualized using Hitachi SU-70 scanning electron microscopes (SEM). Transmission of SSP_m amorphous polycarbonate was scanned in the range of 200-800nm using UV-visible spectrophotometer (CARY 50Bio).

4.3 Results and Discussion

4.3.1 Formation of Insoluble Polycarbonate in Amorphous Micro-Layers

In our first series of experiments, 10 μ m-thick amorphous micro-layers prepared by solvent casting technique was polymerized at 230°C under 10 mmHg. Figure 4.2 shows the evolution of weight average molecular weight and the emergence of insoluble polycarbonate fractions along the reaction times. The molecular weight of 10 μ m-thick amorphous prepolymer micro-layers (Figure 4.2 (\blacktriangle)) increased from 14,000 g/mol (prepolymer MW) to 340,000 g/mol in 180 min. The prepolymer molecular weight is about 14,000 g/mol with stoichiometric imbalance of the end groups ($[-\text{OCO}-\text{C}_6\text{H}_5]/[-\text{OH}] = 0.8$).

In chapters 2 and 3, the increase of the polymer MW was formed to be caused by minimal diffusional resistance for the byproduct (phenol) removal and the formation of nonlinear chain structures polycarbonates (branched and cross-linked PCs). Rearrangement of a carbonate group in linear BPAPC can form a pendant carboxyl group, ortho to an ether link, and through ester exchange reaction with another BPAPC chain, long chain branched structure can be formed. Either the Kolbe-Schmitt rearrangement reaction or the Fries rearrangement reaction leads to the formation of branched structures. The possibility of homolytic scission of carbonate groups at high temperatures between the oxygen and carbonyl group in BPAPC and hydrogen abstraction in the system can generate radicals that may lead to cross-linking reactions [40, 56]. The byproduct, phenol, is known as a radical scavenger. In the SSP_m process, phenol is effectively removed from the system thus recombination of micro-radical species is promoted.

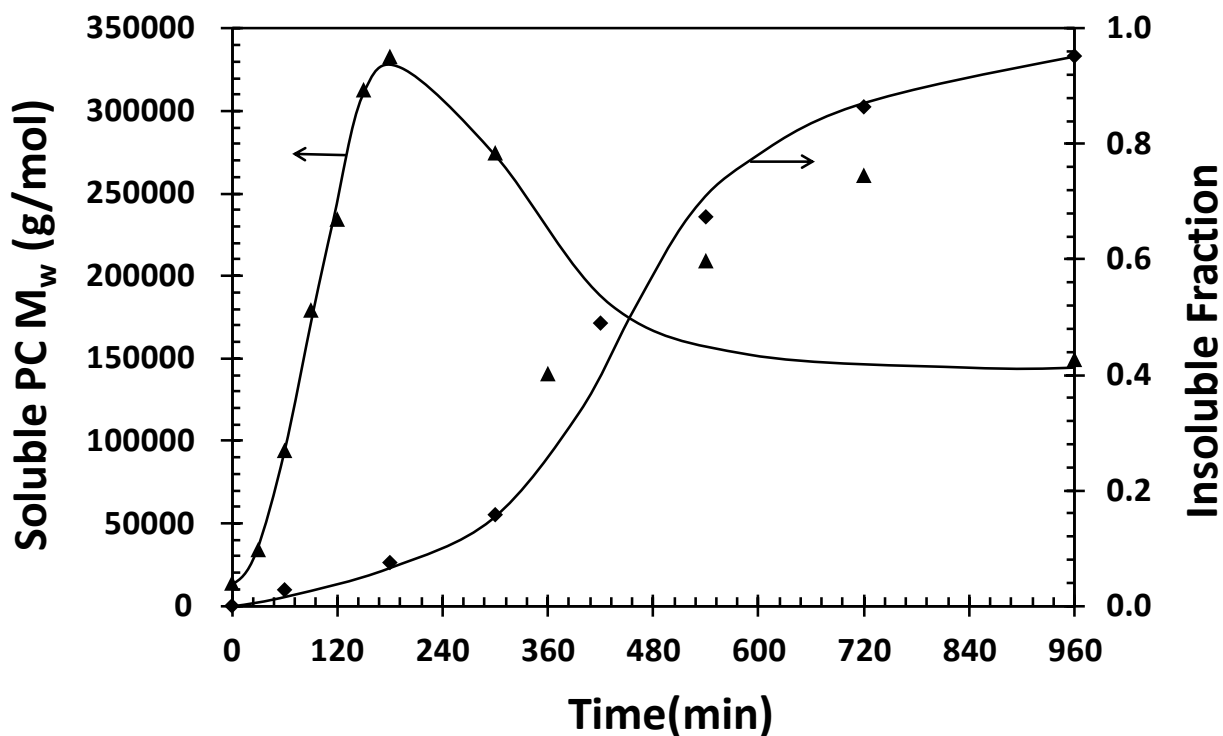


Figure 4.2 Evolution of soluble PC weight average molecular weight (▲) and emergence of insoluble fractions (◆) with the reaction time for 10 μm -thick amorphous micro-layers (Precursor weight average molecular weight=14k g/mol, P= 10 mmHg, T=230°C). Lines are added to guide the eyes.

When longer reaction time is applied in the SSP_m using amorphous micro-layers with 10 μm thickness at 230°C under 10 mmHg the molecular weight decreases after molecular weight reaching a maximum at 180 min (Figure 4.2 (▲)). However, fast increase of insoluble gel fraction is observed after 300 min (see Figure 4.2 (◆)). For the measurement of insoluble fractions, samples (0.5 g) at each reaction time are dissolved in large amount of chloroform (500 ml). The soluble and insoluble gel fractions were separated via filtration using a 0.2 μm pore size membrane followed by washing with a solvent (chloroform) at least 10 times and weighted using

gravimetric method. Only, the soluble fraction was used to measure the molecular weight using GPC and its structure was analyzed using $^1\text{H-NMR}$ analysis. It seems that the polymerization continued even after 180 min of reaction time but high molecular weight polymer chains become insoluble gels. The structure of insoluble fraction was analyzed using pyrolysis gas chromatography.

The fraction of insoluble gels with severe discoloration at high reaction temperatures ($>300^\circ\text{C}$) which is above the polymer melting point ($T_m \sim 260^\circ\text{C}$) are reported in the literature [18, 20, 21, 41, 42]. Yellowish or dark brown color polymers are observed at high reaction temperature. However, the temperature applied in this system is 230°C and the fraction of insoluble gel grows to 0.95 after 960 min with perfect transparency. Recombination of radical species might be mainly responsible for the formation of insoluble gels in that phenolic groups ($[-\text{OH}]$) and phenyl groups ($[-\text{OCO-C}_6\text{H}_5]$) decreased to insignificant levels after the early stages of the reaction ($<30\text{min}$). Thus, step-growth polymerization via end group reactions practically ceases to occur afterwards, but the molecular weight obtained in 30 min is 34,000 g/mol and the highest molecular weight observed in Figure 4.2 is about 333,000 g/mol which is about 10 times higher. Longer polymer chains have a higher probability for the formation of radical sites thus a higher chance of recombination of macro-radical species is expected.

Figures 4.3 and 4.4 show the fraction of insoluble gels with reaction times over 420 min in chloroform (Figure 4.3) and SEM image of insoluble BPAPCs (720min) after separating soluble fraction with 24hr exposure in chloroform in the oven at temperature of 80°C (Figure 4.4). Methylene chloride, tetrahydrofuran (THF) and dimethyl sulfoxide (DMSO) also known as good solvents for the polycarbonates and same results were observed. Almost same amount of

insoluble gel fractions were obtained using these four different types of solvents that listed above. Prepolymer sample thickness was set to $10\mu\text{m}$ before SSP_m and insoluble gels depicted in Figure 4.4 (a) and (b) almost keep its initial shape and has a thickness of nearly $10\mu\text{m}$. As shown in Figure 4.2, about 90% of insoluble fraction was formed in 720 min and porous structures were observed at cross-sectional area of micro-layers as shown in Figure 4.4.

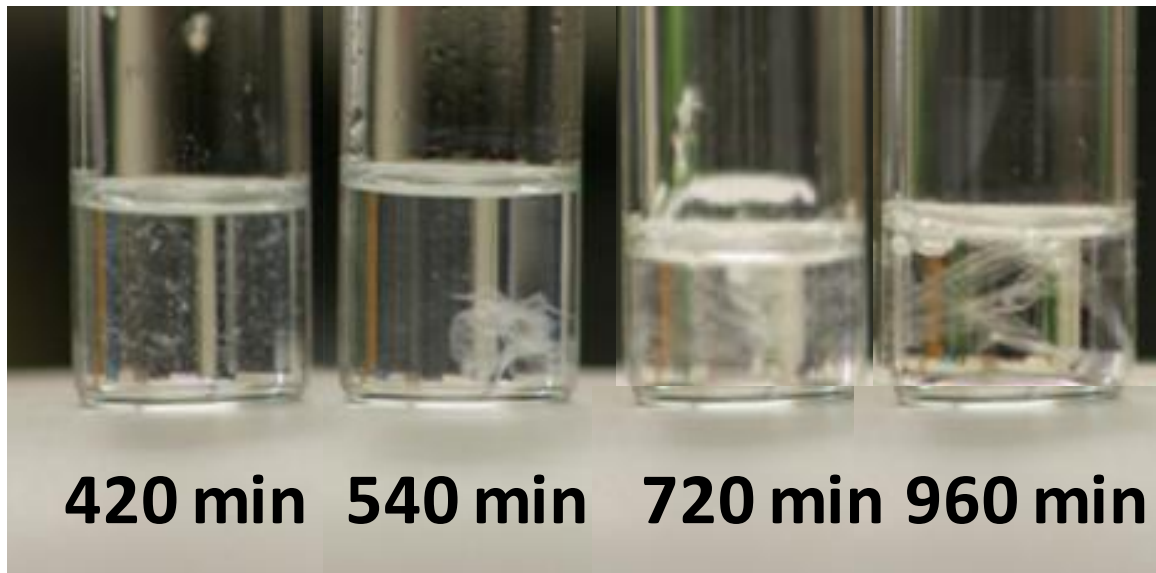


Figure 4.3 Increase of insoluble fraction of BPAPC in solvent (chloroform) as reaction time extend ($T=230\text{ }^\circ\text{C}$, $P=10\text{ mmHg}$, Prepolymer: 14K g/mol).

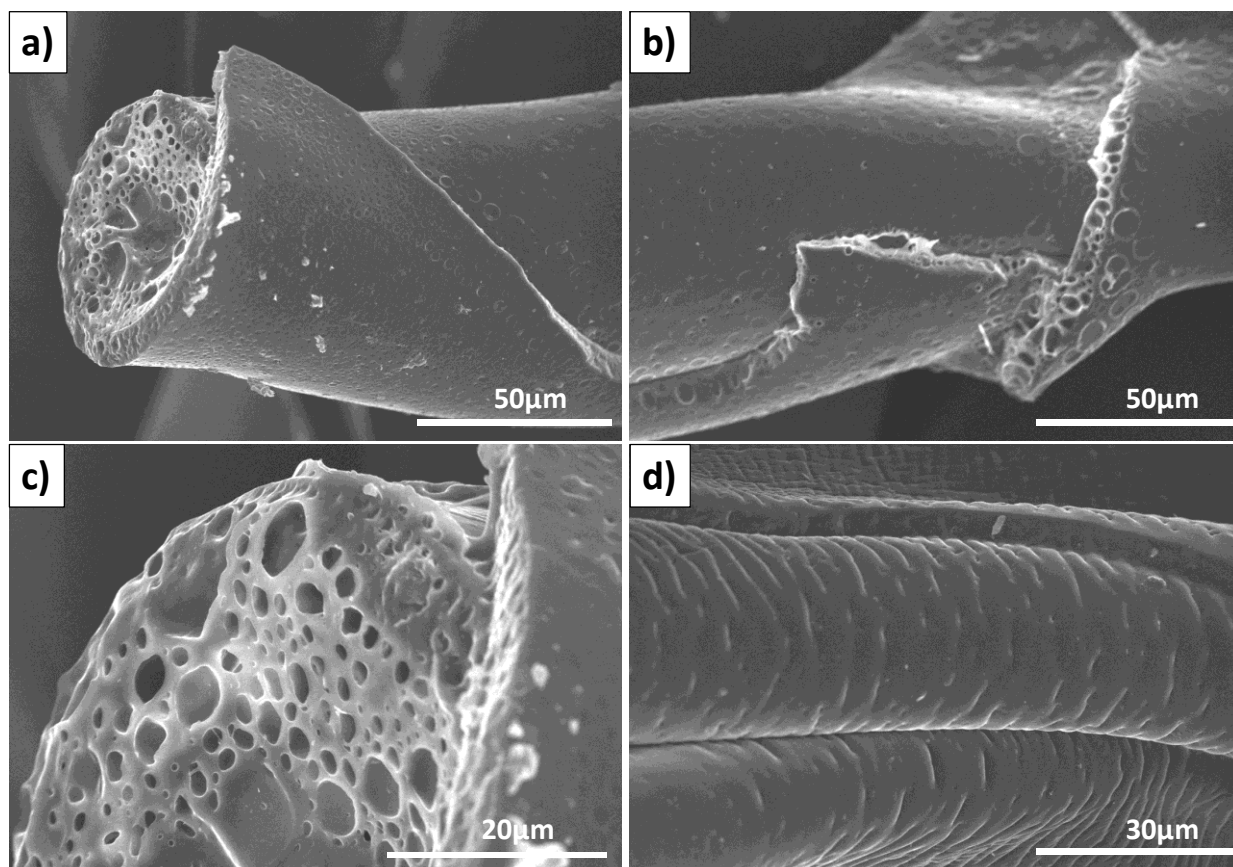


Figure 4.4 SEM image of insoluble BPAPC with reaction time of 720 min ($T=230\text{ }^{\circ}\text{C}$, $P=10\text{ mmHg}$, Prepolymer: 14K g/mol).

In Figure 4.3, we observe the increase of insoluble fraction of BPAPC in chloroform after 420min. Before 420min, no precipitation was visible. However we have shown that about 5% and 16% of insoluble gel were present at the reaction time of 180min and 300min (Figure 4.2(♦)). We have used AFM (D-300) to observe the presence of insoluble gel in amorphous micro-layers at short reaction time. The polymer sample was a 10 μ m-thick amorphous micro-layer polymerized at 230 $^{\circ}$ C for 1800 min to 720 min. The 95% insoluble samples were not tried due to the difficulty of sample preparation. The prepolymer and the SSP_m PC of 0.05mg/ml solutions for the different reaction time were prepared for the sample preparation. And these solutions were coated on the surface of flat substrate using spin coating technique at the spin rate of 2000rpm. We used a tapping mode with the scan rate of 0.5 line/sec. The AFM images were obtained using normal Si 40-50 nm radius probe at a resonance frequency of 334 kHz with the force constant 40 N/m.

Figure 4.5 shows AFM height images of insoluble gel fractions onto the soluble PCs and the insoluble fractions are thicker than soluble PCs. The prepolymer does not contain insoluble gel and amount of insoluble gel increases with reaction time. For the 60min sample, emergence of small particles has larger height was confirmed. These small particles have about 4.5 nm larger heights than soluble PC surface (Figure 4.6). Although it is not shown, soluble PCs have 47.9 nm in height. Area of insoluble PCs was calculated using Image J software and volume fraction of insoluble PCs in 60min sample was 0.06. For the other samples, this calculation was not applied due to the non-uniform surface heights.

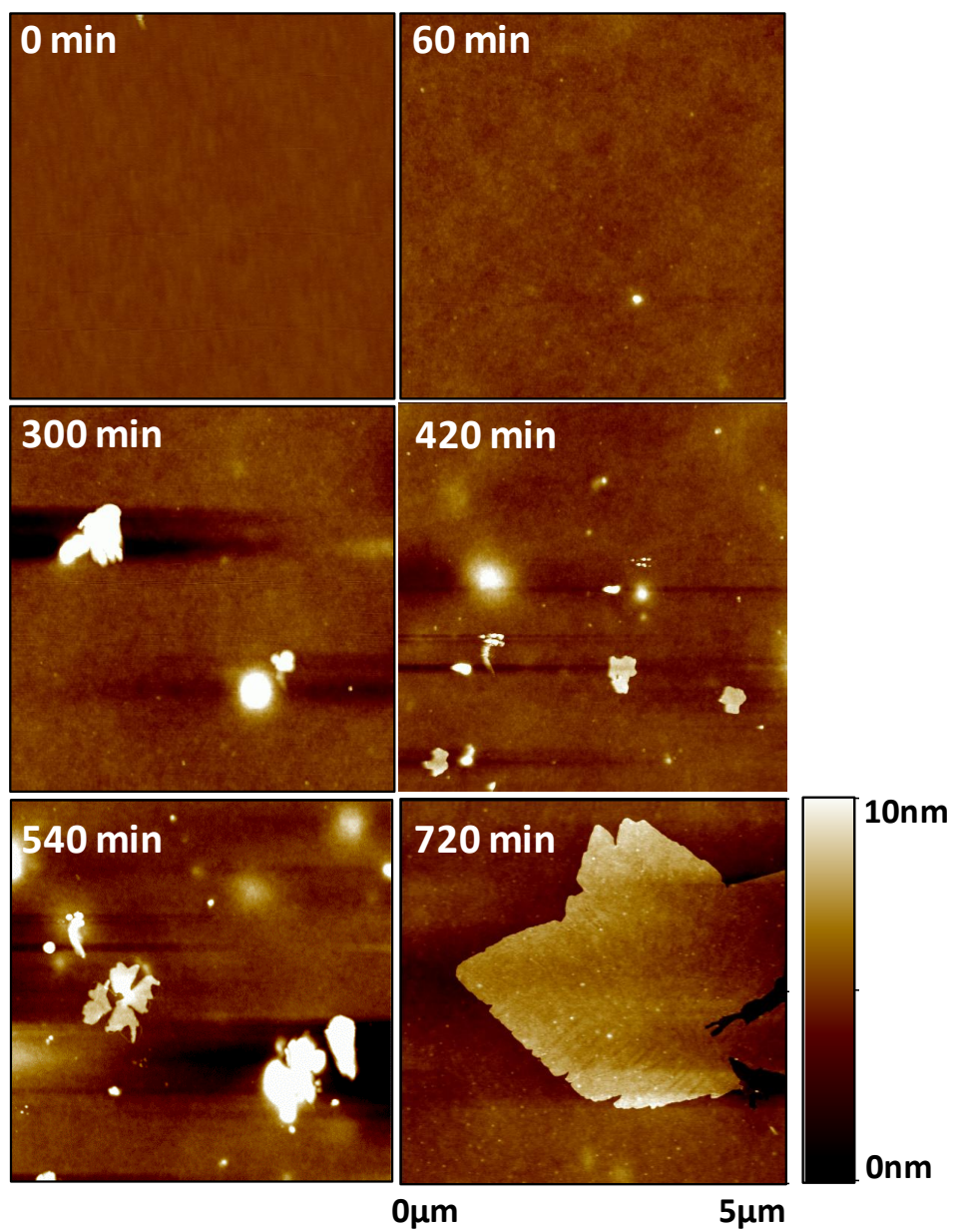


Figure 4.5 AFM height images of insoluble gel fractions onto the soluble PCs. Increment of insoluble gel fractions with reaction extend.

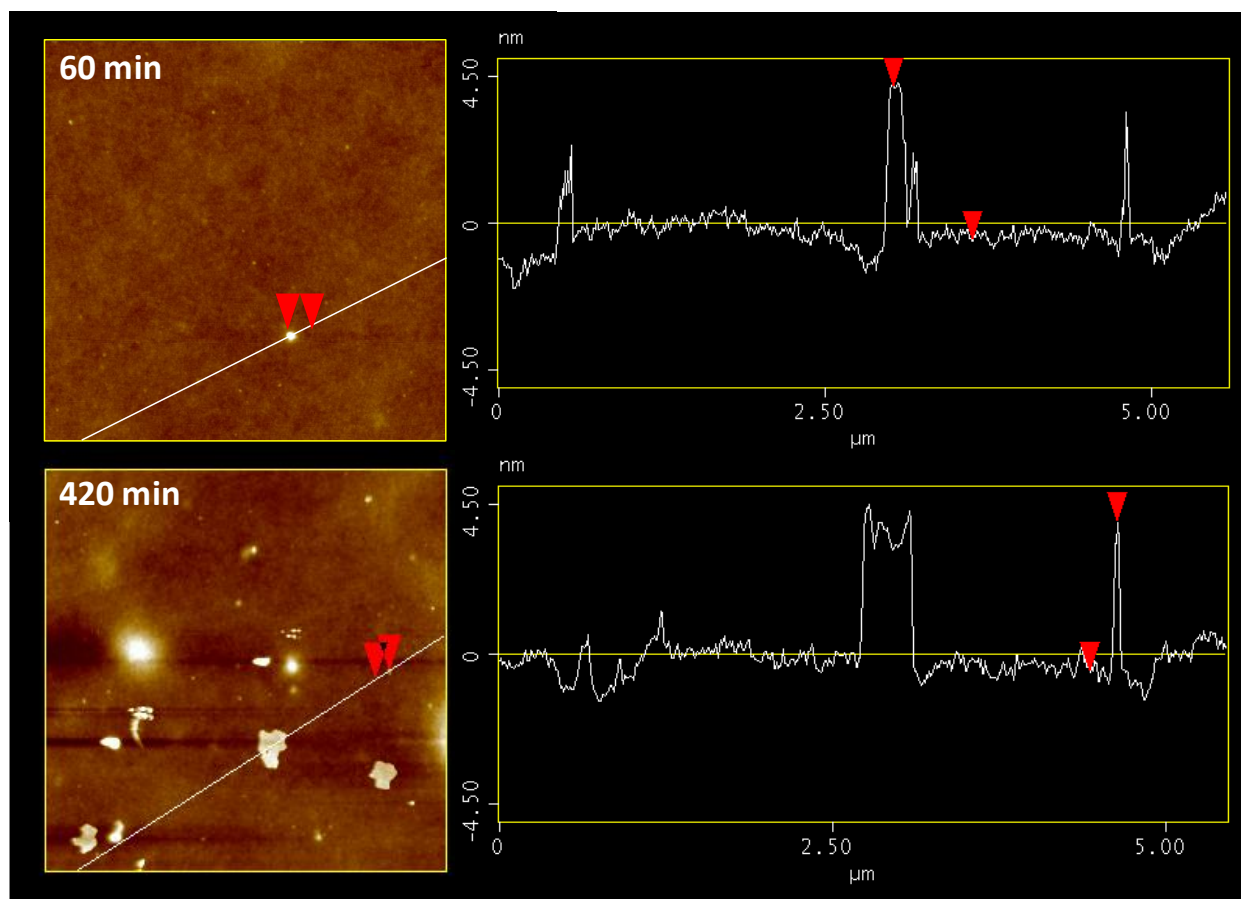


Figure 4.6 Height difference measurement between insoluble gel and soluble PC surface for the 60min and 420min samples.

About 95% insoluble gel fraction is obtained at 960min of reaction time. The chain structures (i.e., branched and cross-linked structures) were investigated using $^1\text{H-NMR}$ analysis and pyrolysis gas chromatography Mass Spectrometry (Py-GC/MS). Soluble and insoluble fractions were separated using $0.2\mu\text{m}$ pore size membrane and the soluble part was analyzed by $^1\text{H-NMR}$ and the insoluble gel was analyzed by Py-GC.

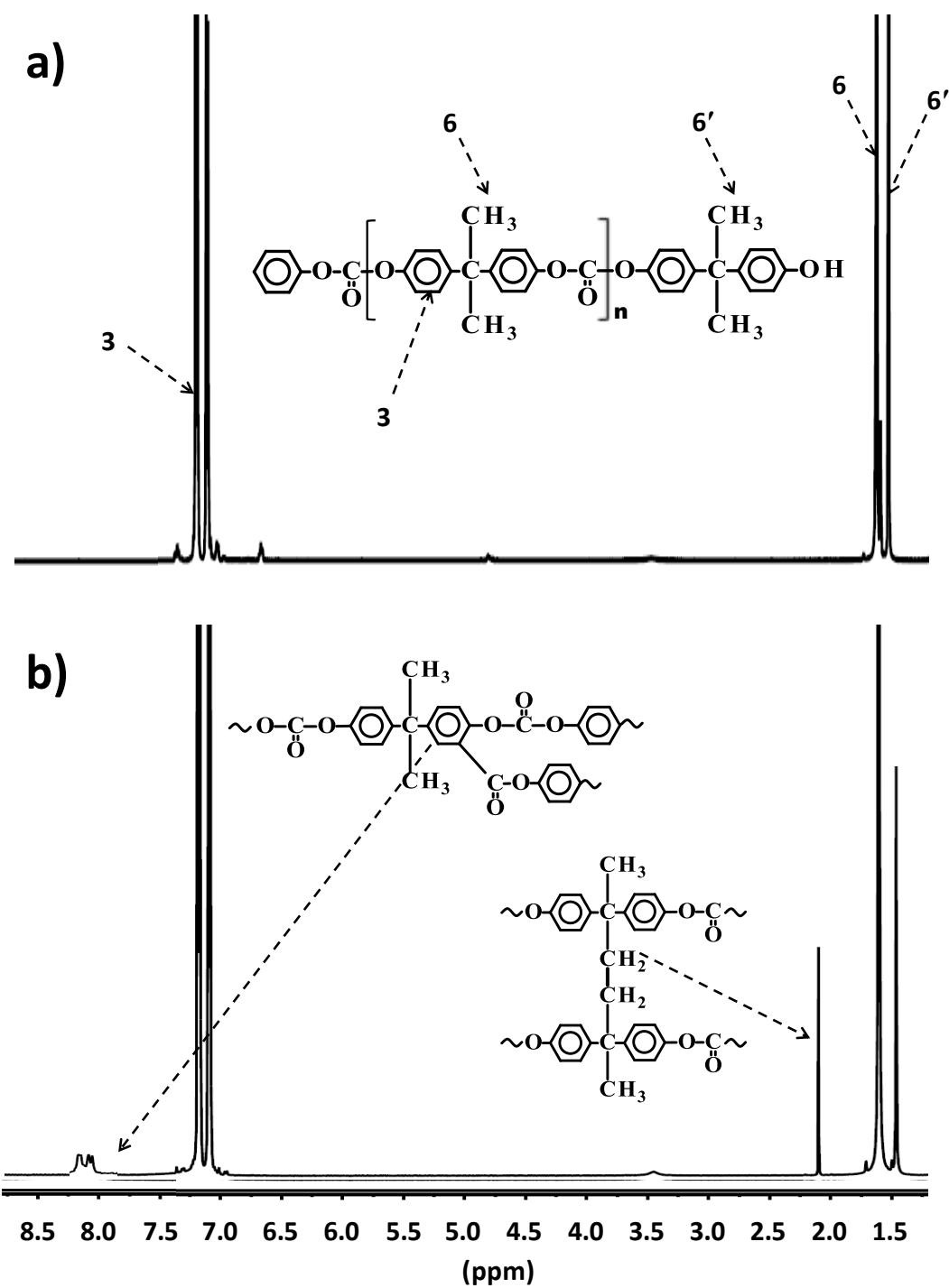


Figure 4.7 ^1H NMR spectroscopic analysis of the amorphous micro-layer: a) prepolymer (14k g/mol), b) soluble fraction of amorphous micro-layer at the reaction time of 960min ($T=230^\circ\text{C}$, layer thickness=10 μm , prepolymer: 14k g/mol).

Figure 4.7 shows the $^1\text{H-NMR}$ spectroscopy data of prepolymer (a) and high molecular weight polycarbonate in the soluble fraction obtained at 960min (b). For the soluble BPAPC, the aromatic regions (peak at 8.0-8.1 ppm) for phenyl salicylate phenyl carbonate (PhSALPhC) and ethyl protons on the linkage of cross-linked structure were confirmed. The mole fractions of cross-linkage was 6.33×10^{-2} which was estimated using area intensity of methyl protons and ethyl protons in repeating units and cross-linkages. As reported in Chapter 3, mole fractions of cross-linkage in the soluble fraction were 3.55×10^{-4} and 4.26×10^{-2} at 30 min and 180min, respectively. At early stages of the reaction, cross-linkages increases about two orders of magnitude. However, the mole fraction of cross-linkages in the soluble fraction does not change much after 180 min of reaction time probably due to the insolubility of highly cross-linked polymer chains and because the $^1\text{H-NMR}$ spectroscopy analysis is limited to the soluble fraction only. This seems to indicate that the insoluble gel formation occurs around the cross-linkage mole fraction of between 4.26×10^{-2} and 6.33×10^{-2} . The molecular weight of soluble polymer chains decreases after 180 min of reaction time at 230°C and that the insoluble gel fraction increases rapidly after 300 min of reaction time (see Figure 4.2).

Recently, Oba et al. reported that the Py-GC/MS method in the presence of tetramethylammonium hydroxide (TMAH) is an effective technique for the qualitative analysis of branched and cross-linked polycarbonate. Through reactive pyrolysis of insoluble gels at a high temperature (400°C), linear, branched and cross-linked polymer chains are selectively decomposed to methyl derivatives of the components which are detected by mass spectrometry. The Pyrogram result in Figure 4.8 shows that the insoluble gel consists of branched and cross-linked structures (structure A-D). Structure A (peak a) can be formed via thermal rearrangement

reaction (Fries and Kolbe-Schmitt Rearrangement reactions) while radical recombination reactions of macro-radical species lead to structure B-D (peak b-d) [40, 56]. According to the structures (B-D) obtained through radical recombination, two macro-radical species would be formed during the SSP_m process, methylene radical via hydrogen abstraction from the methyl group and phenoxy radical through chain scission at the carbonate group. Two methylene radical species may form Structure C that corresponds to peak c while the combination of methylene radical and phenoxy radical species produce Structure D (peak d). Structure B is the reactive pyrolysis component of Structure D which is supporting evidence of the recombination of two different macro-radical species. Note that none of the peaks are related to the byproduct (phenol) which acts as a radical scavenger.

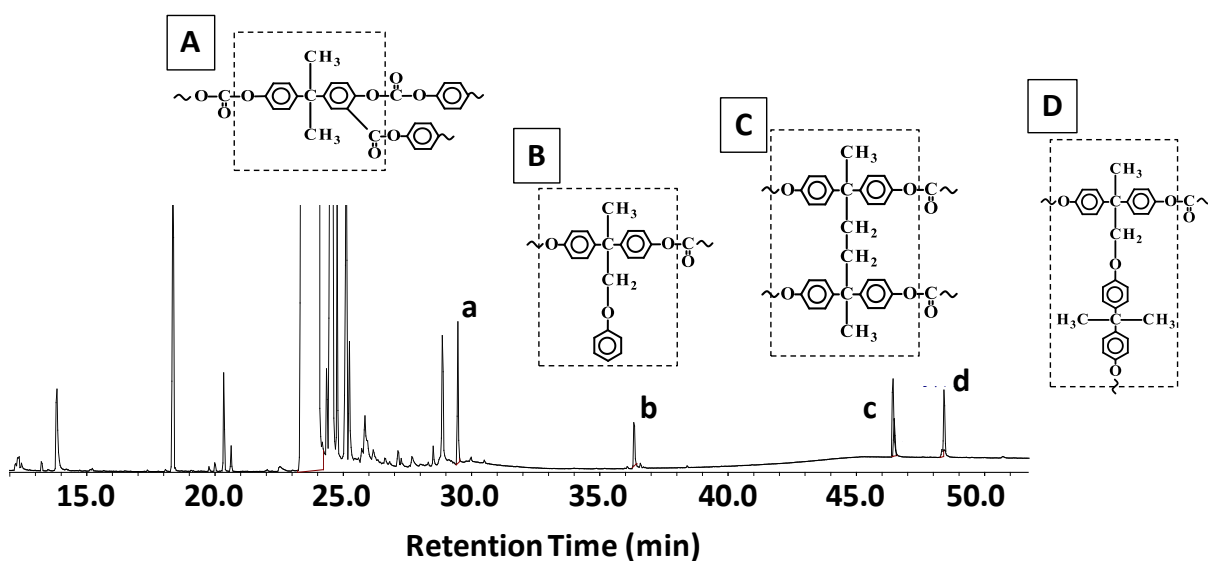


Figure 4.8 Pyrogram of insoluble gel obtained at the reaction time of 960 min ($T=230\text{ }^{\circ}\text{C}$, layer thickness=10 μm , prepolymer: 14k g/mol).

Insoluble PC samples (960 min) were removed from the glass substrate by immersing the polymer/substrate in a water bath and sonicating for over 6 hours. In hydrofluoric acid was also used to remove the micro-layers from the substrate surface. Micro-layers obtained after SSP_m process (960min) have excellent transparency even after long exposure to high reaction temperature at 230°C (Figure 4.9). Also, the amorphous micro-layers were transparent during the polymerization. Improvement of toughness and ductility is another difference in comparison with the starting material (Prepolymer: 14,000 g/mol linear polycarbonate), which will be discussed in Chapter 5. Images of the amorphous micro-layers (960min) recovered from the substrate were presented in Figure 4.9.

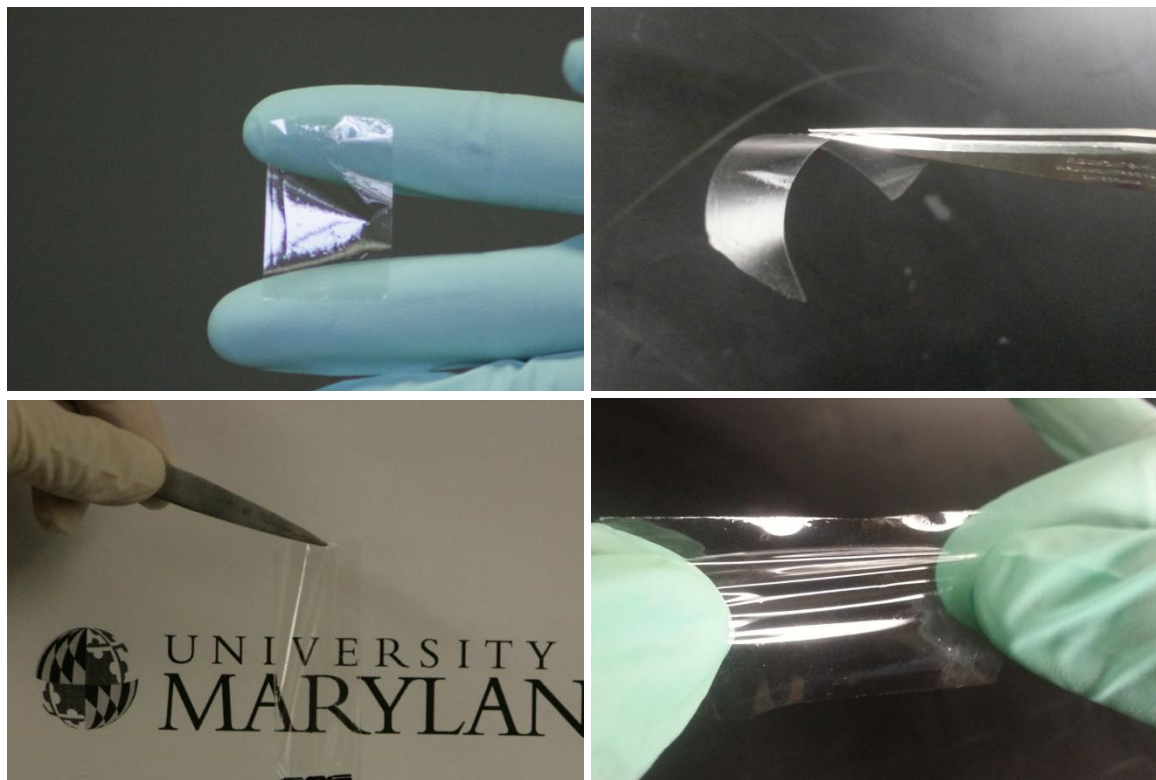


Figure 4.9 Images of stand-alone insoluble PC gel recovered from glass substrate ($T=230\text{ }^{\circ}\text{C}$, layer thickness=10 μm , prepolymer: 14k g/mol, amorphous micro-layer at 960 min).

For the measurement of light transmission of SSP_m PCs, UV-visible spectrophotometer (CARY 50Bio) was used. Figure 4.10 and 4.11 show the UV-vis spectra of prepolymer (B-14k), amorphous micro-layer polymer samples produced via SSP_m and PCs produced by melt process at various reaction times. The prepolymer sample has about 90-93% light transmission at the visible light range (390-700 nm) and the amorphous micro-layers exhibit almost the same transparency throughout the entire range of measurements. Although this is not the best reactor set up of the melt polymerization process, the conventional melt process was conducted in glass vials at 290°C and 10 mmHg, which is within the typical temperature range for the melt process. During the course of the melt process, severe discoloration was observed. After 240 min of reaction, bulk PC turned to dark brown color. In a conventional melt step-growth polymerization, high reaction temperatures, long reaction times (4-5 h), and ineffective removal of phenol often lead to unwanted side reactions, causing discoloration of the final product [12, 16, 17].

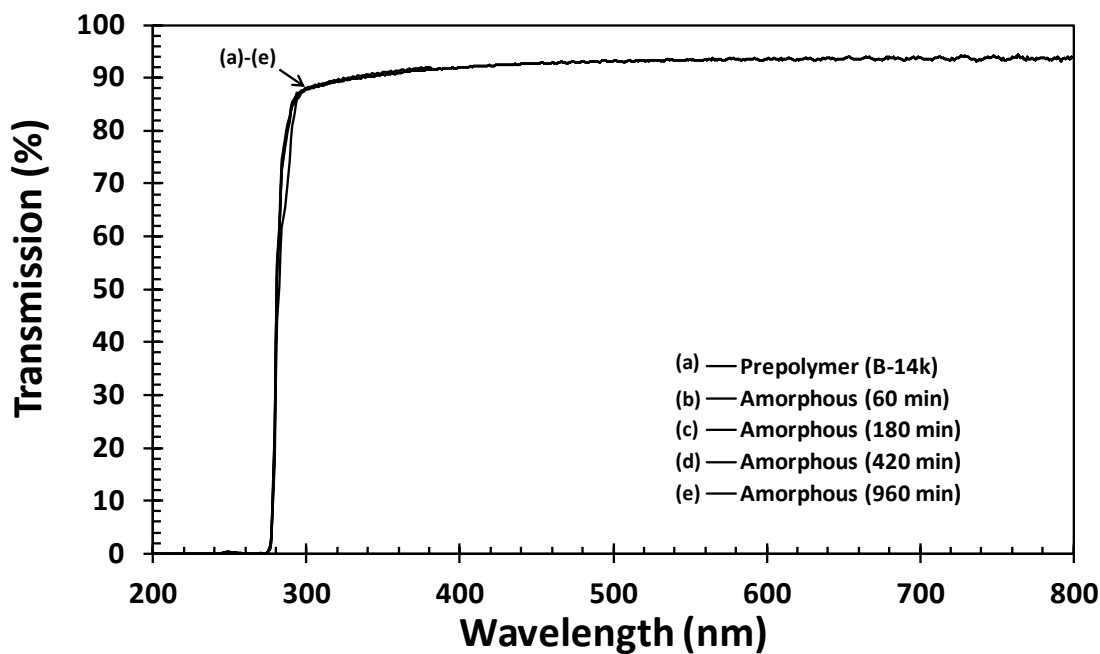


Figure 4.10 UV-vis spectra of (a) prepolymer (B-14k) and (b-e) amorphous micro-layers with reaction time ($T=230\text{ }^{\circ}\text{C}$, $P=10\text{ mmHg}$, Prepolymer B-14k).

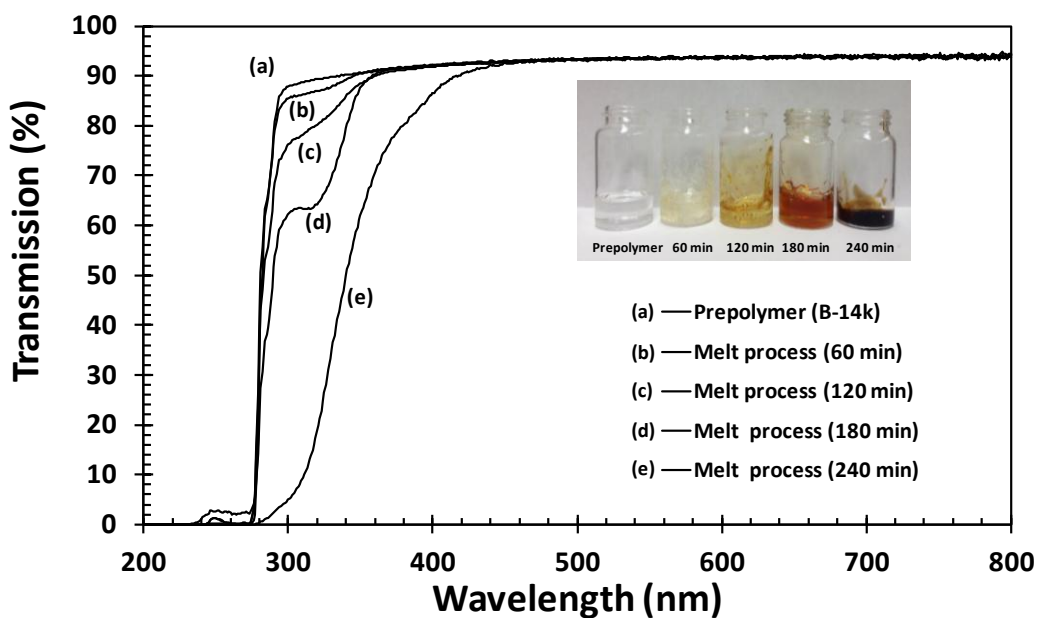


Figure 4.11 UV-vis spectra of (a) prepolymer (B-14k) and (b-e) bulk PCs using melt process with reaction time ($T=290\text{ }^{\circ}\text{C}$, $P=10\text{ mmHg}$, Prepolymer B-14k).

4.3.2 Effect of Layer Thickness

The thickness of a micro-layer is expected to have an effect on the molecular weight and increasing insoluble gel fraction phenomena because it affects the diffusion rate of phenol (condensation byproduct) from the polymer micro-layer. Figure 4.12 shows the molecular weight vs. reaction time profiles for the amorphous micro-layers of thickness ranging from 54nm to 20 μm . All amorphous micro-layer samples maintained transparency during the entire period of polymerization. Even though not shown here, 35 μm thickness samples were partially crystallized when it was cast on the glass substrate, and thermal annealing enhanced the crystallization during the reaction. Thus micro-layer thickness is limited to 20 μm to ensure that all the micro-layers are in an amorphous state.

Figure 4.12 shows that micro-layer thickness has a strong effect on the rate of polymerization and the final molecular weight down to a thickness of about 621 nm, past which point, the effect of the thickness is insignificant. Micro-layers with thicknesses of 54-1021 nm were measured using AFM in tapping mode and the height images were used to obtain precise thickness measurements for each sample. For the micrometer scale samples, the thickness was measured using a Mitutoyo micrometer (Japan). In the range of 54-621 nm, the thickness effect is very minimal and the molecular weights of these samples are in the error range throughout the entire reaction time. Also, the deviation of molecular weight becomes higher as formation of insoluble gel fractions are promoted in thinner micro-layers. Effective removal of phenol in thinner micro-layers may increase the number of available radical sites on the polycarbonate chain thus cross-linking reactions can take place at short reaction times. As shown in Figure 4.13,

the emergence of insoluble gel PCs was observed earlier as micro-layer thickness decreases. The insoluble gel fraction of 10 μ m samples at 180 min is about 5 % while the 54-621 nm-thick micro-layers show about 35 % which is 7 times higher.

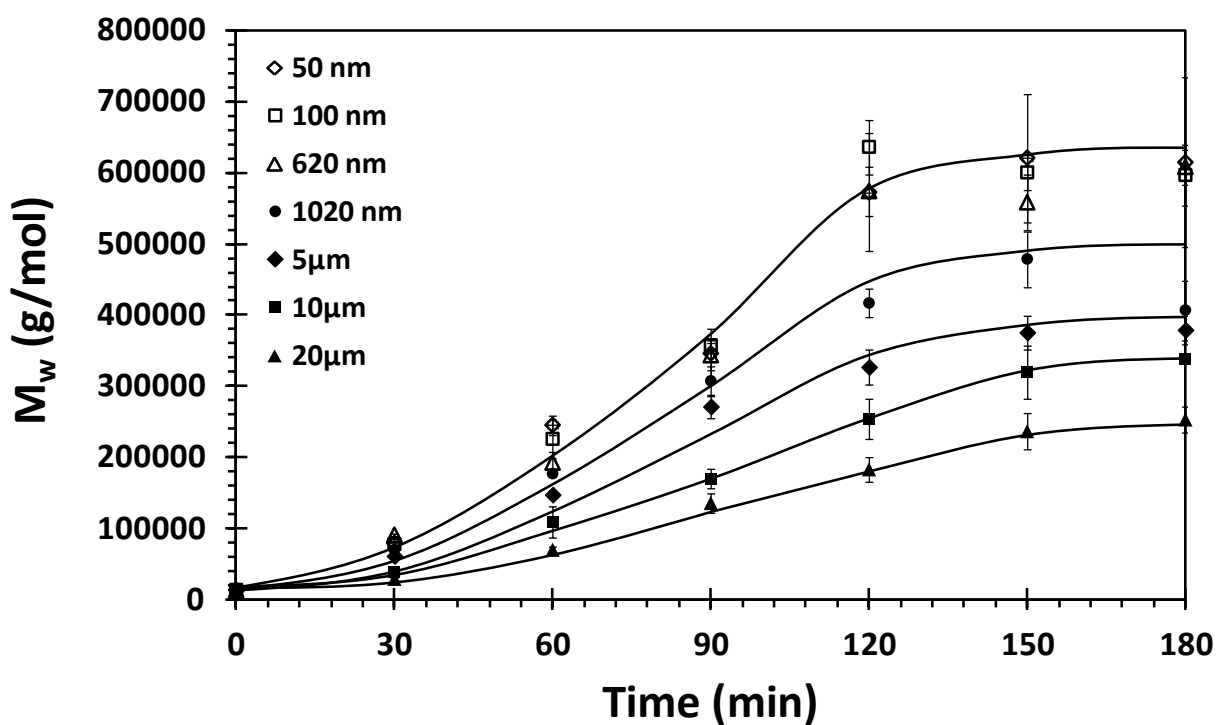


Figure 4.12 Effect of the amorphous micro-layer thickness on the evolution of the polymer molecular weight with the reaction time ($T=230$ °C, $P=10$ mmHg, Prepolymer B-14k). Lines were added to guide the eyes only.

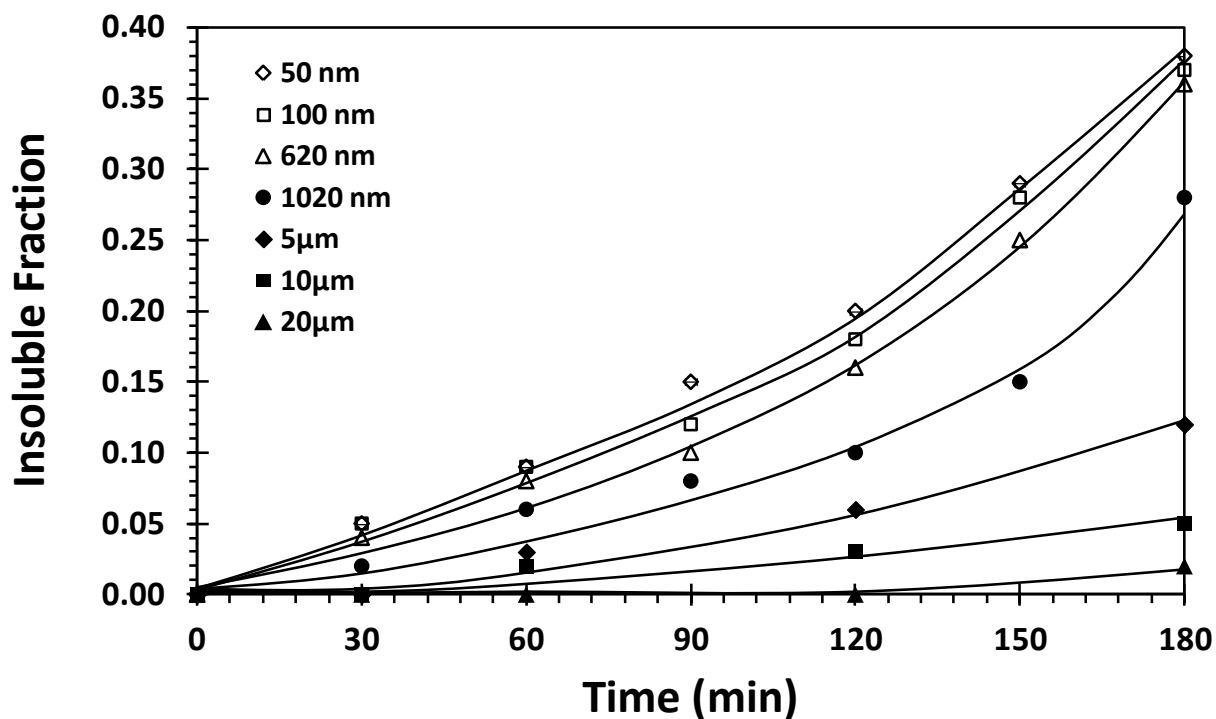


Figure 4.13 Formation of insoluble fraction in amorphous micro-layers depending on thickness ($T=230\text{ }^{\circ}\text{C}$, $P=10\text{ mmHg}$, Prepolymer B-14K). Lines were added to guide the eyes only.

Using the theoretical model provided in Chapter 2, the phenol concentration is estimated. The concentration of phenol affects the molecular weight build up of linear step-growth polymerization and radical recombination reactions as well. Thus, the residual phenol concentration in micro-layers of different thicknesses directly relates to the formation of insoluble gels. The simulation results are shown in Figure 4.14. As expected, thicker layers contain larger amounts of phenol in the reaction space. In the layer thickness range of 54-1021nm, phenol concentrations decrease quickly. The experimental results of different micro-layer thickness samples at 180 min are summarized in Table 4.2.

Table 4.2 Experiment results of different micro-layer thickness (54 nm-20 μ m) at 180 min.

Amorphous-micro layers at 180 min

Thickness	Soluble PC M_w (g/mol)	Polydispersity	Insoluble gel fraction	M_w SD
50 nm	615,742	4.09	0.38	$\pm 89,373$
100 nm	596,854	5.00	0.37	$\pm 42,426$
620 nm	608,350	4.48	0.36	$\pm 39,793$
1020 nm	406,958	4.24	0.28	$\pm 42,132$
5 μ m	379,271	2.68	0.12	$\pm 19,550$
10 μ m	338,346	2.50	0.05	$\pm 17,426$
20 μ m	253,149	2.32	0.02	$\pm 18,595$

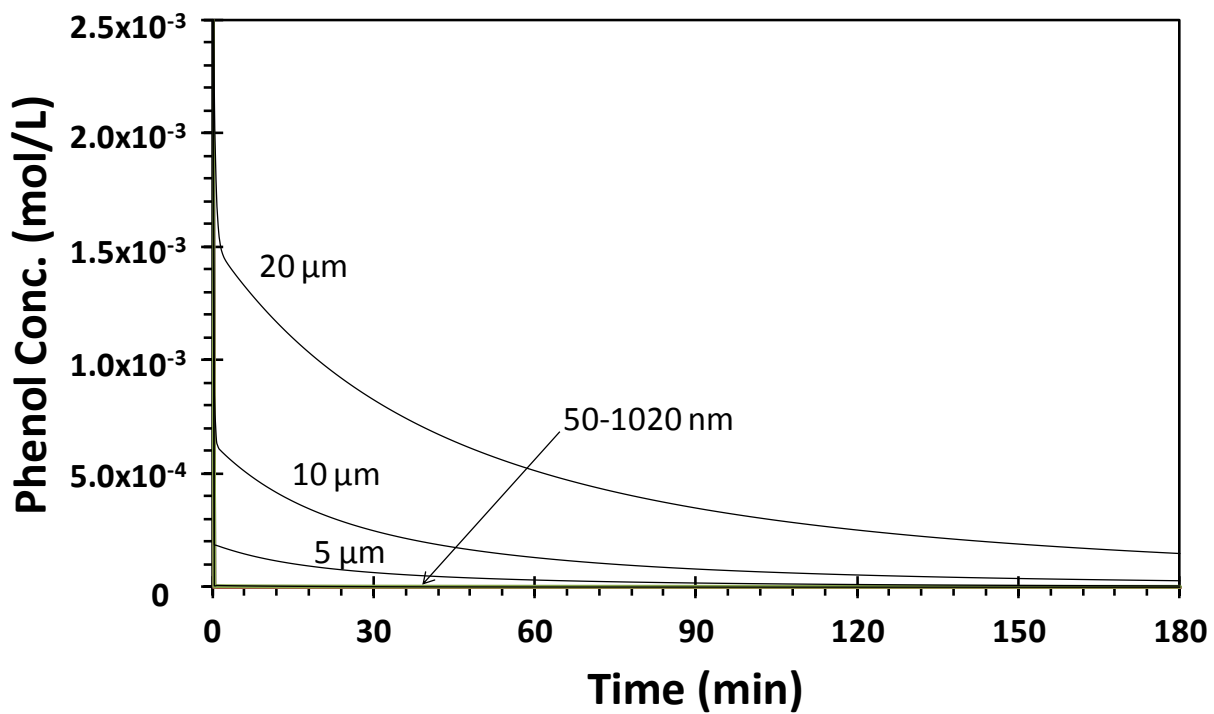


Figure 4.14 Model simulation of phenol concentration depending on micro-layer thickness ($T=230$ °C, $P=10$ mmHg, Prepolymer B-14K).

4.3.3 Effect of Reaction Temperature and formation of Insoluble SSP_m PCs.

In the SSP_m of our study, amorphous polymer micro-layers allow for the employment of higher reaction temperatures than the conventional SSP in that partial melting or fusion of the polymer particles is not of concern. Therefore, higher reaction rates can be achieved without crystallization process. The reaction temperature employed for SSP_m is quite close to the polymer melting point. Figure 4.15 shows the effect of reaction temperature when SSP_m is carried out using 10 μm-thickness amorphous polymer layers prepared by the solvent casting method using a prepolymer sample (14,000 g/mol). In the temperature range of 170-245°C, a strong effect of temperature on the polymerization rate and MW was observed, indicating that the polymerization in micro-layers is kinetically controlled. At 245 °C, the polymer molecular weight at 180 min has reached as high as 850,000 g/mol. Also, it is observed that thermally induced or solvent induced crystallization takes place at temperatures below 200°C during the SSP_m process. Note that the concentrations of residual casting solvent (chloroform) in solvent cast amorphous micro-layer samples at 230 °C were measured by gel permeation chromatography (GPC): 7.51 wt.% (0 min), 1.93 wt.% (30 min), 0.98 wt.% (60 min), and 0.03 wt.% (120 min). The GPC system (Viscotek GPC max with TDA 302 multi detector) equipped with q2500, 3000, 4000, and 5000 columns. HPLC grade THF was used as a mobile phase and predetermined amount of chloroform was used for the calibration.

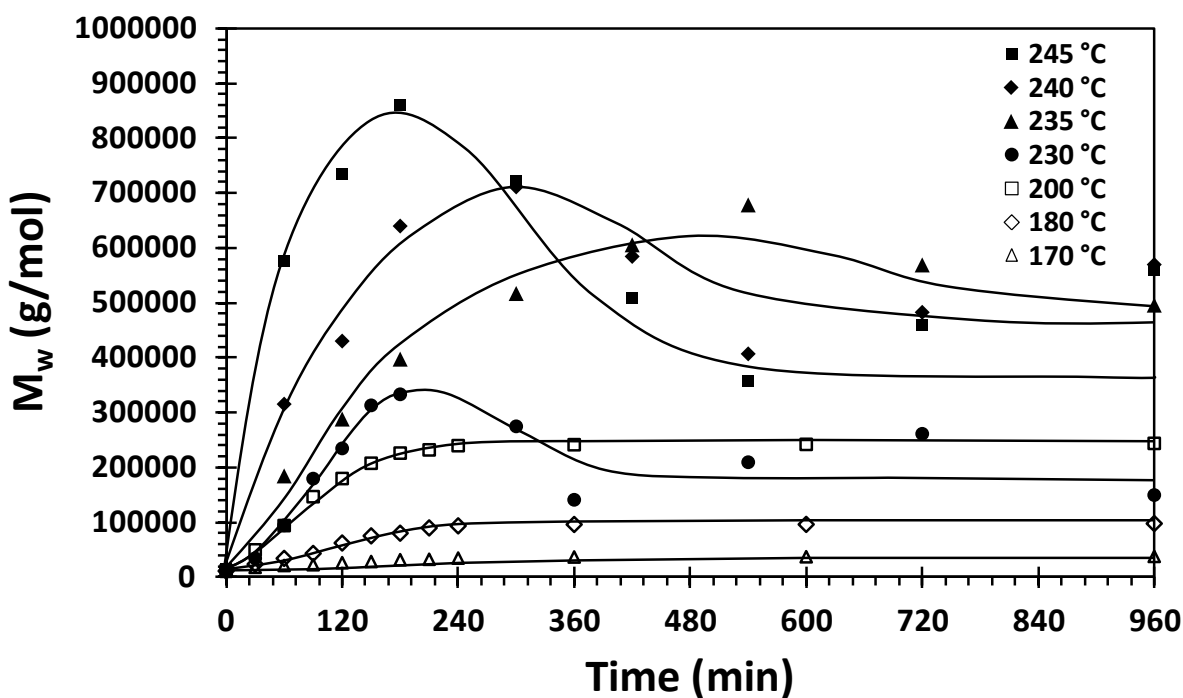


Figure 4.15 Effect of reaction temperature on the evolution of weight average molecular weight of soluble fraction in amorphous polymer micro-layers of 10 μm thickness ($T=170\text{-}245^\circ\text{C}$, $P=10$ mmHg, Prepolymer B-14K). Lines were added to guide the eyes only.

At relatively higher reaction temperature ($>230^\circ\text{C}$), insoluble fraction (in a good solvent such as chloroform, methylene chloride, tetrahydrofuran, or dimethyl sulfoxide) of PC was observed and the amount of insoluble PC increased along the reaction time of the SSP_m process (see Figure 4.16). Insoluble fraction was separated using a $0.2\mu\text{m}$ pore size membrane and weighed using the gravimetric method. Higher reaction temperatures give higher rates of insoluble gel formation. At reaction temperatures of above 230°C , the molecular weight of SSP_m PCs decreases as the insoluble fraction rapidly increases. At temperatures below 200°C , no insoluble gel fraction was observed. Crystalline regions served as diffusion barriers for the

byproduct (phenol) thus higher concentrations of phenol still remained in the crystalline micro-layers. As mentioned earlier, the phenol is a radical scavenger hence higher concentration of phenol will capture the macro-radical species resulting in only a soluble, linear structure polycarbonate. Moreover, decreased mobility of polymer chains in the crystalline polymer results in lower mobility of radical species and lower rate of polymerization. All the crystalline samples (Figure 4.15 at 170°C, 180°C, and 200°C) reach a plateau of molecular weight after 240 min.

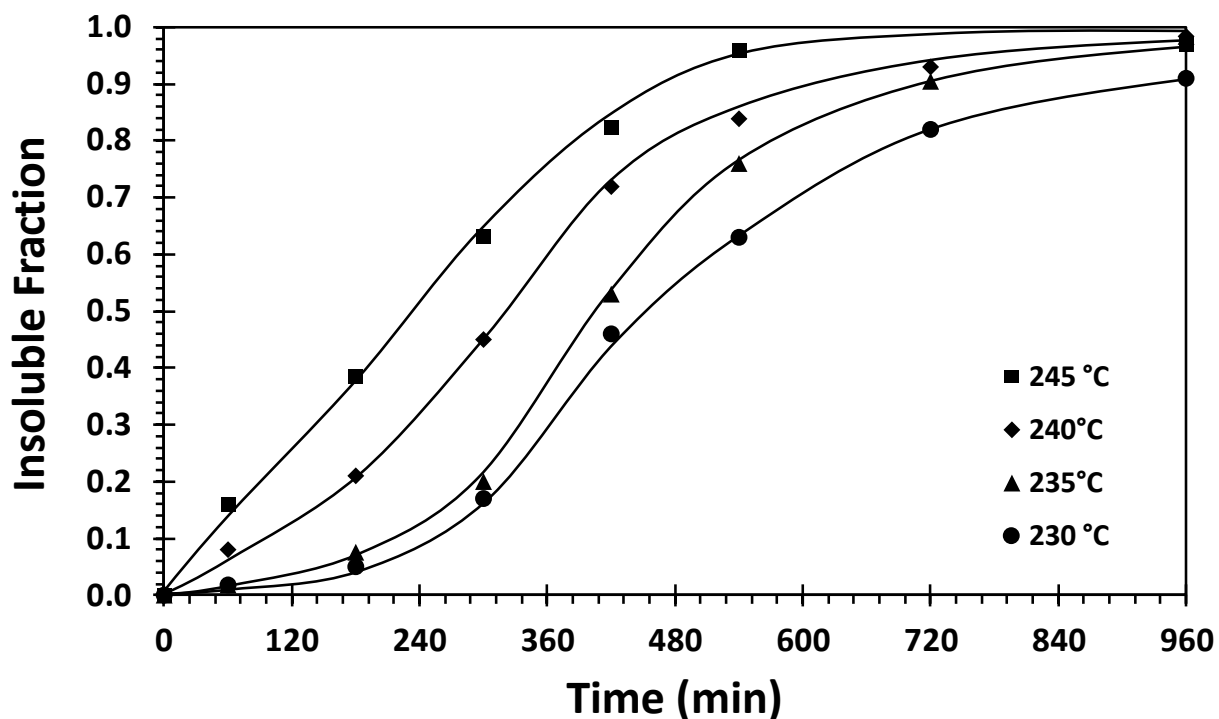


Figure 4.16 Generation of insoluble fraction of BPAPC in amorphous micro-layers of 10 μ m thickness at the reaction temperature above 230°C. Lines were added to guide the eyes only.

4.3.4 Effect of radical inhibitor on the molecular weight and insoluble fraction of PC

The mechanism of cross-linking proposed in this work is radical-induced reaction mechanism (i.e., hydrogen abstraction or chain scission reaction). Unfortunately, the measurement of free radical concentration during the SSP_m process was not possible. To investigate the effect of free radicals, we used an indirect method; free radical inhibitors were added to the polymer micro-layers. The larger the amount of radical inhibitor would decrease the radical concentration in micro-layers hence the buildup of molecular weight is prohibited and the amount of insoluble/infusible polymers would decrease. To avoid the possibility of side reactions between the radical inhibitor and phenyl carbonate end groups in polymer, phenothiazine (see Figure 4.17 (A)) was selected as it does not contain hydroxyl groups. Different concentrations of the radical inhibitor (0.1 wt %, 1.0 wt % and 2.0 wt %) were added to PC-chloroform solutions to prepare the 10µm thick micro-layers. The micro-layers were dried under a fume hood for 2h, and the SSP_m was carried out in a vacuum chamber at 230°C and 10mmHg. Figure 4.17 shows the different molecular weights and insoluble fractions formation at ranging inhibitor concentrations. As expected, SSP_m without any radical inhibitors gives the highest molecular weight buildup until 120min of SSP_m. Moreover, larger amount of the insoluble gel was observed with smaller amount of the radical inhibitor at all reaction times (Figure 4.17 (B)). The molecular weight data in Figure 4.17 (A) represent those that are molecules in chloroform.

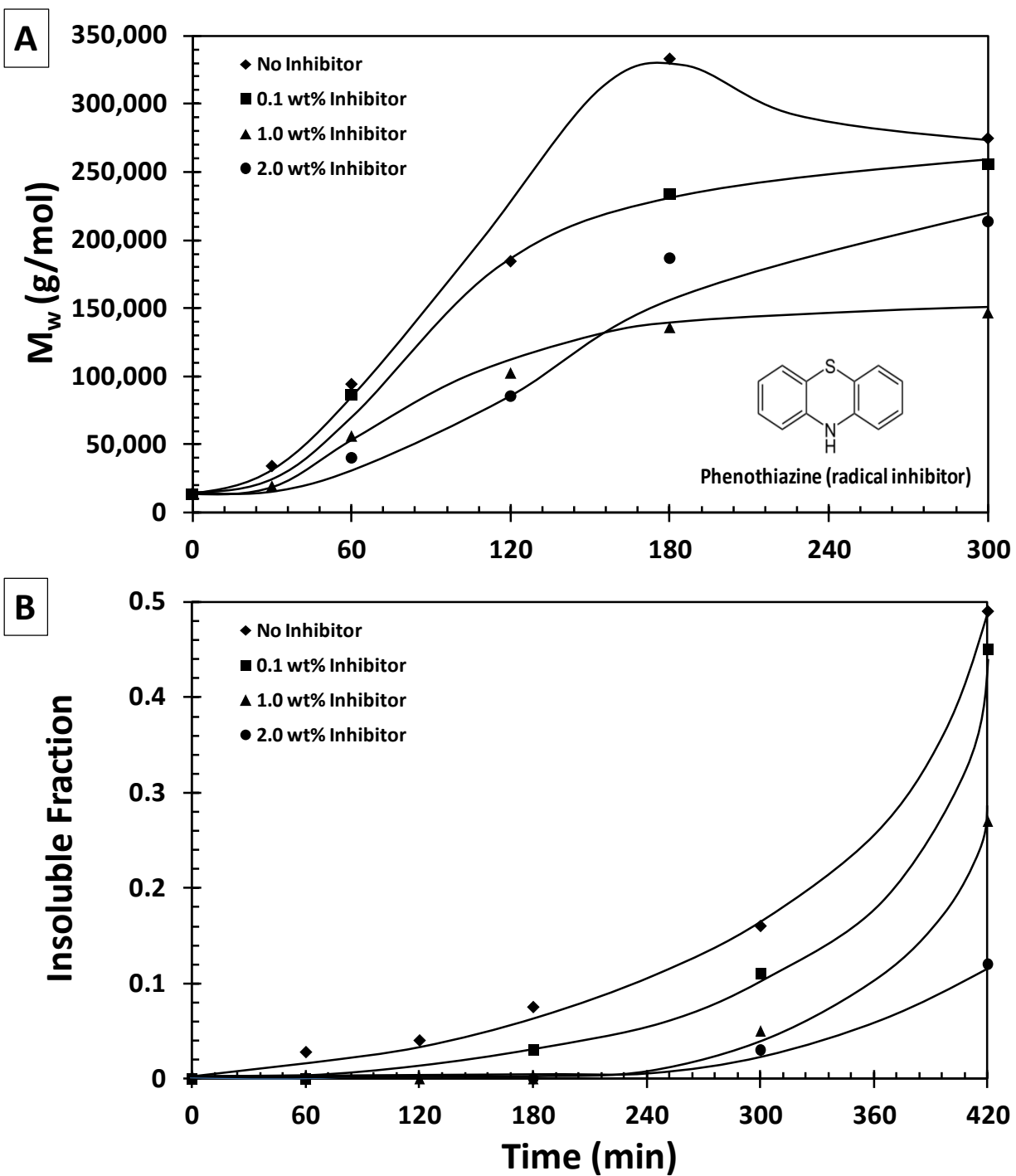


Figure 4.17 Evolution of effect of free radical inhibitor on weight average molecular weight (A) and insoluble fraction (B) with reaction time at 230°C ($T=230$ °C, $P=10$ mmHg, Prepolymer B-14K).

4.3.5 Multi-Layer Deposit & Reaction (MLDR)

When the micro-layers thicker than $35\mu\text{m}$ were prepared by solvent casting or spin coating technique, samples were partially crystallized and thermal annealing enhanced the crystallization during the reaction. Thus the micro-layer thickness was limited to a maximum of $20\mu\text{m}$ to ensure that all the micro-layers remained in an amorphous state. If the layer thickness can be expanded while keeping the merits of the SSP_m technique developed in this study, nonlinear ultrahigh molecular weight polycarbonates can have broader applications. To that purpose, multi-layer deposit and reaction (MLDR) of amorphous polymer was developed. Figure 4.18 shows a schematic description of the MLDR technique. An amorphous micro-layer is polymerized to a high molecular weight PC and then another layer is deposited on top of the original polymer layer by second casing. After the second layer is polymerized, the same procedure is repeated until the desired micro-layer thickness is achieved.

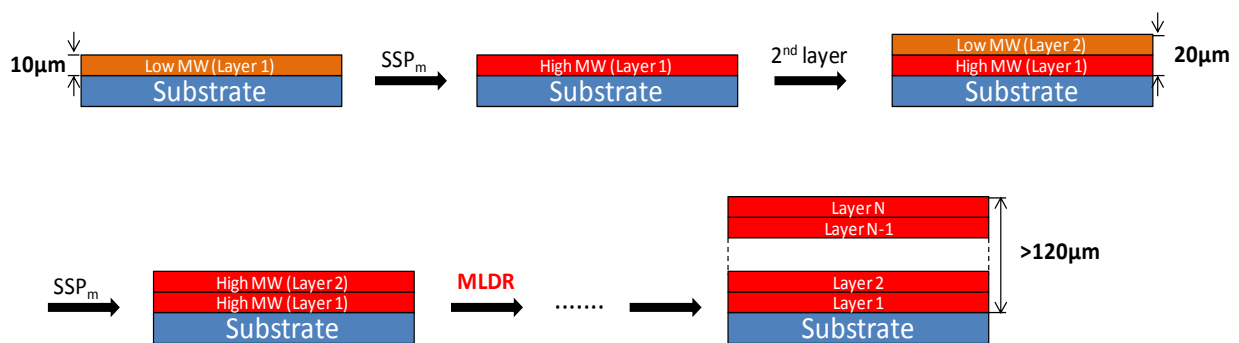


Figure 4.18 Schematic description of Micro-Layer Deposit Reaction (MLDR).

The first series of experiments was carried out with 10 μ m-thick amorphous micro-layers at a reaction temperature of 230 $^{\circ}$ C at 10 mmHg. To prepare the 10 μ m-thick amorphous micro-layers, spin coating technique was used at 2000 rpm with 0.3g/ml PC (14,000 g/mol) solution in chloroform. After 180 min of SSP_m, the 10 μ m amorphous micro-layers have about a 370,000 g/mol weight average molecular weight and 5% insoluble gel which are consistent with the results shown in Figure 4.2. Each additional layer was deposited on the polymer micro-layers after every 180 min of reaction with the same concentrated solution, until a desired thickness was obtained. After the first casting onto the glass substrate, additional micro-layers did not increase the thickness by 10 μ m but rather in increment of 15-25 μ m (Figure 4.19).

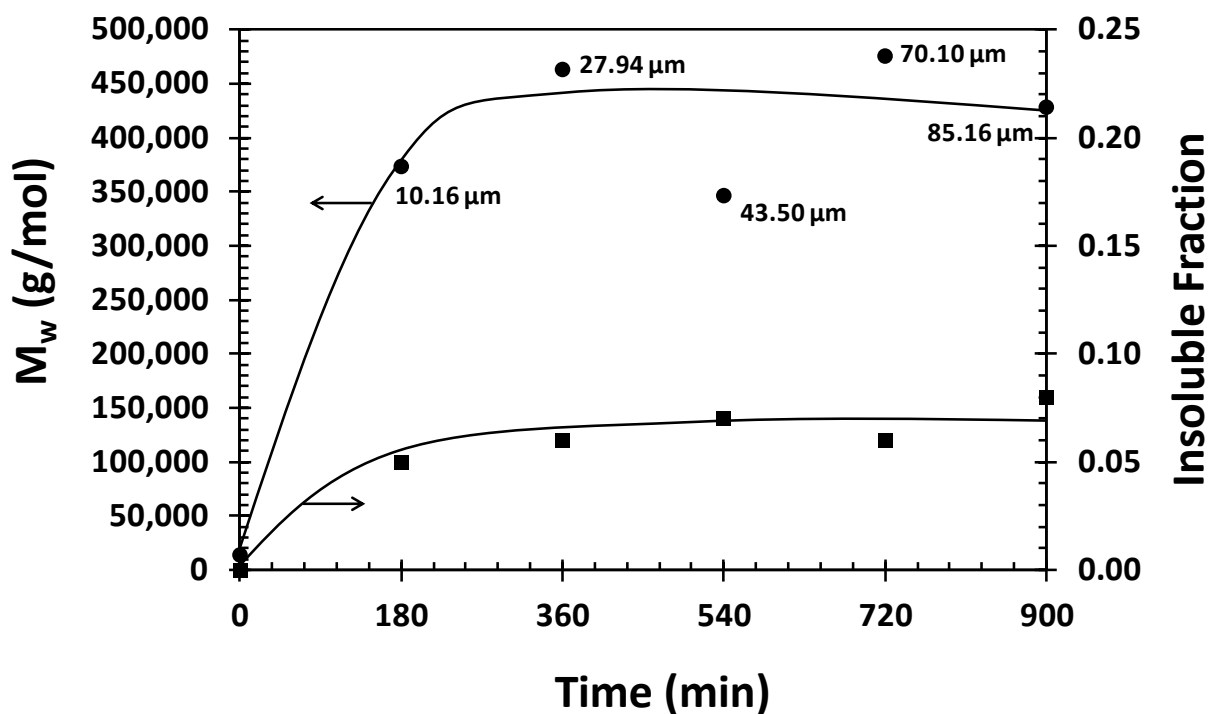


Figure 4.19 Evolution of molecular weight and formation of insoluble gel using MLDR method ($T=230^{\circ}$ C, $P=10$ mmHg, Prepolymer B-14K). Multi layers were deposited every 180 min interval. Solution concentration was set to 10 μ m thickness. Lines are added to guide the eyes.

The molecular weight of each additional multi layer deposited is similar to the molecular weight obtained in the first single amorphous micro-layer (Figure 4.19). This phenomenon is probably due to the fast removal of phenol at the interface of low molecular weight micro-layers and the reaction environment. Thus polymerization on the low molecular weight micro-layer is promoted while the viscous high molecular weight micro-layers underneath have extra diffusion barriers for the removal of the byproduct. In the full range of thicknesses, GPC chromatograms show that samples have unimodal distributions. Also, insoluble gel fractions are around 6% at all reaction times and amorphous micro-layer samples up to 85.16 μm show excellent transparency.

Another experiment was carried out by varying the initial micro-layer thickness (Figure 4.20). Three different concentrated solutions were used to prepare three types of samples with layer thicknesses of 5, 10, and 20 μm . Experiments were carried out at the reaction temperature of 230 $^{\circ}\text{C}$ under evacuate system (10 mmHg). For all samples, multi layers were applied at an interval of every 30 min. The thinner layers produce higher molecular weights but the same phenomenon was observed. The maximum micro-layer thickness obtained from this experiment is 131.32 μm , however, the MLDR technique may produce thicker layers while keeping target properties obtained from first single micro-layer. Figure 4.21 shows polydispersity vs. reaction time for all three micro layer thicknesses.

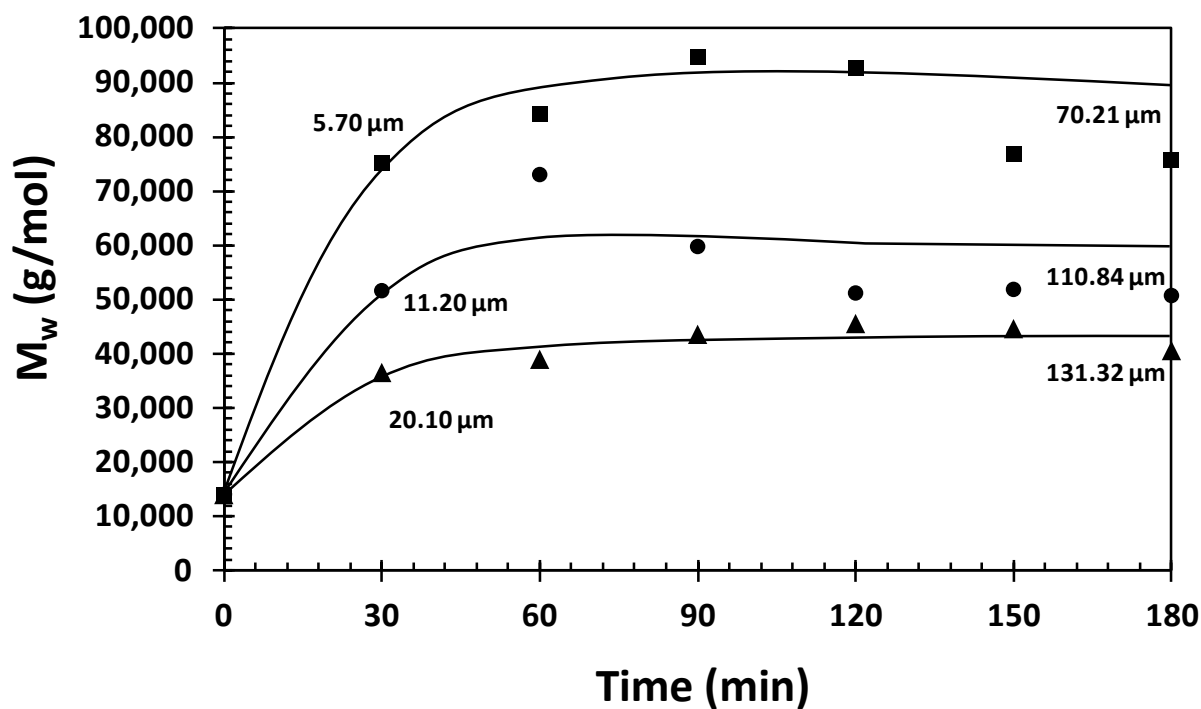


Figure 4.20 Evolution of molecular weight using MLDR method ($T=230\text{ }^\circ\text{C}$, $P=10\text{ mmHg}$, Prepolymer B-14K). Multi layers were deposited at an interval of every 30 min. Solution concentration was set to $5\mu\text{m}$ (\blacksquare), $10\mu\text{m}$ (\bullet), and $20\mu\text{m}$ (\blacktriangle) in thickness.

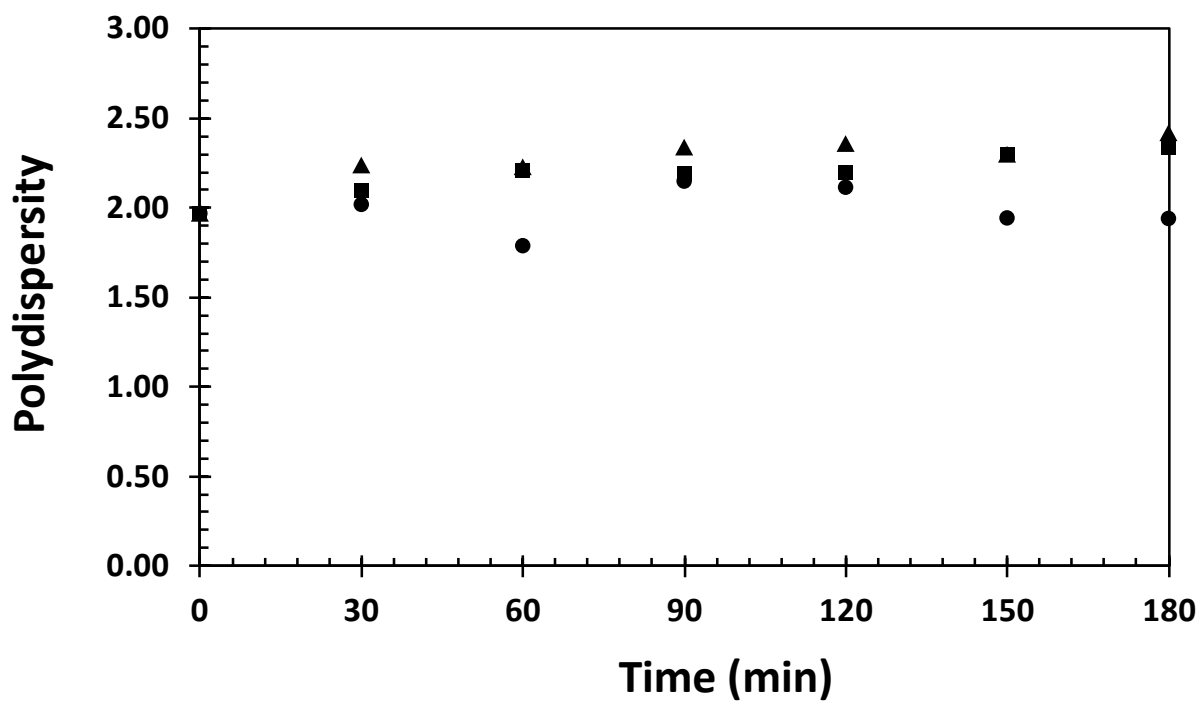


Figure 4.21 Polydispersity of polymers vs. reaction time profile. Multi layers were deposited every 30 min interval ($T=230$ °C, $P=10$ mmHg, Prepolymer B-14K). Solution concentration was set to $5\mu\text{m}$ (■), $10\mu\text{m}$ (●), and $20\mu\text{m}$ (▲) in thickness.

4.4 Conclusions

In this Chapter, the experimental investigation on the formation of insoluble gels during the SSP_m has been presented. The wt. fraction of insoluble gel obtained at 230°C under 10mmHg in 960 min is nearly 0.95 and the polymer has an excellent transparency. Improvement of solvent resistance, toughness and ductility are the major merits of high molecular weight insoluble PCs. The soluble and insoluble fractions were analyzed by ¹H-NMR and Py-GC/MS. Formation of insoluble gels is promoted in thinner micro-layers due to effective removal of the byproduct, phenol. For the layer thicknesses below 621nm, the residual phenol concentration was calculated using a theoretical simulation model. The simulation results indicate that the thickness effect is negligible in that residual phenol concentrations are close to zero. Both the molecular weight build-up and the formation of insoluble gel are affected by the presence of radical inhibitors. The experimental work presented in this chapter provides an indirect evidence of radical-induced reactions to the formation of cross-linked polycarbonates. Micro Layer Deposit Reaction (MLDR) technique tested in this work suggests that the thicker micro-layers of high molecular weight can be prepared.

Chapter5: Thermal, Mechanical and Rheological Properties and Crystalline morphology of SSP_m PCs

5.1 Introduction

In the previous chapters, we have presented that insoluble PC gel was produced at 230°C which is much lower than the melting point and that gel fractions as high as 0.99 was obtained without discoloration [12, 16, 17]. Poor solvent resistance and low surface hardness are known as weaknesses of polycarbonates. Other polymers such as polyimides, poly(ether sulfones), and poly(aryl ethers) can have cross-linking structures that improve the solvent resistance of polymers [81, 93, 94]. In this chapter, the physical, mechanical, and flow properties of partially cross-linked polycarbonates obtained via SSP_m process are presented.

Most studies on nonlinear polycarbonate in the literature are on the synthesis and characterization of branched polycarbonate. The average number of branching units per chain of 0.017-0.434 is reported in the case of melt-polymerized BPAPCs whose branched structure is a result of thermal rearrangement reactions [37]. Depending on the chain length and structure, branched polymers are sorted into short-chain or long-chain branched polymer categories. Long-chain branch polymers are defined as having higher values of weight average molecular weight per arm (M_w/arm) than the critical molecular weight for entanglement, M_c (e.g., 4000-4800 g/mol). The average number of repeating units of M_w/arm for commercially available long-chain

branched BPAPC was estimated at about 39 [7]. Rheological properties and crystallization behavior of polycarbonate depend on its molecular structure as well as molecular weight. For instance, high molecular weight linear PCs are not easy to melt process. However, processing long-chain branched PCs are relatively easier. The higher mobility of polymer chains in long-chain branched polycarbonate compared to linear polycarbonate was investigated using dielectric relaxation analysis [7]. Larger melt elasticity and shear rate sensitivity were observed while mechanical properties were not changed significantly within a wide range of compositions (0-100 wt% of branched BPAPC) of linear and branched BPAPC blends in commercially available long-chain branched polycarbonate [7]. For cross-linked polycarbonates, only the cross-linking of benzocyclobutene-terminated bisphenol A polycarbonate (BCB PC) was studied [81, 95]. Although the cross-linked BCB PC has a different structure than the cross-linked PCs discussed here, the cross-linked BCB PC's glass transition temperature increases up to 210°C depending on the cross-link density. Also, increase of yield stress (59.3-85.5 MPa), ultimate stress (85.5 MPa), and toughness was reported. However, decrease of ultimate elongation (111 to 14%) and film ductility are observed as the cross-link density increases [81]. Figure 5.1 shows the structure of BCB PC and cross-linked BCB PC.

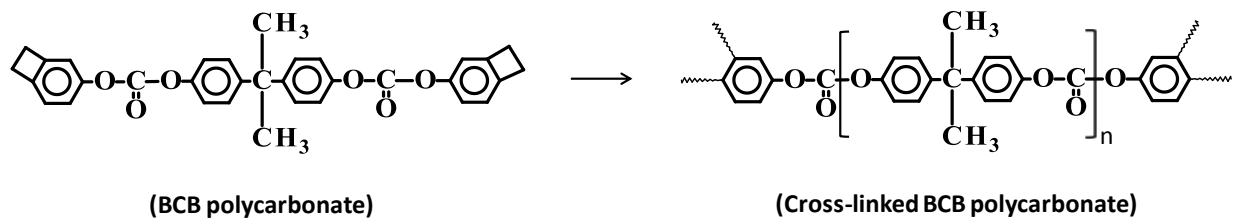


Figure 5.1 Structure of benzocyclobutene-terminated bisphenol A polycarbonate (BCB PC) and cross-linked BCB PC.

5.2 Experimental

5.2.1 Sample Preparation

The samples that are analyzed in this chapter were prepared as described in chapter 4 (see Figure 4.2). Table 5.1 shows the molecular weight (M_w) and the insoluble fractions (mass fractions) with SSP_m reaction time for a 10 μ m-thick micro-layer at 230°C. This Table shows that the amount of insoluble fraction can be controlled by the reaction time. The molecular weights shown in Table 5.1 are for the soluble fraction only.

Table 5.1 Sample weight average molecular weight of soluble PCs, insoluble fraction (mass fraction), polydispersity, and mole fraction of cross-linkage with the reaction time for 10 μ m-thick amorphous micro-layers (Precursor weight average molecular weight=14k g/mol, P= 10 mmHg, T=230°C).

Sample ID	10 μ m Amorphous Micro-Layers (SSP _m at 230°C)				
	Reaction time (min)	M_w in soluble frac. (g/mol)	Insoluble fraction	Polydispersity	Mole fraction of cross-linkage*
PRE-0	0	14,000	0	1.97	0
SSPM-30	30	34,000	-	2.26	3.55×10^{-4}
SSPM-60	60	94,000	0.03	2.32	8.89×10^{-4}
SSPM-180	180	333,000	0.05	2.57	4.26×10^{-2}
SSPM-420	420	187,000	0.49	3.22	6.28×10^{-2}
SSPM-960	960	149,000	0.95	5.46	6.33×10^{-2}

* these values were obtained by ¹H-NMR analysis (soluble fraction only).

5.2.2 Characterizations

The thermal analysis of SSP_m samples obtained from different reaction times was conducted using a differential scanning calorimeter (DSC) (TA Instrument Q1000). All the SSP_m PC samples contain a certain amount of insoluble gel fractions as shown in Table 5.1. About 5-6mg of polymer samples were taken and sealed in a TA Instrument Hermetic aluminum DSC can. A temperature range of 10-300 °C was used to cover both T_g and T_m with a scan rate of 10°C/min. The first cycle of heating and cooling was done to remove solvent effects and former thermal history and data from second cycle was collected to investigate the thermal properties of SSP_m PC samples.

For the dynamic mechanical analysis (DMA, TA Instrument Q800), 40µm and 200µm thick samples was prepared by stacking and fusing 10µm-thick amorphous micro-layers using a Carver Laboratory Heat Press at 200 °C. The 40µm-thick samples were used to obtain strain-stress curves and the 200µm-thick samples were used for the dynamic mechanical analysis using a temperature sweep mode. Different sample thicknesses were applied for the two different analyses due to maximum and minimum static force limits of the instruments. Rectangular shaped samples were prepared using TA Instrument sample cutter (dimension: 5.0 mm (length) × 5.3 mm (width)). For the tensile measurement, analysis conditions were set as follows: initial strain at 0.1%; constant temperature at 25°C; extension rate at 40µm/min; poisson's ratio of 0.37. Dislocation of samples was applied until the micro-layer samples fractured. A temperature sweep was used under a nitrogen environment in order to investigate the glass transition temperature, storage modulus, and phase lag (tanδ). The initial strain was set to 0.5% and a preload force of

0.01N was applied with a constant frequency of 1 Hz. The analysis was carried out from 20°C to 300°C. However, the final data point for each sample varied depending on their disentanglement characteristics. The temperature was raised in increments of 4°C with 2 min given at each analysis temperature to equilibrate the sample at target temperatures.

Flow properties of SSP_m PCs were characterized using a rotational rheometer (RSA III Analyzer (Rheometric Scientific Inc.)) with a parallel-plate (25mm in diameter) geometry with a sample thickness range of 400-500µm. A strain of 5% was used as all samples were in the linear viscoelastic regime. The analysis temperature was set to 260°C for rheological analysis and data collection from DMA analysis was limited to around 250°C. Dynamic storage (G'), loss shear moduli (G''), and complex viscosity (η^*) were obtained at a frequency range of 0.01-100 rad/sec under continuous nitrogen gas flow to prevent side reactions.

5.3 Results and Discussion

5.3.1 Differential Scanning Calorimetry (DSC)

A differential scanning calorimetry (DSC) was used to measure the glass transition temperatures (T_g) of the high molecular weight amorphous micro-layer samples. Figure 5.2 shows the DSC thermograms of the prepolymer (PRE-0 in Table 5.1) and amorphous micro-layers of 10 μm thickness synthesized at 230 $^{\circ}\text{C}$ at different reaction times (SSPM-30 to 960 in Table 5.1). The glass transition temperature of the low molecular weight linear prepolymer (PRE-0) is 131.31 $^{\circ}\text{C}$ but the T_g increased to 150.14 $^{\circ}\text{C}$ after 60min (SSPM-60). After 180 min (SSPM-180) of reaction time, T_g becomes stable at around 159 $^{\circ}\text{C}$ which is higher than the T_g values of commercial BPAPC (e.g., 146 $^{\circ}\text{C}$ (31,000 g/mol), 153 $^{\circ}\text{C}$ (43,000 g/mol)) [7, 96, 97]. The high molecular weight and the observed nonlinear chain structures in our polymer samples are thought to have caused the additional increase in T_g .

At 180 min (SSPM-180), the insoluble gel fraction is about 5% and rapidly increases after 300 min (see Figure 4.2). However, T_g does not seem to increase. Although it is not shown here, the soluble and insoluble fractions of the sample SSPM-960 was separated using its solubility in chloroform and T_g for each fraction was measured. Both soluble and insoluble gel fractions have a glass transition temperature of around 159 $^{\circ}\text{C}$. $^1\text{H-NMR}$ analysis has shown that the soluble fraction also contains branched and cross-linked structures. The mole fractions of cross-linkages in soluble fraction of sample SSPM-960 was 6.33×10^{-2} which was estimated using the area intensity of methyl protons and ethyl protons in repeating units and cross-linkages.

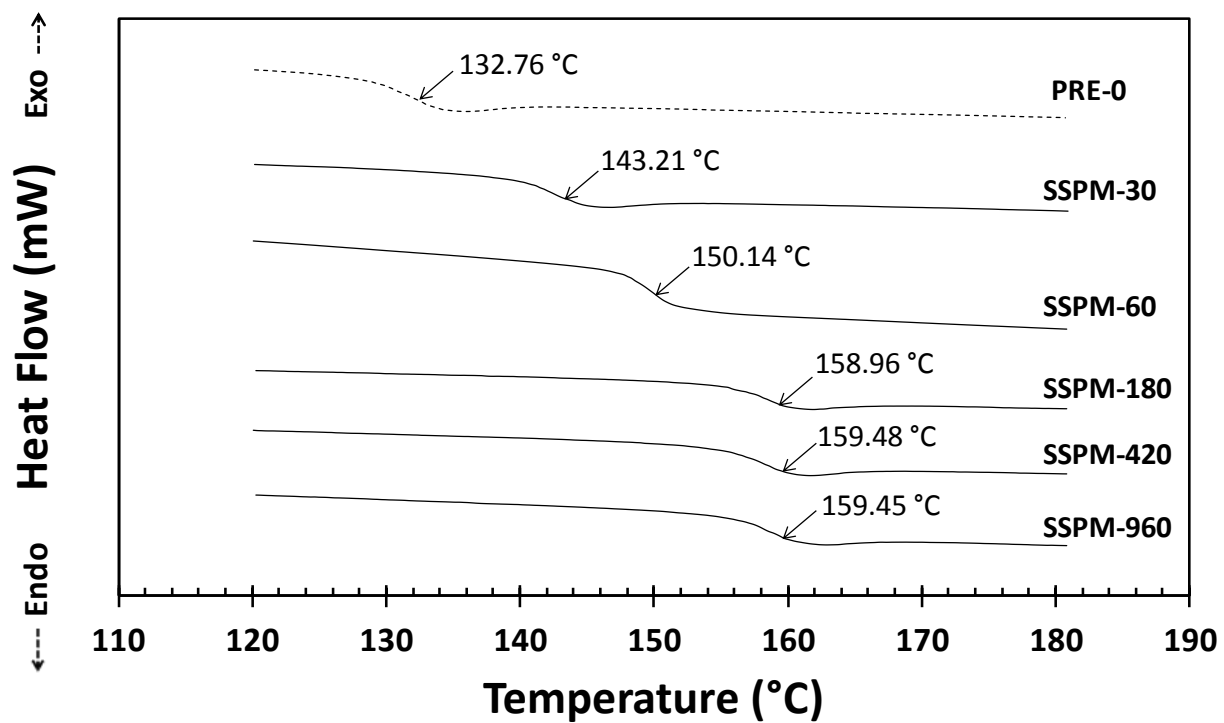


Figure 5.2 DSC thermograms of prepolymer (B-14k), amorphous micro-layers with reaction time ($T=230\text{ }^{\circ}\text{C}$, $P=10\text{ mmHg}$).

5.3.2 Dynamic Mechanical Analysis (DMA)

First series of DMA experiments were carried out for the tensile test of SSP_m PCs at fixed temperature (25°C). The 10µm amorphous samples taken from different reaction times were stacked and melted (fused) to make 40µm-thick films. Strain-stress curves were obtained as shown in Figure 5.3. The prepolymer of MW 14,000 g/mol sample (PRE-0) was also analyzed, though the low molecular weight sample PRE-0 fractured at a strain percent of 0.9. In fact, the prepolymer samples were very brittle making it difficult to prepare stable samples without cracking. For all SSP_m PCs, a great degree of ductility was observed. Tensile moduli of 340-1550 MPa were found for SSP_m amorphous samples, and the tensile modulus and the ultimate tensile strength increases as reaction time proceeds. The increase of ultimate tensile strength is due to the increase in chain length and degree of cross-linking indicating a decrease in rate of stress relaxation as cross-linking inhibits polymer chain flow. Note that Sample c (SSPM-180 in Table 5.1) has soluble weight average molecular weight of 340,000 g/mol with 5% insoluble gel (branched and partially cross-linked PCs) while Sample e (SSPM-960 in Table 5.2) has nearly 95% insoluble PCs. The ultimate elongation of SSP_m PCs increases until 180 min and then decreases with increasing reaction time and insoluble gel fractions. The decreasing of ultimate elongation is a typical phenomena caused by the drop in number of available polymer chain conformational states of cross-linked polymers [81]. Similar behavior was reported for the cross-linked benzocyclobutene-terminated polycarbonate [81]. The ultimate tensile strength and elongation of sample SSPM-960 were 69.5 MPa and 54.6 %, respectively.

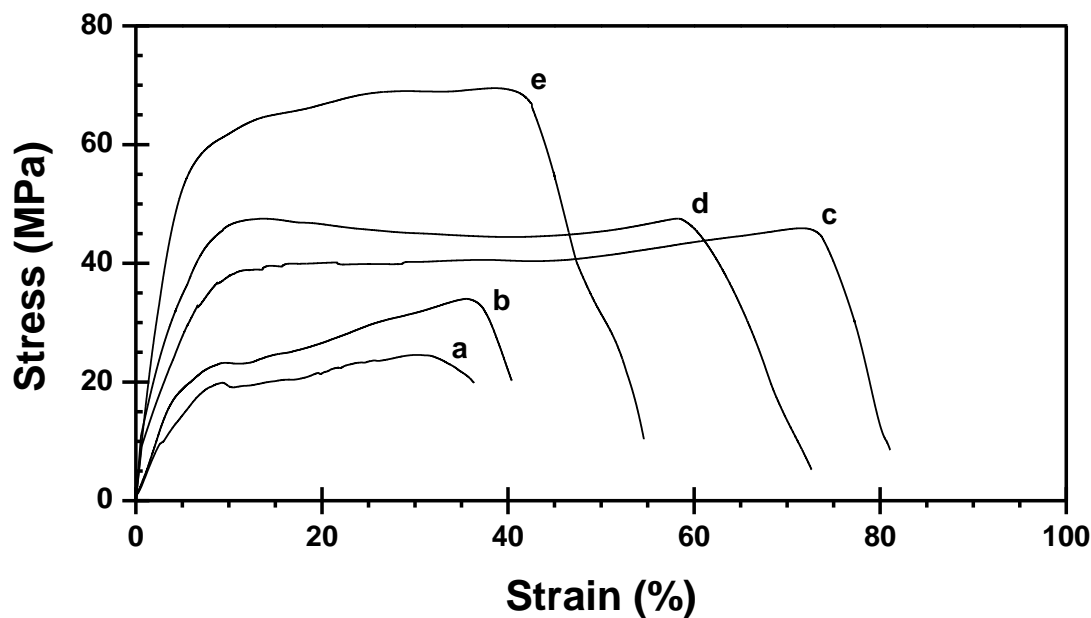


Figure 5.3 Strain-stress curves of SSPm PCs with reaction time: (a) SSPM-30, (b) SSPM-60, (c) SSPM-180, (d) SSPM-420, and (e) SSPM-960.

The results obtained from DMA temperature sweep for the prepolymer (PRE-0) and SSP_m PCs with different reaction time are given in Figure 5.4. Storage modulus versus temperature profiles were obtained using 200 μ m-thick amorphous micro-layer samples which were prepared by fusing 10 μ m-thick samples. SSP_m PCs samples show different dynamic mechanical responses depending on their molecular weight and molecular structures. Second order transition of the prepolymer is 147.2 $^{\circ}$ C. Compared to the T_g obtained from DSC analysis (see Figure 5.2), a value about 15 $^{\circ}$ C higher was observed. The transition point increases until the reaction time of 180 min (SSPM-180) is reached and stabilizes at a temperature of around 164 $^{\circ}$ C. The sample SSPM-180 containing 5% insoluble gel has roughly the same transition temperature

observed in SSPM-420 (49% insoluble) and SSPM-960 (95 % insoluble) samples. Up to a reaction time of 180 min (SSPM-180), there is a clear trend of increasing T_g , which can be attributed to the increase in chain length and degree of cross-linking. Previously reported NMR data in Chapter 3 shows that the mole fraction of cross-linking is 3.55×10^{-4} , 8.89×10^{-4} , and 4.26×10^{-2} for reaction times of 30, 60, and 180 min respectively (see Table 5.1). However, samples SSPM-180, 420, 960 exhibit very similar second order transitions. It seems that the onset of insoluble gel formation does not affect the second order transition of polymer chains. Compared to the mole fraction of cross-linking for the sample SSPM-30, the SSPM-60 shows a slight increase while the SSPM-180 shows an increase of 2 orders of magnitude (see Table 5.1), which has a significant impact on the second order transition. Looking at the soluble fraction of the SSPM-960, the cross-linking mole fraction is 6.33×10^{-2} which is the same order of magnitude as that of the 180 min sample. The sample SSPM-180 have 5% insoluble gel with a cross-linkage mole fraction of 4.26×10^{-2} . Above this point, the insoluble fraction rapidly increases while the T_g remains constant. Thus, this is in good accordance with DSC results which shows that the glass transition temperature stabilize around 159°C after 180 min (sample SSPM-180) (see Figure 5.2). At temperatures below the second order transition, the polymers are in glassy state. The storage modulus of prepolymer (PRE-0) at room temperature (25°C) is about 1000 MPa and this modulus gradually decreases as temperature rises up to the glass transition. For the SSPM-30, the storage modulus increases to 1450 MPa and only slight increments are seen after 180 min of SSP_m (SSPM-180). The sample SSPM-960 containing 95% insoluble has a storage modulus about 1.84 times higher in comparison with linear low molecular weight prepolymer (sample PRE-0).

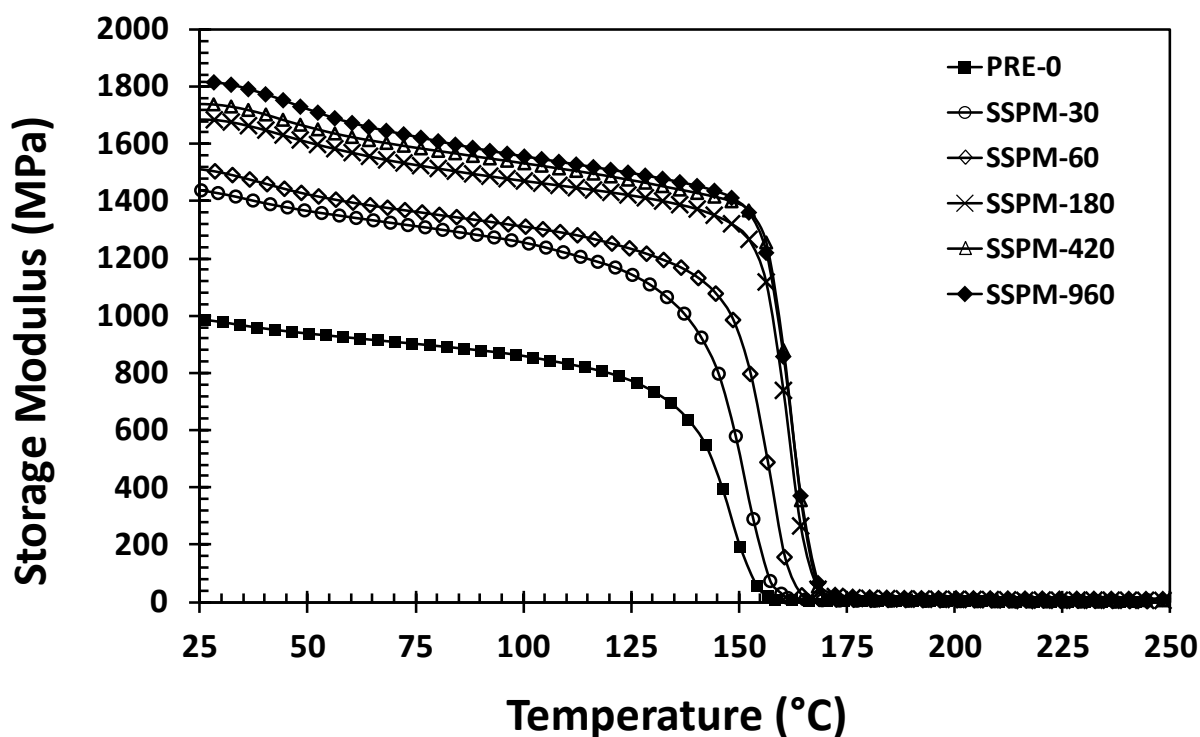


Figure 5.4 SSP_m PCs storage modulus as a function of temperature at 1 Hz with initial strain at 0.5% and preload force at 0.01N. SSP_m PCs were obtained at reaction temperature of 230°C with 10µm thickness micro-layers: PRE-0 (■), SSPM-30 (○), SSPM-60 (◇), SSPM-180 (×), SSPM-420 (△), and SSPM-960 (◆).

Above the glass transition temperature, the polymer chains have full mobility and their entanglement network affect the behavior of dynamic modulus [98]. Difference in molecular weight and molecular structure might affect the polymer chain entanglement at rubbery state. Above T_g , all samples show the drop of storage modulus to significant level about three order of magnitude lower as stress relaxation of polymer chains become higher [99]. To see the different behavior in rubbery state, logarithmic scale was applied as given in Figure 5.5. With prepolymer sample (PRE-0 in Figure 5.5 (■)), storage modulus decreased as temperature is raised and further

temperature increment gives disentanglement of polymer chain at the analysis temperature higher than 230°C. As the SSP_m process proceeds, the storage modulus increases and the slope decreases reaching a plateau, exhibiting elastic behavior in the rubbery state (see SSPM-960 in Figure 5.5 (◆)) [98]. Thus, the partially cross-linked polymer (SSPM-960) containing high fractions of insoluble gel behaves like typical thermosets. Also, disentanglement of polymer chain occurs at higher temperature as the reaction time increases accordingly as cross-linking in amorphous micro-layers is enhanced.

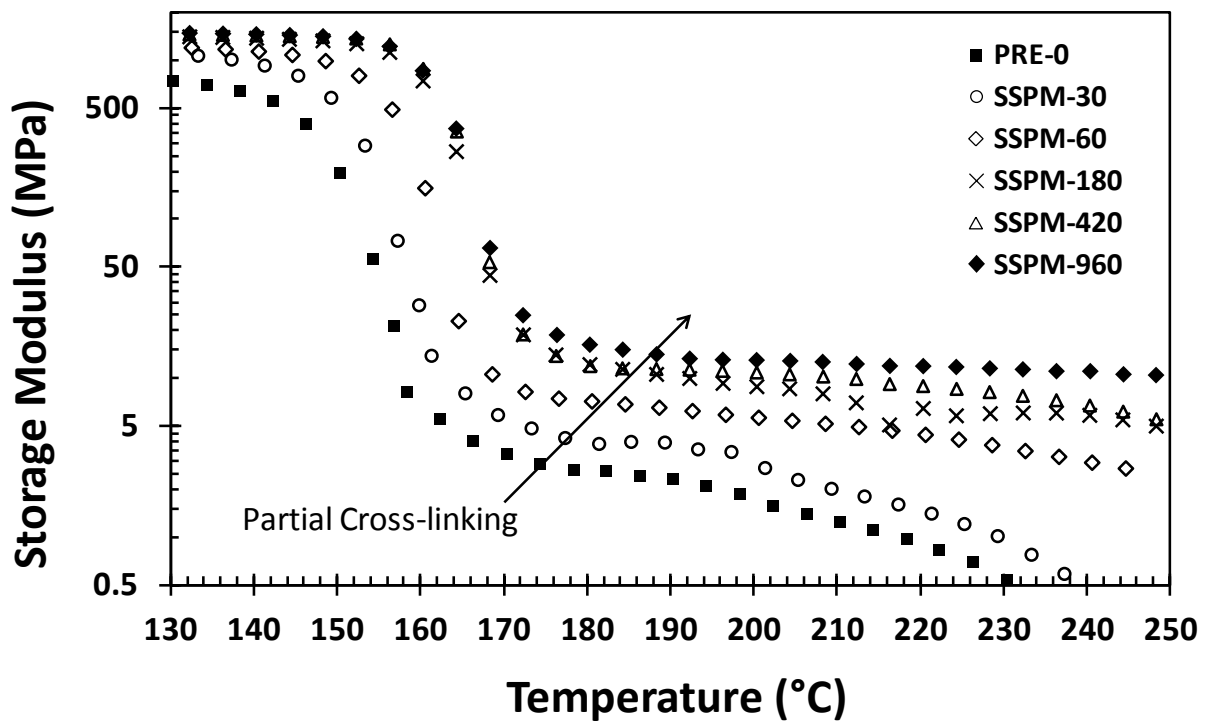


Figure 5.5 Behavior of storage modulus above the glass transition temperature (T_g) with different reaction time samples: PRE-0 (■), SSPM-30 (○), SSPM-60 (◇), SSPM-180 (×), SSPM-420 (△), and SSPM-960 (◆).

The analytical software (Universal Analysis software version 4.5) was used to obtain the loss tangent ($\tan \delta$) curves as given in Figure 5.6. Often, loss tangent is used to define the glass transition temperature (T_g) the ratio of loss modulus (E'') and storage modulus (E') are maximized at the peak values of loss tangent (phase lag).

$$\tan \delta = \frac{E''(\text{loss modulus})}{E'(\text{storage modulus})}$$

As observed in DSC, the loss tangent ($\tan \delta$) peak (in Figure 5.6) positions shift to high temperature until reaction time of 180 min is reached and stays around 168°C until 95% insoluble fraction is obtained. Moreover, the peak height decreases as the reaction time of SSP_m process increases, indicating that the energy loss (phase lag (δ)) becomes lower as molecular weight of polymer increases due to cross-linking. Although glass transition temperature remains nearly constant at 168.5°C after about 5% insoluble fraction (SSPM-180) is formed, the energy loss becomes smaller as insoluble gel formation increases. Figure 5.7 shows the $\tan \delta$ values as temperature is varied through rubbery state until disentanglement of polymer chain occurred for each sample. For all samples, loss tangent (δ) gradually increase as temperature increases indicating polymer loss modulus increases much faster than decreasing of storage modulus as chains are relaxed at higher temperature. When the partially cross-linking density increases with reaction times, $\tan \delta$ (δ) decreases at each given temperature indicating energy loss becomes lower. The SSPM-960 shows a rubber elastic plateau at temperatures above 220°C.

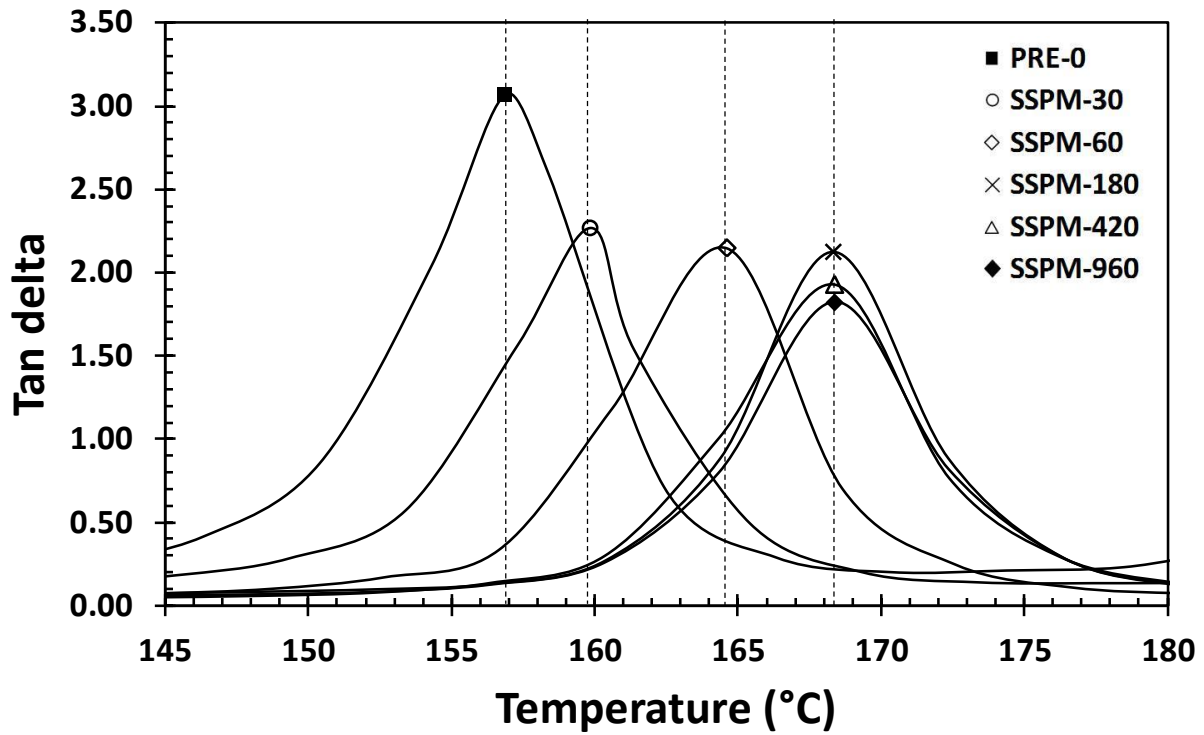


Figure 5.6 Loss tangent ($\tan \delta$) as a function of temperature at 1 Hz with initial strain at 0.5% and preload force at 0.01N. Peak positions are marked as: PRE-0 (■), SSPM-30 (○), SSPM-60 (◇), SSPM-180 (×), SSPM-420 (△), and SSPM-960 (◆).

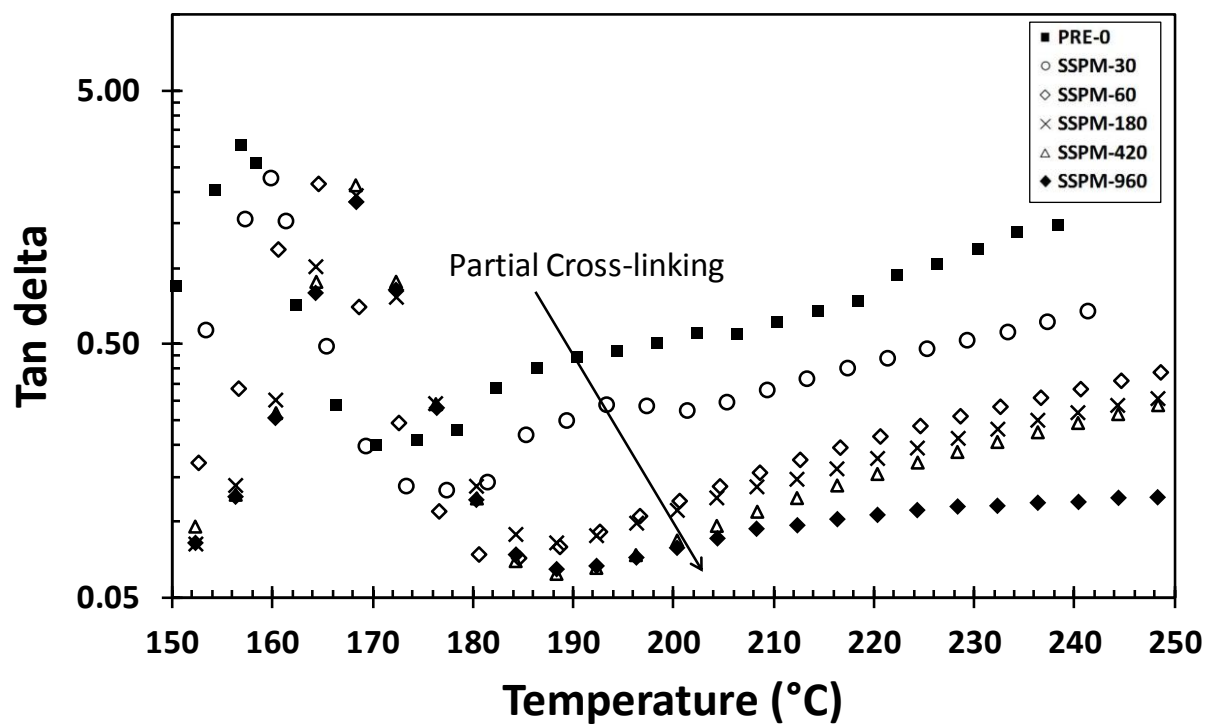


Figure 5.7 Behavior of loss tangent ($\tan \delta$) above the glass transition temperature (T_g) with different reaction time samples: PRE-0 (■), SSPM-30 (○), SSPM-60 (◇), SSPM-180 (×), SSPM-420 (△), and SSPM-960 (◆).

5.3.4 Rheological Properties

Molecular weight (MW), molecular weight distribution (MWD), and chain structures (*i.e.*, branching and cross-linking) are the important parameters that impact the polymer's physical, mechanical, and rheological properties [100]. The mechanical properties of SSP_m PCs in glassy state, glass transition and rubbery state are investigated using dynamic mechanical test. The majority of this part focuses on the flow region. Thus, the flow properties of SSP_m PCs were characterized above the polymer's melting temperature (T_m) using rheological measurements. Since SSP_m PCs have branched and partially cross-linked chemical structures, the flow properties enable us to identify microstructural characteristic. In general, higher molecular weight polymers have lower flow property [7, 101-104]. However, flowability of non-linear structure polymers such as branched and cross-linked polymers depends on the molecular weight and degree of branching and cross-linking as well [105, 106]. The 10 μ m amorphous micro-layers obtained by SSP_m were fused to prepare 400-500 μ m samples prior to the rheological measurement. A strain of 5% was used in the experiments at 260 $^{\circ}$ C which is higher than the polymer's melting point [96, 97] and approximately 10 $^{\circ}$ C higher temperature of polymer chain disentanglement (see Figure 5.7) observed in DMA results. Dynamic storage (G'), loss shear moduli (G''), and complex viscosity (η^*) were obtained at a frequency range of 0.01-100 rad/sec under the continuous nitrogen gas flow to prevent side reactions.

The complex viscosities of linear prepolymer (sample PRE-0) and high molecular weight nonlinear SSP_m PCs (sample SSPMs) are shown in Figure 5.8. The sample PRE-0 (low molecular weight linear polycarbonate) behaves like a typical Newtonian liquid. As molecular

weight is increased with branching and partial cross-linking, zero shear viscosities become two orders of magnitude larger (e.g. sample SSPM-30). The shear thinning effect does not change much in 30 min (sample SSPM-30), approximately 7000 Pa·s drop as frequency increment was observed in both samples PRE-0 and SSPM-30. The complex viscosity increases and the range of the zero shear rate for Newtonian region decreases until 60 min. For the SSPM-180 and 420, the Newtonian behavior is not observed in the frequency range of 0.01-100 rad/sec. As SSP_m reaction extends from 30 min (SSPM-30) to 180min (SSPM-180), the complex viscosities of SSP_m PCs at high shear frequency are very similar while large difference in viscosity was observed as frequency goes to lower range. These phenomena indicate that shear thinning effect become larger as branching and mainly partial cross-linking reaction proceeds in the SSP_m process. It is known that molecular weight, molecular structure, and polymer relaxation rate affect the degree of shear thinning [7, 107]. Lower polymer chain relaxation or diffusion rate from high molecular weight nonlinear (branching and partial cross-linking) polycarbonates give higher shear thinning effect [7, 107]. Linear viscoelastic behaviors were observed for the SSPM-180 and SSPM-420 which contain about 5% and 49% insoluble gel, respectively. For the SSPM-420 (49% insoluble gel), slight increase of shear viscosity is observed in comparison with the SSPM-180. It is reported that cross-linked polymers near gel point the relaxation time becomes large thus steady shear flow is not reached [108].

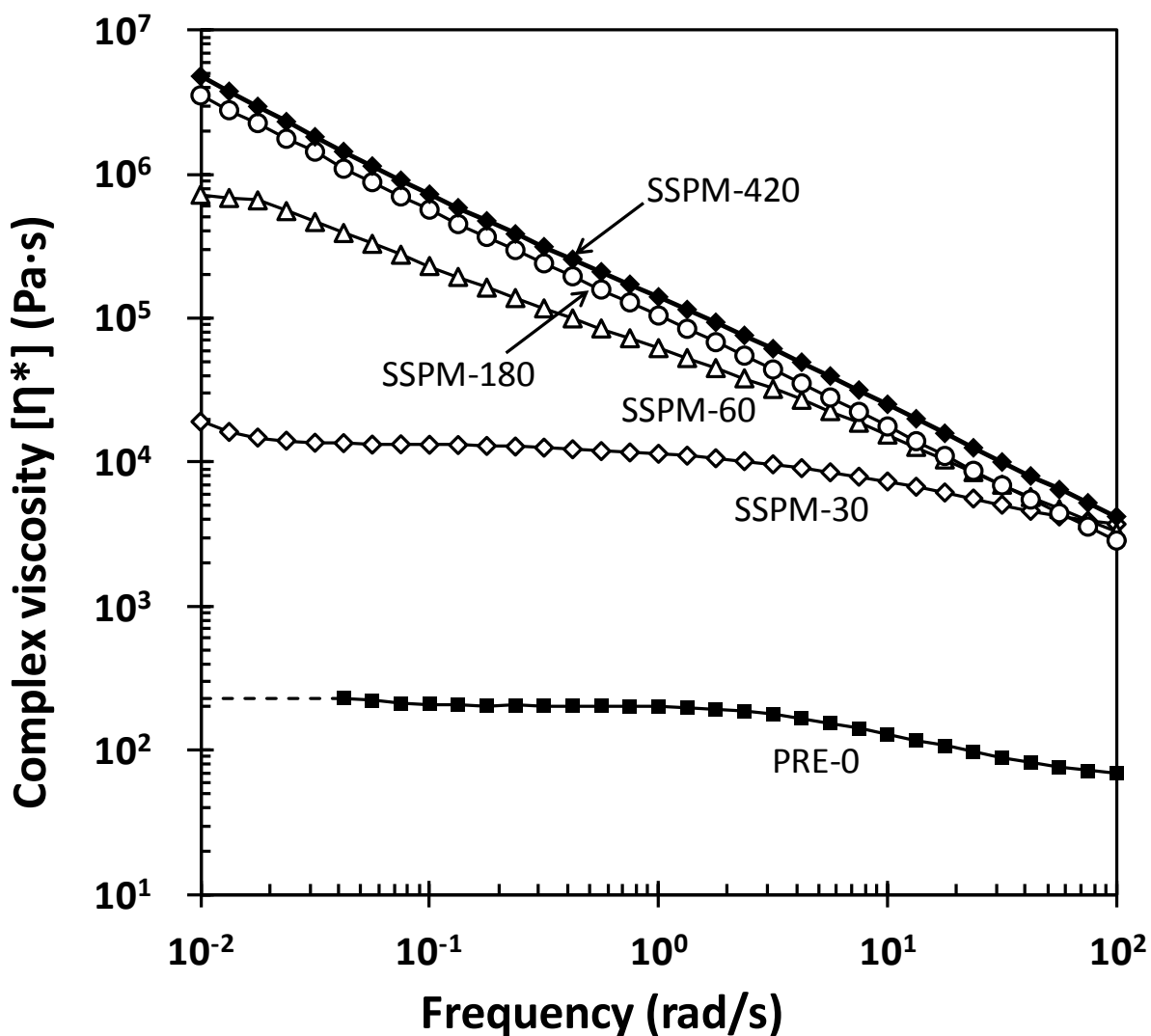


Figure 5.8 Dynamic viscosity of prepolymer and SSP_m PCs over a frequency range of 0.01-100 rad/s. SSP_m PC samples were prepared at 230°C with 10µm thickness: PRE-0 (■), SSPM-30 (◇), SSPM-60 (△), SSPM-180 (○), SSPM-420 (◆).

Figure 5.9 shows shear storage modulus (G') of prepolymer and SSP_m PCs over a frequency range of 0.01-100 rad/s. For the sample PRE-0 (linear low molecular weight polycarbonate), the storage modulus (G') decreases as frequency decreases and the slope is

approximately two which represents a typical behavior of Newtonian fluids. For the SSPM-30, storage modulus increases by about two orders of magnitude but the slope is nearly same. In addition, loss modulus values are higher than the storage modulus at all the range of frequency in that $\tan \delta$ values are higher than 1 (see Figure 5.10 and Figure 5.11). The sample SSPM-30 has gel content below 1 wt%. As gel content increases with reaction time (> 180 min), the complex viscosity (in Figure 5.8) and storage modulus (in Figure 5.9) show that the polymers exhibit more rubber-like behavior in that zero shear viscosity was not observed and the slope of storage modulus approaches zero [108-110]. Recall that in the $^1\text{H-NMR}$ data shown in Chapter 3, the mole fractions of cross-linked polymers are 3.55×10^{-4} , 8.89×10^{-4} , and 4.26×10^{-2} for reaction times of 30, 60, and 180 min, respectively (see Table 5.1). As the amount of cross-linked polycarbonates increases in micro-layers, the storage modulus (G') increases faster than the loss modulus (G'') indicating that melt elasticity of partially cross-linked polycarbonate is much higher than the low molecular weight linear prepolymer (PRE-0) and sample SSPMs with lower contents of cross-linking (Figure 5.11). For the SSPM-180 and SSPM-420, the storage modulus is larger than the loss modulus at all frequency range tested in our experiments.

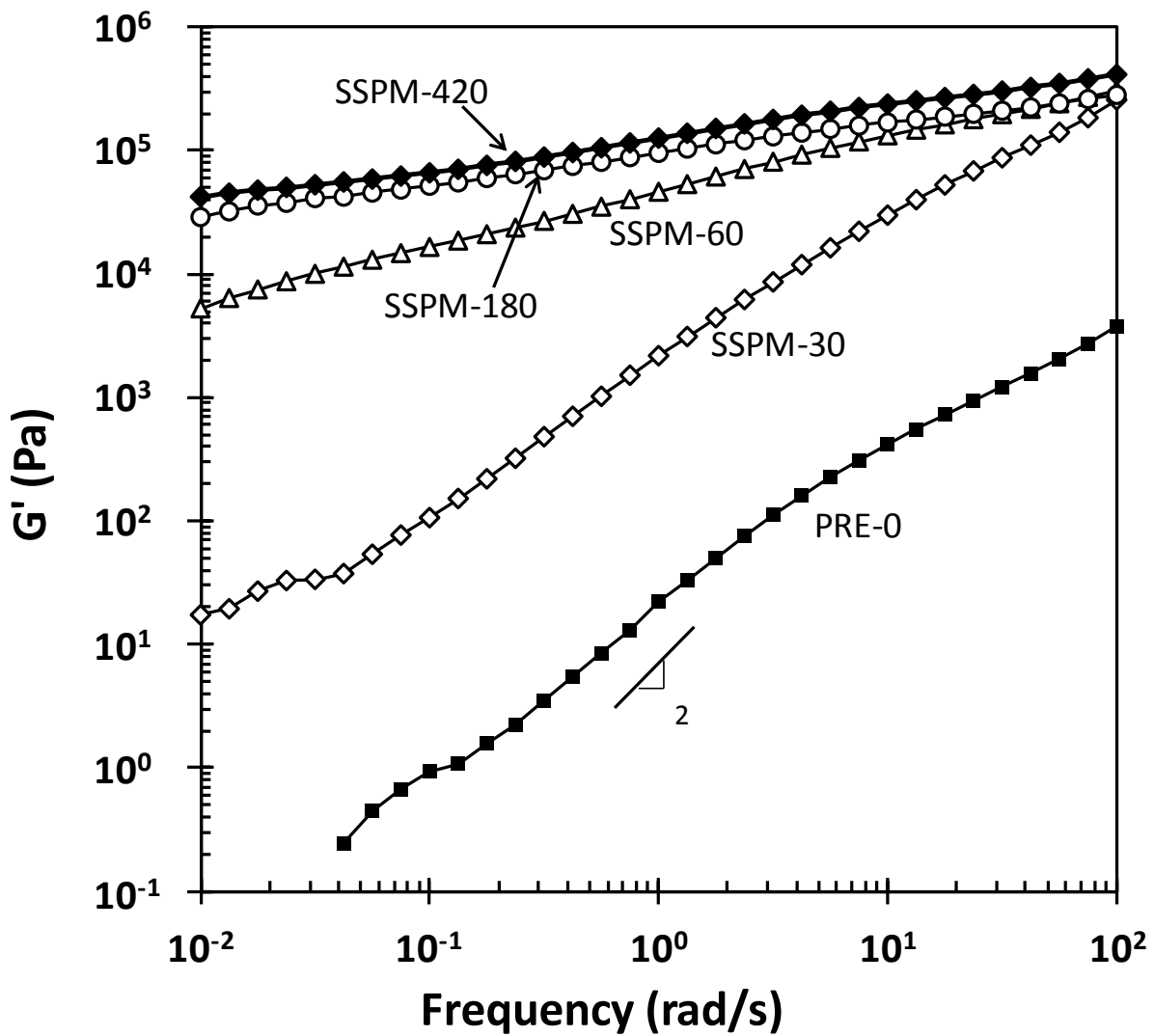


Figure 5.9 Shear storage modulus (G') of prepolymer and SSP_m PCs over a frequency range of 0.01-100 rad/s. SSP_m PC samples were prepared at 230°C with 10μm thickness: PRE-0 (■), SSPM-30 (◇), SSPM-60 (△), SSPM-180 (○), SSPM-420 (◆).

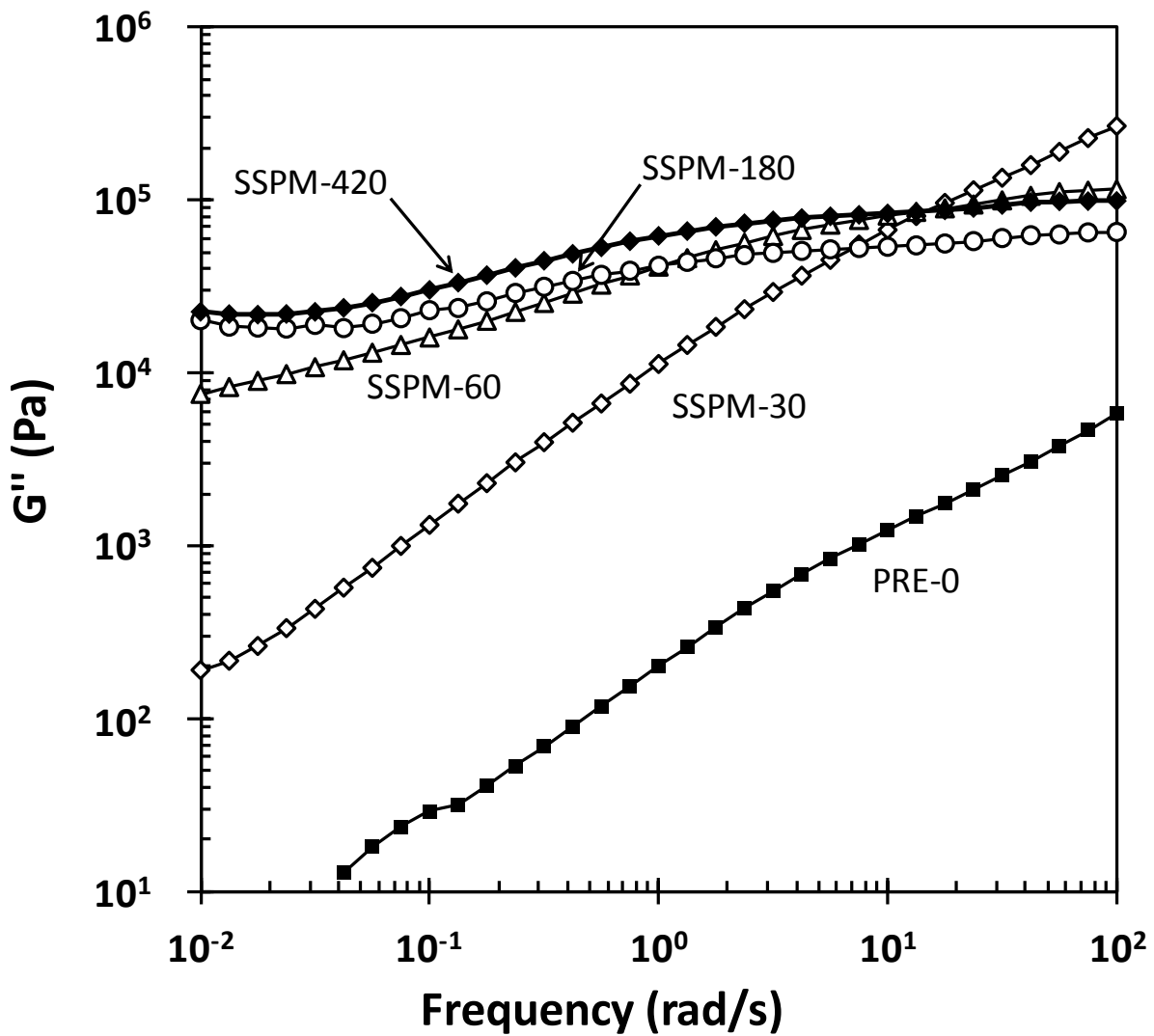


Figure 5.10 Shear loss modulus (G'') of prepolymer and SSP_m PCs over a frequency range of 0.01-100 rad/s. SSP_m PC samples were prepared at 230°C with 10μm thickness: PRE-0 (■), SSPM-30 (◇), SSPM-60 (△), SSPM-180 (○), SSPM-420 (◆).

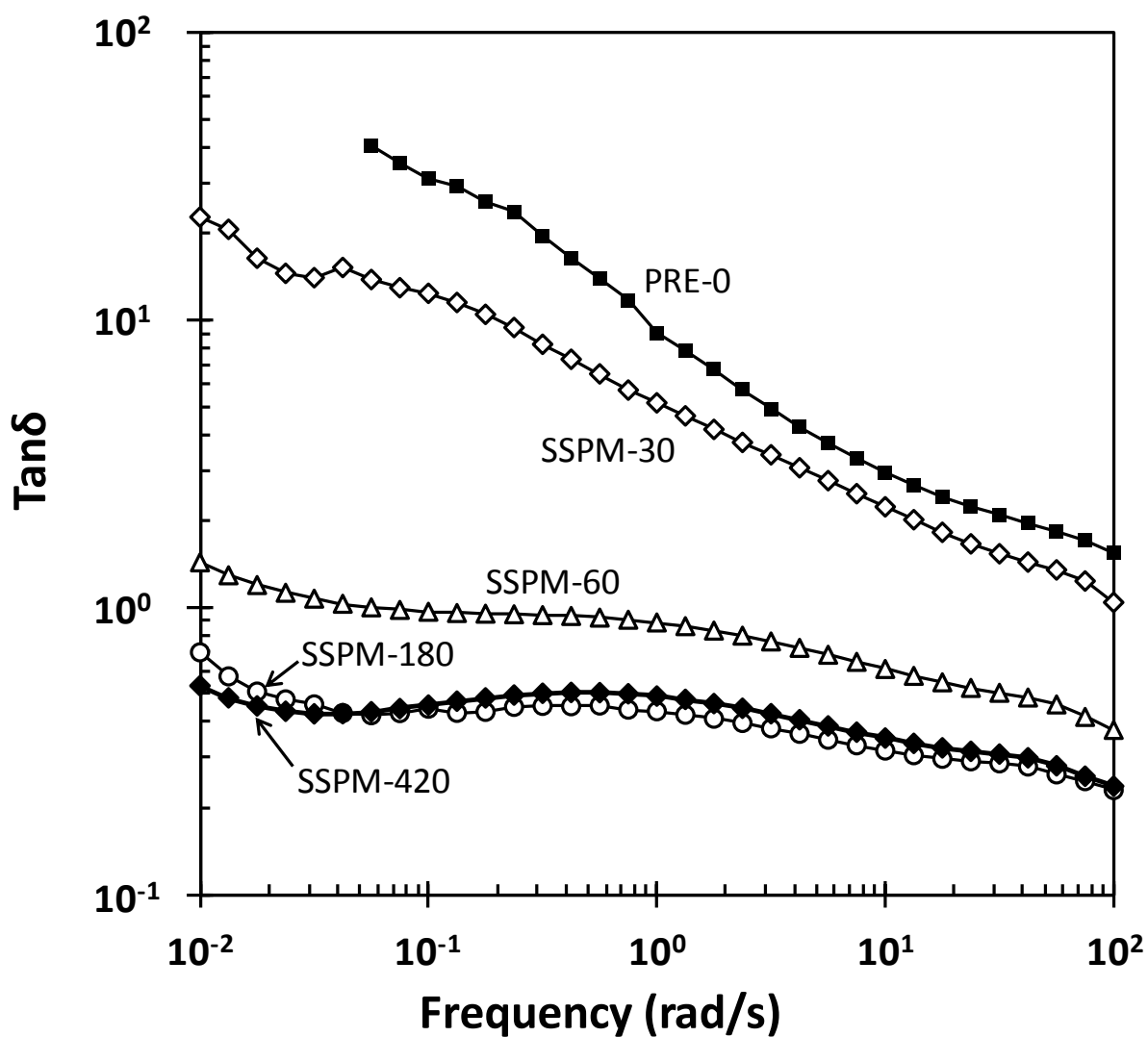


Figure 5.11 Loss tangent ($\tan \delta$) of prepolymer and SSP_m PCs over a frequency range of 0.01-100 rad/s. SSP_m PC samples were prepared at 230°C with 10μm thickness: PRE-0 (■), SSPM-30 (◇), SSPM-60 (Δ), SSPM-180 (○), SSPM-420 (◆).

5.3.5 Crystalline Morphology of SSP_m PCs

When amorphous polycarbonate micro-layers are treated with acetone as a swelling agent, crystallization occurs rapidly in the polymer micro-layer into an aggregate of 3-5 μm-diameter spherulitic polymer particles [48, 49]. Each spherulitic polymer particle consists of very thin leaves, protruding from the center of the particle. Figure 5.12 (a) shows the SEM images of the crystallized linear prepolymer (PRE-0) micro-layer surface of 10μm thickness for 10 sec and 30 sec in acetone. After SSP_m process in amorphous micro-layers at 230°C, the 10 μm-thick micro-layers maintained an amorphous. These micro-layers of nonlinear high molecular weight SSP_m PC s were crystallized using acetone. For the sample PRE-0, the complete spherulitic morphology can be obtained in 30sec. Unlike the original prepolymer crystallized by acetone, the SEM images in Figure 5.12 (b)-(d) show that the high molecular weight nonlinear (branched and partially cross-linked) polycarbonates do not crystallize to discrete spherulites. As the content of cross-linked polycarbonate increases with reaction time, crystallization rate was very slow (see Figure 5.12). Figure 5.13 shows cross-sections of PRE-0 and SSPMs at different reaction time. The prepolymer micro-layers consist of small spherulitic particles across the entire thickness, but the free volume decreases as the content of cross-linked polymers increases. For the sample SSPM-960, acetone induces a rough surface but the spherulitic morphology is not seen at all. High resolution SEM images in Figure 5.14 show that SSPM-960 has non-spherulitic morphology. It is also observed that secondary crystallization occurred at the top of the primary spherulitic structure (Figure 5.15).

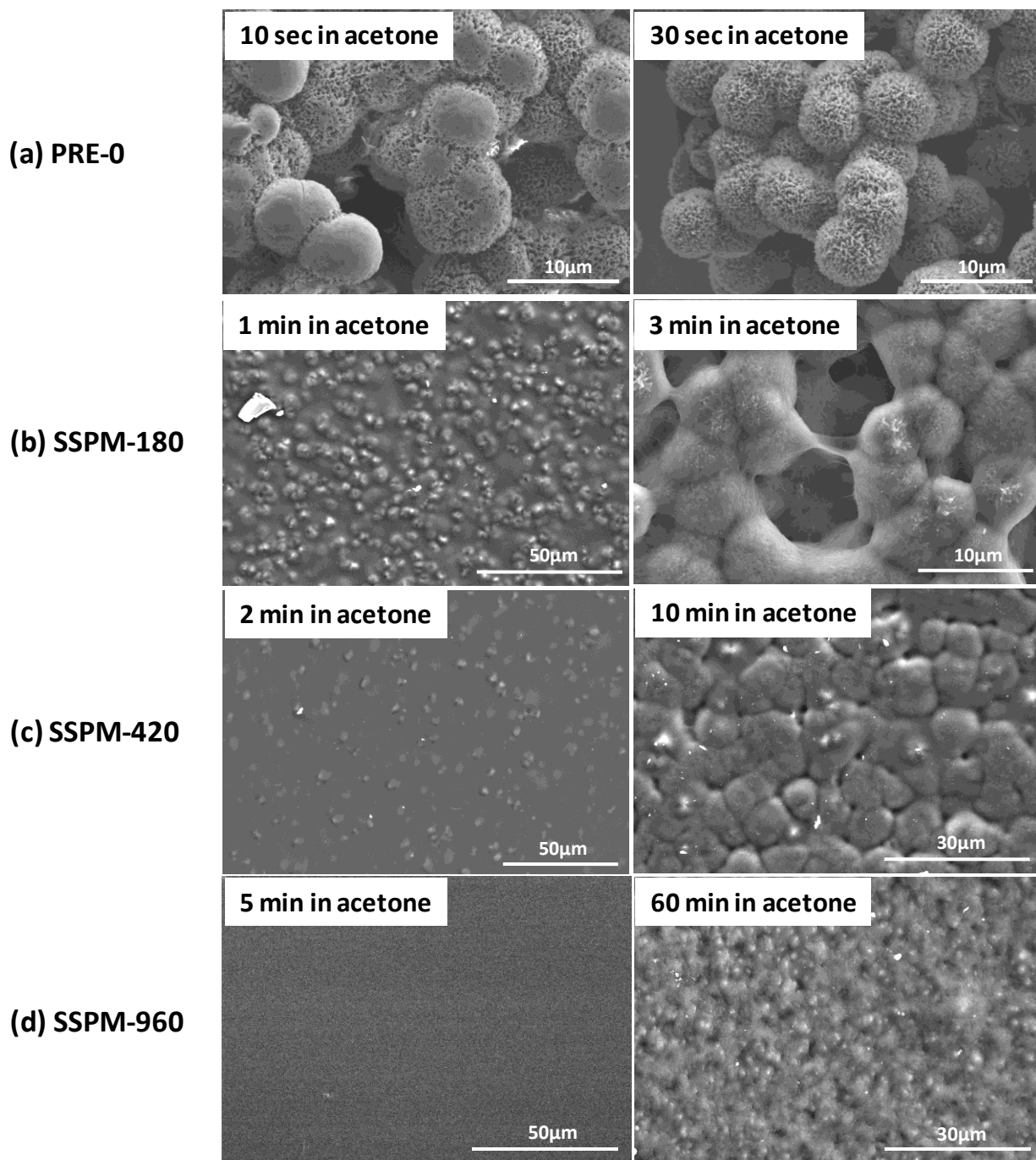


Figure 5.12 Acetone induced crystallization of prepolymer and SSP_m PCs: (a) PRE-0, (b) SSPM-180, (c) SSPM-420, and (d) SSPM-960.

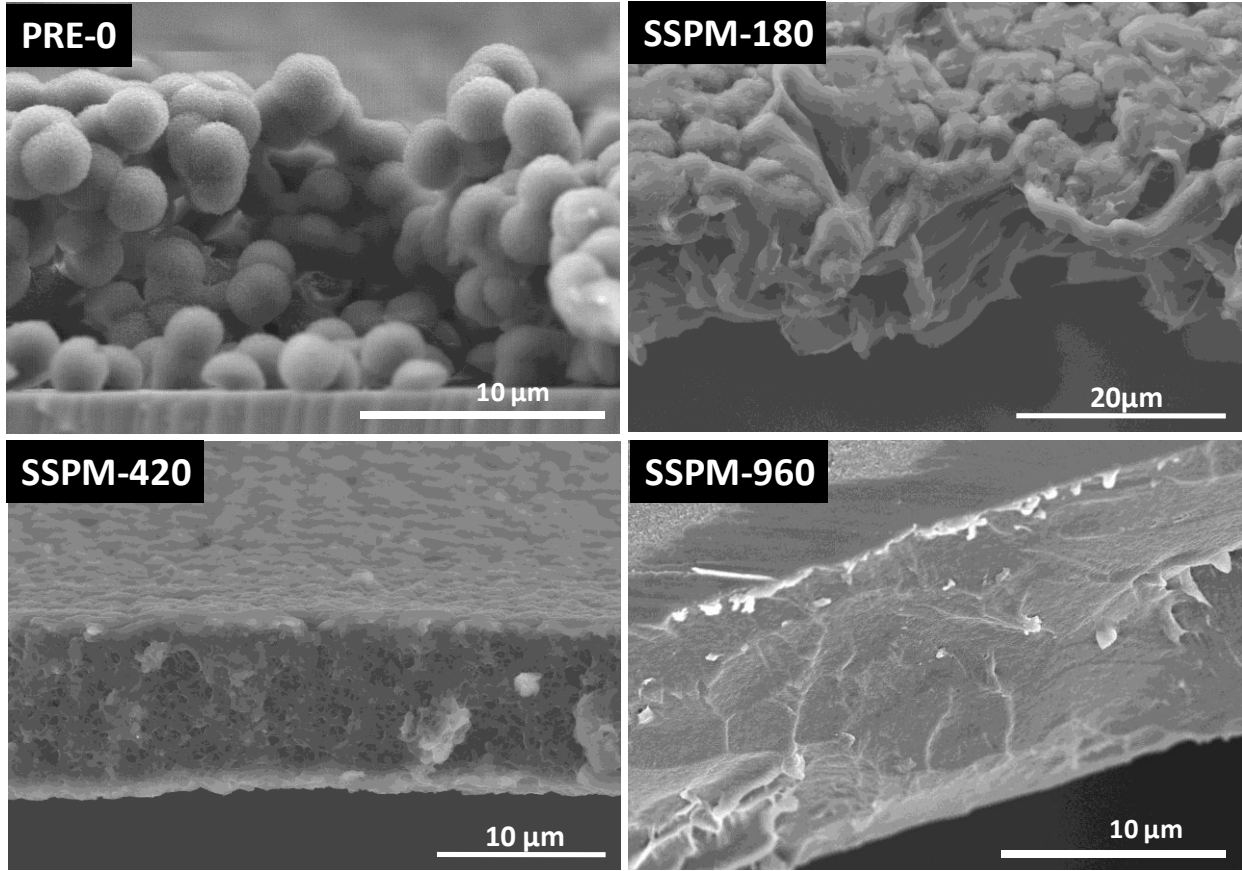


Figure 5.13 Cross-sectional area of prepolymer and SSP_m PCs with reaction time extend.

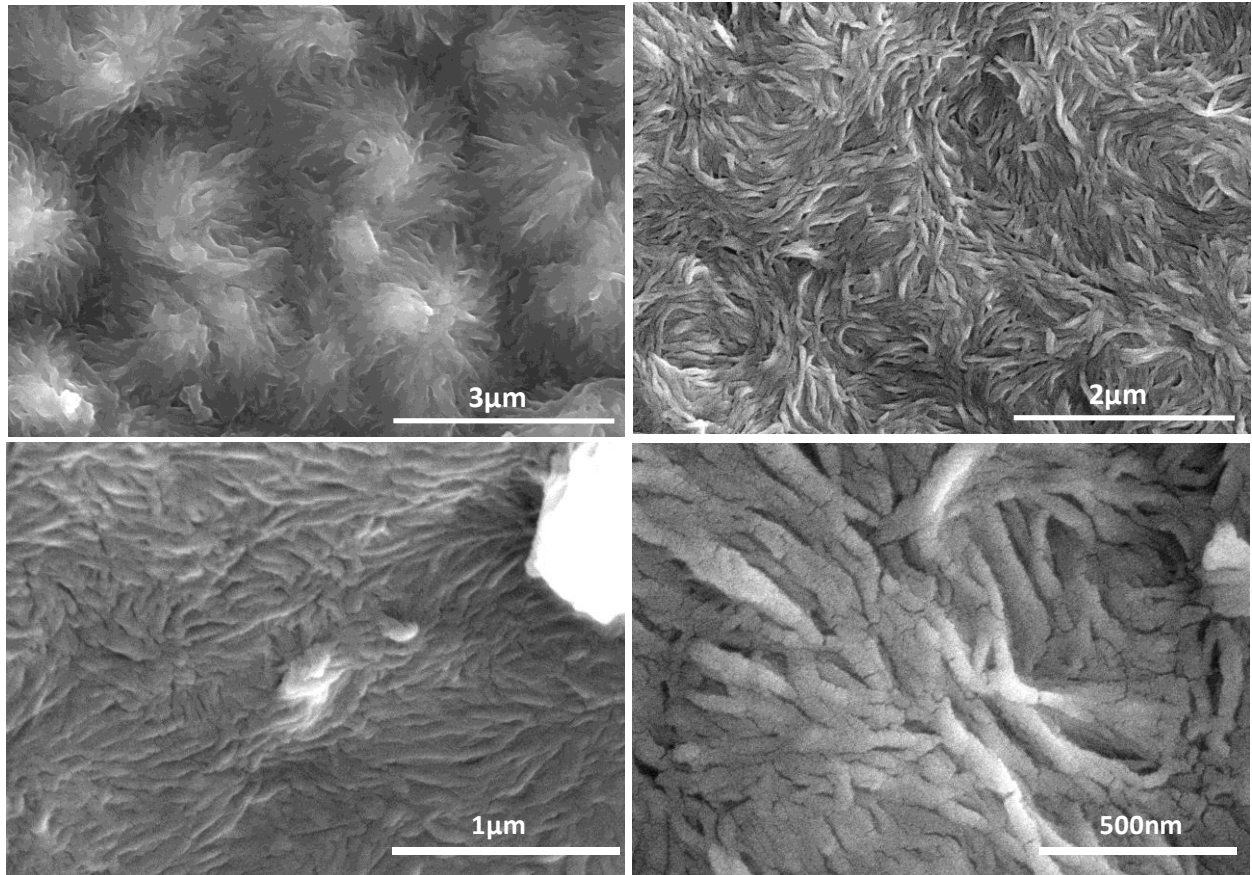


Figure 5.14 Surface morphology of SSPM-960 (about 95% insoluble) samples.

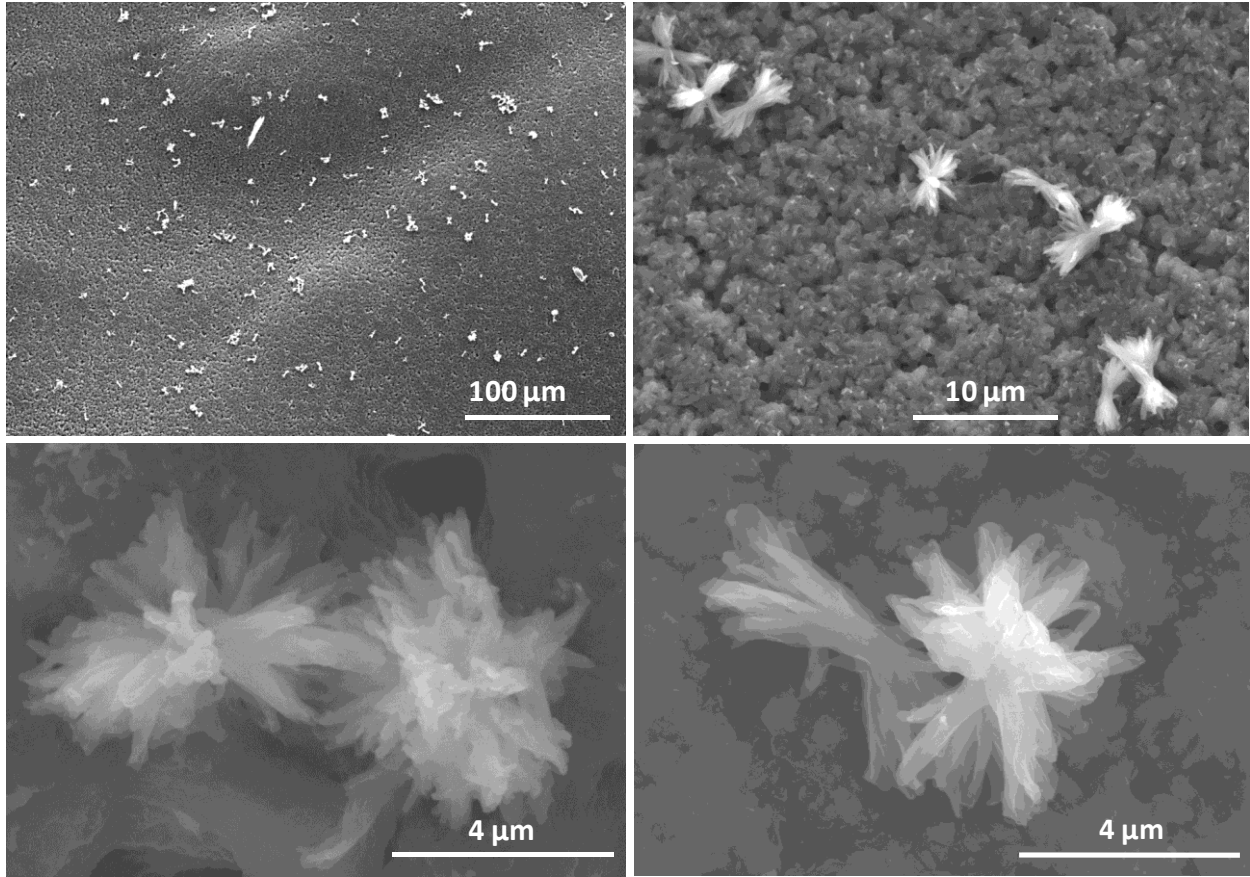


Figure 5.15 The secondary crystallization at the top of the primary structure (sample SSPM-960).

5.4 Conclusions

In this Chapter, thermal, mechanical, and rheological properties of the prepolymer and SSP_m PCs using DSC, DMA, and rheometer were presented. In short reaction times (180 min) of SSP_m, the glass transition temperature rapidly increase to 158.96°C which is 6-10°C higher than the commercially available linear polycarbonates. The T_g remains at this temperature even with a further increase in the insoluble fraction to 95%.

Strain-stress curves obtained using DMA tensile test show that tensile modulus and ultimate tensile strength increase as the reaction time of SSP_m increased. The ultimate elongation increases until the reaction reaches 5% insoluble gel formation but decreases of ultimate elongation was observed as the amount of insoluble gel further increased. Decrease in the ultimate elongation with samples SSPM-420 and SSPM-960 is a typical phenomenon of cross-linked polymers. The maximum ultimate tensile strength was observed at 69 MPa with a sample containing 95% insoluble gel (SSPM-960) and maximum ultimate elongation of SSP_m PCs was about 82% with SSPM-180 (5% insoluble gel). The extension rate of 40µm/min was used to obtain these data. From DMA analysis using temperature sweep mode, the higher storage modulus in glassy state and rubbery state, the decrease of tan δ value on the glass transition temperature, and the decrease of tan δ value in rubbery state region were observed as cross-linking reaction proceeds. The sample containing 95% insoluble gel (SSPM-960) shows the behavior of rubber elastic plateau in both storage modulus and tan δ versus temperature profiles.

The flow properties of SSP_m PCs were characterized above the polymer's melting temperature (T_m) using rheological measurements in the frequency range of 0.01-100 rad/sec.

The high molecular weight branching and partial cross-linking structure yields higher viscosities and about two orders of magnitude increase after 30 min of SSP_m with 10µm amorphous micro-layers. Larger shear thinning effect was observed as branching and partial cross-linking reactions proceed in the SSP_m process.

The crystallization of prepolymer (PRE-0) and SSP_m PCs were also studied. The spherulitic crystalline morphology of low molecular weight prepolymer was not observed in higher molecular weight samples and it is the indirect evidence that these high molecular weight polymers are not linear polymers as the prepolymers used in our experimental study.

Chapter6: Summary and Significance

In this thesis, we have investigated the following: 1) Synthesis of ultra-high molecular weight polycarbonate by solid-state polymerization in micro-layers (SSP_m); 2) Reaction mechanisms for the formation of branched and cross-linked polymers in the SSP_m; 3) Properties of insoluble amorphous polycarbonate synthesized in micro-layers. The specific results and their significances are:

- The ultra-high molecular polycarbonates were synthesized by solid-state polymerization in micro-layers of 5-20µm on stationary glass substrates either in amorphous or crystalline state in the presence of catalyst (lithium hydroxide). It has been found that the polymer molecular weight increases rapidly to above 100,000 g/mol in less than 60 min at 230°C and 10 mmHg. The molecular weight as high as 600,000 g/mol was obtained in 180min when the prepolymer molecular weight of 21,000 g/mol was used at 230°C and 10 mmHg. This is a significant departure from the classical linear step growth polymerization kinetics in that the starting low molecular weight prepolymer had the end group mole ratio far smaller than the stoichiometric ratio of 1.0. The molecular weight is almost linearly dependent on the micro-layer thickness (5-35µm) and its correlation is expressed as $M_w = 4.533 \times 10^5 - 1.083 \times 10^4 \delta$, where δ in µm. For the thicknesses smaller than 621nm, the thickness effect becomes insignificant. The polydispersity of the high molecular weight polymers was broader than the theoretical value (e.g. PD=2.57).

- The molecular structure of the ultrahigh molecular weight polycarbonates has been analyzed by several techniques. ^{13}C -NMR results indicate that the linear step growth polymerization via end group reactions ceases as evidenced by the decrease in the phenolic group to insignificant levels after 30min at 230°C; however, MW continues to increase afterward, indicating that some other reaction mechanisms play a role in the further growth of polymer molecular weight. The ^1H -NMR and Py-GC/MS analysis results revealed that branched molecules and cross-linked molecules are present in the ultrahigh molecular weight polymers. The branched chains are formed by Fries rearrangement reaction or Kolbe-Schmitt rearrangement reaction whereas cross-linked chains are formed by the recombination of radicals generated by chain scission or hydrogen abstraction reactions. At 180min of SSP_m at 230°C, the mole fraction of cross-linked chains was 4.26×10^{-2} by ^1H -NMR spectroscopy analysis. The presence of branched and cross-linked chains or molecules was also confirmed by Py-GC/MS analysis.
- The formation of cross-linked polymers by radical recombination reactions was attributed to the near complete removal of phenol (i.e. radical scavenger) from the micro-layers during the solid state polymerization. The micro-layer thickness was so small that phenol diffusion resistance was practically absent and as a result, the radicals generated by chain scission and hydrogen abstraction reactions were able to engage in further reaction without combining with phenol. For example, in a 5µm-thick micro-layer, the model-calculated phenol concentration decreased rapidly to 1.1×10^{-4} mol/L in 60 sec. The

presence of branched polymer molecules was also observed by AFM. The AFM images show that branch segments have chain lengths of 25-32 repeat units per molecule.

- The formation of branched and cross-linked polymers contributed to the insolubility of the polymer in solvents. The weight fraction of chloroform-insoluble polycarbonate increased with reaction time and at 960min at 230°C of SSP_m, about 95% of the polymer was insoluble. We have also observed that highly cross-linked final polymer micro-layers were highly transparent without any discoloration. About 90-93% light transmission was shown at the visible light range (390-700nm). Higher reaction temperatures give higher rates of insoluble gel formation and the molecular weight buildup indicating both insolubel formation and molecular weight buildip are kinetically controlled. When the degree of cross-linking was low, it appears that some of these polymers dissolve in the solvent, indicating that the cross-linking did not occur globally but locally to enable the dissolution of the polymer in solvents.
- We have developed a Multi-Layer Deposit and Reaction (MLDR) technique to prepare thick layers of high molecular weight polycarbonates. The MLDR technique consists of:
 - 1) Obtaining high molecular weight amorphous polycarbonate micro-layers on the glass substrate;
 - 2) Another layer is deposited on top of the original polymer layer by second casing;
 - 3) After the second layer is polymerized, the same procedure is repeated until the desired micro-layer thickness is achieved. The layer thickness can be expanded while

keeping the merits (e.g. high transparency, good solvent resistance, and obtaining high molecular weight in short reaction time) of the SSP_m technique developed in this study.

- The thermal, mechanical, and rheological properties of high molecular weight polycarbonates were investigated using DSC, DMA, and rheometer. It has been observed that the glass transition temperature increases to about 159°C after 180min of reaction and it was concluded that the glass transition temperature was no longer affected by the degree of cross-linking afterwards. These phenomena were confirmed by the DMA using temperature sweep mode. The sample containing 95% insoluble gel (960min) shows the rubber elastic plateau in both storage modulus and tan δ versus temperature profiles. As the SSP_m process proceeds, the storage modulus increases and the slope decreases reaching a plateau. The shear thinning effect was promoted as branching and partial cross-linking reaction proceeds in the SSP_m process.

Bibliography

- (1). DeRudder, J. L., Commercial Applications of Polycarbonate. In *Commercial Applications of Polycarbonate.*, Eds. Legrand, D.G.; Bendler J.T.; Marcel Dekker Inc: New York, **2000**, p 303.
- (2). Brunelle, D., J., Advances in Polycarbonates. In *Advances in Polycarbonates*, 2005; Vol.; ACS Symposium Series 626; American Chemical Society: Washington, DC, **2005**, pp 1-5.
- (3). Zhai, W.; Yu, J.; Ma, W.; He, J., Influence of Long-Chain Branching on the Crystallization and Melting Behavior of Polycarbonates in Supercritical CO₂. *Macromolecules* **2007**, *40*, 73-80.
- (4). Hachiya, H.; Yoneda, H.; Matsuda, Y.; Yoshida, K.; Takeda, K., Properties of high molecular weight polycarbonate synthesized by using the solid phase polymerization method. *Jan. J. Polym. Sci. Technol.* **2000**, *57*, 15-22.
- (5). Guerrero, H.; Guinea, G. V.; Zoido, J., Mechanical Properties of Polycarbonate Optical Fibers. *Fiber and Integrated Optics* **1998**, *17*, 231-242.
- (6). Yamashita, T.; Kamada, K., Intrinsic Transmission Loss of Polycarbonate Core Optical Fiber. *Jan. J. Appl. Phys.* **1993**, *32*, 2681-2686.
- (7). Lyu, M.-Y.; Lee, J. S.; Pae, Y., Study of mechanical and rheological behaviors of linear and branched polycarbonates blends. *Journal of Applied Polymer Science* **2001**, *80*, 1814-1824.
- (8). Liu, C.; Li, C.; Chen, P.; He, J.; Fan, Q., Influence of long-chain branching on linear viscoelastic flow properties and dielectric relaxation of polycarbonates. *Polymer* **2004**, *45*, 2803-2812.
- (9). Boonstra, T. O.; Olden, D. v.; Woudenberg, R. H., Cross-linked or cross-linkable optical polycarbonates and optical components comprising said optical polycarbonates. U.S. Pat. 5,908,916 A, **1999**.

- (10). Lee, H.-K.; Yuko, Y.; Kim, K.-Y., Photosensitive resin composition, thin film panel made with photosensitive composition, and method for manufacturing thin film panel. U.S. Pat. 7,297,452 B2, **2007**.
- (11). Brydson, J. A., *Plastics Materials*. In *Plastics Materials*, Butterworths, London, **1989**, p 521-545.
- (12). Woo, B.-G.; Choi, K. Y.; Song, K. H., Melt Polycondensation of Bisphenol A Polycarbonate by a Forced Gas Sweeping Process. *Ind. Eng. Chem. Res.* **2001**, *40*, 1312-1319.
- (13). Gu, J.-T.; Wang, C.-S., The interfacial polycarbonate reactions. I. Defining the critical process parameters. *J. Appl. Polym. Sci.* **1992**, *44*, 849-857.
- (14). Fukuoka, S.; Kawamura, M.; Komiya, K.; Tojo, M.; Hachiya, H.; Hasegawa, K.; Aminaka, M.; Okamoto, H.; Fukawa, I.; Konno, S., A novel non-phosgene polycarbonate production process using by-product CO₂ as starting material. *Green Chemistry* **2003**, *5*, 497-507.
- (15). Ignatov, V. N.; Tartari, V.; Carraro, C.; Pippa, R.; Nadali, G.; Berti, C.; Fiorini, M., New Catalysts for Bisphenol A Polycarbonate Melt Polymerisation, 1. Kinetics of Melt Transesterification of Diphenylcarbonate with Bisphenol A. *Macromolecular Chemistry and Physics* **2001**, *202*, 1941-1945.
- (16). Woo, B.-G.; Choi, K. Y.; Song, K. H., Melt Polycondensation of Bisphenol A Polycarbonate by Forced Gas Sweeping Process II. Continuous Rotating-Disk Reactor. *Ind. Eng. Chem. Res.* **2001**, *40*, 3459-3466.
- (17). Sweileh, B. A.; Al-Hiari, Y. M.; Kailani, M. H.; Mohammad, H. A., Synthesis and Characterization of Polycarbonates by Melt Phase Interchange Reactions of Alkylene and Arylene Diacetates with Alkylene and Arylene Diphenyl Dicarbonates. *Molecules* **2010**, *15*, 3661-3682.
- (18). Davis, A.; Golden, J. H., Competition between Scission and Cross-linking Processes in the Thermal Degradation of a Polycarbonate. *Nature* **1965**, *206*, 397-397.
- (19). Davis, A.; Golden, J. H., Thermal degradation of polycarbonate. *J. Chem. Soc. B: Phys. Org.* **1968**, *0*, 45-47.

- (20). Davis, A.; Golden, J. H., Thermally-induced cross-linking of poly[2.2-propane-bis-(4-phenyl carbonate)]. *Die Makromolekulare Chemie* **1967**, *110*, 180-184.
- (21). Davis, A.; Golden, J. H., Degradation of polycarbonates. III. Viscometric study of thermally-induced chain scission. *Die Makromolekulare Chemie* **1964**, *78*, 16-23.
- (22). Fukuoka, S.; Watanabe, T.; Dozono, T., Method for Producing a Crystallized Aromatic Polycarbonate, and a Crystallized Aromatic Polycarbonate Obtained Thereby. U.S. Pat. 4,948,871, **1990**.
- (23). Christopher, W. F.; Fox, D. W., In *Polycarbonates*, Reinhold Publishing, New York, **1962**.
- (24). Fukawa, I.; Fukuoka, S.; Komiya, K.; Sasaki, Y., Porous, Crystallized, Aromatic Polycarbonate Prepolymer, A Porous, Crystallized Aromatic Polycarbonate, and Production Methods. U.S. Pat. 5,204,377, **1993**.
- (25). Ye, Y.; Machado, B.; Choi, K. Y.; Kim, J. H.; Woo, B. G., Modeling of Solid-State Polymerization of Bisphenol A Polycarbonate. *Ind. Eng. Chem. Res.* **2005**, *44*, 2494-2505.
- (26). Kuran, W.; Dębek, C.; Wielgosz, Z.; Kuczyńska, L.; Sobczak, M., Application of a solid-state postpolycondensation method for synthesis of high molecular weight polycarbonates. *J. Appl. Polym. Sci.* **2000**, *77*, 2165-2171.
- (27). Gross, S. M.; Roberts, G. W.; Kiserow, D. J.; DeSimone, J. M., Synthesis of High Molecular Weight Polycarbonate by Solid-State Polymerization. *Macromolecules* **2001**, *34*, 3916-3920.
- (28). Shi, C.; DeSimone, J. M.; Kiserow, D. J.; Roberts, G. W., Reaction Kinetics of the Solid-State Polymerization of Poly(bisphenol A carbonate) Facilitated by Supercritical Carbon Dioxide. *Macromolecules* **2001**, *34*, 7744-7750.
- (29). Shi, C.; Gross, S. M.; DeSimone, J. M.; Kiserow, D. J.; Roberts, G. W., Reaction Kinetics of the Solid State Polymerization of Poly(bisphenol A carbonate). *Macromolecules* **2001**, *34*, 2060-2064.

- (30). Kim, J. H., Solid-state polymerization of bisphenol A polycarbonate with a spray-crystallizing method. *J. Appl. Polym. Sci.* **2009**, *111*, 883-889.
- (31). Kim, Y.; Choi, K. Y., Multistage melt polymerization of bisphenol-A and diphenyl carbonate to polycarbonate. *J. Appl. Polym. Sci.* **1993**, *49*, 747-764.
- (32). Ye, Y.; Choi, K. Y., Optimizing polymer reactivities for the solid-state polycondensation of AA and BB type monomers. *Polymer* **2008**, *49*, 2817-2824.
- (33). Woo, B.-G.; Choi, K. Y.; Song, K. H.; Lee, S. H., Melt polymerization of bisphenol-A and diphenyl carbonate in a semibatch reactor. *Journal of Applied Polymer Science* **2001**, *80*, 1253-1266.
- (34). Brunelle, D. J.; Shannon, T. G., Preparation and polymerization of bisphenol A cyclic oligomeric carbonates. *Macromolecules* **1991**, *24*, 3035-3044.
- (35). Kulig, J. J.; Brittain, W. J.; Gilmour, S.; Perry, J. W., Synthesis of Nonlinear Optical Polycarbonates via the Ring-Opening Polymerization of Macrocyclic Prepolymers. *Macromolecules* **1994**, *27*, 4838-4839.
- (36). Nagahata, R.; Sugiyama, J.-i.; Goyal, M.; Asai, M.; Ueda, M.; Takeuchi, K., Synthesis of ultra high-molecular-weight polycarbonate. *Polym. Adv. Technol.* **2000**, *11*, 727-732.
- (37). Hagenars, A. C.; Pesce, J. J.; Bailly, C.; Wolf, B. A., Characterization of melt-polymerized polycarbonate: preparative fractionation, branching distribution and simulation. *Polymer* **2001**, *42*, 7653-7661.
- (38). Karlik, D.; Brack, H. P.; Verhoogt, H.; Lemmon, J. P.; Kamps, J. H.; Sederel, W. L.; Goossens, J. M. D., Process for the production of branched melt polycarbonate by late addition of fries-inducing catalyst. U.S. Pat. 6504002 B1, **2003**.
- (39). Marks, M. J.; Munjal, S.; Namhata, S.; Scott, D. C.; Bosscher, F.; De Letter, J. A.; Klumperman, B., Randomly branched bisphenol A polycarbonates. I. Molecular weight distribution modeling, interfacial synthesis, and characterization. *Journal of Polymer Science Part A: Polymer Chemistry* **2000**, *38*, 560-570.

- (40). Oba, K.; Ishida, Y.; Ito, Y.; Ohtani, H.; Tsuge, S., Characterization of Branching and/or Cross-Linking Structures in Polycarbonate by Reactive Pyrolysis-Gas Chromatography in the Presence of Organic Alkali. *Macromolecules* **2000**, *33*, 8173-8183.
- (41). McNeill, I. C.; Rincon, A., Degradation studies of some polyesters and polycarbonates. Bisphenol A polycarbonate. *Polymer Degradation and Stability* **1991**, *31*, 163-180.
- (42). Montaudo, G.; Puglisi, C.; Samperi, F., Chemical reactions which occur in the thermal treatment of polycarbonate/polyethyleneterephthalate blends, investigated by direct pyrolysis mass spectrometry. *Polymer Degradation and Stability* **1991**, *31*, 291-326.
- (43). Goodner, M. D.; Gross, S. M.; Desimone, J. M.; Roberts, G. W.; Kiserow, D. J., Broadening of molecular-weight distribution in solid-state polymerization resulting from condensate diffusion. *J. Appl. Polym. Sci.* **2001**, *79*, 928-943.
- (44). Ye, Y.; Choi, K. Y., Estimation of Initial Conditions of a Prepolymer for a Solid-State Step-Growth Polymerization Process. *Macromol. React. Eng.* **2010**, *4*, 613-620.
- (45). Kim, J.; Roberts, G. W.; Kiserow, D. J., Effect of prepolymer molecular weight on solid state polymerization of poly(bisphenol a carbonate) with nitrogen as a sweep fluid. *J. Polym. Sci. Part A: Polym. Chem.* **2008**, *46*, 4959-4969.
- (46). Kim, J.; Dong, L. B.; Kiserow, D. J.; Roberts, G. W., Complex Effects of the Sweep Fluid on Solid-State Polymerization: Poly(bisphenol A carbonate) in Supercritical Carbon Dioxide. *Macromolecules* **2009**, *42*, 2472-2479.
- (47). Kim, Y.; Choi, K. Y.; Chamberlin, T. A., Kinetics of melt transesterification of diphenyl carbonate and bisphenol A to polycarbonate with lithium hydroxide monohydrate catalyst. *Ind. Eng. Chem. Res.* **1992**, *31*, 2118-2127.
- (48). Ye, Y.; Choi, K. Y., Preparation of Micron-Sized Spherulitic Bisphenol A Polycarbonate Particles in Thin Films. *Macromol. Mater. Eng.* **2009**, *294*, 847-854.
- (49). Ye, Y.; Kim, B.; Seog, J.; Yong Choi, K., Transitions of morphological patterns of crystallizing polycarbonate in thin films. *J. Appl. Polym. Sci.* **2012**, *124*, 560-567.
- (50). Odian, G., *Principles of polymerization. 4th edition.* 2004.

- (51). Hout, H. H. M. v.; Akio Ikeda, T. K.; McCloskey, P. J.; Shimoda, T., Method of manufacturing polycarbonates. U.S. Pat. 6,339,138, **2002**.
- (52). Hachiya, H.; Adachi, T., Polycarbonate resin composition for use in the production of a substrate for an optical information medium. US Pat. 7,307,114 B2, **2007**.
- (53). Hachiya, H.; Kazunori, M.; Komiya, K., Polycarbonate comprising different kinds of bonding units and process for the preparation thereof. Pat. 0,885,912 A1, **1998**.
- (54). Fukuda, Y.; Kanno, T.; Kuwana, T.; Okano, Y.; Oshino, Y.; Tanigawa, M.; Yamato, T.; Weniger, Process for the preparation of polycarbonate. US Pat. 5,468,936 A, **1995**.
- (55). Flory, P. J., Molecular Size Distribution in Linear Condensation Polymers¹. *J. Am. Chem. Soc.* **1936**, 58, 1877-1885.
- (56). Oba, K.; Ishida, Y.; Ohtani, H.; Tsuge, S., Characterization of abnormal structures in thermally treated liquid crystalline aromatic polyesters by pyrolysis-gas chromatography in the presence of organic alkali. *Polym. Degrad. Stab.* **2002**, 76, 85-94.
- (57). Diepens, M.; Gijsman, P., Photodegradation of bisphenol A polycarbonate. *Poly. Degrad. Stab.* **2007**, 92, 397-406.
- (58). Potyrailo, R. A.; Lemmon, J. P.; Leib, T. K., Aromatic polycarbonate characterization. U.S. Pat. 6,541,264, **2000**.
- (59). Davis, A.; Golden, J. H., Stability of Polycarbonate. *Journal of Macromolecular Science, Part C* **1969**, 3, 49-68.
- (60). Puglisi, C.; Sturiale, L.; Montaudo, G., Thermal Decomposition Processes in Aromatic Polycarbonates Investigated by Mass Spectrometry. *Macromolecules* **1999**, 32, 2194-2203.
- (61). Kim, J.; Gracz, H. S.; Roberts, G. W.; Kiserow, D. J., Spectroscopic analysis of poly(bisphenol A carbonate) using high resolution ¹³C and ¹H NMR. *Polymer* **2008**, 49, 394-404.

- (62). Uozumi, T.; Kwon, T. S.; Takeuchi, K.; Hayashi, T.; Tanaka, M., Thermal behavior of poly(bisphenol A carbonate) in the presence of phosphorus compounds. *J. Polym. Sci. Part A: Polym. Chem.* **2004**, *42*, 1069-1074.
- (63). Foti, M.; Ingold, K. U.; Lusztyk, J., The Surprisingly High Reactivity of Phenoxy Radicals. *J. Am. Chem. Soc.* **1994**, *116*, 9440-9447.
- (64). Valdebenito, A.; Lissi, E. A.; Encinas, M. V., Effect of Phenols on the Free-Radical Photopolymerization of Vinyl Monomers in Aqueous Solution. *Macromol. Chem. Phys.* **2001**, *202*, 2581-2585.
- (65). Semeluk, G. P.; Bernstein, R. B., The Thermal Decomposition of Chloroform. I. Products 1a. *J. Am. Chem. Soc.* **1954**, *76*, 3793-3796.
- (66). Semeluk, G. P.; Bernstein, R. B., The Thermal Decomposition of Chloroform. II. Kinetics 1a. *J. Am. Chem. Soc.* **1956**, *79*, 46-49.
- (67). Zanetti, J. E.; Egloff, G., The Thermal Decomposition of Benzene. *Journal of Industrial & Engineering Chemistry* **1917**, *9*, 350-356.
- (68). Hou, K. C.; Palmer, H. B., The Kinetics of Thermal Decomposition of Benzene in a Flow System. *The Journal of Physical Chemistry* **1965**, *69*, 863-868.
- (69). Sankey, B. M.; White, A. M., Thermal stabilization of N-methyl-2-pyrrolidone. U.S. Pat. 4,168,226 A, **1979**.
- (70). Klute, C. H.; Walters, W. D., The Thermal Decomposition of Tetrahydrofuran. *Journal of the American Chemical Society* **1946**, *68*, 506-511.
- (71). Rice, F. O.; Herzfeld, K. F., The Thermal Decomposition of Organic Compounds from the Standpoint of Free Radicals. VI. The Mechanism of Some Chain Reactions. *Journal of the American Chemical Society* **1934**, *56*, 284-289.
- (72). Boyce, J. R.; Shirvanyants, D.; Sheiko, S. S.; Ivanov, D. A.; Qin, S.; B. 철 rner, H.; Matyjaszewski, K., Multiarm Molecular Brushes: Effect of the Number of Arms on the Molecular Weight Polydispersity and Surface Ordering. *Langmuir* **2004**, *20*, 6005-6011.

- (73). Glagola, C. P.; Miceli, L. M.; Milchak, M. A.; Halle, E. H.; Logan, J. L., Polystyrene-Poly(ethylene oxide) Diblock Copolymer: The Effect of Polystyrene and Spreading Concentration at the Air/Water Interface. *Langmuir* **2012**, *28*, 5048-5058.
- (74). Sorokin, A. V.; Bai, M.; Ducharme, S.; Poulsen, M., Langmuir-Blodgett films of polyethylene. *Journal of Applied Physics* **2002**, *92*, 5977-5981.
- (75). Beers, K. L.; Gaynor, S. G.; Matyjaszewski, K.; Sheiko, S. S.; Moller, M., The Synthesis of Densely Grafted Copolymers by Atom Transfer Radical Polymerization. *Macromolecules* **1998**, *31*, 9413-9415.
- (76). Djalali, R.; Li, S.-Y.; Schmidt, M., Amphipolar Core-shell Cylindrical Brushes as Templates for the Formation of Gold Clusters and Nanowires. *Macromolecules* **2002**, *35*, 4282-4288.
- (77). Zhai, W.; Yu, J.; Ma, W.; He, J., Influence of Long-Chain Branching on the Crystallization and Melting Behavior of Polycarbonates in Supercritical CO₂. *Macromolecules* **2006**, *40*, 73-80.
- (78). Roiter, Y.; Jaeger, W.; Minko, S., Conformation of single polyelectrolyte chains vs. salt concentration: Effects of sample history and solid substrate. *Polymer* **2006**, *47*, 2493-2498.
- (79). Roiter, Y.; Minko, S., Adsorption of Polyelectrolyte versus Surface Charge: in Situ Single-Molecule Atomic Force Microscopy Experiments on Similarly, Oppositely, and Heterogeneously Charged Surfaces. *The Journal of Physical Chemistry B* **2007**, *111*, 8597-8604.
- (80). Roiter, Y.; Minko, S., AFM Single Molecule Experiments at the Solid-liquid Interface: In Situ Conformation of Adsorbed Flexible Polyelectrolyte Chains. *Journal of the American Chemical Society* **2005**, *127*, 15688-15689.
- (81). Marks, M. J.; Sekinger, J. K., Synthesis, Crosslinking, and Properties of Benzocyclobutene-Terminated Bisphenol A Polycarbonates. *Macromolecules* **1994**, *27*, 4106-4113.
- (82). Adelman, S.; Margotte, D.; Vernaleken, H., Polycarbonates with end groups containing bonds which can be crosslinked by UV light. U.S. Pat. 4,230,548, **1980**.

- (83). Schnell, H., Chemistry and Physics of Polycarbonates. In Interscience Publisher; Wiley: New York, **1964**, Chapter 3.
- (84). McNeill, I. C.; Rincon, A., Thermal degradation of polycarbonates: Reaction conditions and reaction mechanisms. *Polymer Degradation and Stability* **1993**, *39*, 13-19.
- (85). Montaudo, G.; Puglisi, C., Thermal decomposition processes in bisphenol a polycarbonate. *Polymer Degradation and Stability* **1992**, *37*, 91-96.
- (86). Montaudo, G.; Puglisi, C.; Samperi, F., Chemical reactions occurring in the thermal treatment of polymer blends investigated by direct pyrolysis mass spectrometry: Polycarbonate/polybutyleneterephthalate. *Journal of Polymer Science Part A: Polymer Chemistry* **1993**, *31*, 13-25.
- (87). Foti, S.; Giuffrida, M.; Maravigna, P.; Montaudo, G., Direct mass spectrometry of polymers. VII. Primary thermal fragmentation processes in polycarbonates. *Journal of Polymer Science: Polymer Chemistry Edition* **1983**, *21*, 1567-1581.
- (88). Tsuge, S.; Ohtani, H.; Oba, K., Novel characterization of branching and/or cross-linking structures in condensation polymers by reactive pyrolysis-gas chromatography in the presence of organic alkaline. *Macromolecular Symposia* **2003**, *195*, 287-292.
- (89). Ito, Y.; Ogasawara, H.; Ishida, Y.; Ohtani, H.; Tsuge, S., Characterization of End Groups in Polycarbonates by Reactive Pyrolysis-Gas Chromatography. *Polym J* **1996**, *28*, 1090-1095.
- (90). Ohtani, H.; Fujii, R.; Tsuge, S., Pyrolysis – capillary gas chromatography combined with on-line alkylation for the compositional analysis of liquid crystalline aromatic polyesters. *Journal of High Resolution Chromatography* **1991**, *14*, 388-391.
- (91). Levy, L. B., Inhibition of acrylic acid polymerization by phenothiazine and p-methoxyphenol. II. Catalytic inhibition by phenothiazine. *Journal of Polymer Science Part A: Polymer Chemistry* **1992**, *30*, 569-576.
- (92). Levy, L. B., Inhibition of acrylic acid polymerization by phenothiazine and p-methoxyphenol. *Journal of Polymer Science: Polymer Chemistry Edition* **1985**, *23*, 1505-1515.

- (93). Alam, S.; Kandpal, L. D.; Varma, I. K., Ethynyl-Terminated Imide Oligomers. *Journal of Macromolecular Science, Part C* **1993**, *33*, 291-320.
- (94). Garapon, J.; Stille, J. K., Biphenylene as Cross-Linking Sites for Polyquinolines. *Macromolecules* **1977**, *10*, 627-632.
- (95). Aharoni, S.; Marks, M., Crosslink Products, Mechanism, and Network Structure of Benzocyclobutene Terminated Bisphenol a Polycarbonates. In *Synthesis, Characterization, and Theory of Polymeric Networks and Gels*, Springer US: 1992; pp 165-177.
- (96). Xu, L.; Weiss, R. A., Melt Crystallization of Bisphenol A Polycarbonate in Blends of Polycarbonate with Zinc Salts of Sulfonated Polystyrene Ionomers. *Macromolecules* **2003**, *36*, 9075-9084.
- (97). Delbreilh, L.; Dargent, E.; Grenet, J.; Saiter, J. M.; Bernes, A.; Lacabanne, C., Study of poly(bisphenol A carbonate) relaxation kinetics at the glass transition temperature. *European Polymer Journal* **2007**, *43*, 249-254.
- (98). van Melick, H. G. H.; Govaert, L. E.; Meijer, H. E. H., On the origin of strain hardening in glassy polymers. *Polymer* **2003**, *44*, 2493-2502.
- (99). Mulliken, A. D.; Boyce, M. C., Polycarbonate and a Polycarbonate-POSS Nanocomposite at High Rates of Deformation. *Journal of Engineering Materials and Technology* **2006**, *128*, 543-550.
- (100). LeGrand, D. G.; Bendler, J. T., *Handbook of polycarbonate science and technology*. Marcel Dekker: New York.
- (101). Fox, T. G.; Flory, P. J., Viscosity-Molecular Weight and Viscosity-Temperature Relationships for Polystyrene and Polyisobutylene^{1,2}. *Journal of the American Chemical Society* **1948**, *70*, 2384-2395.
- (102). Fox, T. G.; Flory, P. J., Second order Transition Temperatures and Related Properties of Polystyrene. I. Influence of Molecular Weight. *Journal of Applied Physics* **1950**, *21*, 581-591.
- (103). Fox, T. G.; Flory, P. J., Further Studies on the Melt Viscosity of Polyisobutylene. *The Journal of Physical Chemistry* **1951**, *55*, 221-234.

- (104). Folt, V. L., The Effects of Mechanical Degradation on Rheological Properties of Elastomers. *Rubber Chemistry and Technology* **1969**, *42*, 1294-1313.
- (105). Schaefgen, J. R.; Flory, P. J., Synthesis of Multichain Polymers and Investigation of their Viscosities. *Journal of the American Chemical Society* **1948**, *70*, 2709-2718.
- (106). Masuda, T.; Ohta, Y.; Onogi, S., Rheological Properties of Anionic Polystyrenes. III. Characterization and Rheological Properties of Four-Branch Polystyrenes. *Macromolecules* **1971**, *4*, 763-768.
- (107). Romani, F.; Corrieri, R.; Braga, V.; Ciardelli, F., Monitoring the chemical crosslinking of propylene polymers through rheology. *Polymer* **2002**, *43*, 1115-1131.
- (108). Winter, H. H., Evolution of rheology during chemical gelation. In *Permanent and Transient Networks*, Steinkopff: 1987; Vol. 75, pp 104-110.
- (109). Tian, J.; Yu, W.; Zhou, C., The preparation and rheology characterization of long chain branching polypropylene. *Polymer* **2006**, *47*, 7962-7969.
- (110). Al-Muntasheri, G. A.; Hussein, I. A.; Nasr-El-Din, H. A.; Amin, M. B., Viscoelastic properties of a high temperature cross-linked water shut-off polymeric gel. *Journal of Petroleum Science and Engineering* **2007**, *55*, 56-66.

List of Publications

- (1) Emdadi, L.; Luciani, C. V.; Lee, S. Y.; **Baick, In Hak.**; Choi, K. Y., Experimental and theoretical study of the reaction locus during the dispersion polymerization of methyl methacrylate in a nonpolar hydrocarbon solvent at low temperature. *Polymer Engineering & Science*, **2011**, *51*, 1969-1986.
- (2) Luciani, C. V.; Emdadi, L.; Lee, S. Y.; **Baick, In Hak.**; Choi, K. Y., Modeling of Phase Inversion and Particle Stability in the Dispersion Polymerization of Methyl Methacrylate in a Non-polar Hydrocarbon Solvent. *Macromolecular Reaction Engineering*, **2011**, *5*, 340-351.
- (3) Choi, K. Y.; Luciani, C. V.; Emdadi, L.; Lee, S. Y.; **Baick, In Hak.**; Lim, J. S., Spherical Pseudo-Inverse Opal Silica with Pomegranate-Like Polymer Microparticles as Templates. *Macromolecular Materials and Engineering*, **2012**, *297*, 1021-1027.
- (4) **Baick, In Hak.**; Luciani, C. V.; Park, S. Y.; Lim, T.; Choi, K. Y., Kinetics of Reversible Oligomerization of l-Lactic Acid with a $\text{SnCl}_2 \cdot 2\text{H}_2\text{O}$ /p-Toluenesulfonic Acid Catalyst. *Industrial & Engineering Chemistry Research*, **2012**, *51*, 16617-16625.
- (5) **Baick, In Hak.**; Ye, Y.; Luciani, C. V.; Ahn, Y. G.; Song, K. H.; Choi, K. Y., Ultra-High Molecular Weight Nonlinear Polycarbonates Synthesized in Micro-Layers. *Industrial & Engineering Chemistry Research*, **2013**, **Nov**, **15** (under final review).
- (6) **Baick, In Hak.**; Yang W. J.; Luciani, C. V.; Choi, K. Y., Synthesis of Partially Cross-linked Bisphenol A Polycarbonates via Radical Recombination, **2013** (In preparation)

Inventions

Invention Title: Ultra Molecular Weight Step-Growth Polymers

Description: A novel polymerization technique is disclosed to synthesize condensation polymers of ultra-high molecular weight, branching, and crosslinking with excellent solvent and heat resistances with optical transparency in short reaction time starting with low molecular weight polymer precursors.

Inventor (s): Kyu Yong Choi, In Hak Baick, Yuesheng Ye, Carla Luciani

List of Conference Presentations

(1) A Two-Step Process for the Synthesis of Poly(L-lactic Acid)

In Hak Baick, Yuesheng Ye, and Kyu Yong Choi

Presenter: **In Hak Baick**

Conference: 2008 AIChE Annual Meeting

(2) A Two-Step Process for the Synthesis of Poly(L-lactic Acid)

In Hak Baick, Yuesheng Ye, and Kyu Yong Choi

Speaker: **In Hak Baick**

Conference: 2009 UMD Research Fest

(3) Pseudo-Solid State Polymerization In Amorphous Polymer Micro-Layers: A Novel Route to Ultra-High Molecular Weight Polycarbonate

In Hak Baick, Carla Vanesa Luciani, Woojic Yang, and Kyu Yong Choi

Speaker: **In Hak Baick**

Conference: 2011 AIChE Annual Meeting

(4) Understanding Rapid pseudo-Solid State Step-Growth Polymerization in Micro-Layers Leading to Ultrahigh Molecular Weight Polymers

In Hak Baick, and Kyu Yong Choi

Presenter: **Kyu Yong Choi**

Conference: CBET/NSF Conference 2012

(5) Pseudo-Solid State Polymerization in Amorphous Polymer Micro-Layers: A Novel Route to Produce Ultra-High Molecular Weight Polycarbonate

In Hak Baick, Carla Vanesa Luciani, Yuesheng Ye, and Kyu Yong Choi

Speaker: **In Hak Baick**

Conference: 2012 UMD Research Fest

(6) Polymerization in Confined Reaction Space: New Tools for Designed Polymers

In Hak Baick, and Kyu Yong Choi

Speaker: **Kyu Yong Choi**

Conference: KAIST-UMD Symposium on Projections in the Physical Sciences for Future 2012

(7) Pseudo-Solid State Polymerization In Amorphous Polymer Micro-Layers: A Novel Route to Produce Ultra-High Molecular Weight Polycarbonate

In Hak Baick, Carla Vanesa Luciani, Woojic Yang, and Kyu Yong Choi

Presenter: **Kyu Yong Choi**

Conference: Polymer Reaction Engineering Conference 2012

(8) Ultra-high Molecular weight Bisphenol A Polycarbonate via Solid State Polymerization in Geometrically Confined Reaction Space

In Hak Baick, Yuesheng Ye, Carla Vanesa Luciani, and Kyu Yong Choi

Speaker: **Kyu Yong Choi**

Conference: US Korea Conference 2013

(9) Ultrahigh Molecular Weight Polycarbonate via pseudo-Solid State Polymerization (p-SSP) in Geometrically Confined Reaction Space.

In Hak Baick, and Kyu Yong Choi

Speaker: **Kyu Yong Choi**

Conference: 11th International Workshop on Polymer Reaction